
INTERACTIONS BETWEEN BIOLOGICAL MACROMOLECULES: PRION PROTEIN AND ITS LIGANDS

Paola M. G. Cavaliere

Dottorato in Scienze Biotecnologiche – XXIV ciclo
Indirizzo Biotecnologie Industriali e Molecolari
Università di Napoli Federico II





INTERACTIONS BETWEEN BIOLOGICAL MACROMOLECULES: PRION PROTEIN AND ITS LIGANDS

Paola M. G. Cavaliere

Dottoranda: Paola M. G. Cavaliere

Relatore: Prof.ssa Adriana Zagari

Coordinatore: Prof. Giovanni Sannia

To whom taught me everything

Table of Contents

Riassunto	pag.	1
Summary	pag.	6
Abbreviations	pag.	8
Chapter I <i>Introduction</i>		
1.1 The main issue of the Prion Protein	pag.	9
1.2 Prion protein: a structural and functional overview	pag.	11
1.3 The dark side of prion protein: PrP as a disease-causing agent	pag.	17
1.3.1 Mechanisms of PrP conversion	pag.	18
1.3.2 Intermediates in prion protein conversion: PrP polymerization	pag.	19
1.3.3 The uncertain landscape of therapeutic strategies in prion diseases	pag.	20
1.4 Thesis aims	pag.	21
Chapter II <i>Prion Protein and Methylene Blue</i>		
2.1 Methylene blue and its role in the therapeutic world	pag.	23
2.2 Experimental Procedures	pag.	26
2.3 Results	pag.	29
2.4 Discussion	pag.	39
Chapter III <i>Prion Protein and Aptamers</i>		
3.1 Nucleic-acid-binding properties of prion protein	pag.	44
3.1.1 Are nucleic acids involved in the physiology and/or in the pathology of prion protein?	pag.	44
3.1.2 Prion protein and DNA/RNA aptamers	pag.	47
3.1.3 D12 and R12 aptamers against prion protein	pag.	49
3.2 Experimental Procedures	pag.	51
3.3 Results	pag.	53
3.4 Discussion	pag.	64
Chapter IV <i>Prion Protein and Aldolase C</i>		
4.1 The glycolytic enzyme Aldolase	pag.	68
4.1.1 The possible physiological role of the PrP-AldoC complex	pag.	70
4.2 Experimental Procedures	pag.	71
4.3 Results	pag.	72
4.4 Discussion	pag.	76
Chapter V <i>Conclusion</i>	pag.	78
Appendix I <i>Other protein-misfolding diseases: the case of phenylalanine hydroxylase</i>	pag.	80

Appendix II <i>List of publication, communications and research activity in scientific institution abroad and in Italy</i>	pag.	82
Acknowledgments	pag.	84
References	pag.	86

Riassunto

Una famiglia di malattie neurodegenerative, molto rara ma fatale non solo per gli esseri umani ma anche per varie specie animali, è correlata al misfolding della proteina prionica (PrP). Negli esseri umani, sono collegate a questa proteina le malattie di Creutzfeldt-Jakob, di Gerstmann-Straussler-Scheinker e l'insonnia fatale, mentre negli animali, la malattia è stata inizialmente riscontrata nelle pecore (da cui il termine scrapie), ma può colpire anche i bovini (Prusiner, 1998) ed altri animali. Le malattie prioniche possono sorgere spontaneamente, per induzione mediante mutazioni del gene della proteina prionica oppure per acquisizione tramite infezione. In quest'ultimo caso le malattie prendono il nome di encefalopatie spongiformi trasmissibili (TSE). La patogenesi di queste malattie è associata all'accumulo di aggregati amiloidi insolubili nel cervello, seguita dalla morte delle cellule neuronali. L'evento centrale di questo tipo di malattie neurodegenerative è la conversione dell'isoforma cellulare della proteina prionica, PrP^{C} , in quella patologica, PrP^{Sc} . La conversione $\text{PrP}^{\text{C}} \rightarrow \text{PrP}^{\text{Sc}}$ prevede una variazione conformazionale della PrP, prevalentemente α -elicoidale, in una struttura ricca di β -sheet (Caughey et al., 2001). Il conformero patologico presenta altre caratteristiche, oltre a quelle strutturali, che lo distinguono dall'isoforma cellulare. Infatti, la PrP^{C} è monomerica ed è sensibile alla proteinasi K mentre la PrP^{Sc} è un multimerico caratterizzato da un'elevata resistenza alla digestione da parte della proteinasi K (Caughey et al., 1991).

La caratteristica più importante e inusuale delle malattie TSE è la natura dell'agente patogeno. Anche se non è stato definitivamente dimostrato, si pensa che l'agente patogeno sia la proteina prionica stessa e questa asserzione viene indicata come "*protein-only hypothesis*". Secondo questa ipotesi, la PrP^{Sc} auto-catalizza la propagazione della propria conformazione patologica usando l'isoforma PrP^{C} come substrato (Prusiner, 1998). Infatti, il conformero patologico della proteina prionica, PrP^{Sc} , potrebbe indurre la conversione di altre molecole di PrP^{C} verso la forma amiloidogena PrP^{Sc} .

Dal punto di vista strutturale, la proteina prionica cellulare è una glicoproteina, costituita da circa 210 amminoacidi (nella forma matura) e composta da una regione N-terminale non strutturata e da un dominio C-terminale globulare strutturato (Hornemann et al., 2004). La proteina prionica è espressa maggiormente nel cervello, ma è stata riscontrata anche in altri tessuti non neuronali come le cellule linfoidi, il cuore, il tratto gastrointestinale, i muscoli, i reni e le ghiandole mammarie. Nonostante la PrP sia altamente conservata lungo le specie e presente in molti tessuti, il suo ruolo biologico non è stato ancora chiaramente delucidato. Da studi effettuati, sono stati ipotizzati diversi ruoli per la proteina prionica; in particolare, nel metabolismo neurotrasmettitore, nell'attivazione delle cellule immunologiche, nell'adesione cellulare, nella trasduzione del segnale, nel metabolismo del rame, nell'attività antiossidante e nella morte cellulare (Aguzzi et al., 2008).

L'obiettivo di questo lavoro di tesi è quello di studiare le possibili interazioni della proteina prionica con altri partner biologici (proteine e acidi nucleici) e con piccole molecole organiche, utilizzando molteplici metodologie. In particolare, questo lavoro di tesi è stato condotto percorrendo tre linee diverse: a) lo studio dei possibili effetti di una piccola molecola organica, il blu di metilene (MB), sui meccanismi di formazione

degli oligomeri e degli aggregati amiloidi in modo tale da avere una possibile applicazione in ambito farmaceutico, b) lo studio dell'interazione della PrP con piccoli aptameri DNA ed RNA, i quali legano in modo specifico la proteina e possono quindi essere utilizzati nell'ambito della diagnostica, e infine c) lo studio dell'interazione della PrP con un enzima glicolitico, l'aldolasi C, allo scopo di indagare sui possibili ruoli biologici della proteina in relazione alla glicolisi (Gawinecka et al., 2010).

La proteina prionica e il blu di metilene. Un importante campo di ricerca nell'ambito del prione è la valutazione, *in vitro*, di composti che possano interferire con il meccanismo di conversione della proteina prionica e quindi possano essere utilizzati come farmaci contro le malattie prioniche. Per questo scopo, nel presente lavoro è stata ricercata una molecola organica con determinate caratteristiche da poter essere usata in futuri test clinici. Il blu di metilene soddisfa tutti i criteri richiesti per un possibile futuro farmaco nell'ambito delle malattie prioniche: primo, è una molecola già utilizzata in ambito farmaceutico, per cui si conoscono le sue caratteristiche tossiche e farmacologiche; secondo, è una molecola capace di attraversare la barriera encefalica, e quindi in grado di agire nel cervello sui meccanismi che portano all'insorgenza di queste malattie; e terzo, il blu di metilene, ha una tossicità limitata per gli essere umani e gli animali.

Il blu di metilene è oggi considerato un membro di una nuova classe di inibitori del processo di oligomerizzazione e/o fibrillazione delle proteine coinvolte nelle malattie neurodegenerative. L'MB è utilizzata in campo medico da più di 120 anni, per diversi scopi (Schirmer et al., 2011). Recentemente, l'MB sta riscuotendo molto successo grazie agli incoraggianti risultati ottenuti in una fase clinica II in cui questa molecola è stata testata su pazienti affetti di Alzheimer (Gura, 2008). Dopo sei mesi di somministrazione, i pazienti hanno mostrato un netto miglioramento delle funzioni cognitive. L'MB si è dimostrato efficace anche su altre proteine amiloidogeniche, come per esempio, nella formazione dei filamenti tau e nella degradazione delle poliglutammine (Van Bebber et al., 2010). Inoltre, MB agisce sulla deposizione della proteina TAR DNA (TDP-43), la quale ha una elevata tendenza ad aggregare (Yamashita et al., 2009). Questi risultati inducono a pensare che l'MB può avere proprietà anti-aggreganti che lo rendono adatto ad agire su tutte le proteine coinvolte nelle amiloidosi. Nonostante ciò, fino ad ora, non ci sono lavori in cui l'MB sia stato testato sui meccanismi di conversione della proteina prionica.

Nella ricerca delle specie tossiche che portano alla morte neuronale nelle amiloidosi cerebrali, ci sono evidenze sperimentali che dimostrano la tossicità degli aggregati solubili prefibrillari oltre che delle fibrille insolubili (Stefani et al., 2003). Per la proteina prionica, è stato visto che gli oligomeri sono neurotossici sia *in vitro*, nelle colture primarie neuronali, sia *in vivo* dopo iniezione subcorticale (Simoneau et al., 2007). Su queste basi, nel presente lavoro si è valutato per la prima volta l'azione inibitoria del blu di metilene sia sui processi di oligomerizzazione che di fibrillazione della proteina prionica, *in vitro*, mediante l'utilizzo di varie metodologie, come la fluorescenza, la risonanza plasmonica di superficie (SPR), la calorimetria differenziale a scansione, la risonanza magnetica nucleare, light scattering statico, la microscopia elettronica a trasmissione. I risultati ottenuti dimostrano che l'MB è in grado di rallentare la formazione degli oligomeri della PrP, ed inoltre di ridurre la quantità di oligomeri che si formano. Inoltre, MB inibisce completamente la formazione delle fibrille amiloidi della PrP. In definitiva, i risultati ottenuti pongono le

basi per la valutazione del blu di metilene per test in modelli animali, come successivo passo verso un possibile utilizzo in fase clinica.

La proteina prionica e gli aptameri del DNA e RNA. L'interazione tra la proteina prionica e gli acidi nucleici (NA) è sempre stata una tematica di dibattito nel campo del prione, da quando la "*protein only hypothesis*" ha portato ad un nuovo paradigma nella biologia. La proteina prionica è in grado di formare complessi con gli acidi nucleici per cui una nuova ed interessante linea di ricerca riguarda lo studio dell'interazione della PrP con piccole sequenze di DNA ed RNA (aptameri). Tali aptameri hanno una elevata affinità per la PrP e, alcuni di essi, sono in grado di discriminare tra le due forme della proteina, i. e., quella cellulare e quella patologica. Ciò trova riscontro nell'ambito della diagnostica delle malattie prioniche. Infatti, questo campo, nonostante gli innumerevoli sforzi compiuti, è ancora privo di valide strategie che permettano la diagnosi precoce di queste malattie, sia negli esseri umani sia negli animali. Lo studio dell'interazione della proteina prionica con queste piccole sequenze nucleotidiche ha permesso anche di indagare sul significato di queste interazioni a livello fisiologico.

Nel tentativo di cercare delle caratteristiche comuni tra gli aptameri di DNA e RNA preposti ad interagire con la proteina prionica e finora studiati, ne sono emerse due riguardanti sia la sequenza degli acidi nucleici, sia la struttura che questi aptameri adottano in soluzione. In particolare, molte delle sequenze sintetizzate, e che hanno dimostrato un'elevata affinità per la proteina prionica, presentano triplette contigue di guanine nella sequenza (Mercey et al., 2006). La presenza di guanine favorisce la formazione delle quadruple eliche o G-quadruplex. Le quadruple eliche di DNA/RNA sono strutture gerarchiche composte da due o più tetradi di guanine (G-tetradi) coplanari. Molti lavori indicano che questa strutturazione è indispensabile per l'interazione con la PrP (Gatto et al., 2009).

In un precedente lavoro, mediante la tecnica SELEX, un metodo di selezione e sintesi di acidi nucleici in grado di interagire con uno specifico target, sono stati isolati una serie di RNA capaci di legare in modo specifico la proteina prionica bovina (Murakami et al., 2008). Questi aptameri RNA presentano un *core* di sequenza (GGA)₄ e si ripiegano in una struttura a quadrupla elica. Gli autori hanno pertanto isolato questo core costituito da quattro ripetizioni GGA, dimostrando che questa sequenza minima è sufficiente per mantenere un'elevata affinità verso la PrP.

Sulla base di questi risultati, per questo lavoro sono stati presi in considerazione gli aptameri DNA ed RNA della stessa sequenza minima studiati da Murakami, *et al.*, (GGAGGAGGAGGA), di cui si riferisce più semplicemente come D12 e R12. Anche queste sequenze sono in grado di adottare una struttura G-quadruplex, in presenza di ioni K⁺, ed inoltre formano un dimero grazie alle interazioni di stacking che si stabiliscono tra le G-tetradi di ogni monomero (Mashima et al., 2009). Durante questo progetto di dottorato è stato condotto uno studio cinetico e termodinamico completo relativo all'interazione tra la proteina prionica e gli aptameri, D12 e R12, mediante l'uso dell'SPR e della calorimetria isoterma a titolazione. Questo studio ha permesso di ottenere ulteriori informazioni riguardo le forze che guidano questa interazione e le energie connesse. Inoltre, utilizzando diversi domini della PrP (sia la PrP (23-234) intera, sia la proteina troncata (103-234)), è stato possibile indagare sui siti di legame della proteina prionica. I risultati ottenuti chiaramente dimostrano che: i) le forze coinvolte nell'interazione della PrP con il D12 e l'R12 sono diverse; ii)

l'interazione tra la PrP intera e l'R12 avviene mediante la formazione di un complesso in cui una molecola di PrP interagisce con un dimerico R12; iii) l'interazione tra la proteina troncata e gli aptameri avviene mediante la formazione di un complesso con stechiometria diversa rispetto a quella ottenuta con la proteina intera; iv) l'interazione della PrP con questi aptameri coinvolge entrambi i domini della proteina, sia l'N-terminale (in cui sono presenti due siti di legame per gli acidi nucleici), sia il dominio strutturato C-terminale (in cui è presente un terzo sito di legame). Infine, mediante dicroismo circolare (CD), sono state studiate anche le variazioni strutturali che avvengono in seguito alla formazione del complesso PrP-aptamero. L'interazione provoca variazioni strutturali nella proteina, indipendentemente dall'aptamero con cui interagisce, mentre è stata osservata una variazione strutturale solo dell'R12, in seguito alla formazione del complesso.

Proteina prionica e Aldolasi C. Sebbene molti studi siano stati condotti allo scopo di comprendere il ruolo fisiologico della proteina prionica nelle cellule, la sua funzione biologica rimane tuttora un mistero. Questi studi sono stati principalmente rivolti alla ricerca di possibili interattori biologici che potrebbero chiarire alcuni dei processi cellulari in cui è coinvolta la PrP. Infatti, lo studio dell'interazione relativa ad una specifica proteina può delucidare non solo le funzioni della proteina considerata, ma anche dei suoi rispettivi partner. Strom, *et al.* (Strom et al., 2006), hanno individuato per la prima volta, mediante tecniche di proteomica, l'interazione tra la PrP e l'enzima aldolasi C (AldoC), una delle tre isoforme della famiglia delle aldolasi, localizzata principalmente nel cervello. L'aldolasi, un enzima della via glicolitica, catalizza la scissione aldolica reversibile del fruttosio-1,6-bis-fosfato e del fruttosio-1-fosfato a diidrossiacetone fosfato e gliceraldeide-3-fosfato o gliceraldeide, rispettivamente. Questo enzima, nei vertebrati, può essere presente in tre isoforme diverse: aldolasi A, B e C le quali hanno una distribuzione differente nei tessuti. L'AldoC è localizzata principalmente nelle cellule Purkinje e in altre cellule neuronali, non presenta varianti naturali e ha proprietà catalitiche intermedie tra le isoforme A e B (Paoletta et al., 1990).

In particolare, l'interazione della proteina prionica con l'aldolasi C è stata collegata alla perdita delle cellule Purkinje nel cervello di topi PrP^{0/0}. Infatti, l'aldolasi C è espressa in queste cellule, e l'interazione con la proteina prionica potrebbe essere necessaria per la loro sopravvivenza (Strom et al., 2006). Questa interazione è di particolare interesse poiché rafforza l'esistenza di una correlazione fisiologica tra la PrP e le aldolasi. Infatti, recenti lavori riportano un aumento dell'espressione di molte proteine glicolitiche, tra cui l'aldolasi A e C, in pazienti affetti della malattia di Creutzfeldt-Jakob ed inoltre, un aumento dei livelli del trascritto dell'aldolasi C mRNA (Dandoy-Dron et al., 2000; Gawinecka et al., 2010).

Mentre per l'aldolasi A e B si conosce in dettaglio il ruolo biologico nella glicolisi e nella gluconeogenesi, il ruolo fisiologico dell'aldolasi C nel cervello è molto dibattuto. Inoltre, non sono stati ancora riportati dati riguardanti la forza di interazione tra la PrP e l'AldoC, per cui l'obiettivo di questo lavoro di tesi è stato quello di caratterizzare l'AldoC, dal punto di vista biofisico utilizzando varie tecniche come il CD, la cromatografia ad esclusione molecolare e light scattering dinamico, e successivamente, di effettuare una dettagliata analisi termodinamica e cinetica della formazione del complesso PrP-AldoC mediante SPR. Lo studio di interazione è stato esteso anche alle altre isoforme, A e B, le quali hanno una struttura tridimensionale

molto simile all'aldolasi C ed hanno contribuito a delineare il tipo di interazione esistente tra la proteina prionica e questo enzima.

I risultati ottenuti da questo studio mostrano per la prima volta una caratteristica strutturale della proteina prionica che può contribuire a delucidare un possibile coinvolgimento della PrP nella regolazione delle proteine glicolitiche, e quindi nella glicolisi. Dai risultati ottenuti si evince che la proteina prionica interagisce con tutte le isoforme dell'aldolasi, con comparabile affinità, ed in particolare, l'interazione avviene sul dominio C-terminale della PrP. Su queste basi è possibile presumere che l'interazione sia basata su un riconoscimento strutturale tra la PrP e le tre aldolasi che adottano la stessa struttura tridimensionale.

Summary

A family of rare but all fatal neurodegenerative diseases which affect not only humans but also various animal species is related to the prion protein (PrP). The unique feature of these diseases is that, in addition to sporadic and inherited forms, they may be acquired by transmission of an infectious agent, which is represented by a misfolded form of prion protein, called PrP^{Sc}. Despite great efforts in the prion field, many questions remain unresolved related to the pathogenic mechanisms underlying prion diseases. The understanding of the mechanisms that lead to oligomerization and aggregation of PrP is necessary to find effective therapeutic strategies to antagonize prionopathies. In addition to the role of PrP on prionopathies, the physiological function of this protein in the cell is still a mystery. Many biological roles have been assigned to PrP, leading to presume that this protein can act in multicellular process, interacting with many biological macromolecules.

Taking in consideration the above main issues on prion field, this thesis work was focused on the study of the interaction between PrP and three different molecules: a heterocyclic aromatic molecule, methylene blue (MB); small DNA and RNA aptamers with a sequence (GGA)₄; and a glycolytic enzyme, Aldolase C. These molecules were chosen for different aims, in order to obtain further information about: i) the possibility to use a compound, such as MB, for therapy against prionopathies; ii) the affinity of the interaction between PrP and DNA and RNA aptamers with specific features, that could be used for diagnosis of prion diseases and could give information about the biological meaning of these interactions; and finally iii) a possible physiological function of PrP regulated by the interaction with aldolases.

In searching for a compound that could interfere with the PrP^C->PrP^{Sc} conversion, and be potentially used as drug against prion diseases, we chose methylene blue for its many properties: first, MB fulfills the safety features required for drugs delivery to humans and animals, and secondly, it is able to cross the blood brain barrier and, thus, suitable to target the toxic species formed in the brain, leading to prion diseases. In this thesis work, MB was tested to evaluate its potential inhibition action on both oligomerization and fibrillization processes that are thought to be on the pathway to the PrP disease occurrence. To this aim, several methodologies were used, such as fluorescence, surface plasmon resonance (SPR), nuclear magnetic resonance, differential scanning calorimetry, static light scattering and transmission electron microscopy. This work is the first that shows the effective action of MB on the PrP conversion *in vitro*. We demonstrate that MB can slow down the formation of PrP oligomers and limit the amount of oligomers. Its mechanism of action seems to be dependent on the oligomerization pathway of PrP. Finally we demonstrate that MB is able to completely suppress the formation of PrP fibrils. As a consequence, we believe that our findings deserve the evaluation of MB for *in vivo* studies and preclinical testing for prion disease.

The nucleic acids (NA) correlation with prion protein has ever been an issue of debate since the “protein only” hypothesis brought a new biological paradigm. The nucleic acids DNA and RNA form an interesting group of PrP molecular partners, and although the biological meaning of these interactions is not fully clear, several evidences suggest that NAs could have a relevant role for prion physiology and

pathology. Small DNA and RNA aptamers have shown to interact with PrP with high affinity. In an attempt to find a common shared sequence among the aptamers studied, it was found that some of them contain contiguous GG, and moreover, they can adopt a quadruplex structure. On this basis, we have studied the interaction of PrP with two reported DNA and RNA aptamers of sequence (GGAGGAGGAGGA), called D12 and R12. These aptamers, that fold in a G-quadruplex structure and are dimers, have shown a specific interaction with the native form of PrP. In this thesis work, a complete thermodynamic and kinetic investigation was performed using SPR, isothermal titration calorimetry and circular dichroism, in order to gain further information about the forces that drive this interaction. Using various PrP domains, it was possible to investigate also the nucleic acids-binding regions of PrP. The results here obtained demonstrate that the interaction between the full-length PrP and both D12 and R12 is driven by different types of forces. Moreover, the binding between full-length PrP and R12 occurs through the formation of a complex in which one molecule of PrP interacts with one R12 dimer. Differently, both aptamers bind to a deleted PrP form with a diverse stoichiometry. Finally, three putative binding sites on PrP are presumably involved in the interaction with these aptamers. This study has also allowed to evaluate the conformational changes induced by the PrP-nucleic acids complex formation, highlighting that PrP undergoes structural changes upon D12 and R12 interaction, whereas structural variations were also observed for R12, but not for D12. The binding study of DNA and RNA aptamers is an useful tool for the development of diagnostic strategies, since aptamers can be used to concentrate PrP from biological fluids to remove normal prions from a sample, and consequently enrich PrP^{Sc}.

The lack of a deep understanding of PrP role in the complex machinery of living cells has led to an intensive study of the biological prion partners. In fact, PrP has a considerable number of interactors. One of these is the glycolytic enzyme Aldolase C, belonging to the fructose-bisphosphate aldolase family and mainly expressed in the brain. In our work, taking into account that, so far, no data regarding the binding strength of PrP-AldoC interaction have been reported, a detailed thermodynamic and kinetic analysis of the binding of PrP to AldoC by SPR was conducted. Our interaction study was extended to the other two aldolase isoenzymes, aldolase A and B, that share a high sequence identity, to investigate whether the binding was sequence specific or not. Our results showed that all three aldolases interact with PrP with a binding constant within the micromolar range. Moreover, using various PrP domains, we identify the C-terminal domain of prion protein as the binding region for aldolases. We surmise that the binding process between PrP and aldolase enzymes occurs through a 3D-structural recognition. Further research is required to determine the relationship between PrP^C and its biological ligands, how the absence of the interaction is compensated, and whether the loss-of-function of PrP and its interactors is related to prion diseases.

Ultimately, the interaction study conducted during the doctorate has brought a little contribution to different branches of the prion field, broadening, through several approaches, the knowledge of the energetics and the kinetics of the interaction of the prion protein with some biological interactors, such as aldolase C and nucleic acids. Moreover, we trust that the work on methylene blue will be taken in consideration for future studies and further development in prion diseases therapy.

Abbreviations

Δ PrP	Truncated protein (103-234)
Aa	Amino acid
A β	Amyloid β -peptide
AldoA	Aldolase A
AldoB	Aldolase B
AldoC	Aldolase C
bPrP	Bovine prion protein
bPrP- β	β isoform of bovine prion protein, oligomer
BBB	Blood brain barrier
BSE	Bovine spongiform encephalopathies
CD	Circular dichroism
CJD	Creutzfeldt-Jakob disease
CNS	Central nervous system
CM	Carboxymethylated dextran
DSC	Differential scanning calorimetry
Fru-1,6-P ₂	Fructose-1,6- (bis)phosphate
Fru-1-P	Fructose 1-phosphate
GSS	Gerstmann-Sträussler-Scheinker syndrome
HuPrP	Human prion protein
ITC	Isothermal titration calorimetry
MALS	Multi-angle light scattering
MB	Methylene blue
MoPrP	Mouse prion protein
NA	Nucleic acid
NMR	Nuclear magnetic resonance
OvPrP	Ovine prion protein
PAH	Phenylalanine hydroxylase
PKU	Phenylketonuria
PMCA	Protein misfolding cyclic amplification
PrP ^C	Cellular prion protein
PrP ^{Sc}	Scrapie prion protein
rPrP	Recombinant prion protein
SAXS	Small-angle X-ray scattering
SELEX	Systematic evolution of ligands by exponential enrichment
SLS	Static light scattering
SPR	Surface plasmon resonance
SEC	Size exclusion chromatography
TEM	Transmission electron microscopy
ThT	Thioflavin T
TSE	Transmissible spongiform encephalopathies
Wt	Wild-type

Chapter I Introduction

1.1 The main issue of the Prion Protein

Prion protein is currently associated with neurodegenerative disorders that affect animals and humans. PrP belongs to the class of misfolded proteins that cause diseases by conformational changes coupled to aggregation. Besides this general concept, PrP diseases are unique among the misfolding-caused pathologies because of its causative agent. Prion diseases, in addition to sporadic and inherited forms, may be acquired by transmission of an infectious agent. It is near-universal accepted that the infectious principle consists merely of protein and is capable of replicating and transmitting infections without the need for informational nucleic acids (Griffith, 1967; Prusiner, 1982; Prusiner, 1998). In fact, the origin of the word “prion” stems from the anagram of “proteinaceous infectious particle” resistant to inactivation by most procedures that modify nucleic acids, coined by Prusiner to describe such a unique pathogen (Prusiner, 1982).

Since prion diseases are characterized by their transmissibility, they are also termed transmissible spongiform encephalopathies. The number of human and animal diseases recognized as TSEs has increased steadily and now includes Creutzfeldt-Jakob disease, Gerstmann-Sträussler-Scheinker syndrome, fatal familial insomnia, and Kuru in humans, BSE in cattle, chronic wasting disease in deer and elk, and transmissible mink encephalopathy. BSE has been inadvertently transmitted to a variety of captive animals, causing feline spongiform encephalopathy and a plethora of diseases in zoo animals including kudus, nyalas, and greater cats.

The fact that prions could function as infectious agents despite the absence of a nucleic acid genome led to the formulation of the “protein only” or prion hypothesis. According to this theory, the infectious agent is a self-perpetuating conformer of PrP (Prusiner, 1982; Prusiner, 1998). In particular, there are two conformers of this protein: cellular PrP^{C} , which is the normal conformer, and scrapie PrP^{Sc} , which is the infectious conformer. PrP^{Sc} was predicted to replicate during infection by contacting specific regions on PrP^{C} to recruit this protein and convert it into PrP^{Sc} . Therefore, the conformational conversion of PrP^{C} into PrP^{Sc} is thought to be the fundamental molecular event underlying all prion diseases.

Although PrP^{C} and PrP^{Sc} appear to share the same primary structure, they differ profoundly in biochemical and biophysical properties (Stahl et al., 1993). Cellular PrP^{C} is monomeric, soluble in non-ionic detergents and proteinase-sensitive, whereas PrP^{Sc} forms large aggregates (and often appears as amyloid fibrils) which are insoluble in non-denaturing detergents and shows partial resistance to proteinase K (PK) digestion (Caughey et al., 2001; Collinge, 2001; Weissmann, 2004). Consistent with NMR structural data for recombinant prion protein, PrP^{C} isolated from normal brain is primarily α -helical, whereas low-resolution optical spectroscopic measurements reveal that PrP^{Sc} isolated from diseased brain contains mostly β -sheet structure (Pan et al., 1993; Riek et al., 1997). This suggests that the differences in biophysical properties between these two isoforms result from distinct protein conformations.

According to the current hypothesis, the replication of prions occurs by self-propagation of infectious PrP^{Sc} via impression of its own abnormal conformation on PrP^{C} , thereby generating additional molecules of PrP^{Sc} in an autocatalytic reaction. Two prevalent hypotheses exist to explain the molecular mechanism of prion propagation. The conversion reaction is thought to occur either by a template-assisted refolding mechanism, in which binding of PrP^{Sc} to PrP^{C} decreases the activation energy that separates the two states (Cohen, 1999), or via a nucleated polymerization process, in which PrP^{Sc} serves as a seed that recruits and stabilizes abnormal conformations of PrP, that are in dynamic equilibrium with PrP^{C} (Caughey, 2001). On the other side, familial prion diseases are presumed to arise because germline mutations in the *PrnP* gene favor conformational conversion of mutant PrP^{C} molecules into PrP^{Sc} , without the necessity for contact with exogenous prions. Finally, sporadic cases are thought to be due to spontaneous conversion of wild-type PrP^{C} molecules to the PrP^{Sc} state at a low frequency, or alternatively, to rare somatic mutations in the *PrnP* gene.

A great deal of evidence now supports the validity of the prion hypothesis. A strong proof of this hypothesis is that expression of PrP by the host is necessary for the propagation of the infectious agent and for the development of the disease. It has been convincingly shown that *Prn-p^{0/0}* mice, in which the prion protein gene has been inactivated, are resistant to prion infection and do not sustain replication of the infectious agent (Büeler et al., 1993). There is also compelling evidence that the sequence of PrP encoded by the host is a major determinant of the species-specificity, incubation time, and neuropathological characteristics of prion transmission (Westaway et al., 1987; Scott et al., 1989; Prusiner et al., 1990). Indeed, the existence of prion strains, that are associated to different incubation times and neuropathological profiles in a single host, was considered at the beginning as a significant argument against the prion hypothesis. Anyhow, recent evidences show that each strain may represent a distinct self-propagating conformation of PrP^{Sc} (Telling et al., 1996; Safar et al., 1998).

Another important result supporting the prion hypothesis came from the PMCA method, in which PrP^{Sc} can be amplified by incubating and sonicating PrP^{Sc} -containing brain homogenate, diluted in normal brain homogenate. Soto and coworkers amplified PrP^{Sc} derived from scrapie-infected hamsters indefinitely by using PMCA in serial dilutions. Amplification of PrP^{Sc} was accompanied by amplification of infectivity (Castilla et al., 2005). In a fascinating study, there were identified the minimal components (PrP^{C} , copurified lipids, and single-stranded polyanionic molecules) required for amplification of PrP^{Sc} , and they convincingly showed that prion infectivity can be generated *de novo* in brain homogenates derived from healthy hamsters using PMCA (Deleault et al., 2007). Inoculation of further healthy hamsters with the *de novo*-formed prions caused a transmissible prion disease. This study might be regarded as the final proof of the prion hypothesis.

Despite great efforts in the prion field, many questions remain unresolved related to the pathogenic mechanisms underlying prion diseases. In fact, prion hypothesis does not explain the neuronal death observed in prion-affected brains, thus, it is still unclear if the neuronal damage is caused by a loss of the normal function of PrP^{C} or by acquisition of a toxic property of PrP^{Sc} . Moreover, the evidence that neuropathology can develop in the apparent absence of PrP^{Sc} , and that PrP^{Sc} can

accumulate without causing clinical symptoms, argues that PrP^{Sc} itself might not be highly neurotoxic and that molecules other than PrP^{Sc} could be responsible for prion-induced neurodegeneration (Lasmézas et al., 1997; Manson et al., 1999; Flechsig et al., 2000).

Prions have assumed much wider relevance in understanding other neurodegenerative disorders since prionopathies are often associated with the deposition of amyloid-like fibrils similar to those observed in other amyloidogenic diseases as Alzheimer's, Huntington's and Parkinson's diseases (Caughey et al., 2003; Chiti et al., 2006). Moreover, other studies are moving toward the hypothesis that prion-like transmission could be a common property of all amyloid disorders (Walker et al., 2002).

Finally, the most newly fascinating speculation comes from the similarities between prion propagation in mammals and fungi, suggesting that prions should no longer be considered as a disease-causing biological anomaly but should be thought as a novel regulator of cell phenotype (Tuite et al., 2010).

1.2 Prion protein: a structural and functional overview

Structural features of prion protein. Cellular prion protein is mostly a plasma membrane-anchored extracellular glycoprotein. This protein is encoded by a single exon as a polypeptide chain of 250 to 260 amino acids, depending on the species, containing at the both termini signal sequences of ca. 22 aa each (Oesch et al., 1985). In the mature form, through post-translational modifications, the N-terminal signal peptide (ER SP) is removed during entry into the lumen of the endoplasmic reticulum (ER), whereas the C-terminal signal (GPI SP) is cleaved off, upon attachment of a glycosyl phosphatidylinositol (GPI) moiety to Ser230 (Basler et al., 1986; Stahl et al., 1987; Turk et al., 1988). Additionally, inside the ER, PrP^C may be variably glycosylated at two asparagine residues (N181 and N197) giving rise to di-, mono- and un-glycosylated species (Haraguchi et al., 1989).

PrP contains a long NH₂-proximal flexible sequence, which is followed by a globular COOH-proximal domain. The structurally less-defined N-terminus consists of residues 23–124 and contains a stretch of several octapeptide repeats (OR), flanked by two positively charged clusters, CC1 (aa 23–27) and CC2 (aa 95–110) (Fig. 1.1A). Both N-terminus and C-terminus of PrP are linked by a hydrophobic stretch of amino acids known as the HC region (aa 111–134). Although NMR experiments showed a flexible disorder of the N-terminal region at pH 4.5 without any detectable secondary structure (Donne et al., 1997), at pH 6.2, the HGGGW and GWGQ segments of the octarepeats were shown to adopt a loop and a β -turn-like conformation respectively (Zahn, 2003). Moreover, each octarepeat has displayed a particular affinity for Cu²⁺ (Millhauser, 2004) and weaker binding with other divalent cations such as Zn²⁺, Fe²⁺, Ni²⁺ and Mn²⁺ (Choi et al., 2006).

In contrast, the C-terminus of PrP is structured and presents a globular fold of three α -helices (H1, H2 and H3) and a short, double-stranded, antiparallel β -sheet (S1, S2) (Wüthrich et al., 2001). A disulfide bridge between Cys179 and Cys214 (human

sequence numbering) links H2 and H3 (Fig. I.1B). In particular, the high degree of sequence identity (generally above 90%) among the known mammalian prion protein sequences implies an identical three-dimensional fold of the C-terminal domain. In Figure I.2 the sequence alignment of three PrP species (MoPrP, HuPrP and OvPrP) is shown.

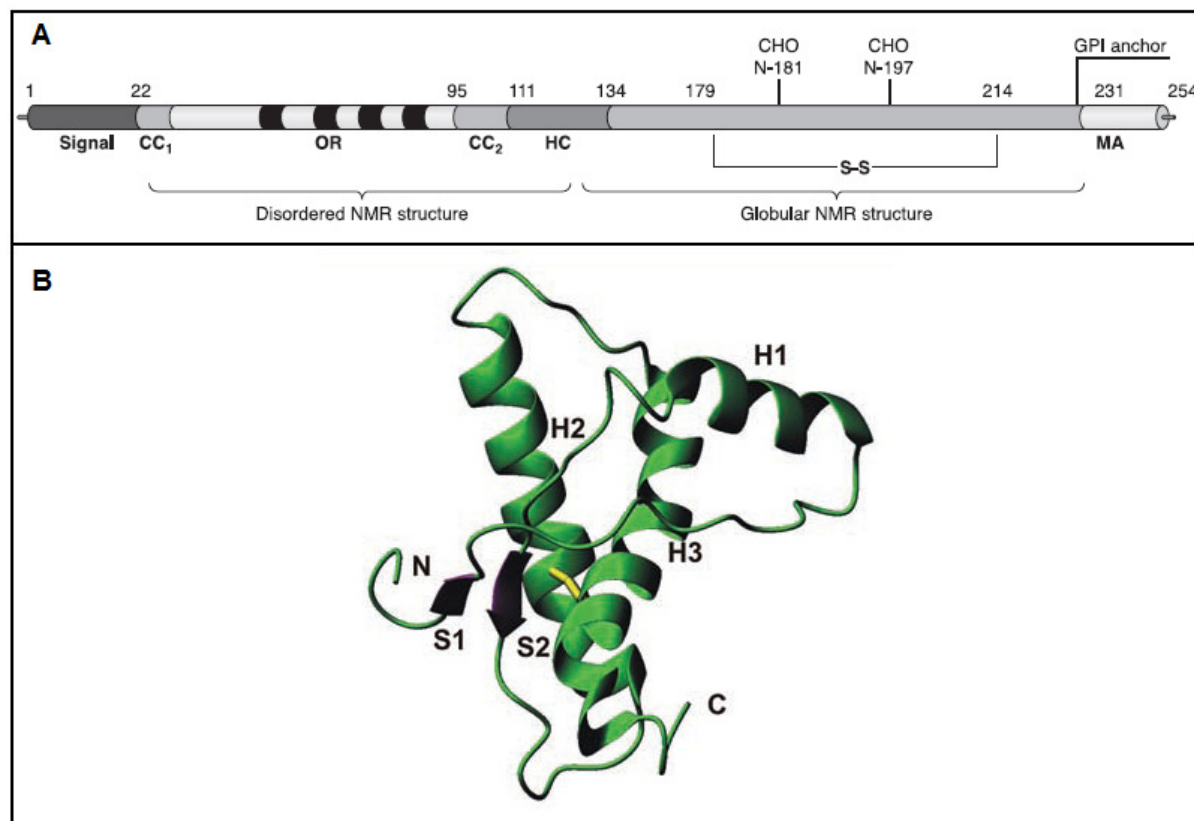


Figure I.1 Overview of the sequence and overall fold of PrP. A) Outline of the primary structure of the PrP^C. CC1 and CC2 define the charged clusters. OR indicates the four octapeptide repeats. HC defines the hydrophobic core. MA denotes the membrane anchor region. S-S indicates the single disulfide bridge, and the glycosylation sites are designated as CHO. The numbers describe the position of the respective amino acids. B) Ribbon representation of the C-terminal domain of mouse PrP. The secondary structure elements and the N- and C-termini are labelled. The sulphur bridge is indicated in yellow.

Since the first NMR structure of the C-terminal domain of mouse PrP, solved in 1996 (Riek et al., 1996), the number of PrP entries in the PDB database has increased continuously. Most of them were solved by NMR, having in solution either the full-length or truncated forms of PrP, while the X-ray structures are few and restricted to the C-terminal domains of the human, ovine and rabbit proteins. This could suggest an intrinsic tendency of these proteins to elude crystallization, presumably due to intrinsic heterogeneity or, more likely, to local flexibility (Pastore et al., 2007).

It is worth noting that all available PrP structures were expressed in simplified host organisms such as *E. coli*, leading to overexpressed recombinant exogenous proteins which is neither glycosylated nor GPI anchored. Since PrP is a glycoprotein anchored to the lipid membrane, some concern was put into demonstrating that recombinant PrP is a relevant model of the native PrP^C. A study on PrP^C extracted from healthy calf brain demonstrated that native bovine PrP exhibits the same

PrP. During zebrafish development, knockdown of either of the duplicated *PrnP* genes induces loss of cell adhesion and altered localization of epithelial-cadherin and FYN Tyr kinase, phenotypes that are suppressed by the expression of mouse PrP (Málaga-Trillo et al., 2009). In addition, in adult mice regulated proteolysis and expression of PrP on the neuronal cell surface are required for the maintenance of myelination through a non-cell autonomous route (Bremer et al., 2010). Together, these studies indicate that PrP might have a pleiotropic role *in vivo*, perhaps mediating its broad effects by affecting cell signalling pathways. Figure I.3 depicts some theoretical models of how PrP^C might influence cell signaling, endocytosis, and cell adhesion.

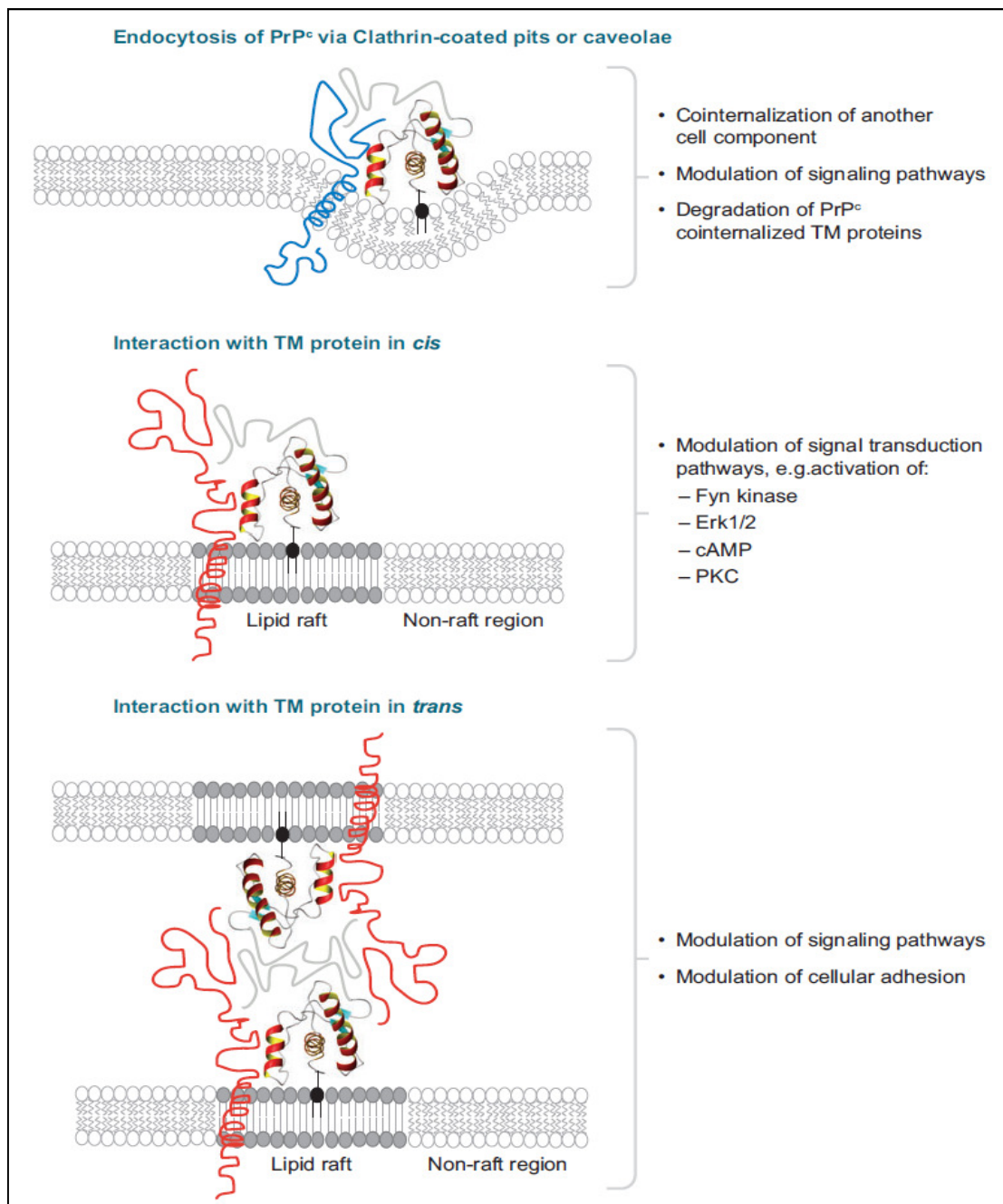


Figure I.3 Models of the possible ways by which PrP^C could exert its physiological function.

Endocytosis of PrP^C via clathrin-coated pits or caveolae may represent a mechanism for the downregulation of PrP^C on the cell surface. Alternatively, or additionally, endocytosis of PrP^C leads to cointernalization of another cell component, e.g., a proteinaceous interacting partner, thereby regulating the presence of the latter on the cell surface. This regulation could positively or negatively modulate the activity of signal transduction pathways, e.g., via inducing degradation of the cointernalized partner. Moreover, an interaction with a transmembrane protein may lead to modulation of signal transduction pathways in the cell carrying PrP^C on its cell surface and modulation of adhesion to adjacent cells (Aguzzi et al., 2008).

Perhaps PrP^C and PrP^{Sc} do not possess any intrinsic biological activity of their own, but modify the function of other proteins. GPI-anchored proteins must interact with transmembrane adaptors on the same cell or an adjacent cell to influence intracellular signal transduction pathway. This supposition has led to the search for PrP-interacting partners. In Table I.1 are summarized some of the PrP^C interaction partners identified thus far, such as membrane proteins (receptors, enzymes, Caveolin-1, Na-K-ATPase, and a potassium channel), cytoplasmic proteins (components of the cytoskeleton, heat-shock proteins, and adaptor proteins involved in signaling), and even the nuclear protein CBP70.

Table I.1 Molecules identified as interaction partners to PrP^C or PrP^{Sc}

Interaction partner	Subcellular localization	Binding Site	Function of interaction partner and references
Hsp60 and GoEL	Mitochondria	180-210	Chaperone (Edenhofer et al., 1996)
Laminin	Extracellular, basement membrane	Unknown	Signal transduction, cell adhesion, neuritogenesis (Graner et al., 2000)
Synapsin Ib	Synaptic vesicles	23–100 and 90–231	Synaptic vesicle formation, modulation of neurotransmitter release and in synaptogenesis (Spielhauer et al., 2001)
Grb2	Cytoplasm	23–100 and 90–231	Adaptor protein mediating signal transduction (Spielhauer et al., 2001)
N-CAM	Plasma membrane (transmembrane/ GPI-anchored)	141–176	Cell adhesion, signaling, etc. (Maness et al., 2007)
Caveolin-1	Caveolae, plasma membrane (transmembrane)	Unknown	Caveolae formation and endocytosis; cross-linking of PrP induces Fyn activation (Mouillet-Richard et al., 2000)
Fyn kinase	Cytoplasm, associated with cytosolic side of plasma membrane	Unknown	Signal transducer molecule (Mouillet-Richard et al., 2000)
β-dystroglycan	Plasma membrane (transmembrane, part of the dystroglycan complex)	Unknown	Transmembrane protein, binds extracellularly to α-dystroglycan and, intracellularly, to dystrophin (Keshet et al., 2000)
Dp71 (dystrophin)	Cytoplasmic face of plasma	Unknown	Cytoskeletal protein (Keshet et al., 2000)

	membrane (part of the dystroglycan complex)		
α-syntrophin	Cytoplasmic face of Membrane	Unknown	Adaptor protein, in sarcolemma and the neuromuscular junction (Keshet et al., 2000)
α-tubulin	Microtubules, cytoplasm	Unknown	Microtubule subunit (Keshet et al., 2000)
B-actin	Intracellular cytoskeleton protein	Unknown	Subunit of microfilaments of the cytoskeleton (Keshet et al., 2000)
BACE-1	Plasma membrane (transmembrane)	Unknown	APP processing (Parkin et al., 2007)
TREK-1	Plasma membrane (transmembrane)	128–230	Two-pore potassium channel protein (Azzalin et al., 2006)
Bcl-2	Cytoplasmic face of mitochondrial outer membrane, nuclear envelop, and ER	72–254	Inhibition of apoptosis (Kurschner et al., 1995)
Mouse amyloid precursor-like protein 1 (APLP1)	Plasma membrane (transmembrane)	Unknown	Neuronal survival and neurite outgrowth (Sakai et al., 2006)
αB-crystalline	Cytoplasm	Unknown	Small heat-shock protein, chaperone (Sun et al., 2005)
Clathrin heavy chain 1	Cytosolic face of coated vesicles and coated pits	Unknown	Involved in intracellular trafficking of receptors and endocytosis (Petrakis et al., 2006)
Na⁺/K⁺ ATPase α3	Plasma membrane	Unknown	Catalytic subunit of P-type ATPase, active transport of cations across cell membranes (Petrakis et al., 2006)
Vitronectin	Extracellular matrix glycoprotein	105–119	Axonal growth in the peripheral nervous system (Hajj et al., 2007)
CBP70	Nuclear and cytoplasmatic		Lectin (Rybner et al., 2002)
Glycosaminoglycans (GAG)	Connective tissues, covalently linked to proteins to form proteoglycans	23–35, 23–52, 53–93, 110–128	Various functions (Pan et al., 2002)
Aldolase C	Cytoplasm	Unknown	Enzymatic activity in the glycolytic pathway (Strom et al., 2006)
ApoE	Secreted	23–90 109–141	Main apolipoprotein of chylomicrons, involved in neurodegenerative diseases such as Alzheimer disease (Gao et al., 2006)
Plasminogen	Secreted	Unknown	Inactive zymogen form of plasmin, which participates in thrombolysis or extracellular matrix degradation (Ellis et al., 2002)

Unfortunately, the physiological relevance of most of the proposed interaction partners remains unconfirmed. Proteins that are not even localized to the outer leaflet of the cell membrane, where PrP^C is located and believed to exert its function, would at least require an additional interacting cell component, meaning that their interaction with PrP^C must be indirect (Aguzzi et al., 2008).

Another intensive field of research is the interaction of PrP with nucleic acids. The exact biochemical nature of the scrapie agent is still a matter of debate, and some studies revealed the presence of residual amounts of nonspecific nucleic acids in purified preparations of PrP infectious material. These findings have motivated the studies of prion protein's binding with nucleic acids (Kellings et al., 1994; Safar et al., 2005).

Many studies, in fact, have shown the more or less specifically interaction of PrP with various nucleic acids or nucleic acid-like molecules (Adler et al., 2003; Kocisko et al., 2006; Lima et al., 2006). In particular, the recently developed SELEX method has allowed to select both DNA (Takemura et al., 2006) and RNA aptamers (Weiss et al., 1997; Mercey et al., 2006) to specifically bind to PrP and/or PrP^{Sc}. Regarding the nucleic acid-binding site on PrP, some reports indicate the N-terminal half of the protein as a binding site of low specificity and high affinity primarily based on charge interaction, coinciding with the two lysine cluster (Rhie et al., 2003; Mercey et al., 2006). On the other hand, data from small angle X-ray scattering and NMR spectroscopy showed that both the globular and unstructured domains of PrP are involved in its interaction with nucleic acids (Lima et al., 2006).

The biological significance of PrP binding to nucleic acids is perhaps suggested by the modifications induced in both partners as a result of their interaction. Specific DNA sequences could reduce PrP^{Sc} accumulation (Proske et al., 2002; Rhie et al., 2003) or, in contrast, induce conversion of recombinant PrP to a soluble β -sheet isoform (Cordeiro et al., 2001). Reciprocally, PrP also modified the conformation of nucleic acid (Gabus et al., 2001).

The physiological meaning of the complexes PrP-NAs, certainly, depends upon the subcellular topology of PrP. If one takes into account only the location of PrP at the outer face of the cell membrane, the probability of encountering nucleic acids is low. On the other hand, both cytosolic and transmembrane forms of PrP are likely to interact with cellular nucleic acids.

1.3 The dark side of prion protein: PrP as a disease-causing agent

In the case of TSEs, a clear and irrefutable role for PrP in the appearance of phenotypic manifestation and spread of disease has been established. PrP is the major constituent of biochemically enriched preparations of the TSE agent (Prusiner, 1998), and mice devoid of *PrnP* gene cannot replicate the infectious agent and are resistant to TSEs (Aguzzi et al., 2008). In addition, depletion of PrP, after infection, extends incubation times and reverses both neuropathology and behavioral defects induced by the infection (Mallucci et al., 2007). These observations are consistent

with a main role of PrP in TSE aetiology. However, an important question remains: what is the molecular basis of prion replication?

1.3.1 Mechanisms of PrP conversion

Transgenic mouse studies have provided genetic (Prusiner et al., 1990) and biochemical (Meier et al., 2003) evidence that the conversion of PrP^C to PrP^{Sc} occurs through the formation of a PrP^C/PrP^{Sc} complex. However, such a complex has never been isolated to purity.

There are two models to explain the conformational conversion of PrP^C into PrP^{Sc}. The “template-directed refolding” hypothesis predicates an instructionist role for PrP^{Sc} on PrP^C. This model postulates an interaction between exogenously introduced PrP^{Sc} and endogenous PrP^C, which is induced to transform itself into further PrP^{Sc} (Fig. 1.4A). An important concept involved in this mechanism is that PrP^C is thermodynamically less stable than PrP^{Sc}, but spontaneous conversion is kinetically limited. Alternatively, the seeded nucleation hypothesis suggests that PrP^{Sc} exists in equilibrium with PrP^C. In a non-disease state, such an equilibrium would be heavily shifted toward the PrP^C conformation, such that only minute amounts of PrP^{Sc} would coexist with PrP^C. According to this “seeded nucleation” hypothesis, the infectious agent would consist of a highly ordered aggregate of PrP^{Sc} molecules and only if several monomeric PrP^{Sc} molecules are mounted into this ordered seed, further monomeric PrP^{Sc} can be recruited and eventually aggregate to amyloid. Therefore, monomeric PrP^{Sc} would be harmless, but it might be prone to incorporation into nascent PrP^{Sc} aggregates (Fig. 1.4B) (Aguzzi et al., 2004).

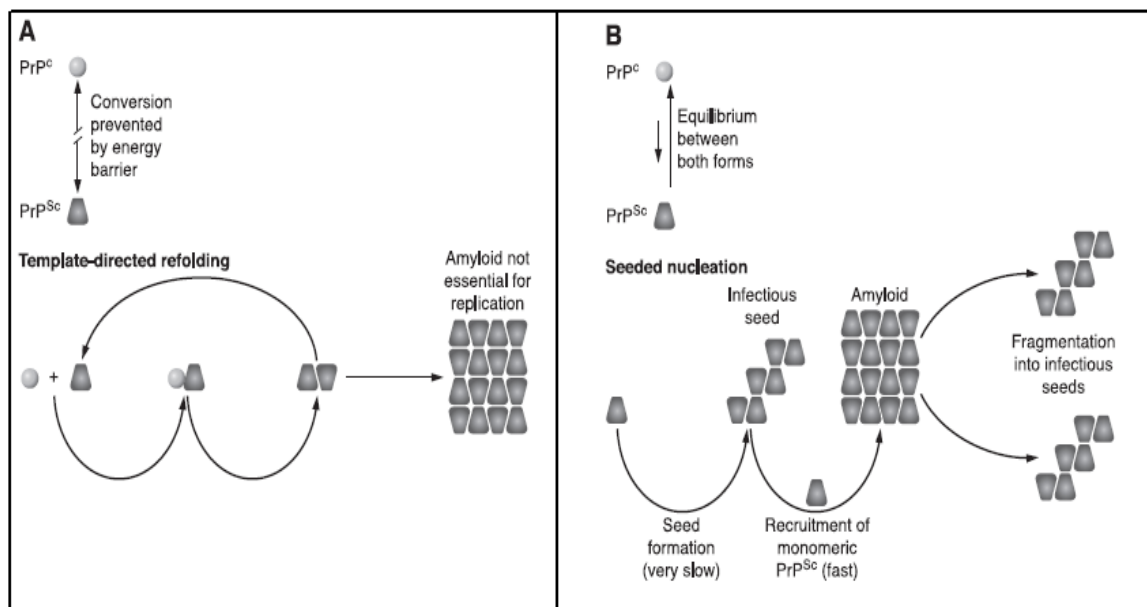


Figure 1.4 Models for the conformational conversion of PrP^C into PrP^{Sc}. A) The refolding or template assistance model. A high-energy barrier may prevent spontaneous conversion of PrP^C into PrP^{Sc}. B) The seeding or nucleation-polymerization model proposes that both PrP isoforms are in a reversible thermodynamic equilibrium. Fragmentation of PrP^{Sc} aggregates increases the number of nuclei, which can recruit further PrP^{Sc} and thus results in apparent replication of the agent.

In the seeding or nucleation-polymerization model, it is necessary to evoke a mechanism for generating new templates, since the seeded polymerization process

cannot account for the exponential increase in infectious titre, that is observed over the course of disease in mammals. Thus, in addition to the seeded-polymerization step, there must be ongoing polymer fragmentation to generate new templates, known as propagons (Masel et al., 1999) (Fig. 1.3B). These “propagons” or shorter fibrils, which may result from breakage of frangible structures, should be more infectious than longer fibrils (Silveira et al., 2005), an observation consistent with the fact that a larger number of free ends in a short fibril population leads to more rapid conversion of soluble cellular prion protein into misfolded fibrillar form (Aguzzi et al., 2009). Furthermore, in *in vitro* growth assays of many amyloid fibril systems, it has been noted that agitation significantly enhances the overall conversion rate of proteins into fibrillar forms (Kim et al., 2007), indicating that fibril breakage is an essential factor determining the rate of amyloid formation.

The polymer fragmentation mechanism that would follow the first step of PrP^{Sc} oligomer-growth is now well supported by experimental studies with yeast prions, in which the fragmentation of prion polymers is catalyzed by the molecular chaperone heat shock protein 104 (Hsp104), in conjunction with other co-chaperones (Haslberger et al., 2010). Analogously, there are indications that similar processes govern the growth of mammalian prions (Legname et al., 2004; Castilla et al., 2005) as well as non-prion-related amyloid fibrils (Dobson, 2003).

1.3.2 Intermediates in prion protein conversion: PrP polymerization

In the evolution of prion pathology, the conformational change of PrP is accompanied by an increase in β -sheet content and in the same way an increase of the amyloidogenic propensity of the PrP (Mckinley et al., 1983). The amyloid property of PrP^{Sc} implicates an important specificity that is the polymeric state of the pathological protein. Thus, the acquisition of amyloidic properties during PrP conversion underlines the importance of the polymerization process (i.e. acquisition of a quaternary structure) in the evolution of the pathology.

Many efforts have been made to characterize the quaternary structure of PrP^{Sc} to better understand the mechanism underlying PrP conversion, and to establish what is the toxic PrP form that ultimately leads to neuronal death. Indeed, while the PrP fibrillization conditions were widely studied previously (Swietnicki et al., 2000; Baskakov et al., 2002; Rezaei et al., 2005), only recently, amyloidogenic oligomeric structures have been associated with the manifested biological effects, highlighting the neurotoxic activity of recombinant PrP oligomers, *in vitro* and *in vivo* (Kazlauskaitė et al., 2005; Simoneau et al., 2007), in agreement with other studies on neurodegenerative diseases (Lashuel et al., 2002). A few years ago, Silveira *et al.* (Silveira et al., 2005) determined the smallest size of infectious PrP assemblage. This investigation revealed that 15 to 28 mer of PrP harbour the necessary information for the replication of the infectious agent whereas smaller (less than 5mer) and larger PrP oligomers show less or no infectivity. Thus, *in vitro* and *in vivo* independent studies converge on the key role of PrP oligomers.

It has been shown that the folding pathway of PrP differs depending on the species considered and the physico-chemical conditions used (Chakroun et al., 2010). There are several types of conditions that lead to the formation of either β -enriched PrP oligomers or PrP amyloid fibrils. The first condition used was a partial unfolding

induced by chaotropic agent as urea or Guanidine HCl at acidic pH (Bjorndahl et al., 2011). Further, formation of β -enriched oligomers was induced by heating and acidic pH or neutral pH without using other agents (Lu et al., 2002; Rezaei et al., 2002; Rezaei et al., 2005). The latter condition has the advantage of affecting exclusively the folding energetics of the protein, whereas either chaotropic agents or detergents may also impact the surrounding water molecules and/or participate to the newly formed structure as either cofactors or chemical chaperon (Rezaei, 2008).

With the assumption that oligomeric intermediates, having a peculiar structure, are the neurotoxic initiators in prion diseases, a consequent question arises: why these PrP forms are toxic to cells?. The conversion of a protein from its native state into an oligomeric form invariably generates a wide distribution of misfolded species, which expose an array of groups that are normally masked in globular proteins. The improper interactions between oligomers and cellular components, such as membranes, small metabolites, proteins, or other macromolecules, may conceivably lead to the malfunctioning of the cellular machinery. Depending on the cell type involved, the result could be impairment of axonal transport, oxidative stress, sequestration of essential proteins, or a combination of disparate factors, ultimately leading to apoptosis or other forms of cell death. For this reason, an optimal strategy used in the research of possible anti-prion agents, is to prevent aggregation or even production of the amyloidogenic protein before it can generate any potentially damaging intermediates.

1.3.3 The uncertain landscape of therapeutic strategies in prion diseases

The current therapeutic strategies for prion diseases are not fully satisfactory. Thus far, no vaccine, nor disease reversing therapeutic compounds nor strategies (cure) exist. The current therapeutic strategies are primarily aimed at preventing the $\text{PrP}^{\text{C}} \rightarrow \text{PrP}^{\text{Sc}}$ conversion. Indeed, different strategies can be applied in order to prevent the interaction of cellular PrP with the pathological isoform and so averting subsequent conversion.

Targeting PrP^{C} expression is one of the strategies that have been experimented to avoid the prion conversion, and is based on the following observations: i) PrP^{C} is required for susceptibility to prion disease (Brandner et al., 1996), and ii) a reversal of neuropathological and behavioral abnormalities has been observed in scrapie-inoculated mice when neuronal expression of PrP^{C} was eliminated, despite the continued presence of PrP^{Sc} deposits and accumulation of infectivity (Mallucci et al., 2003; Mallucci et al., 2007). Effective methods for reducing PrP^{C} expression in cell culture include the use of small interfering RNA (siRNA) to the *Prnp* gene (Tilly et al., 2003), and recently, a lentivirus vector, designed to express a short hairpin RNA (shRNA) had significant effect *in vitro* and in a chimeric mouse infected with scrapie (Pfeifer et al., 2006).

Another strategy takes into account that compatibility of PrP^{C} and PrP^{Sc} is necessary for efficient conversion of PrP^{C} by a particular PrP^{Sc} strain. Indeed, incompatibility can be a result of differences in prion protein between species (Horiuchi et al., 2000) or specific amino acid substitutions (Palmer et al., 1991). These studies indicate that incompatible PrP^{C} not only resists to conversion but is also capable of blocking the conversion of compatible sensitive PrP^{C} molecules. Alternatively, PrP^{Sc} may be

prevented from migrating to the central nervous system (CNS) or measures may be taken to increase clearance of PrP^{Sc} using branched polyamines or β -breaker peptides.

Finally, an impressive wealth of molecules has been considered as potential antiprion compounds capable to bind PrP^C and, thus, rendering the cellular form inaccessible or incompatible for conversion to PrP^{Sc}. Even if many of these compounds were shown to be able to slow down the progression of prion disease *in vitro* or in rodent models, few have made their way into human trials or case reports, including early or prophylactic treatments and later stage therapies. The unsatisfactory conclusion is that none of these therapeutic lead compounds has yet proven their usefulness in clinical settings, and some have conspicuously failed.

A non-exhaustive list includes compounds as diverse as Congo red (Caughey et al., 1992), amphotericin B, anthracyclins (Tagliavini et al., 1997), sulfated polyanions (Caughey et al., 1993), porphyrins and phthalocyanines (Caughey et al., 1998), lysosomotropic factors as quinacrine (Barret et al., 2003), acridines and phenothiazines (Korth et al., 2001), the spice curcumin (Caughey et al., 2003), and the single-stranded phosphorothioated analogs of natural nucleic acids (Kocisko et al., 2006).

Additional hurdles may lie in the identification of compounds that have specific features to act in the CNS. They must be effective *in vivo*, with a low toxicity for humans and animals, must have a well-known pharmacological behavior and a safety profile to allow for applicability in the clinical phase of disease. Finally, but not less important, they must be able to cross the blood-brain barrier. This is a feature that has been underestimated in the past, in finding suitable anti-prion agents. In fact, some of the compounds that showed good results on the inhibition of prion conversion *in vitro*, inevitably failed *in vivo*, for the simple reason that they are not able to pass the blood-brain barrier.

However, many compounds show some prophylactic or early treatment effect in TSE-infected animals. Therefore, there are hopes that future advances on drug-research could bring better clinical results.

1.4 Thesis aims

The main protagonist of this work is the prion protein, a complex entity, involved in fatal neurodegenerative disorders. Although prion field has undergone excellent progress in recent years, many questions still need to find an answer, starting from the physiological role of this protein in the cell, to the actual propagation mechanism of the infectious disease and the possible diagnosis and cures for prionopathies.

This thesis work was focused on the study of the interaction between PrP and three different molecules: a heterocyclic aromatic molecule, methylene blue; small DNA and RNA aptamers with a sequence (GGA)₄; and a glycolytic enzyme, Aldolase C. These molecules were chosen for different aims, in order to obtain further information about: i) the possibility to use a compound, such as MB, for therapy against

prionopathies; ii) the affinity of the interaction between PrP and DNA and RNA aptamers with specific features, that could be used for diagnosis of prion diseases and could clarify the biological meaning of these interactions; and finally iii) a possible physiological function of PrP regulated by the interaction with aldolases.

In Chapter II, the study of the effects of methylene blue on both oligomerization and fibrillization process of prion protein is addressed. A widely explored field in prion is the evaluation, primarily *in vitro*, of compounds that can interfere with the PrP^C → PrP^{Sc} conversion, and be potentially used as drugs to avoid, suppress or ameliorate the clinical phase of prion diseases. To this purpose, we have not added a new molecule to the large ensemble of existing compounds and alleged anti-prion agent. Conversely, we sought a known molecule that, firstly, fulfilled safety features to act in humans and animals, and secondly, can actually be considered for future *in vivo* tests. Methylene blue has satisfactorily answered all the requests that we demanded for an anti-prion agent. Therefore, in this work, methylene blue was tested to evaluate its potential inhibition action on both oligomerization and fibrillization processes that are thought to be on the pathway forward the disease occurrence. The results obtained could be taken in consideration for future test of MB on animal models.

In Chapter III, the specific interaction of two DNA and RNA sequence aptamers, (GGAGGAGGAGGA), with prion protein is described. Small DNA and RNA aptamers form an interesting group, that is gaining increasing attention as tools to investigate the biological meaning of the interactions of PrP with nucleic acids and to develop new diagnostic assays for prion diseases. In this thesis work, a complete thermodynamic and kinetic investigation was performed to gain further information about the forces that drive this interaction. Moreover, using various PrP domains, it was possible to investigate also the putative nucleic acids-binding sites of PrP. This study has allowed also to evaluate the effects of the PrP-nucleic acids complexes formation on both complex partners.

Finally, one of the most intriguing puzzles of prion biology is the physiological role of prion protein in the cell. The lack of a deep understanding of PrP role in the complex machinery of living cells has led to an intensive study of the biological prion partners that might help to fill the gap still present in this field. In fact, the prion protein has a considerable number of interactors that can give rise to simple complexes or supramolecular systems, in which PrP interacts with more proteins. One of these interactors is the glycolytic enzyme Aldolase C, belonging to the fructose-bisphosphate aldolase family. Therefore, we carried out a detailed thermodynamic and kinetic analysis of the binding of PrP to AldoC, that is presented in Chapter IV. Our interaction study was extended to the other two aldolase isoenzymes, aldolase A and B, to investigate whether the binding was sequence specific or not. This study has afforded to add a gusset over the mysterious backdrop of the biological interactions of prion protein.

Chapter II Prion Protein and Methylene Blue

2.1 Methylene Blue and its role in the therapeutic world

In the field of prion disease therapies, many classes of compounds have been evaluated *in vitro* and in animal models to prevent and treat these diseases in animals and humans. Of the many compounds studied, a few have made their way into human trials or case reports, and the effectiveness of treatment administered at the onset of clinical symptoms, or at late stage, is low. The development of successful treatments has been hindered by the incomplete understanding of prion disease pathogenesis. Indeed, it is not known how PrP^{Sc} formation and/or accumulation leads to pathology. Large aggregates of PrP^{Sc} are neither necessary nor sufficient to cause clinical disease in all cases, and it may be that soluble oligomeric forms of prion protein (PrP) are more relevant to mechanisms of infection, conversion and toxicity (Silveira et al., 2005).

The research of prion disease treatment moves on two different tracks. One is referred to the early treatment regimes, that include various prophylactic compounds and immunotherapies, and it has sought efficacy through neutralization of infectious sources, blockade of infection *via* the most common peripheral routes, and/or blockade of neuroinvasion. This research line has encountered many difficulties due to the lack of early diagnosis methods for prionopathies. Therapies targeting later disease, that are initiated after the appearance of clinical signs, are included in the second track of research. These therapies would involve some combination of inhibiting pathogenic PrP formation, destabilizing or enhancing clearance of existing pathogenic PrP^{Sc}, blocking neurotoxic effects of the infection, and/or promoting the recovery of lost functions in the CNS.

Most of the studies searching for anti-aggregation compounds, not only for prion diseases, but also for all the pathologies that involve formation and deposition of amyloid aggregates in the brain, have been conducted *in vitro*. Although *in vivo* tests provide the most rigorous evaluations of anti-TSE treatments, the low occurrence of this type of test is due to their slowness, high cost, and impracticability for screening purposes. On the contrary, a great variety of relatively high throughput, low cost, cell culture models and noncellular *in vitro* assays have enabled the identification of a number of different classes of anti-prion compounds, that then have shown efficacy in animal models. Moreover, *in vitro* assays have allowed investigation of the mechanisms of prion inhibition (Sim et al., 2009).

Some screened and tested *in vitro* class of compounds, aimed to inhibit the PrP^C → PrP^{Sc} conversion, are polyanions, sulphonated dyes as congo red and curcumin, cyclic tetrapyrroles, lysosomotropic factors as quinacrine, acridines and phenothiazines, peptide aptamers and β-sheet breakers. Many inhibitors prevent conversion by directly binding to PrP^C (Caspi et al., 1998; Kuwata et al., 2007) or to PrP^{Sc} (Nicolla et al., 2010) and, thus, blocking interactions between them. Others affect conversion by interfering with intermediates formed during the PrP conversion, or by altering PrP^C expression and distribution (Caughey et al., 2006).

Recent investigations are increasingly devoted to seek anti-aggregation compounds that may help to treat a whole set of independent proteinopathies. This new approach is grounded on the common structure of amyloids. In this scenario, a phenothiazine derivative, methylene blue, has shown to possess anti-aggregation activity for many misfolded-proteins associated to amyloidogenic diseases. Indeed, it was reported that MB is able to inhibit the beta amyloid A β_{42} oligomerization (Necula et al., 2007), as well as tau filament formation, *in vitro* (Taniguchi et al., 2005; Van Bebber et al., 2010). Moreover, MB prevents deposition of the TAR DNA-binding protein of 43 kDa (TDP-43) in a cell culture model based on ectopic overexpression of TDP-43 variants, lacking their nuclear localization signals and thus facilitating cytoplasmic accumulation and aggregation (Yamashita et al., 2009). Finally, MB has recently attracted an increasing attention, since the outcome of a phase II clinical trial of MB treatment for AD patients has shown encouraging results as significant improvement of cognitive functions (Oz et al., 2009).

Although other molecules, belonging to the phenothiazine class, have been evaluated, *in vitro*, in order to test their inhibition action on prion protein (Korth et al., 2001; Barret et al., 2003), MB was almost neglected for investigations on prion diseases. Nevertheless, MB gathers several properties required for drug candidates expected to act in the central nervous system: it has a low toxicity in rats and humans (Riha et al., 2005), is able to cross the blood-brain barrier (Peter et al., 2000) and is approved for use in humans (Di Santo et al., 1972).

MB is a tricyclic phenothiazine drug (Wainwright et al., 2005). Under physiological conditions it is a blue cation which undergoes a catalytic redox cycle: MB is reduced by nicotinamide adenine dinucleotide phosphate (NADPH) or thioredoxin to give leucoMB, an uncharged colorless compound. LeucoMB is then spontaneously reoxidized by O₂ to MB (Fig. II.1). The typical redoxcycling of MB *in vivo* can be illustrated *in vitro* using the famous blue bottle experiment: MB is visibly reduced by glucose to give leucoMB and then, by opening the lid of the bottle it is reoxidized by atmospheric O₂: the blue color comes back. After closing the lid, there is a lag phase and then MB is reduced again (Schirmer et al., 2011).

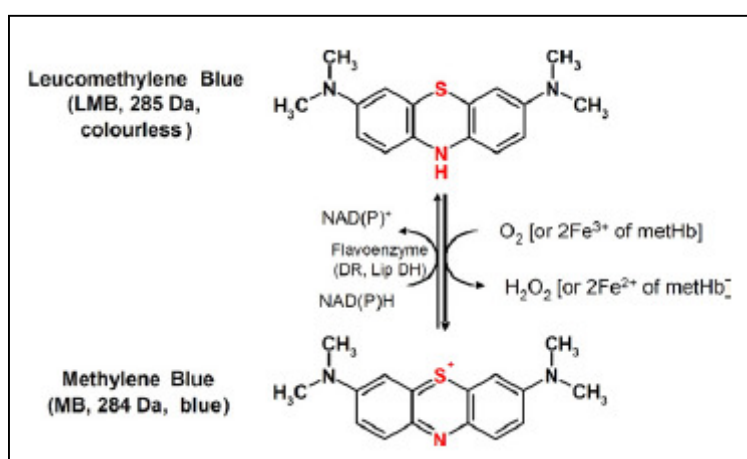
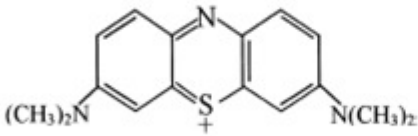
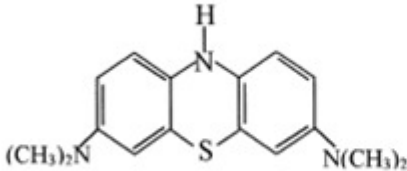


Figure II.1 The catalytic redox cycle of methylene blue *in vivo*.

The chemico-physical properties corresponding to both MB reduced and oxidized forms are summarized in Table II.1. It is worth mentioning that, at concentrations higher than 10 μ M, MB forms dimers.

Table II.1 Chemico-physical properties of both MB forms

Species	Structure	Abbreviation	p <i>K</i> _s	λ ^{max}	Other properties *
Methylene blue		MB	0	660, 614, 292	<i>K</i> _D = 3970 dm ³ mol ⁻¹
Leuco methylene blue		LMB	4.5, 5.8	2562	

* *K*_D corresponds to the dissociation process of the MB dimer: (MB)₂ ⇌ 2MB

MB, the first synthetic drug used, has 120-year history in several areas of medicine, and one of its first uses was in the treatment of malaria (Guttmann et al., 1891). It has shown to exhibit effects on several cellular targets including NO synthase, cythochrome c oxidase, and the 70-kDa heat shock protein (Callaway et al., 2002; Atamna et al., 2008; Jinwal et al., 2009). Furthermore, its biochemical properties make it a very effective redox cycling compound, with antioxidant and neuroprotective properties (Hajieva et al., 2009).

Current indications for MB, approved by the US Food and Drug Administration, are enzymopenic hereditary met-hemoglobinemia and acute acquired met-hemoglobinemia (Cawein et al., 1964), prevention of urinary tract infections in elderly patients, and intra-operative visualization of nerves, nerve tissues, and endocrine glands as well as of pathologic fistulae (O'leary et al., 1968). Of great practical importance is also the administration of MB for the prevention and treatment of ifosfamid-induced neurotoxicity in cancer patients (Kupfer et al., 1994).

In clinical practice, MB is available as a solution (1%, w/v; 10 g/l or 26.74 mM) and the recommended safe dose appears to be within 1-4 mg/kg (Clifton II et al., 2003). Typically, MB is administered i.v. or orally (50–300 mg), but interosseous MB infusion has also been described (Herman et al., 1999). After oral administration of 100 mg MB, whole blood MB concentrations in healthy individuals were reported to be one order of magnitude lower than after i.v. administration of the same dosage (Peter et al., 2000). However, a recent study comparing the administration of single doses of MB (50 mg i.v. versus 500 mg orally) indicated that the absolute bioavailability of MB after oral administration was 72.3% (Walter-Sack et al., 2009).

From the toxicological point of view, MB is relatively non-toxic and has an enviable safety record. In one notable pediatric case report (Blass et al., 1976), a child was given a dose that was 16 times the recommended maximum. The child's skin was intensely blue, but there were no other documented ill effects. Most side effects of MB appear to be dose-dependent and do not occur with doses < 2 mg/kg, a dose range that is widely used in the clinical applications of MB. In *in vitro* studies, MB demonstrates biological actions at a wide range of concentrations, from 0.1 nM to 10 mM, and toxic effects have only been reported at concentrations higher than 100 mM.

Aware of the fact that in the prion field there is an urgent need to find an effective treatment for prion diseases, and that the extreme cost of drug development is the major obstacle when new drug programs have to be processed, we aimed to give a little contribution, looking for a known molecule, that fulfills all the safety features required to be used in animals and humans, and furthermore, a molecule with specific properties to act in the CNS. MB satisfies the criteria for a BONARIA drug. In the acronym BONARIA, BON stands for safe and efficacious, A stands for affordable, R stands for registered, and IA stands for internationally accessible.

In particular, we carried out an *in vitro* study, testing the action of methylene blue on the oligomerization and fibrillization of prion protein, the two main processes on the pathogenic pathway of the disease. We have found that MB is able to slow down the PrP oligomer formation, and completely suppress the fibril formation. In this work we finally propose a possible mechanism of action of MB on prion conversion.

2.2 Experimental procedures

- *Protein production*

The full-length PrP from sheep OvPrP (A¹³⁶ R¹⁵⁴ Q¹⁷¹ variant), the truncated form Δ OvPrP (103-234) and the mouse PrP (MoPrP) were produced in *Escherichia coli* and purified as previously described (Rezaei et al., 2000). All the mutants from sheep, OvPrP_H190A, OvPrP_H190KI208M and Δ OvPrP_I206W were obtained by introducing the respective mutations into the ARQ gene cloned in a pET22bC vector by using the QuickChange mutagenesis kit (Stratagene, La Jolla, CA). The mutants were purified through the protocol used for the wild-type prion protein. Different buffers were used to desalt the protein on a HiPrep desalting column using an FPLC equipment (GE Healthcare): sodium citrate 20 mM, pH 3.4; sodium acetate 20 mM, pH 4.6; MOPS 20 mM, pH 7.0. Final protein concentration was measured by optical density at 280 nm using an extinction coefficient of 58718 M⁻¹ cm² for OvPrP (wt ad mutants) and MoPrP, and an extinction coefficient of 18005 and 23505 M⁻¹ cm² for Δ OvPrP and for Δ OvPrP_I206W, respectively, deduced from the aminoacid sequence.

The generation of oligomers from OvPrP and MoPrP was performed in sodium citrate 20 mM, pH 3.4. Both protein solutions, at a concentration of 100 μ M were incubated in a thermocycler Perkin Elmer GenAmp2400 and heated at 60 °C for 12 hours and at 50 °C for 8 minutes for OvPrP and MoPrP, respectively. Then the samples were cooled down to 15 °C and eluted with sodium citrate 20mM, pH 3.4 on a TSK 4000SW (60 x 0.78 cm) column. Homogeneous fractions of each oligomer were collected.

- *Fluorescence experiments*

Fluorescence spectra were recorded at 20 °C on a Jasco 6200 spectrofluorimeter with a 2 mm x 10 mm optical path-length cuvette. An excitation wavelength of 285 nm was chosen and for all the experiments the protein concentration range used was 20-30 μ M in sodium acetate 20 mM, pH 4.6.

Concentration of MB varied from 0 up to a molar ratio PrP:MB of 1:5. Each solution of the mixture PrP-MB was prepared independently without successive additions of MB in the PrP solution to avoid complications due to dilution effects within titration type

experiments. Each measurement was repeated in triplicate and appropriate blanks corresponding to the buffer were subtracted to correct the fluorescence background. It was used the Stern-Volmer equation to evaluate the type of quenching resulting from fluorescence experiments performed (Lakowicz, 1999).

$$\frac{F_0}{F} = (1 + K_{eq} [Q])(1 + k_q \tau_0 [Q]) \quad \text{Eq.1}$$

where F_0 and F are the fluorescence intensities before and after the addition of the quencher respectively. The first factor on the right-hand side describes the static quenching, resulting by formation of a complex between quencher and fluorophore, with K_{eq} as the equilibrium constant of the binding reaction. The second factor is related to the dynamic quenching, resulting from encounters of quencher and fluorophore during the fluorescence lifetime where k_q is the bimolecular quenching constant, τ_0 is the lifetime of the fluorophore in the absence of quencher and $[Q]$ is the concentration of the quencher.

- *Surface Plasmon Resonance*

The SPR experiments were performed using a Biacore T100 system (GE Healthcare, Uppsala, Sweden). The full-length OvPrP and the truncated Δ OvPrP were immobilized on a CM5 using a standard amine coupling procedure, using HBS-EP buffer (HEPES 10 mM, NaCl 150 mM, EDTA 3 mM, 0.005% Surfactant P20, pH 7.4) as running buffer. The PrP forms were immobilized through activation of the sensor chip with 60 μ L of N-hydroxysuccinimide (NHS) and N-ethyl-N-(dimethylaminopropyl) carbodiimide (EDC), followed by 30 μ L injection of PrP forms diluted in 10 mM sodium acetate buffer pH 5.0. Unreacted activated groups were blocked by a 15 μ L injection of 1 M ethanolamine.

Various concentrations of MB were prepared in running buffer up to 500 μ M, since the completely regeneration of the sensor surface was not possible at higher concentrations. Then, MB was injected over the flow cell of the chip for 1 minute at a flow rate of 30 μ L/min. Data were corrected using a blank sensor chip as control. The analysis of the SPR sensorgram was made using BIAevaluation software.

- *Circular Dichroism*

CD spectra were recorded with a Jasco J-815 spectropolarimeter equipped with a Peltier type temperature control system (Model PTC-423S). The instrument was calibrated with an aqueous solution of d-10-(+)-camphorsulfonic acid at 290 nm. Molar ellipticity per mean residue, $[\theta]$ in $\text{deg cm}^2 \text{ dmol}^{-1}$, was calculated from the equation: $[\theta] = [\theta]_{\text{obs}} \cdot \text{mrw} / 10 \cdot l \cdot C$, where $[\theta]_{\text{obs}}$ is the ellipticity measured in degrees, mrw is the mean residue molecular weight, 109 Da, C is the protein concentration in g L^{-1} and l is the optical path length of the cell in cm.). Far-UV CD spectra of full-length OvPrP in absence and presence of MB were recorded in the range 260 \div 190 nm at 20 $^{\circ}\text{C}$, using a 0.2-cm optical path length quartz cuvette. The protein concentration used was 6 μ M in sodium acetate 15 mM, pH 4.6. Each CD spectrum was obtained by averaging 3 scans collected with a time constant of 4 s, a 2-nm bandwidth, and a scan rate of 5 nm min^{-1} . The baseline was corrected by subtracting the buffer spectrum. Thermal denaturation curves of full-length OvPrP with and without MB were recorded over the 20 \div 90 $^{\circ}\text{C}$ temperature range and by monitoring the CD signal at 222 nm. All curves were obtained using a scan rate of 1.0 $^{\circ}\text{C min}^{-1}$.

Reversibility of the denaturation was evaluated by recording, after cooling to 20 °C, the spectra of samples subjected to a first temperature scan.

For all CD measurements, concentration of MB varied from 0 up to a molar ratio PrP:MB of 1:20. Each solution of the mixture PrP-MB was prepared independently.

- *Size exclusion chromatography*

The oligomerization pathways of each PrP forms were analyzed using Akta FPLC chromatography equipment (GE Healthcare) on a TSK 4000SW (60 x 0.78 cm) column. The column was previously calibrated for molecular mass using a Gel Filtration High Molecular Weight calibration kit (GE Healthcare) constituted by ovalbumin (44 kDa), conalbumin (75 kDa) and aldolase A (158 kDa). Before each run, the column was equilibrated with at least two column volumes of elution buffer and each run was performed at room temperature. The elution buffer was sodium citrate 20 mM, pH 3.4 and the eluent flow was 1 mL min⁻¹. The elution profile was monitored at two UV absorption wavelengths (280 nm and 215 nm). The concentration of proteins used was 40 µM and each protein solution was incubated at 50 °C at different incubation time, ranging from 0 to 90 minutes.

- *Static light-scattering Experiments*

The static light-scattering kinetics experiments were performed on a homemade device with four lasers beams (407, 473, 533, and 633 nm) using a 2 mm cuvette. The oligomerization of OvPrP, MoPrP and the mutants OvPrPH190A and OvPrPH190KI208M was monitored at 50 °C. The concentration of protein samples was in the range 30 ÷ 50 µM in 20 mM citrate sodium, pH 3.4 or MOPS 20 mM, pH 7.0, depending on the pH condition tested. To estimate the percent decrease of the SLS intensity signal in the presence of MB with respect to the one of the protein without MB, the SLS values, at the maximum recorded time, were considered for each curve.

For depolymerization experiments, O1 and O3 oligomers obtained from SEC purification were incubated, at a concentration of 8 µM, in the SLS device at 75 °C and 55 °C, respectively. Signal processing was achieved by a homemade MatLab program.

- *Differential scanning calorimetry*

DSC thermograms were obtained by a MicroCal DSC instrument with cell volumes of 0.5 mL, at a scan rate of 60 and 90 °C/hour. All the experiments were performed with the full-length OvPrP at 50 µM, using three different pH conditions: sodium citrate 20 mM, pH 3.4, sodium acetate 15 mM, pH 4.6 and MOPS 20 mM, pH 7.0. For each condition, at least two thermograms were recorded with and without MB at a molar ratio PrP:MB of 1:4. DSC thermograms were analyzed with ORIGINLab software. Deconvolution of DSC curves obtained at pH 7.0 was achieved by a homemade MatLab program applying the Lumry–Eyring model (Sanchez-Ruiz, 1992). To estimate the percentage of oligomers formed in the absence and in the presence of MB, we calculated the area of the deconvoluted peaks corresponding to the second transition.

- *PrP fibrillization and electron microscopy*

All solvents and solutions prepared for fibril formation were filtered using 0.02-µm filters prior any usage. Lyophilized HuPrP and OvPrP were dissolved in MES 50 mM, pH 6.0. The fibrillization reaction was started diluting the PrP stock solution (44 µM)

to a final concentration of 22 μ M in 2.0 M GdnHCl and 0.5 mM MES, pH 6.0. For the samples with methylene blue, MB was dissolved in water to a final concentration of 22 \div 220 μ M. All the samples were incubated at 37 $^{\circ}$ C.

The kinetics of fibril formation was monitored using a ThT binding assay. During incubation at 37 $^{\circ}$ C, aliquots of the solutions were collected at regular time intervals and diluted in sodium acetate 10 mM, pH 5.0 to a PrP final concentration of 0.3 μ M. Then, ThT was added to a final concentration of 10 μ M. For each sample, emission spectra were recorded using a Jasco 6200 spectrofluorimeter with a 2 mm x 10 mm optical path-length cuvette and an excitation wavelength of 445 nm. Both excitation and emission slits were 5 nm. Spectra were averaged upon three measurements (n) and the fluorescence intensity at emission maximum (482 nm) was determined. To evaluate if MB could interfere with the ThT emission, fluorescence spectra of the solutions containing alternatively only ThT and both ThT and MB were recorded, at the maximum concentration used for the samples PrP-MB. The emission of ThT was the same with and without MB.

Fibril morphology was analyzed by TEM using a Zeiss EM902 (80kV) microscope. Briefly, 10 μ L of the protein samples were adsorbed onto carbon-coated Formvar grids (Agar Scientific). Then, each grid was washed three times with water, stained with 2% uranyl acetate and finally air-dried.

2.3 Results

Interaction between the native monomeric PrP and methylene blue.

In order to evaluate if there is a specific binding of prion protein with MB at pH 4.6, we used different approaches, namely, Trp fluorescence and SPR. In the prion primary structure, there are seven tryptophan residues, all located within the N-terminal domain. This domain is highly flexible and lacks any identifiable secondary structure (Donne et al., 1997; Riek et al., 1997), leading to a complete exposure of all the Trp residues. This particular arrangement of the tryptophans in a restricted region of the protein allows to identify the binding region of prion protein to MB. Indeed, for fluorescence experiments we used the full-length OvPrP (23-234) and the truncated form Δ OvPrP (103-234) with the mutation I206W, since the C-terminal domain lacks tryptophan. In Δ OvPrP, a Trp was placed at position 206 replacing the residue Ile, that in the 3D structure is exposed on the protein surface.

Figure II.2 shows the fluorescence spectra recorded for the full-length OvPrP and Δ OvPrP_I206W in the presence of MB at increasing molar ratio PrP:MB up to 1:5. The quenching phenomena of MB on the full-length OvPrP and Δ OvPrP results in a decrease of the intensity fluorescence with the increase of MB concentration. Such effects are indicative of fluorescence quenching and can be used to characterize the PrP-MB interaction by the well-known Stern-Volmer equation (Lakowicz, 1999).

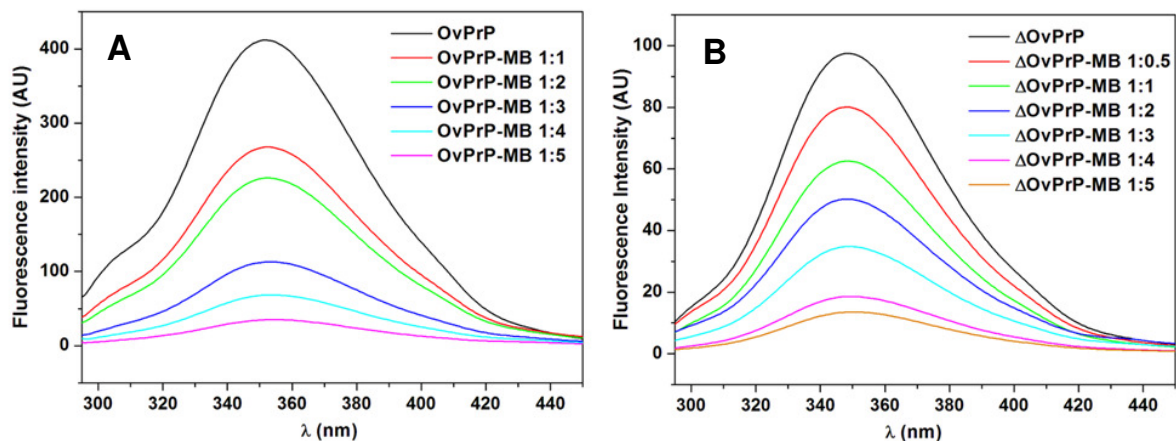


Figure II.2 Fluorescence titrations for the interaction of prion protein with MB. A) Spectra related to the full-length OvPrP with MB; B) Spectra related to Δ OvPrP_I206W with MB

Figure II.3 shows the Stern-Volmer plot of the PrP proteins quenching caused by the presence of methylene blue. The Stern-Volmer plot was found to be linear for both the full-length OvPrP and Δ OvPrP_I206W, which means that only a dynamic quenching occurs.

It has to be taken into account that the full-length OvPrP embodies seven Trp and all of them contribute to the Stern-Volmer equation with their own dynamic and static constants. In general, when there are more fluorophores in a protein, if the difference between the quenching constants is not large, the Stern-Volmer plots may appear approximately linear (Calhoun et al., 1986). Thus, for the full-length OvPrP all the tryptophans are dynamically quenched by MB with similar dynamic quenching constants, that is reliable since the N-terminal domain of the protein is not structured and all the Trp are similarly exposed.

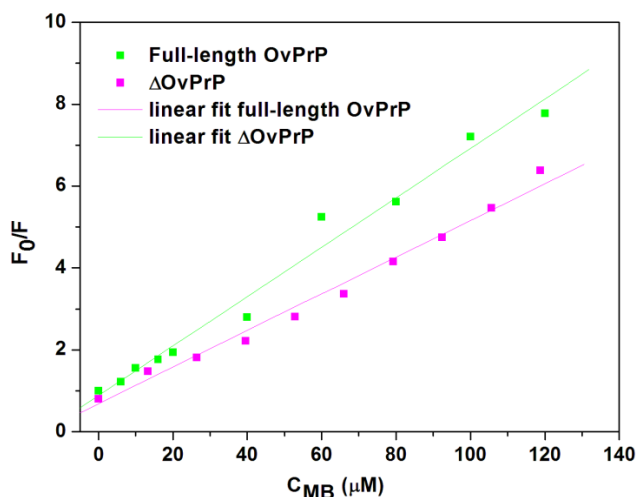


Figure II.3 Stern-Volmer plot of the full-length and the truncated PrP quenching caused by the presence of MB

Because both full-length and truncated OvPrP fluorescence intensity progressively decrease with increasing concentrations of MB, without reaching saturation, MB does not establish a specific interaction with PrP.

It is noteworthy that fluorescence measurements provide only information about the structural integrity of the immediate environment of the fluorophores, thus, SPR experiments have been performed to further study the interaction between PrP and MB. The full-length OvPrP and Δ OvPrP were immobilized on the sensor surface chip and various concentrations of MB were injected over the sensor chip up to 500 μ M.

The SPR sensorgrams obtained for the full-length OvPrP, shown in Figure II.4A as example, demonstrated that, albeit the signal responses increase with increasing MB concentration, the responses remain constant within a few seconds and returns to the baseline very rapidly after dissociation. Reliable kinetic constants cannot be obtained by fitting the SPR sensorgrams with any models available in the BIAevaluation software. A similar behavior was observed with Δ OvPrP.

In Figure II.4B is reported the SPR response curve of the full-length OvPrP *versus* MB concentration. The linear dose-response curve suggests that no saturation is reached, and this precludes the possibility to determine the dissociation constant value (K_D). These results may be indicative of multiple binding sites and/or a low affinity for OvPrP (Hosokawa-Muto et al., 2008).

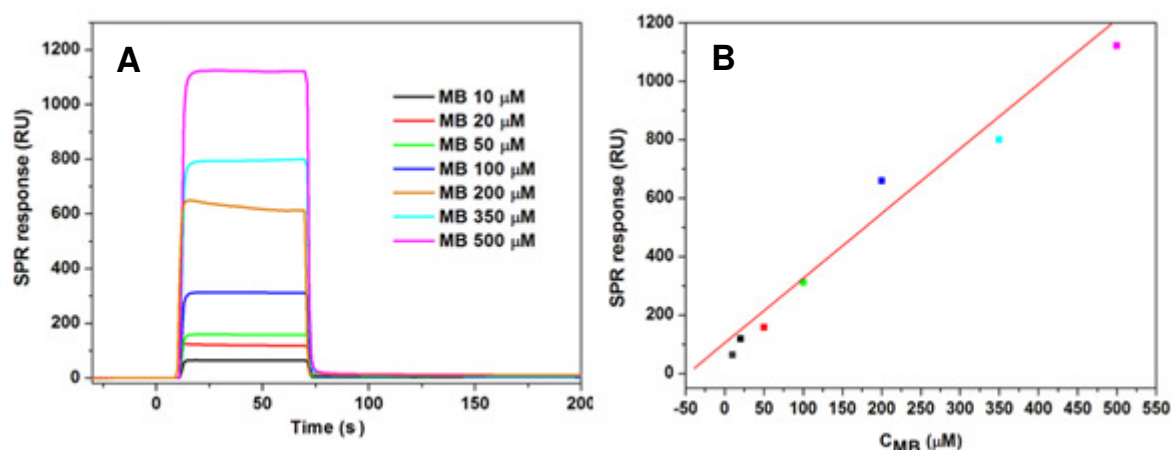


Figure II.4 SPR experiments for the interaction of the full-length PrP with MB. A) Time evolution of SPR response at various MB concentrations up to 500 μ M. B) Dose response curve of the SPR response *versus* MB concentration

Finally, 15 N-HSQC spectra of the 15 N-labeled Δ OvPrP in the presence of MB up to a molar ratio PrP:MB of 1:10 were recorded by Dr. Annalisa Pastore at the National Institute for Medical Research-MRC (The Ridgeway London, United Kingdom). No chemical shift changes of nitrogen resonance frequencies were observed in the presence of MB (data not shown), in agreement with fluorescence and SPR data.

To analyze the effects of MB on the stability of PrP, CD and DSC experiments were also performed, at pH 4.6, and results are shown in Figure II.5. The inset in Figure II.5A, shows the normalized CD spectra recorded for the native monomeric protein with and without MB, up to a molar ratio PrP:MB of 1:20. All spectra show a characteristic α -helical structure and are perfectly superimposable. Furthermore, thermal denaturation curves were recorded by monitoring the molar ellipticity at 222 nm (Fig. II.5A) going up to a molar ratio PrP:MB of 1:20. In all cases, there is no change on the melting temperature of the unfolding process. Either in the presence

or in the absence of MB, the unfolding process was reversible with complete recovery, after cooling, of the secondary structure of the protein (data not shown).

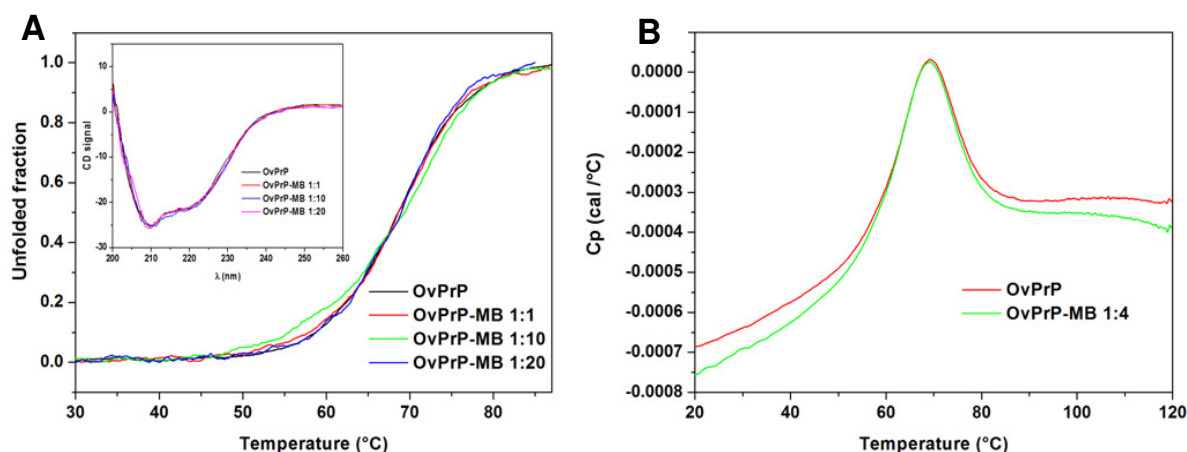


Figure II.5 Analysis of the stability effects on prion protein mediated by MB at pH 4.6. A) CD thermal unfolding of OvPrP in the absence and in the presence of MB up to a molar ratio PrP:MB of 1:20 (In the inset are displayed the corresponding CD spectra). B) DSC thermograms recorded for OvPrP in the absence and in the presence of MB at a molar ratio PrP:MB of 1:4

Similar results were obtained from DSC experiments (Fig. II.5B). Indeed, the DSC thermogram related to PrP in the presence of MB at a molar ratio PrP-MB of 1:4, showed no variations of T_m ($69.1 \text{ }^{\circ}\text{C} \pm 1 \text{ }^{\circ}\text{C}$) with respect to the thermogram obtained in the absence of MB.

Effects of methylene blue on the kinetics of PrP polymerization and depolymerization.

In previous works, it has been shown that the thermal treatment of either OvPrP and MoPrP leads to the formation of oligomers, although the oligomerization pathway is not the same, with oligomer ratio differing as a function of PrP type (Eghiaian et al., 2007). In particular, the thermal refolding of the OvPrP, in acidic ($\text{pH} < 4.5$) conditions, induces the formation of three different oligomers referred to as O1, O2 and O3 corresponding to 36, 24 and 12 mers, respectively. In addition, it was shown that only O1 is able to fibrilize giving rise to a fiber-like aggregate, referred to as P0. The thermal refolding of MoPrP predominantly leads to the formation of the oligomer O3, with small amounts of O1 and O2 (Chakroun et al., 2010).

In order to evaluate the effect of MB on the oligomerization process of PrP, we analyzed, through SLS, the kinetics of the oligomerization for both OvPrP (wt and properly selected mutants) and MoPrP in the presence of MB, at pH 3.4 and 7.0. The PrP mutants were selected on the following criteria: i) to evaluate the influence of MB on the oligomerization rate of the PrP mutants that give rise to only one type of oligomer and, ii) to evaluate the influence of MB on the oligomerization rate of the type of PrP that leads to the formation of higher aggregates. For the first aim, wt-MoPrP and the mutant OvPrP_H190A were selected, as they lead to the formation of only O3 and O1 oligomer, respectively (Chakroun et al., 2010), using wt-OvPrP as control. On the other hand, the influence of MB on aggregates was evaluated through the design and the production of a new mutant, OvPrP_H190KI208M, which leads to the formation of P0 fibrillar assemblies.

In Figure II.6 the SEC profiles of all the PrP forms, obtained at pH 3.4, at 50 °C and at various incubation times (See Experimental Procedures, Section 2.2), are shown together with the schematic oligomerization reaction. The chromatogram referred to wt-OvPrP showed the formation of the three oligomers O3, O2 and O1 (Fig. II.6A), whereas MoPrP and the mutant OvPrP_H190A showed the formation of only one oligomer, O3 and O1 respectively (Fig. II.6B,C), as previously reported (Chakroun et al., 2010). The new mutant OvPrP_H190KI208M is characterized by the formation of P0 fibrils assemblies, in addition to the oligomer O3 (Fig. II.6D).

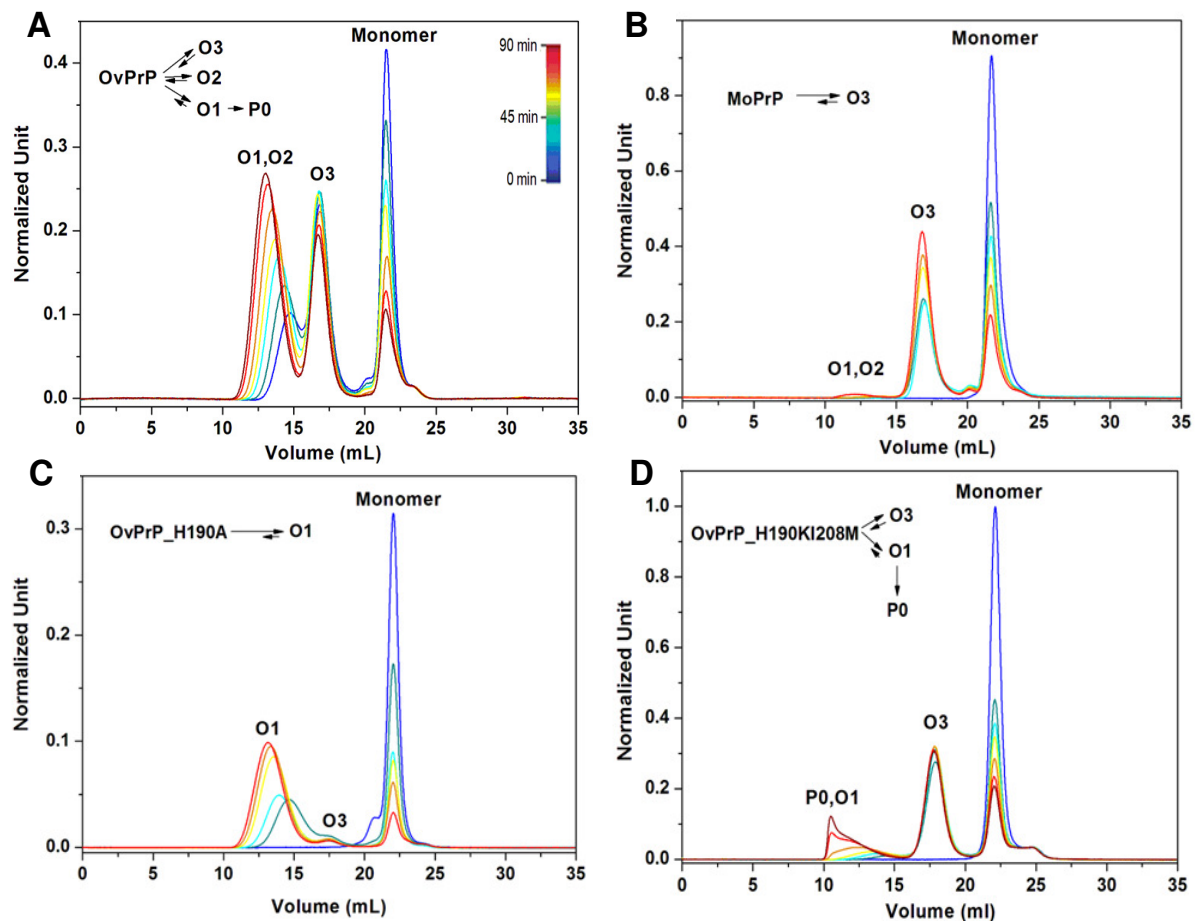


Figure II.6 Oligomerization pathways obtained by thermal treatment, at pH 3.4 and at various incubation times. A) SEC profiles of wt-OvPrP; B) SEC profiles of wt-MoPrP; C) SEC profiles of OvPrP_H190A; D) SEC profiles of OvPrP_H190KI208M. The color curves correspond to increasing incubation times from 0 to 90 minutes.

In Figure II.7, the kinetic curves of all PrP protein forms tested in the presence of MB at pH 3.4 are shown. In all cases, the kinetic profiles obtained in the presence of MB differed from those obtained using the protein alone, and the higher the MB concentration was, the more the SLS intensity signal decreased. The estimation of the SLS signal decrease, performed at the maximum recorded time, is indicative of the oligomerization rate. In particular, the decrease suggests that at molar ratio PrP:MB of 1:1, the signal of OvPrP, MoPrP and OvPrP_H190A decreased about 10 % and at molar ratio PrP:MB of 1:3 about 18 % with respect to the protein without MB. The decrease of the SLS intensity signal of the variant OvPrP_H190KI208M was 17 % and 30 % lesser with respect to the protein alone, at molar ratios PrP:MB of 1:1

and 1:3, respectively. This general behavior clearly shows the MB influence on the PrP oligomerization rate.

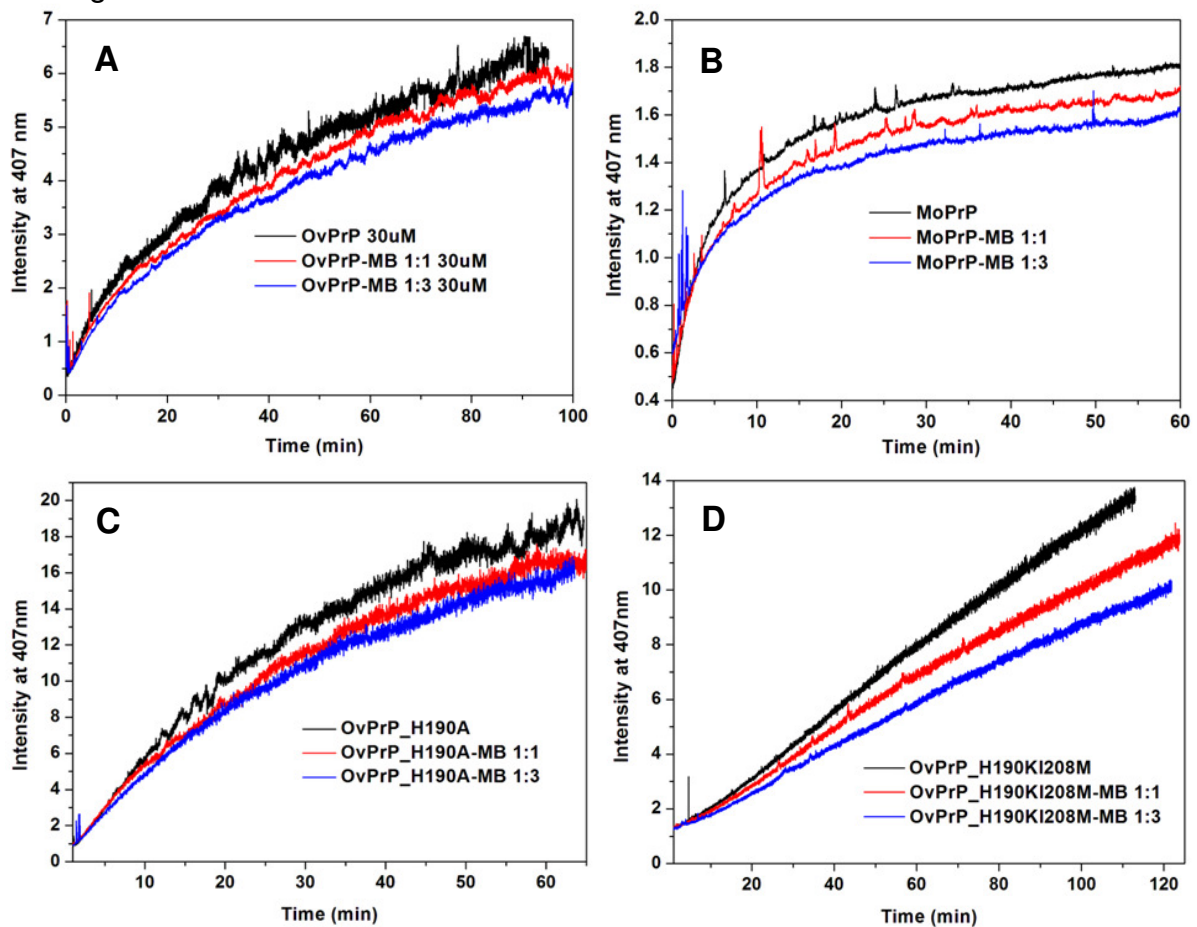


Figure II.7 Effect of MB on the kinetics of the PrP oligomerization, at pH 3.4. A) SLS curves of wt-OvPrP; B) SLS curves of MoPrP; C) SLS curves of OvPrP_H190A; D) SLS curves of OvPrP_H190KI208M

It has been shown that in neutral conditions, the thermal treatment of wt-OvPrP leads to an oligomerization pattern in which the formation of O1 oligomer, rather than O2 and O3 oligomers, is favored and further heating produces the formation of aggregates (Prigent et al, 2011). For comparison, SEC profiles related to the oligomerization pathways of OvPrP, at pH 3.4, 4.5 and 7.1, is displayed in Figure II. 8A.

SLS kinetic experiments on wt-OvPrP, at pH 7.0, showed a drastically slow down of the kinetics in the presence of MB, already at a molar ratio of MB:PrP equal to 1 (Fig. II.8B). It is noteworthy that the SLS intensity signal of OvPrP in the presence of MB was about 40 % lesser than the one of the protein alone at the end of the measure. A conclusive finding of SLS polymerization experiments is that PrP oligomerization rate is affected by MB.

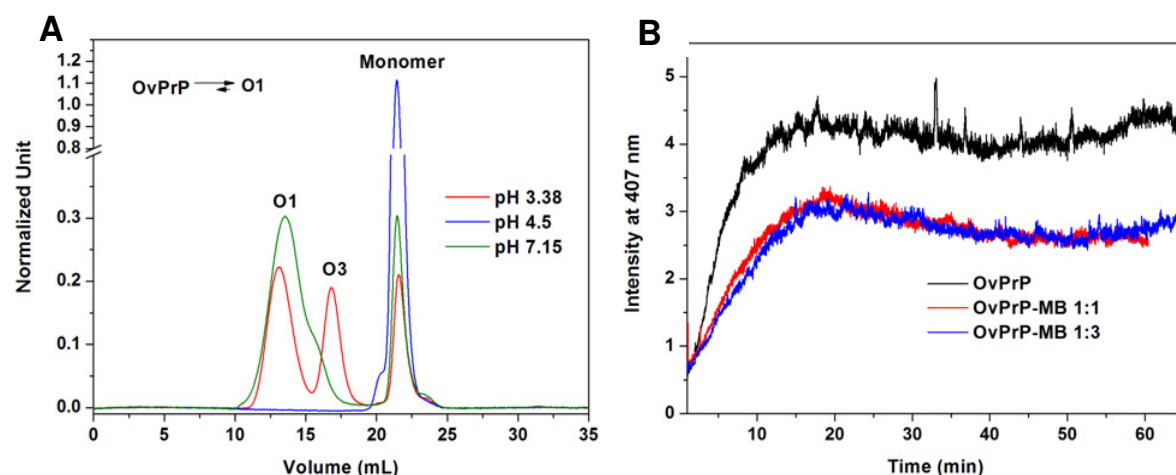


Figure II.8 A) Comparison of the SEC profiles corresponding to the oligomerization pathways of OvPrP at pH 3.4, 4.5 and 7.1; B) SLS kinetic curves describing the effects of MB on the oligomerization of OvPrP, at pH 7.0.

At this junction a question arises: does MB directly interact with oligomers or with intermediate species? If MB interacted with PrP oligomers they should undergo some changes in their properties and behavior such as depolymerization, that is a well characterized one-step process that leads to monomers generation (Eghiaian, 2007). To address this question, we carried out depolymerization experiments on the two most representative oligomers O1 and O3. They were obtained and purified respectively from OvPrP and MoPrP, and their depolymerization was monitored by SLS in the presence of MB and at a molar ratio PrP:MB of 1:4. The SLS curves, shown in Fig. II.9, indicate that the depolymerization rate of both oligomers is the same with and without MB, excluding the possibility of a direct interaction between MB and PrP oligomers.

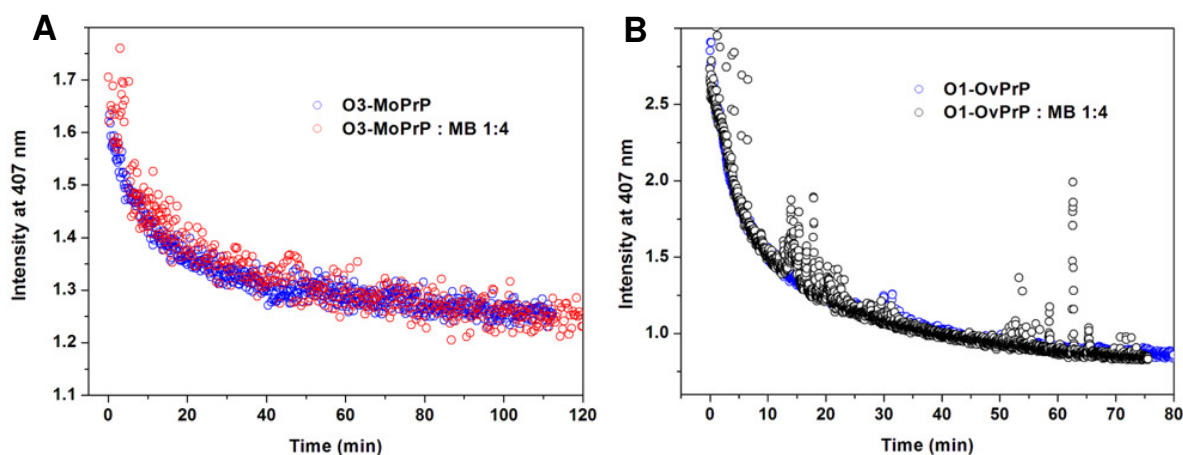


Figure II.9 SLS kinetics of the depolymerization of O3 oligomer (A), and O1 oligomer (B) at pH 3.4

The unfolding process of PrP in the presence of methylene blue.

It was previously reported that the thermal unfolding of OvPrP within the pH interval $4.5 < \text{pH} < 7.0$ showed two peaks interpreted as a polymerization and depolymerization phenomena (Rezaei et al., 2002). Thus, the effects of MB on the oligomerization process of PrP was also studied by DSC, recording the thermograms at pH 3.4 and

pH 7.0, in the presence of MB. In Figure II.10, the DSC thermograms recorded for OvPrP, in the absence and the presence of MB at a ratio PrP:MB of 1:4, are shown. The denaturation process, at both pH, consists of two transitions, in agreement with previous data (Rezaei et al., 2002).

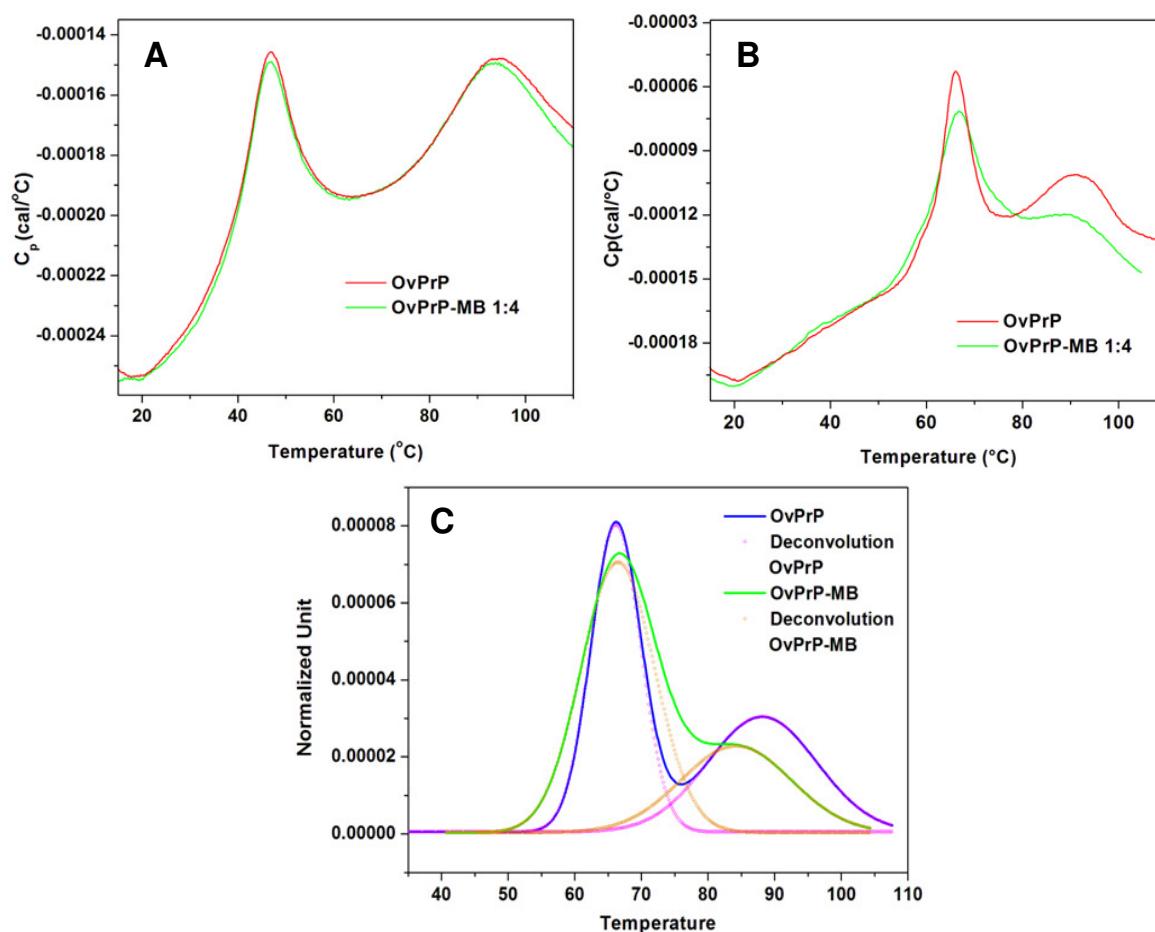


Figure II.10 Unfolding of OvPrP followed by DSC at two different pH in the absence and in the presence of MB, at a molar ratio PrP:MB of 1:4. A) DSC thermogram at pH 3.4; B) DSC thermogram at pH 7.0; C) Deconvolution of the DSC curves obtained at pH 7.0, with and without MB. Continuous lines correspond to the experimental C_p data. Symbols represent the predicted C_p curves of each transition peak in which the global curves can be deconvoluted.

At pH 3.4, the first transition occurs around 47 °C and the second one around 94 °C (Fig. II.10A). For both thermograms, with and without MB, these temperatures are preserved and the area of both peaks is similar, even if a small reduction on the area of the second peak was observed in the presence of MB.

Interestingly, at pH 7.0, the DSC thermogram of OvPrP without MB showed a first transition temperature around 66 °C and a second transition temperature around 88 °C (Fig. II.10B). In the presence of MB, the DSC thermogram was markedly different compared to that one of the protein only. Indeed, both peak area decrease, in particular, the second peak is considerably reduced. Therefore, to compare the oligomers amount formed during the first transition in the absence and in the presence of MB, thermograms have been deconvoluted, as shown in Figure II.10C. Particularly, deconvolution of the first peak shows no significant differences with and without MB. Differently, deconvolution of the second peak reveals meaningful

differences in both the surface area and the transition temperature. Indeed, in the presence of MB, the peak area, which is proportional to the total protein concentration, is reduced by about 28 % and the transition temperature (84 °C) is about 4 °C lower in comparison to the protein alone (88 °C), in good agreement with the Lumry–Eyring equation (Sanchez-Ruiz, 1992). As result from DSC experiments, MB significantly interferes with polymerization of PrP and particularly limits the amount of oligomers formed along the polymerization pathway, at the physiologic pH 7.0.

Effect of methylene blue on PrP fibrillization

Finally, the action of MB on fibril formation was studied. HuPrP and OvPrP fibrils were generated at pH 6.0 in the absence (as control) and in the presence of MB. The PrP fibril formation was monitored using a ThT binding assay. In Figure II.11 the kinetics of fibril formation is shown for HuPrP and OvPrP, with and without MB, at different molar ratios.

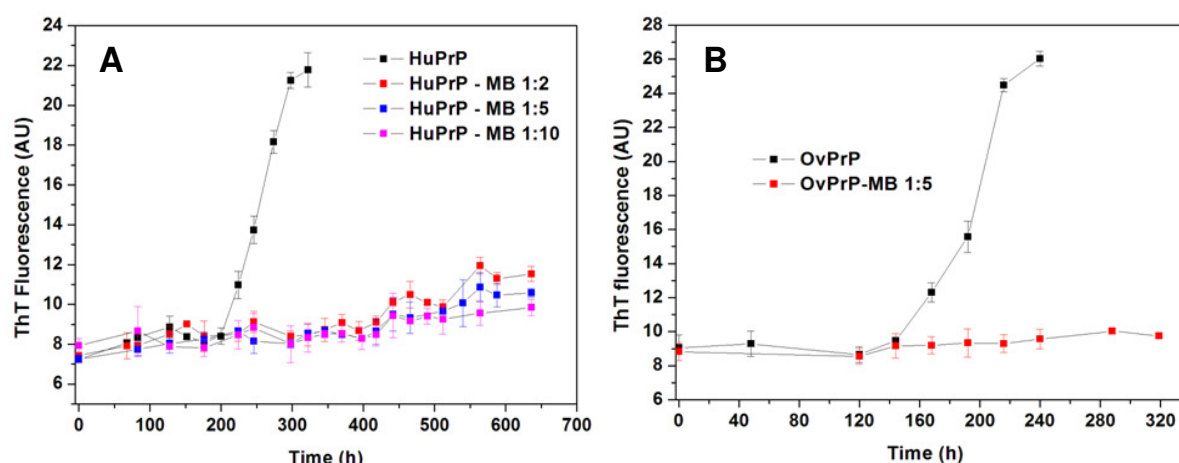


Figure II.11 ThT binding assay for PrP fibril formation in the absence and in the presence of MB at low PrP:MB molar ratios, as indicated. A) ThT fluorescence of HuPrP; B) ThT fluorescence for OvPrP. Results represent means \pm s.d (n=3).

For both HuPrP and OvPrP, in the absence of MB, the ThT signal gradually rises with a sigmoidal shape, indicating the formation of PrP fibrils. In contrast, the fibril formation was completely inhibited by the presence of MB, at molar ratios PrP:MB equal or lesser than 1:2.

In the range $1:0 \leq \text{PrP:MB} \leq 1:1$, there is no inhibition of fibril formation, but a longer lag phase is observed at equimolar concentration of MB relative to PrP, compared to the control (Fig. II.12).

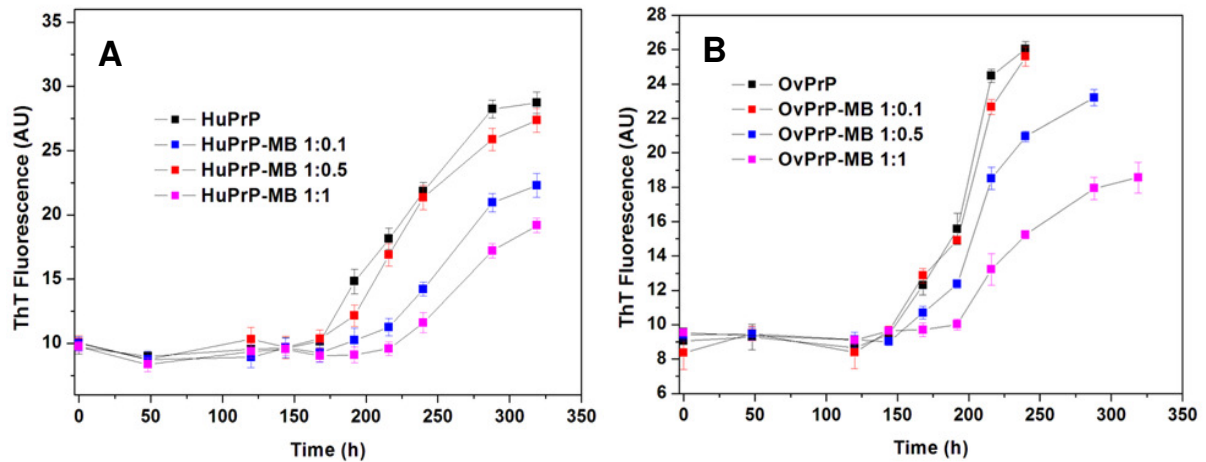


Figure II.12 ThT binding assay for PrP fibril formation with and without MB at high PrP-MB molar ratios, as indicated. A) ThT fluorescence of HuPrP; B) ThT fluorescence of OvPrP. Results represent means \pm s.d (n = 3).

A valuable confirmation that the fibril formation is suppressed by MB, at molar ratios lesser than 1:2, was obtained by TEM images. For both HuPrP and OvPrP, typical fibrillar structures were observed in the absence of MB, (Fig. II.13A,E). On the other hand, very little fibrillar material was observed for samples incubated with MB at molar ratios PrP:MB lower than 1:2 (Fig. II.13B-D,F).

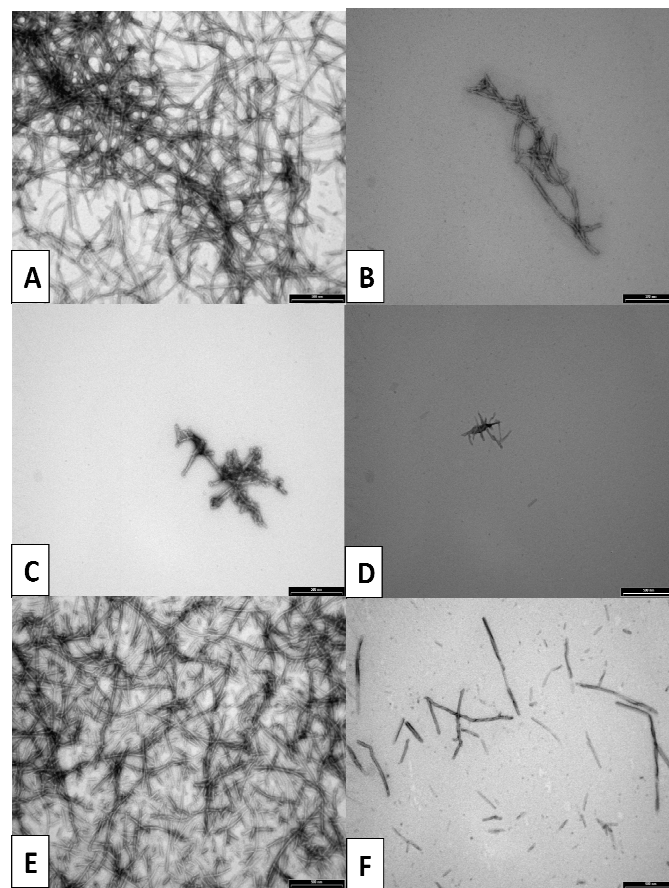


Figure II.13 TEM images of HuPrP fibrils formed in the absence of MB (control) (A), and in the presence of MB at molar ratios HuPrP:MB of 1:2 (B), 1:5 (C), 1:10 (D); TEM images of OvPrP fibrils formed in the absence of MB (control) (E), and in the presence of MB, at a molar ratio OvPrP-MB of 1:5 (F). Scale bar: 0.5 μ m.

The EM images of the samples HuPrP and OvPrP in the presence of MB, at equimolar concentration, confirm the results obtained by ThT fluorescence assays, showing the formation of PrP fibrils also for the samples containing MB, even if a little decrease on the fibril amount was detected (Fig. II.14). These findings demonstrate that MB efficiently prevents the amyloidogenesis of PrP, at a PrP:MB ratio equal to 1:2.

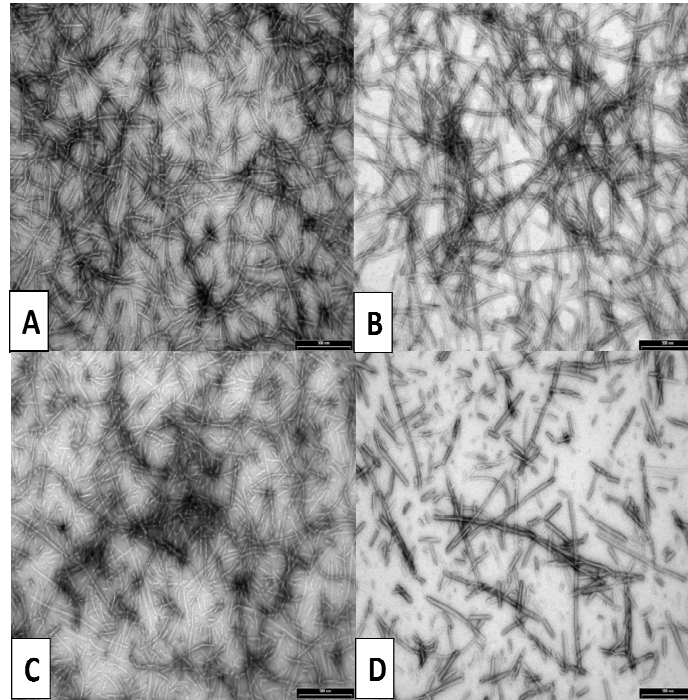


Figure II.14 TEM images related to HuPrP fibrils without MB (control) (A), HuPrP fibrils at a molar ratio HuPrP:MB of 1:1 (B), OvPrP fibrils without MB (control) (C), and OvPrP fibrils at a molar ratio 1:1 (D). Scale bar: 0.5 μ m.

2.4 Discussion

MB does not specifically interact with the native monomeric PrP

The potential anti-prion agents hitherto evaluated have different ways of inference on the prionogenesis. In fact, they can act in a specific step of the conversion mechanism, interacting with different PrP forms and blocking the chain reaction. Indeed, many of these compounds antagonize the PrP conversion through a ground state stabilization of the protein by a direct interaction with the native PrP conformation (Vogtherr et al., 2003; Kuwata et al., 2007; Nicolla et al., 2010). Other molecules, as Congo red, reinforce PrP^{Sc} structure and stabilize the PrP^{Sc} template, so that the partial denaturation essential for the conversion of additional PrP^C cannot occur (Caspi et al., 1998). Therefore, to understand how MB could act on the transconformation of PrP, we first studied its interaction with the monomeric native PrP using fluorescence, SPR and NMR approaches. To this purpose, we used both the full-length PrP (103-234) and the deleted protein (103-234).

Results from both fluorescence and SPR showed that MB does not specifically interact with the native conformation of both full-length and truncated PrP. In addition, NMR data shows no interaction of MB with Δ OvPrP.

CD spectra at room temperature, and both DSC and CD thermal unfolding experiments carried out at pH 4.6 (which is the optimal pH for prion protein) on the full-length OvPrP in the presence of MB showed that neither the secondary structure or the stability of the protein is pertubated by MB. Collectively, all results demonstrate that MB does not have any effect on the native monomeric form of PrP.

MB interferes with PrP oligomerization but not with depolymerization

It has been underlined the importance of the polymerization process during PrP conversion for the acquisition of amyloidogenic properties (Rezaei, 2008). In fact, all the $\text{PrP}^{\text{C}} \rightarrow \text{PrP}^{\text{Sc}}$ mechanism models include at least a polymerization step (Griffith, 1967; Come et al., 1993). Therefore, the kinetic formation of PrP oligomers in the presence of MB was analyzed by SLS. In particular, using PrP from various species, and different kind of mutants under various experimental conditions, we studied the effects of MB on different oligomerization pathways of the prion protein.

Taking into account that OvPrP undergoes parallel unfolding/refolding processes upon heating, and thus, each oligomer directly originates from the native state (Eghiaian, 2007), our SLS data on the PrP oligomerization demonstrate that MB is able to slow down the formation rate of all oligomers, independently. In particular, MB reduces the SLS intensity signal of the PrP variant OvPrP_H190KI208M, at pH 3.4 and wt-OvPrP at pH 7.0, that give rise to aggregates in addition to O1 oligomer (Eghiaian, 2007). In the latter case a decrement of SLS signal of 40 % was observed, at the end of the measurements. The above results from SLS support the hypothesis of a direct action of MB on a partial or completely unfolded transient state that precedes the formation of oligomers, either at pH 3.4 or at the physiological pH 7.0. This hypothesis could explain the diverse observed effects of MB on the oligomerization of the various PrP forms, that are characterized by distinct pathways.

Furthermore, depolymerization experiments performed on the purified oligomers in the presence of MB did not show a variation on the kinetics, indicating that MB does not interact with the oligomers, but acts as a simple spectator in this process. It is noteworthy that depolymerization is a one-step process, without the formation of intermediate states or intermediate oligomers (Eghiaian, 2007). Therefore, considering the action of MB on the kinetics of PrP oligomerization, together with the fact that there is not a direct specific interaction neither with the α -monomeric PrP or the oligomers, we conclude that MB may specifically target the partially unfolded intermediates that precede the formation of the oligomers. In fact, many experimental data have provided evidence for the existence of a partially unfolded state that precedes the formation of oligomers (Kuwata et al., 2002; Rezaei et al., 2005; Eghiaian, 2007; Jenkins et al., 2008).

MB limits the amount of oligomers and suppresses the fibril formation

DSC thermograms at pH 3.4 and 7.0 revealed a different action of MB on the PrP conversion depending on the pH, and hence, depending on the PrP oligomerization

pathway, in agreement with SLS experiments. The unfolding process of OvPrP in acidic ($\text{pH} < 4.5$) and neutral ($\text{pH} > 6.0$) conditions gives rise to two peaks on the DSC thermograms (Rezaei et al., 2002). This multimolecular process was explained assuming that the endothermic unfolding of the protein is immediately followed by an irreversible polymerization in the first transition and an irreversible depolymerization in the second one. Following this assumption, the second transition on the thermograms should be directly related to the amount of oligomers formed during the first transition. Thereby, DSC experiments provided a direct proof that MB is able to reduce the amount of oligomer formed during polymerization, at pH 7.0 (Eghiaian, 2007; Eghiaian et al., 2007). The second peak area decrement is related to a fewer amount of oligomers formed during the first transition, corresponding to a net oligomer loss of about 28 %.

The experimental evidences presented here support the idea that MB has a dual effect both on the kinetics and the thermodynamics of the prion conversion. MB is able to decrease the oligomerization rate of all PrP oligomers independently, and significantly decreases the amount of oligomers. It is worth point out that the ability to decrease the PrP oligomerization rate is an advisable feature of this compound, since MB can be therapeutically useful to enhance the incubation period in prion diseases.

Finally, we investigated the effect of MB on the PrP fibrillization by promoting fiber formation of recombinant PrP. Our experiments on fibrillization of both HuPrP and OvPrP, with and without MB, carried out by means of ThT assay and TEM, successfully demonstrated a complete inhibition of the fibril formation in the presence of MB, at a molar ratio PrP:MB of 1:2 or lesser. However, TEM images provided evidence for a little reduction of the fiber formation, with respect to the control, already at an equimolar PrP:MB ratio.

Data of the the actual PrP form (oligomer and/or amyloid fibrils) that carry the toxicity and the infectivity on prion diseases are still matter of debate. However, fibrils obtained from recombinant PrP are reported to be toxic and also infectious (Legname et al., 2004; Lee et al., 2011), thus the effectiveness of MB also on the PrP fibrillization is a relevant feature, being fiber formation an essential step of the conversion process.

Possible mechanism of action of MB on the PrP conversion

MB belongs to a new class of inhibitor compounds that can prevent the oligomerization and fibrillization of proteins associated to amyloidogenic diseases. In fact, the action of MB was evaluated for several proteins, including A β , polyglutamine and TDP-43 (Necula et al., 2007; Gura, 2008; Yamashita et al., 2009).

Although many studies have reported the beneficial effects of MB on other amyloidogenic proteins, this molecule has been rarely considered for studies on prion conversion. In a previous work, MB showed no inhibition effect on PrP^{Sc} formation, together with high toxicity in neuroblastoma ScN2a cells (Korth et al., 2001). Anyhow, the authors have considered that some of the compounds tested, that could not be reliably examined because of their cytotoxicity forward ScN2a cells, might be

effective anti-prion drugs. Therefore, nowadays it would be worthwhile to conduct further studies, preliminarily *in vitro*. More recently, positive data were obtained about MB treated prion-filtered red cells utilized for neonatal exchange transfusion to reduce the risk of variant Creutzfeldt-Jakob disease transmission (Hornsey et al., 2010).

Several works, that already tested MB on other amyloidogenic proteins, have attempted to explain the mechanism by which MB interferes with the amyloidogenesis. In fact, MB might have distinct modes of anti-aggregation action. It has been reported that MB inhibits the A β 40 aggregation (Taniguchi et al., 2005). Differently, Necula *et al.* reported that MB inhibits A β 42 oligomerization but promotes fibrillization, suggesting that oligomer and fibril formation are distinct and competing pathways (Necula et al., 2007). Another protein, that has to be taken into account in AD, is the tau protein and MB was shown to be able to block the tau-tau binding interaction inhibiting tau filament formation (Wisichik et al., 1996; Taniguchi et al., 2005). It was also shown that MB could be useful for the treatment of TDP-43 proteinopathies. In this case, MB may bind to dimers and oligomers of TDP-43 and thereby inhibit fibril formation (Yamashita et al., 2009). All these studies lead to presume a general action of MB on those proteins that are correlated to misfolding diseases. However, it is worth pointing out that the mechanism underlying oligomerization and fibril formation still requires clarification, and could occur by different pathways for each disease-associated amyloid-forming proteins.

As far as PrP oligomerization and fibrillization is concerned (Griffith, 1967; Come et al., 1993), structural analysis and MD simulations revealed that OvPrP oligomerization requires a full detachment of the unfolded S1-H1-S2 segment from the H2-H3 α -helical bundle and the type of oligomer produced is controlled by the site where this protein expansion takes place (De Simone et al., 2007; Eghiaian et al., 2007). On this basis, we put forward a mechanism that might explain how MB antagonizes PrP oligomerization and fibrillization. Taking into account that MB slows down the oligomerization rate of all oligomers, but reduces the amount of only O1 oligomer, MB may modulate the PrP structural expansion in a reaction dependent manner i) by reducing local structural fluctuations of the intermediates that precede O2 and O3 oligomer, and thus, slowing down their formation rate, and ii) by stabilizing the intermediate state that leads to O1 oligomer formation through hydrophobic and electrostatic interactions, and thus, preventing the formation of this oligomer (Fig. II.15). Moreover, it was shown that O1 is the only oligomer able to fibrillize giving rise to a fiber-like aggregate (Eghiaian et al., 2007), thus, it is conceivable to presume that this oligomer may be the responsible for the fibril assemblies formation. Therefore, the stabilization of the intermediate which precedes O1 oligomer by a direct interaction with MB, could explain also the complete suppression of fibrillization.

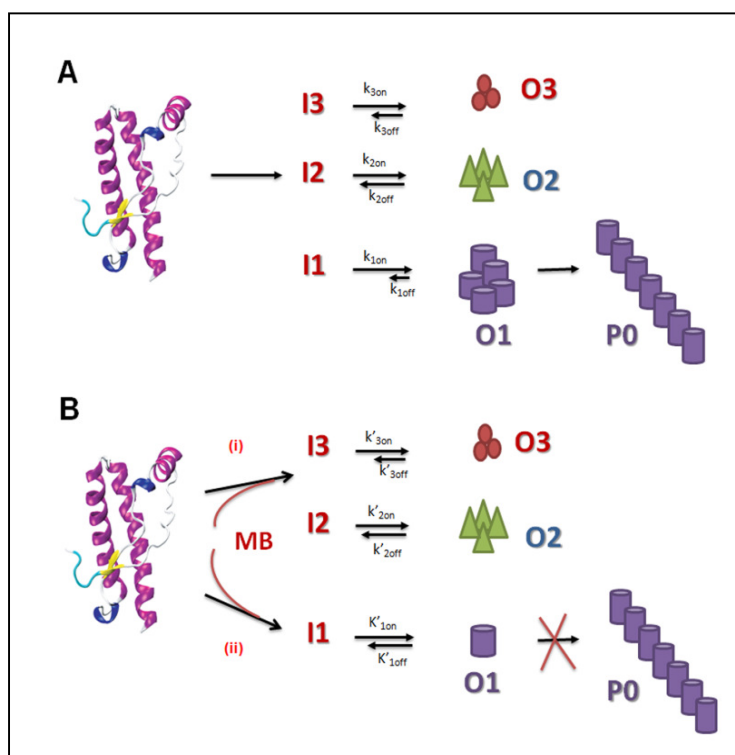


Figure II.15 Proposed mechanism of action of MB on the oligomerization/fibrillization of PrP. The PrP oligomerization process starts from a structural protein expansion leading to the formation of distinct intermediates, denoted by I, that precede each oligomer (A). MB may interact with the intermediates that precede each oligomer (B), (i) by slowing down the formation rate of all oligomers, and in addition (ii) by reducing the amount of the O1 oligomer and hence suppressing the fibrillization.

Currently, there are growing evidences that in other brain amyloidoses, soluble oligomers, as well as insoluble fibrils are toxic (Stefani et al., 2003; Lee et al., 2011). In particular, it has been reported that the oligomers generated from recombinant PrP are neurotoxic, *in vitro* and *in vivo* (Simoneau et al., 2007). On the other hand, PrP fibrils were shown to be infectious *in vivo* (Legname et al., 2004). Therefore, the action of MB on both PrP oligomers and fibrils is a highly valuable mark, since MB would act in both the PrP forms that are related to prion toxicity and infectivity, respectively.

To sum up, this thesis work is the first that shows the effective action of MB on the PrP conversion, *in vitro*. We demonstrate that MB can slow down the formation of PrP oligomers and limit the amount of higher assemblies. Finally, we demonstrate that MB is able to completely suppress the formation of PrP fibrils. As oligomerization and fibrillization are essential steps in the PrP^C to PrP^{Sc} conversion, MB acts as an antiprion agent. As a consequence, our findings deserve the evaluation of MB for *in vivo* studies and preclinical testing also for prion disease.

Chapter III Prion Protein and Aptamers

3.1 Nucleic-acid-binding properties of prion protein

The concept that a protein is the causative agent for TSEs challenged the traditional paradigm that disease transmission results solely from an agent that carries genetic information. Many independent studies all failed to identify specific nucleic acids in the scrapie agent, including viroid-like molecules, as well as to demonstrate any infectivity associated with nucleic acids extracted from the brains of infected animals (Marsh et al., 1974). This is also consistent with the exceptional resistance of the agent against physical, chemical and enzymatic treatments that degrade nucleic acids (Ward et al., 1974; Alper et al., 1987).

Although no additional molecule implicated in the pathogenesis has been found in PrP^{Sc} samples, the presence of a cofactor is still not completely ruled out. It has been suggested by several groups that an additional, as yet unknown, factor might initiate or modulate the PrP^C-to-PrP^{Sc} conversion (Telling et al., 1995; Nandi et al., 1999; Cordeiro et al., 2001). Several host macromolecules have been suggested as candidates for conversion catalysts: cellular adhesion molecules, nucleic acids, basal membrane molecules and sulfated glycans. These molecules have been reported to interact with PrP^C and to induce or modulate its conversion into a β -sheet-rich structure that shares many features with the infectious PrP (Caughey et al., 1994; Cordeiro et al., 2001; Horonchik et al., 2005).

The nucleic acids DNA and RNA form an interesting group of PrP molecular partners and several scientists have demonstrated that PrP can bind small NAs *in vitro* and *in vivo* with varying affinities (Beaudoin, 2008; Gomes, 2008b; Mercey, 2006). Moreover, the interaction of PrP with DNA or RNA can lead to conformational changes both to the protein and to the NA molecule (Cordeiro et al., 2001; Adler et al., 2003), which could suggest a biological significance of PrP binding to nucleic acids.

Anyhow, if the proteinaceous nature of the TSE agent now seems firmly established, the involvement of nucleic acids in triggering the initial polymerization events remains a possible scenario. In addition, mysteries still obscure the status and biological functions of the cellular protein, the knowledge of which could help understand many aspects of the pathophysiology of prion diseases (Marc, 2010). These open questions have also motivated the studies of prion protein's interaction with nucleic acids.

3.1.1 Are the nucleic acids involved in the physiology and/or in the pathology of prion protein?

The nucleic acid-binding properties of the prion protein (both RNA and DNA) might have broader implications either for its native function or for disease.

From a structural point of view, the 3D-structure of mouse PrP in complex with an 18 bp double-stranded DNA (dsDNA) was derived from SAXS and NMR measurements (Lima et al., 2006). In particular, NMR HSQC spectra revealed changes that are

clustered in two major domains: one in the disordered N-terminal part of PrP and the other in the C-terminal globular domain. Another *in silico* study (Tjong et al., 2007), predicted that the PrP globular domain recognizes DNA mainly through the α -helix H1. As result, both PrP domains show the ability to bind DNA.

On the other hand, an NMR study of the interaction between murine rPrP and a synthetic RNA sequence (SAF93^{43–59}) revealed that part of the N-terminal domain has undergone modifications upon RNA binding (Gomes et al., 2008^b). Moreover, a rPrP mutant lacking residues 23–90 was not able to bind RNA, demonstrating that the amino-terminal region is crucial for RNA interactions (Gomes et al., 2008^a; Gomes et al., 2008^b).

Physiology of the nucleic acid binding to PrP.

It is worth mentioning that the nucleic acid segments (DNA or RNA) that have been hitherto described to bind or affect PrP conversion are very different from those of a genomic NA. The described NA-dependent effects occur *via* sequences with unknown cellular functions and that are also much smaller than those that could carry enough genetic information. So is there any *in vivo* functional implication for the NA binding properties of PrP^C? The *in vitro* studies showed nanomolar affinities for some complexes with DNA or RNA, suggesting that these molecules represent interesting candidates for *in vivo* PrP binding (Cordeiro et al., 2001; Takemura et al., 2006). In fact, PrP shares similarities with nucleic acid binding proteins (Gabus et al., 2001) and has a mapped DNA-binding region on its globular domain (Lima et al., 2006). Therefore, several findings point to a physiological role for PrP as an NA-binding protein.

Furthermore, the idea of an NA chaperoning properties possessed by PrP has recently emerged, since NA-binding by PrP^C can lead to structural rearrangements in both binding partners, with folding/refolding of the NA and folding/oligomerization of the protein (Nandi et al., 1999; Gabus et al., 2001). This hypothesis could be supported also by the fact that, so far, no specific NA sequence was recognized by PrP and the RNA-chaperoning activity includes specific and non-specific RNA (Clodi et al., 1999). Moreover, with the capacity to bind both small RNAs and DNAs, PrP might exert its function by participating in the gene regulation array at the post-transcriptional level, acting as a NA chaperone (Bera et al., 2007).

Finally, it is worth mentioning that a general overview of nucleic acids so far studied suggests that long molecules of RNAs and DNAs generally induce the formation of large nucleoprotein aggregates, while the interaction with short RNAs or DNAs results in a soluble or oligomerized β -sheet PrP (Cordeiro et al., 2001; Gabus et al., 2001; Gomes et al., 2008^b). This has led to speculate that the transition of PrP to a beta-rich structure could represent a physiological mechanism. On the contrary, some DNA and RNA molecules seem to prevent or stop PrP aggregation in infected cells (Silva et al., 2010). This capacity has been explored in possible therapeutic and diagnostic strategies for prion disease.

Pathology of the nucleic acid binding to PrP.

Besides the potential physiological role of the PrP-NA complexes, one of the most intriguing features of the interaction between PrP and NAs is the finding that some NA sequences can act as catalysts for the formation of a scrapie-like PrP

conformation. Indeed, previous works have shown that the binding of PrP to small double-stranded NA sequences increases the β -sheet content of the protein and, depending on the PrP:NA molar ratio, protein aggregates can be formed (Cordeiro et al., 2001). These aggregates are mainly amorphous although, under some conditions, NA binding can promote partial unfolding of PrP, triggering formation of an amyloid-like structure that resembles PrP^{Sc} in its resistance to proteinase-K digestion (Deleault et al., 2003; Gomes et al., 2008^b). Moreover, highly structured RNAs can also convert human PrP^C into PrP^{Sc}-like forms (Adler et al., 2003), and some RNA aptamers bind with high specificity to PrP^{Sc} (Rhie et al., 2003).

An interesting study brought compelling evidence to the hypothesis that NAs might catalyze PrP conversion, with the use of PMCA technique. PMCA occurs through the incubation of PrP^C with an excess of PrP^{Sc}, either from brain homogenates or from a purified source (Deleault et al., 2007). Using this approach, with a preparation containing only native PrP^C and co-purified lipid and mouse liver RNA, it was obtained successful PMCA propagation of PrP^{Sc} molecules. The conversion was confirmed by the observation of the disease occurrence after inoculation of the *de novo* PrP^{Sc} molecules formed into mice (Wang et al., 2010). This seminal work shows that infectious prions can be formed from a minimal set of components including synthetic NA, stressing the possible role of nucleic acids in PrP^{Sc} generation. These results led to propose the hypothesis of NA-catalyzed PrP conversion (Cordeiro et al., 2005). Accordingly, host NAs might catalyze the PrP^C->PrP^{Sc} conversion by acting as a scaffold or surfaces and thereby facilitating the interaction between PrP^C and PrP^{Sc} molecules. From the energetic point of view, NA molecules would act by lowering the free-energy barrier between PrP^C and PrP^{Sc}, thus triggering conversion.

Figure III.1 shows the template assistance model of PrP conversion together with the models proposed for the catalyst action and/or molecular chaperone of NAs on the PrP^C-to-PrP^{Sc} conversion (Cordeiro et al., 2005). In the NA-catalyst models, the formation of large aggregates of PrP^{Sc} would need the presence of exogenous PrP^{Sc} (or generated from spontaneous conversion of PrP^C into PrP^{Sc}), which would rescue the already converted PrP^{Sc} from the NA. The freed NA would then be able to catalyze another conversion, amplifying the process (Silva et al., 2008).

However, *in vitro* studies showed the dependency of the extent of aggregation on the molar ratio between PrP and NA, so that an apparently irreversible process, in the direction of PrP aggregation, predominates within a high PrP to NA ratio (Cordeiro et al., 2001). However, the precise mechanism behind this catalyzed conversion is still not completely understood and further studies must be done in order to determine how NAs play in the PrP conversion mechanism.

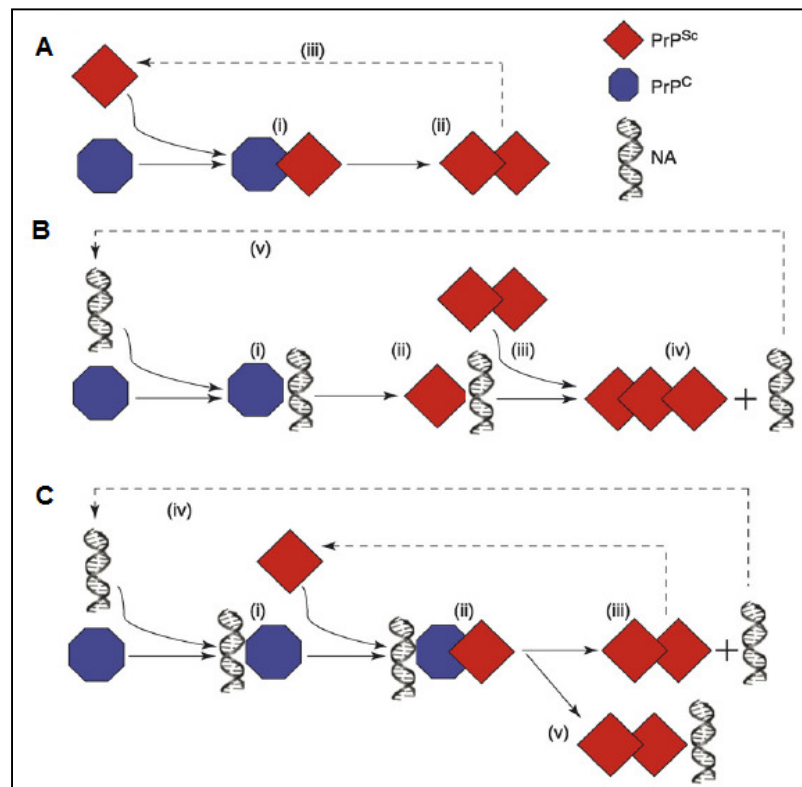


Figure III.1 Models for nucleic acid-mediated prion propagation. The models propose how a NA (gray) can act on the PrP^C (blue) to PrP^{Sc} (red) conversion. A) Template-assisted refolding model. PrP^{Sc} interacts directly with PrP^C (i) and helps the latter to assume the PrP^{Sc}-like conformation (ii). Formed PrP^{Sc} is able to catalyze conversion of more PrP^C into the infectious species (iii). B) Binding of NA by PrP^C (i) induces the acquisition of the β -sheet-rich conformation (ii). Following the addition of PrP^{Sc} oligomers (iii), larger aggregates are formed and the nucleic acid is released from the complex (iv). It is then able to catalyze another conversion event (v). C) Formation of the PrP^C-NA complex (i) would act as a scaffold for binding of PrP^{Sc} to the protein part of the complex (ii), leading to conversion into scrapie-like conformation and giving rise into the net conversion of more PrP^{Sc} (iii). The NA could be released from the complex, after PrP^{Sc} formation (iii) being able to contribute to further conversion (iv), or could be irreversibly incorporated into the infectious aggregated particle (v). After (Silva et al., 2008)

3.1.2 Prion protein and DNA/RNA aptamers

Originally, the term “aptamer” designated synthetic RNA or DNA molecules selected from combinatorial libraries to specifically bind small molecules or proteins. SELEX is the most employed *in vitro* method used to isolate, starting from a very large pool of random sequences, one or a few families of nucleic acid sequences that satisfy the selection criteria (Tuerk et al., 1990). Indeed, in the search for nucleic acids that could bind with high affinity and specificity to prion protein, several authors used SELEX method. This method has allowed to identify DNA and/or RNA sequences capable to bind PrP^C and/or PrP^{Sc}.

To the purpose of isolating aptamers that could distinguish PrP^C from its pathological isoform PrP^{Sc}, Weiss *et al.* were the first authors to carry out the SELEX method in the prion field, with the selection of various RNA aptamers able to bind to the recombinant Syrian golden hamster PrP (Weiss et al., 1997).

Beside the highly specific ligands that can be selected by SELEX method, PrP has been shown to bind a variety of DNAs or RNAs, that have proved very useful in covering many aspects of the PrP-nucleic acids interaction.

Therefore, a question arises regard the selected DNA and RNA aptamers by SELEX hitherto studied: Do these aptamers share a common sequence or a structural motif? Unluckily, a sequence analysis of the reported PrP specific-aptamers reveals no obvious sequence motif for DNA and RNA aptamers. Anyhow, a comparison of the RNA- or DNA-ligands that were isolated from independent laboratories has revealed: i) conserved sequence patterns that were present in a few independently obtained aptamers, and ii) a relatively frequent structural feature consisting of a guanine quadruplex. Regarding the shared sequence of the aptamers, some of them were characterized by the following pattern: AAG(A or G)(C or U)GUCGGGG-N₀₋₁-UUGGCA-N₀₋₁-AA, where N₀₋₁ is zero or one nucleotide (Marc, 2010). In other cases, the aptamers presented repeated guanine triplets (GGG....GGG....GGG...GGG). Anyhow, in both cases, the sequence contains repeated guanine duplets or triplets. Besides the common sequence, these aptamers share also a common structure. Indeed, they can adopt a guanine quadruplex-structure (Weiss et al., 1997). Many works have reported that this structure seems necessary for the interaction, since its disruption, by replacing the guanosine with uridines, completely abolishes the interaction with PrP. Thus, G-quadruplexes may represent a common recognition motif (Gatto et al., 2009). Guanine-quadruplexes are a structural motif composed of two or more tetrads of coplanar guanosines (G-quartets) that are stacked on top of each other (Keniry, 2000).

It is worth mentioning that beside G-quadruplexes, other structural motifs have been described in RNA- and DNA-aptamers raised against PrP (Adler et al., 2003; Mercey et al., 2006; Takemura et al., 2006). In some cases, the requirement of these structures for PrP-binding has been probed by various methods. However, the absence of any obvious relation between them, precludes the identification of a consensus structural pattern.

From a structural point of view, taking together the results of several studies, the interaction of PrP with nucleic acids seems to involve at least three distinct sites in the protein: two of them located at the ends of the unstructured N-terminal domain, and the third in the C-terminal globular part. In particular, there are two lysine clusters located in the N-terminal domain of PrP that were assigned as possible binding sites of NAs. The first one encompasses the residues K²⁵KRPKPGGGW³⁴ in OvPrP and it was reported to be the major nucleic-acid binding site (Mercey, 2006 ;Weiss, 1997). NAs could interact with these aa through charge interaction with low specificity and high affinity. The second binding site in PrP for nucleic acids is another lysine cluster (W¹⁰¹NKPSKPKT¹¹⁰ in sheep PrP) (Lima et al., 2006; Mercey et al., 2006). Interestingly, both lysine-clusters contain alternating proline and basic residues, a feature that is reminiscent of the binding motifs found in proteins that are known to interact with nucleotides and nucleic acids. The binding to this second lysine cluster does not rely solely on charge interaction but may also involve stacking interactions with tryptophan residue 101. In fact, the overlapping peptide K¹⁰³PSKPKTNM¹¹², lacking residue W¹⁰¹, did not bind in spite of its three basic lysine residues.

Beside these two interaction sites in its disordered N-terminal domain, the structured C-terminal domain of PrP also contributes to nucleic acid binding. Studies based on SAXS and NMR spectroscopy have shown that the globular and unstructured domains of PrP are both involved in the interaction with nucleic acids. A comparison of the chemical shifts between the NMR spectra of free and DNA-bound hamster PrP

point to several residues in the structured domain from arginine 136 to alanine 224, that interact with E2DBS, a 18 bp DNA (Lima et al., 2006). Therefore, each of these three sites in PrP may cooperate in binding nucleic acids through either of the two main modes through which proteins are known to interact with nucleic acids: i) binding to the groove of a nucleic-acid helix, through charge interactions with the backbone, and/or ii) sequence-specific recognition of unstacked bases into binding pockets of the protein (Shulman-Peleg et al., 2008).

Finally, regarding the recognition of PrP toward nucleic acid, most of the aptamers that have been raised against PrP from one species, also recognized PrP from other species (Weiss et al., 1997; Mercey et al., 2006; Takemura et al., 2006). This is not unexpected, considering the high conservation of PrP polypeptide sequence, which is close to 100% in the PrP regions involved in nucleic acid binding. In addition, most of these aptamers recognize both PrP^C and its pathological isoform PrP^{Sc}, except for some of them that show some specificity towards PrP^{Sc} or the β -oligomeric isoform of recombinant PrP, as a result of the selection process (Weiss et al., 1997; Rhie et al., 2003). Considering the interaction from the other side, PrP was shown to bind a large variety of nucleic acids that were either identified through SELEX, or tested individually. As no obvious consensus sequence or structural pattern could be extracted from the comparison of these ligands, NA aptamers include both single-stranded and double stranded DNAs, as well as RNAs with diverse structures. However, this diversity should not lead to the conclusion that PrP binds any nucleic acid with no specificity, since modifications of RNA or DNA aptamer often reduce binding (Takemura et al., 2006). Moreover, most of the nucleic acid-binding proteins do not bind only one well defined sequence, but may instead functionally interact with more than one structural or sequential pattern, suggesting that the large group of NAs capable to bind PrP do not rule out a physiological meaning of this interaction.

3.1.3 D12 and R12 aptamers against prion protein

In a previous work, RNA aptamers against recombinant bPrP and its amyloidogenic β isoform (bPrP- β) were obtained by means of SELEX method (Tuerk et al., 1990) from RNA pools containing a 55-nt randomized region (Murakami et al., 2008). The recombinant amyloidogenic prion protein, bPrP- β , was generated through chemical treatment of recombinant bPrP, with the assumption that bPrP- β resembles PrP^{Sc} in terms of structural and biochemical properties (Baskakov et al., 2002).

Interestingly, all RNAs contained tandem GGA repeats, mainly four continuous GGA triplet repeats (GGA)₄. These RNA aptamers showed high affinity to both bPrP and bPrP- β and moreover, were able to detect PrP^C in a bovine brain homogenate on northwestern blotting assay (Murakami et al., 2008). Since the conserved region (GGA)₄ plays an important role for specific binding to bPrP and bPrP- β , the authors minimized the selected aptamers to a 12-nt RNA, r(GGA)₄, in order to evaluate if this region is the minimal sequence required to keep the interaction with the PrP. In this manner, they could demonstrate that the minimized 12-nt RNA retained the binding ability toward bPrP and bPrP- β and thus, the conserved core sequence of tandem GGA repeat (GGA)₄ is the region relevant for this binding. Moreover, it is worth mentioning that the appearance of the tandem GGA in anti-PrP RNA aptamers is relatively high, thus GGA repeat must be meaningful for specific binding to PrP (Weiss et al., 1997; Proske et al., 2002; Gatto et al., 2009). This is further

confirmed by experiments in which substitutions were applied in the conserved region (GGA)₄. The results revealed a decrease of the binding ability of the aptamer mutants toward bPrP- β while a moderate decrease in binding affinity was observed with bPrP (Murakami et al., 2008).

Another intriguing feature of the aptamers containing a GGA repeat is the ability to adopt a unique quadruplex structure in the presence of K⁺ ions (Kettani et al., 2000). NMR experiments, performed under physiological K⁺ conditions, have been made on the 12-nt RNA r(GGA)₄, (R12), and 12-nt DNA d(GGA)₄, (D12), showing that one R12 molecule folds into an intramolecular parallel quadruplex with a G:G:G:G tetrad plane and a G(:A):G:G(:A):G hexad one. Then, two R12 quadruplexes form a dimer in a tail-to-tail manner, through hexad–hexad stacking (Mashima et al., 2009). Analogously, one D12 strand forms a quadruplex with four G-G segments aligned parallel to each other, and then two D12 quadruplex form a dimer in a tail-to-tail manner (Matsugami et al., 2001). Although the R12 structure shares several common features with the structure formed by the DNA counterpart molecule, remarkable differences between the R12 and D12 structures have also been noted. In Figure III.2 both structures of R12 and D12 are schematically shown. The R12 quadruplex comprises a G(:A):G:G(:A):G hexad plane in addition to a G:G:G:G tetrad plane, while the D12 quadruplex comprises a G(:A):G(:A):G(:A):G heptad plane in addition to a G:G:G:G tetrad plane; the dimerization occurs through heptad-heptad staking (Mashima et al., 2009). Moreover, the dyad axis correlating two monomers is along the A3-A9 direction for R12, but is perpendicular to the A3-A9 direction for D12.

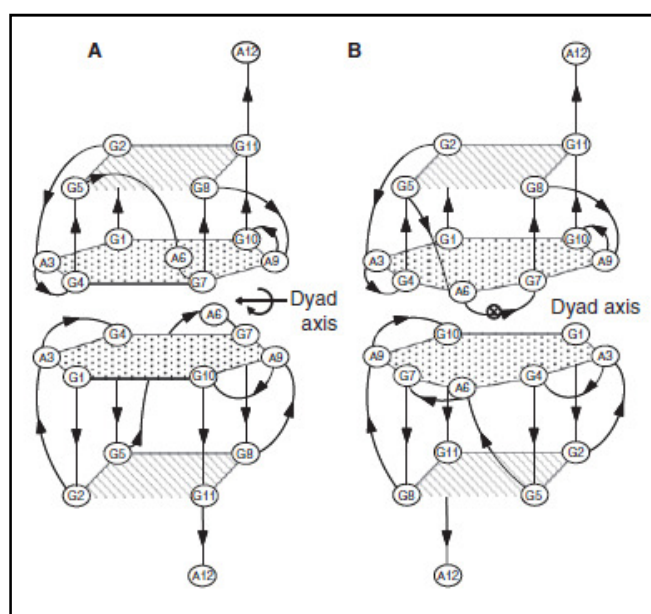


Figure III.2 Schematic representation of the R12 structure (A) and the D12 structure (B). A dyad axis correlating the two monomers is indicated for each structure.

The quadruplex fold, adopted by PrP-binding aptamers, seems an essential feature for the PrP recognition. Indeed, a work on RNA aptamers, selected against recombinant Syrian golden hamster PrP, reported that the G quartet scaffold is required for the interaction with PrP, since the replacement of guanosine with uridine completely hampers the binding with PrP (Weiss et al., 1997).

Summarizing, DNA and RNA aptamers must have two essential features to be able to specifically interact with both α -rich PrP isoform and β -PrP: i) the presence of a minimal sequence core of four tandem GGA repeat (GGA)₄, and ii) a G quadruplex architecture.

In this context, taking into account the minimal sequence of both DNA and RNA aptamers required for a specific interaction with PrP, calorimetric, spectroscopic and SPR studies were here performed in order to characterize thermodynamically, kinetically and structurally the interactions between OvPrP and both D12 and R12. Moreover, structural investigations were conducted using various PrP domains in order to obtain insight into the PrP regions involved in the interaction and the nature of the forces that drive these bindings.

3.2 Experimental procedures

- *Sample preparation*

The full-length PrP from sheep PrP (23-234) and the truncated form Δ OvPrP (103-234) were produced as described in Section 2. 2. The buffer used to desalt the protein, on a HiPrep desalting column, was MES 15 mM pH 6.0, KCl 70 mM. Protein concentration was measured by optical density at 280 nm with the procedure described in Section 2.2.

Aptamers were purchased from PRIMM (Milan). The aptamer samples were prepared by dissolving the lyophilized compound in MES 15 mM, KCl 70 mM at pH 6.0. The solution has been annealed by heating at 95 °C for 5 min and slowly cooling to room temperature. The concentration of the dissolved oligonucleotide has been evaluated by UV measurement at 95 °C, using as molar extinction coefficient the value calculated by the nearest-neighbor model (Cantor et al., 1970) for the sequence d(GGAGGAGGAGGA), r(GGAGGAGGAGGA) and d(TGGGGT).

The unfolded D12 solutions were obtained by dialysis against MES 15 mM pH 6.0, to remove the K⁺ ions.

- *Isothermal Titration calorimetry.*

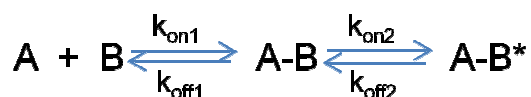
ITC experiments were carried out at 298 K using a high-sensitivity CSC-5300 Nano-ITC microcalorimeter from Calorimetry Science Corporation (Lindon, Utah) with a cell volume of 1ml. Only after reaching the baseline stability, the experiments were launched. In each titration experiment, volumes of 10 μ L of a solution containing D12, R12 and d[(TGGGGT)₄] at a concentration of 80÷130 μ M were injected into a solution with the prion protein in the same buffer (MES 15 mM pH 6.0 KCl 70 mM), using a computer-controlled 250 μ L microsyringe. The OvPrP forms were prepared at a concentration of 16 μ M. In order to allow the system to reach the equilibrium, we applied a time interval of 300 or 400 s between each ligand injection. Heat produced by ligands dilution was evaluated by performing a control experiment, titrating each ligand into the buffer alone. The interaction heat for each injection was calculated after correction for the heat of ligand dilution. The corrected heat values were plotted as a function of the molar ratio aptamer:PrP, to give the corresponding binding isotherms. The resulting isotherms were fitted to a single set of identical sites model employing a nonlinear least-squares minimization algorithm to a theoretical titration curve, using the program Bindwork from Calorimetry Science Inc. $\Delta_b H^\circ$ (reaction

enthalpy change in kJ mol^{-1}), K_b (binding constant in M^{-1}), and n (number of binding sites) were the fitting parameters. The Gibbs energy and the entropic contribution were calculated using the relationships $\Delta_b G^\circ = -RT \ln K_b$, ($R = 8.314 \text{ J mol}^{-1} \text{ K}^{-1}$, $T = 298 \text{ K}$) and $-\Delta_b S^\circ = \Delta_b G^\circ - \Delta_b H^\circ$.

- *Surface Plasmon Resonance.*

For technical and instrument details see Section 2.2. SPR experiments were performed immobilizing the full-length OvPrP and ΔOvPrP domain on the sensor surface of a CM5 chip, using a standard amine coupling procedure. Then, D12 and R12 aptamers, as well as $d[(\text{TGGGGT})_4]$, were injected as analytes at various concentrations (from 200 nM to 50 μM) and using MES 15 mM, pH 6.0 KCl 70 mM as running buffer. OvPrP covalently immobilized chip was subsequently regenerated by removed bound analytes using the mobile phase buffer Glycine 10 mM, pH 2.5, injected 180 s after the analyte injection. Data were corrected using a blank sensor chip as control.

The SPR sensorgram for each protein-aptamer interaction were analyzed by curve-fitting using BIAevaluation software provided with the Biacore device. Various reaction models were applied to perform complete kinetic analysis of the protein sensorgram. The fitting was performed in such a way that the χ^2 value, representing the statistical closeness of curve-fitting, became the lowest. It was recommended ideally to be below 10. The best fitting was achieved by the two-state reaction (conformation change) model which is described by the following equation:



where A is the immobilized protein, B is the aptamer, AB represents the protein-aptamer complex and AB* represents the complex after the conformational change.

- *Circular Dichroism.*

For technical and instrument details see Section 2.2. Far-UV measurements (190 ÷ 250 nm) were carried out in MES 15 mM pH 6.0 KCl 70 mM at 20 °C using a 0.1 cm optical path length cell. CD titration was performed on the full-length and truncated OvPrP, keeping the concentration of PrP constant (10 μM), and increasing the concentration of the aptamers up to a molar ratio PrP/aptamer of 1:2.

Each solution of the mixture PrP-aptamer was prepared independently, without successive additions of the aptamers in the PrP solution to avoid complications due to dilution effects within titration experiments. CD spectra, recorded with a time constant of 4 s, a 2 nm band width, and a scan rate of 20 nm min^{-1} , were signal-averaged over at least three scans. The baseline was corrected by subtracting the buffer spectrum.

3.3 Results

Binding analysis of the interaction between prion protein and quadruplex structures

In order to study the kinetics and the thermodynamics of the binding between OvPrP and both D12 and R12 aptamers, we used ITC and SPR. Various PrP forms were investigated to identify the regions involved in the interaction with both DNA and RNA, as well as the type of interactions that take place. In particular, the following PrP proteins were used: i) the full-length OvPrP (23-234), and ii) the deleted Δ OvPrP (103-234) which partially lacks the unstructured N-terminal part. All experiments were conducted at pH 6.0. It is worth mentioning that the full-length PrP contains all the three potential binding sites, i.e., the two lysine clusters (aa 25-34 and 101-110 in OvPrP) in the N-terminal region and the third site consisting of various aa located in the structured C-terminal domain, whereas the deleted form (Δ OvPrP) lacks the first lysine cluster (Fig. III.3).

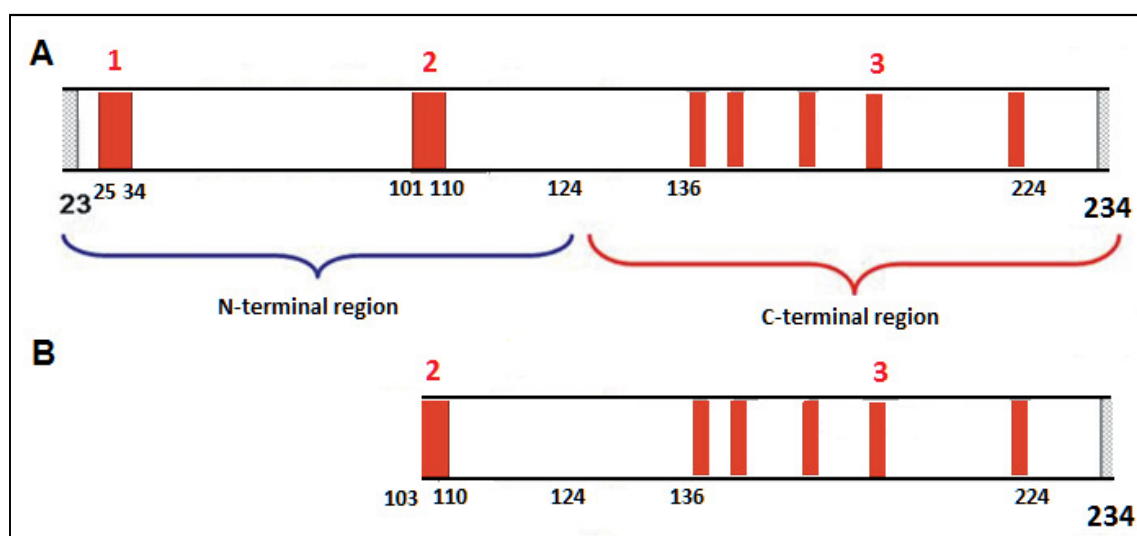


Figure III.3 Schematic representation of the OvPrP forms used. A) Full-length OvPrP (23-234); B) Δ OvPrP (103-234). The areas in the sequence, depicted in red, and the related numbers, correspond to the putative PrP binding sites for NAs.

Since for this study, only the ovine prion protein species was used, the protein is reported as PrP, for simplification.

Thermodynamic data obtained by ITC experiments

The integrated heat data, along with the corresponding raw ITC profiles (insets) obtained by ITC measurements for the titration of the full-length PrP and Δ PrP with both D12 and R12, are shown in Figure III.4. The raw data for all the titration experiments indicate an exothermic interaction, based on the positive values observed for the peaks. Thermodynamic parameters, obtained from the fitting of the binding isotherms, are summarized in Table III.1, with the exception of the system full-length PrP and D12, from which no thermodynamic parameters were derived. Indeed, although the corresponding raw ITC has the typical profile of an exothermic reaction, precipitation was observed at the end of ITC experiments, precluding the

possibility to obtain the thermodynamic parameters related to this system. Differently, no precipitation was detected for the interaction between the full-length PrP and R12, as well as for Δ PrP with both D12 and R12 aptamers. For the determination of the thermodynamic parameters, both D12 and R12 aptamers were considered to be dimeric.

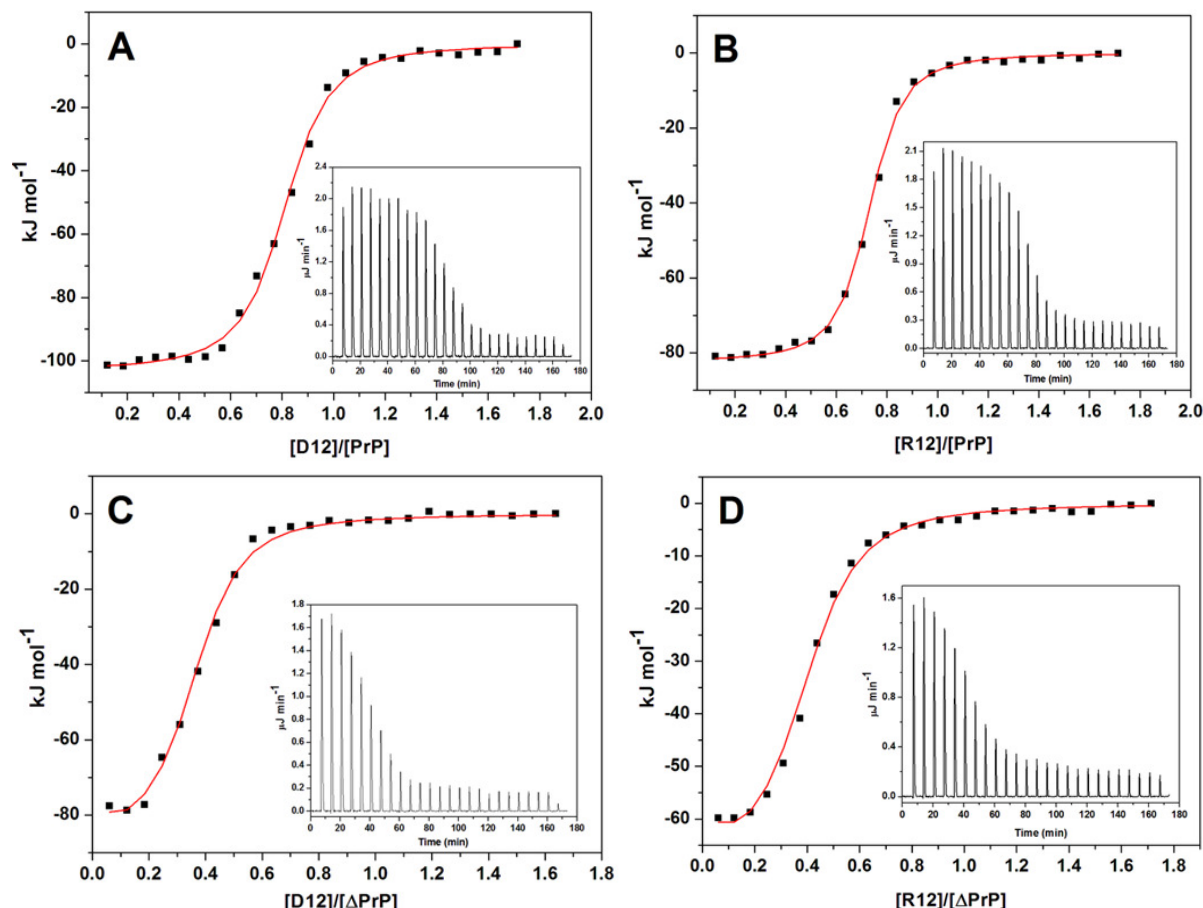


Figure III.4 ITC titration experiments. Binding isotherms and raw ITC profiles (insets) for full-length PrP with D12 (A) and R12 (B); and for Δ PrP with D12 (C) and R12 (D).

The ITC data for R12 binding to full-length PrP indicate the formation of a 1:1 protein-aptamer complex with the highest binding affinity ($K_b = 1.3 \times 10^7 \text{ M}^{-1}$). Another kind of complex is formed with the truncated protein, since the binding stoichiometry of Δ PrP, with both D12 and R12, was 1:0.5 with similar K_b values. Comparison of the thermodynamic constants related to the interaction of the full-length and the truncated protein with R12 show that K_b is one order of magnitude higher for the full-length PrP than for Δ PrP. Anyhow, the values of the Gibbs energy variations indicate that, from a thermodynamic point of view, the interaction of prion protein with the aptamer molecules is strongly favored at 25 °C.

The favorable enthalpy variation values (from -86.2 to -68.4 kJ mol^{-1}) and the unfavorable entropies (from -49 to -32 kJ mol^{-1}) indicate that, in all cases, the binding processes are enthalpically driven. Anyhow, R12 binding to Δ PrP has a lesser favorable enthalpy ($\Delta_b H^\circ = -68.4 \text{ kJ mol}^{-1}$) as compared to the other systems.

Table III.1 Thermodynamic parameters for the interaction of the full-length PrP and the truncated PrP with D12 and R12 aptamers, and d[(TGGGGT)₄] determined by ITC at 25 °C and pH 6.0.

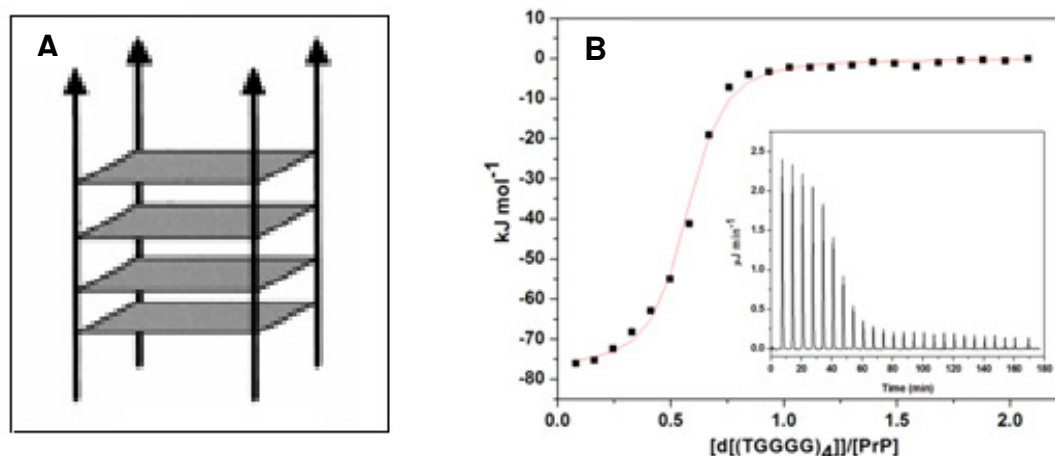
	n	K_b (M ⁻¹)	$\Delta_b H^\circ$ (kJ mol ⁻¹)	$T\Delta_b S^\circ$ (kJ mol ⁻¹)	$\Delta_b G^\circ$ (kJ mol ⁻¹)
PrP + D12	ND	ND	ND	ND	ND
ΔPrP + D12	0.5 ± 0.1	(3.1 ± 0.2) × 10 ⁶	-86.2 ± 2.0	-49 ± 2	-37 ± 2
PrP + R12	0.9 ± 0.2	(1.3 ± 0.1) × 10 ⁷	-81.6 ± 1.0	-41 ± 2	-41 ± 2
ΔPrP + R12	0.5 ± 0.1	(2.2 ± 0.3) × 10 ⁶	-68.4 ± 1.0	-32 ± 2	-36 ± 2
PrP + d[(TGGGGT)₄]	0.5 ± 0.2	(5.2 ± 0.1) × 10 ⁶	-76.4 ± 1.0	-38 ± 2	-38 ± 2

ND = not determined

n = number of PrP binding sites

We tested also the interaction of the full-length PrP with the truncated sequence of *Tetrahymena* telomeric DNA, d(TGGGGT), which forms a parallel tetramolecular quadruplex in the presence of K⁺ ions, containing four equivalent grooves (Laughlan et al., 1994). Although this sequence differs from the sequence of D12 and R12 (containing four GGA repeated triplets), it still contains contiguous guanine and, furthermore, folds in a G-quadruplex, [d(TGGGGT)₄].

In Figure III.5A the schematic structure of a parallel tetramolecular G-quadruplex is shown. Raw ITC data relative to the interaction of the full-length PrP with [d(TGGGGT)₄] showed a similar profile to those obtained with both D12 and R12 aptamers (Fig. III.5B).

**Figure III.5** A) Schematic structure of a parallel tetramolecular G-quadruplex. B) Binding isotherm and raw ITC data (inset) for titration of the full length PrP with d[(TGGGGT)₄].

The thermodynamic parameters obtained from ITC titration revealed a high affinity of PrP also toward this quadruplex ($K_b = 5.2 \times 10^6$ M⁻¹), but with a binding stoichiometry

of 1:0.5 (Table III.1). The binding enthalpy change is in between the values corresponding to the interaction of R12 with the full-length and the truncated PrP. ITC results suggest that the high affinity of PrP toward these nucleic acids is presumably due to the presence of contiguous guanines in the sequence. Moreover, PrP seems to specifically interact with DNA and RNA that fold into quadruplex structures. To confirm the specificity of PrP toward the quadruplex DNA and RNA, D12 was unfolded by removing K^+ ions from the solution, and an ITC titration was performed using only Δ PrP, to avoid difficulties due to precipitation with the full-length PrP. As shown in Figure III.6, the heat changes obtained upon addition of the unfolded D12 correspond to the heat of the ligand dilution. Therefore, the results fully demonstrated the failure of Δ PrP interaction with the unfolded D12, lacking the quadruplex structure.

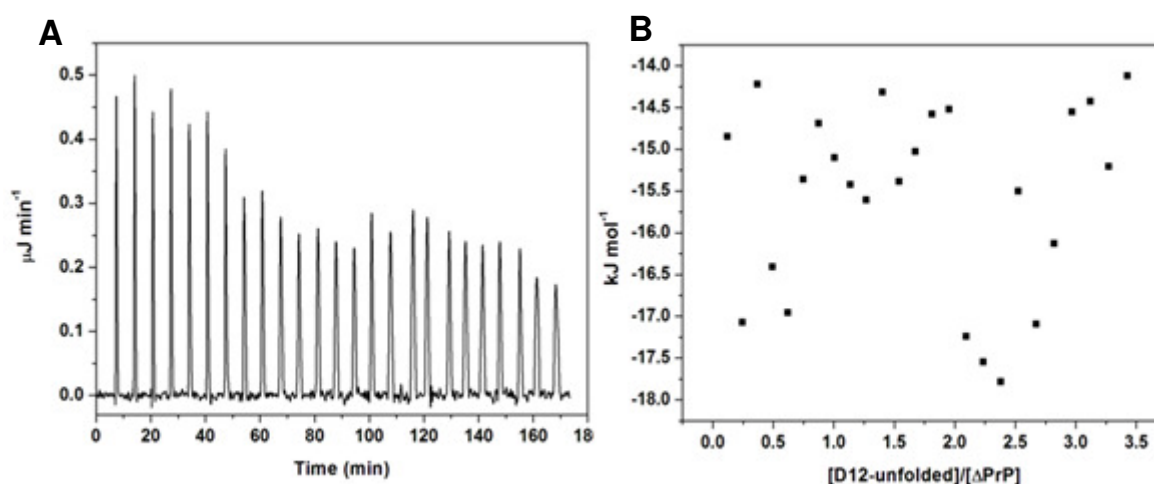


Figure III.6 ITC titration experiments related to the binding of Δ PrP with the unfolded D12. A) Raw ITC profile; B) Plot of heat change on ligand addition against the ligand:PrP molar ratio.

Kinetic and binding data obtained by SPR experiments

To validate the ITC data and to get insights into the kinetics of the interactions, SPR experiments were performed testing the interaction of both D12 and R12 aptamers with the same PrP forms used for ITC experiments. In particular, the PrP proteins were immobilized on different channels of a sensor chip and solutions of various concentrations of D12 and R12 were injected over the surface chip.

As previously mentioned, the interaction of D12 with the full-length PrP leads to precipitation, thus, no information was obtained by ITC analysis. In contrast, SPR experiments allowed the estimation of the affinity of this interaction, since the binding reaction occurs in a solution-independent manner. In Figure III.7, the SPR sensorgrams corresponding to the interaction of D12 and R12 aptamers with both the immobilized full-length and truncated PrP, are shown.

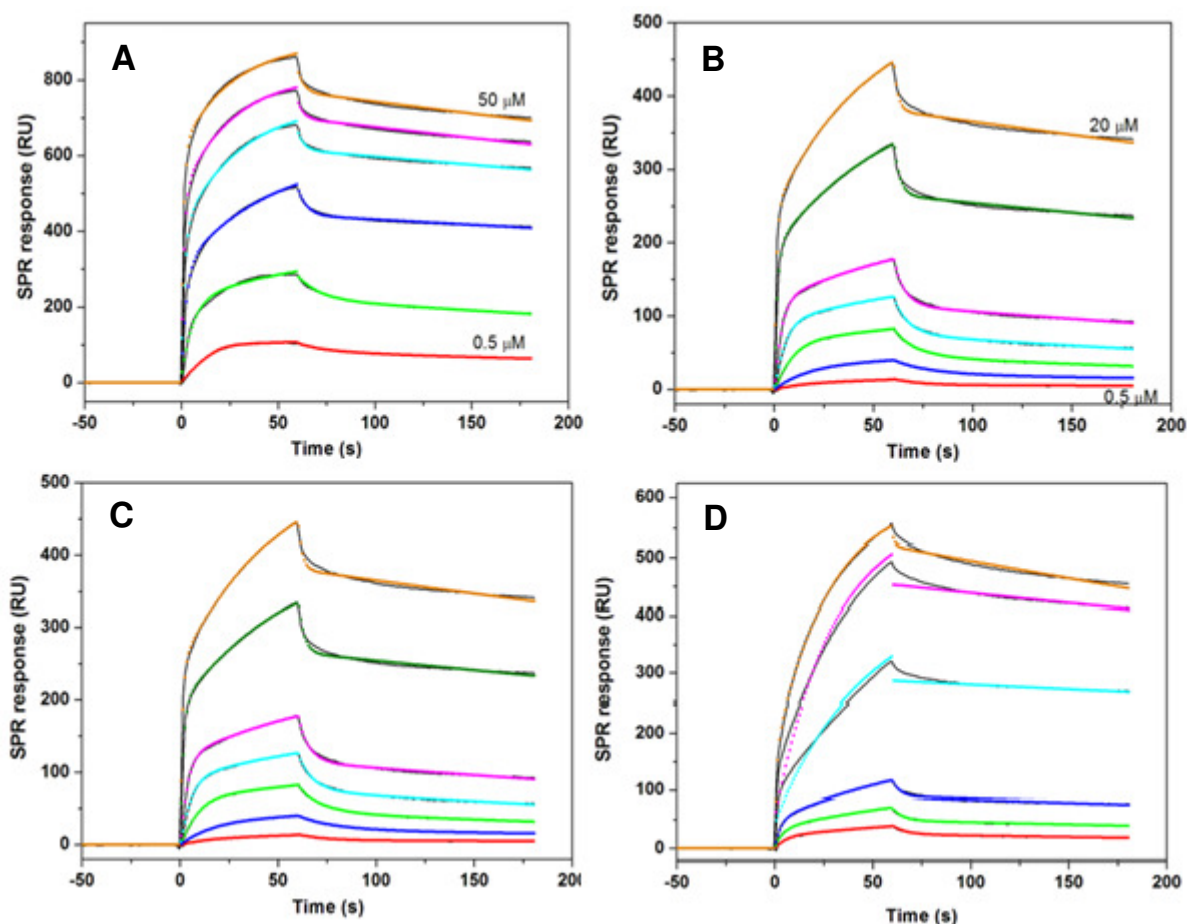


Figure III.7 Time Evolution of the SPR sensorgrams obtained at various concentrations of the aptamers (in the range from 0.5 μM to 50 μM). Sensorgrams related to the full-length PrP with D12 (A) and R12 (B). Sensorgrams related to ΔPrP with D12 (C) and R12 (D). Each SPR sensorgrams is reported with the corresponding fit (dot lines), based on a two state reaction model which includes a conformational change.

All SPR sensorgrams were analyzed, by applying various kinetic models. The best fits were yielded with the two state reaction model that takes into account a conformational change upon complex formation. The two states reaction model can be described by two steps: i) the formation of the initial protein-aptamer complex, and ii) the subsequent conformation rearrangement that can take place on the protein and/or on the aptamers (Fig. III.8). Thus, SPR experiments allowed not only to kinetically characterize these systems, but also to obtain structural information regarding the systems studied. Indeed, these results are in agreement with previous studies in which structural variations for both PrP and NAs were reported.

From the fitting of the SPR sensorgrams, the association ($k_{\text{on}1}$, $k_{\text{on}2}$) and dissociation rate constant ($k_{\text{off}1}$, $k_{\text{off}2}$) of the two reaction steps were derived. In Table III.2 the kinetic constants for the PrP-aptamers interactions are summarized.

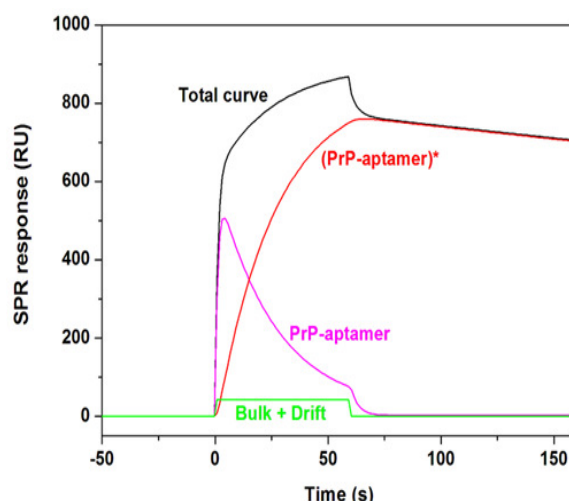


Figure III.8 Separation of individual components of the actual SPR curves characterizing the interactions PrP-aptamers: formation of the complex PrP-aptamer (in magenta); conformational changes upon complex formation (in red); contribution of bulk and drifts (in green)

The association rate constants ($k_{on,1}$) related to the first interaction step were significantly higher with respect to those obtained for the second step ($k_{on,2}$), for the full-length and the truncated PrP with D12 and R12, respectively. In more detail, the $k_{on,1}$ values, for both the full-length and the truncated PrP, are within the same order of magnitude (10^3), either for the interaction with D12 and R12, revealing a fast association phase of these aptamers to PrP. Analogously, $k_{off,2}$ values are very similar among all the systems, indicating that the dissociation process is relatively slow.

Table III.2 Kinetic parameters for the interaction of the full-length PrP and the truncated PrP with D12, R12, and d[(TGGGGT)₄] determined by SPR. The values of K_D were determined by the dose response curves.

	$k_{on,1}$ ($M^{-1} s^{-1}$)	$k_{off,1}$ (s^{-1})	$k_{on,2}$ (s^{-1})	$k_{off,2}$ (s^{-1})	K_D (M)
PrP + D12	$(5.4 \pm 0.1) \times 10^3$	$(1.0 \pm 0.1) \times 10^{-1}$	$(3.6 \pm 0.1) \times 10^{-2}$	$(5.9 \pm 0.5) \times 10^{-3}$	$(2.8 \pm 0.3) \times 10^{-6}$
ΔPrP + D12	$(6.7 \pm 0.1) \times 10^3$	$(5.1 \pm 0.2) \times 10^{-2}$	$(2.7 \pm 0.3) \times 10^{-2}$	$(5.1 \pm 0.7) \times 10^{-3}$	$(4.3 \pm 0.4) \times 10^{-6}$
PrP + R12	$(1.8 \pm 0.3) \times 10^3$	$(9.9 \pm 0.2) \times 10^{-1}$	$(4.0 \pm 0.2) \times 10^{-2}$	$(5.7 \pm 0.6) \times 10^{-3}$	$(2.9 \pm 0.5) \times 10^{-6}$
ΔPrP + R12	$(7.1 \pm 0.3) \times 10^3$	$(5.4 \pm 0.1) \times 10^{-2}$	$(2.8 \pm 0.2) \times 10^{-2}$	$(5.7 \pm 0.7) \times 10^{-3}$	$(4.8 \pm 0.5) \times 10^{-6}$
PrP + d[(TGGGGT)]	$(6.0 \pm 0.7) \times 10^4$	$(8.8 \pm 0.1) \times 10^{-2}$	$(1.4 \pm 0.1) \times 10^{-2}$	$(1.5 \pm 0.6) \times 10^{-3}$	$(1.3 \pm 0.5) \times 10^{-5}$
ΔPrP + d[(TGGGGT)]	$(8.8 \pm 0.2) \times 10^3$	$(1.9 \pm 0.2) \times 10^{-1}$	$(1.9 \pm 0.2) \times 10^{-2}$	$(1.4 \pm 0.5) \times 10^{-2}$	$(1.8 \pm 0.5) \times 10^{-5}$

To determine the binding dissociation constant, the dose response curves were obtained by plotting the SPR responses at equilibrium against aptamer concentration, from which it was possible to estimate the K_D values (Table III.2). The dose response curves for the interaction of the full-length PrP and Δ PrP with D12 and R12 are depicted in Figure III.9. The values of the binding constants are within the micromolar range and are very similar among all the systems. These results suggest that the binding of PrP with D12 and R12 aptamers occurs through

interactions with both the N-terminal and C-terminal domain, and thus, it is conceivable to presume that all the three binding sites reported in PrP for nucleic acids are involved in these bindings.

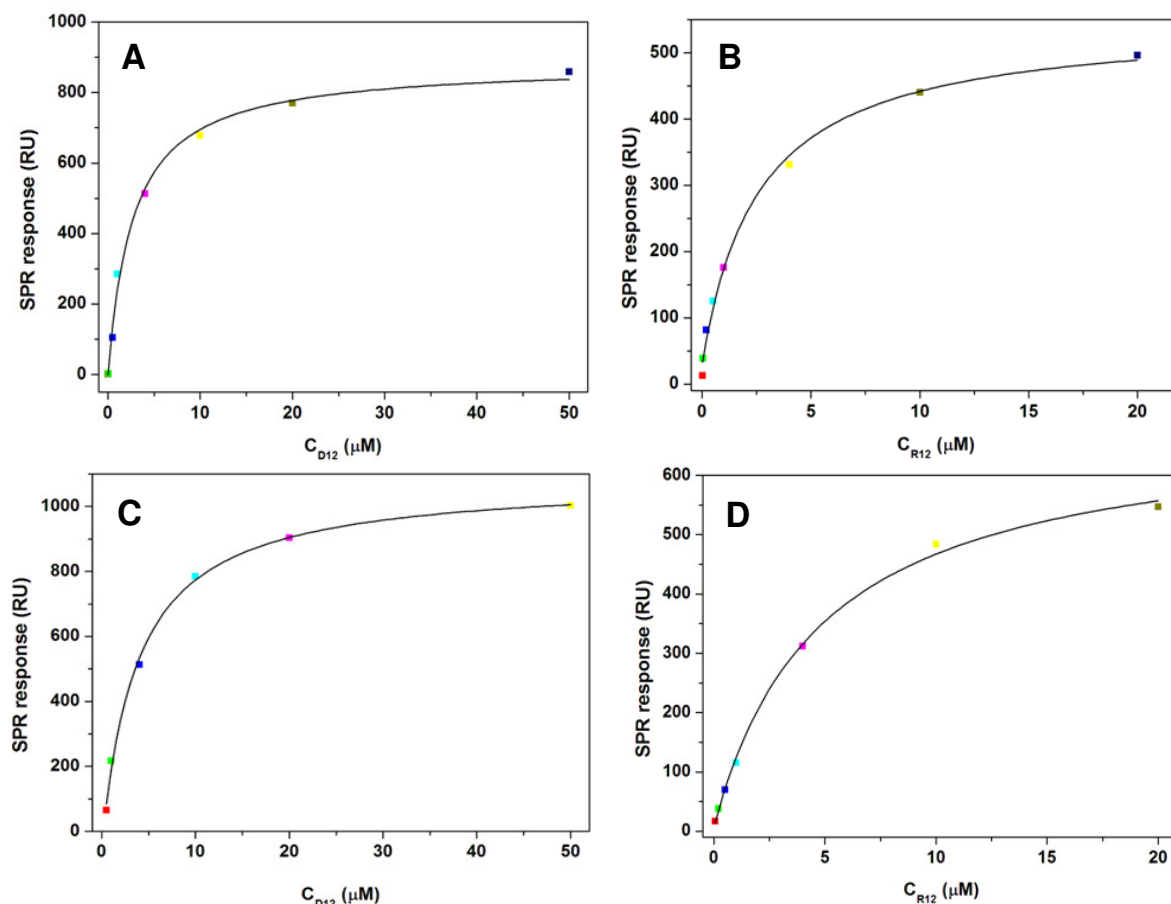


Figure III. 9 SPR binding analysis. Dose-response curves for the interaction of the full-length PrP with D12 (A) and R12 (B). Dose-response curves for the interaction of ΔPrP with D12 (C) and R12 (D).

SPR experiments were performed to kinetically characterize also the interaction of the full-length and the truncated PrP with the tetramolecular quadruplex $d[(\text{TGGGGT})_4]$. In Figure III.10, the corresponding sensorgrams are shown.

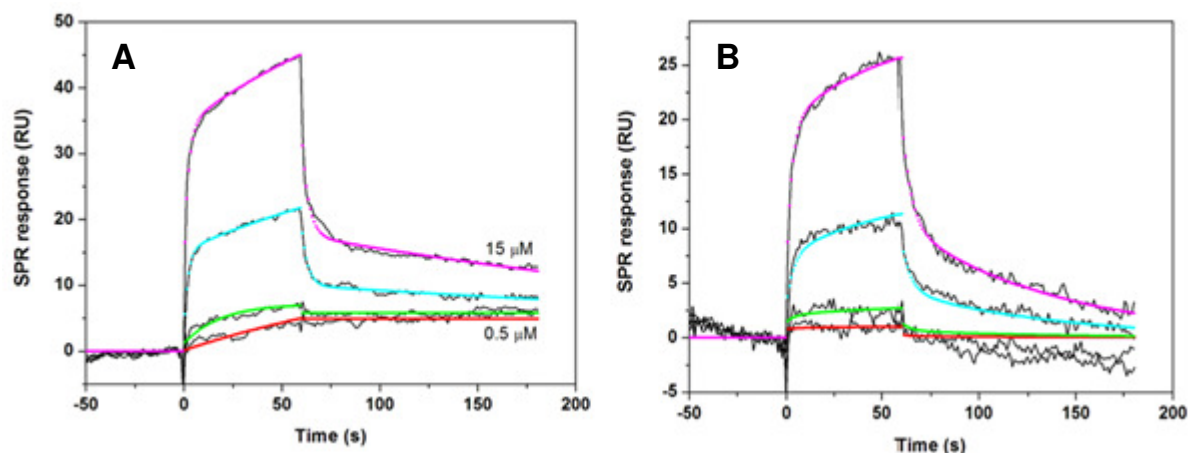


Figure III.10 SPR sensorgrams corresponding to the interaction of the quadruplex $d[(\text{TGGGGT})_4]$ with the full-length PrP (A), and ΔPrP (B) together with the fit obtained applying the two state reaction model (dot lines).

As for D12 and R12, the SPR sensorgrams relative to the interaction between PrP and d[(TGGGGT)₄] were best fitted by the two state reaction model, giving rise to kinetic constants that follow a similar trend as that related to the interaction between PrPs and D12 and R12.

The fitting of the dose response curves (Fig. III.11) led to K_D values of one order of magnitude higher than those determined for D12 and R12, indicating a lower affinity of PrP toward the quadruplex d[(TGGGGT)₄]. Moreover, the values obtained for both PrP forms are very similar, suggesting that the interaction of PrP with the quadruplex d[(TGGGGT)₄] may be mediated by the two binding sites present in the deleted PrP used in this study and does not involve the first lysine cluster in the N-terminal part.

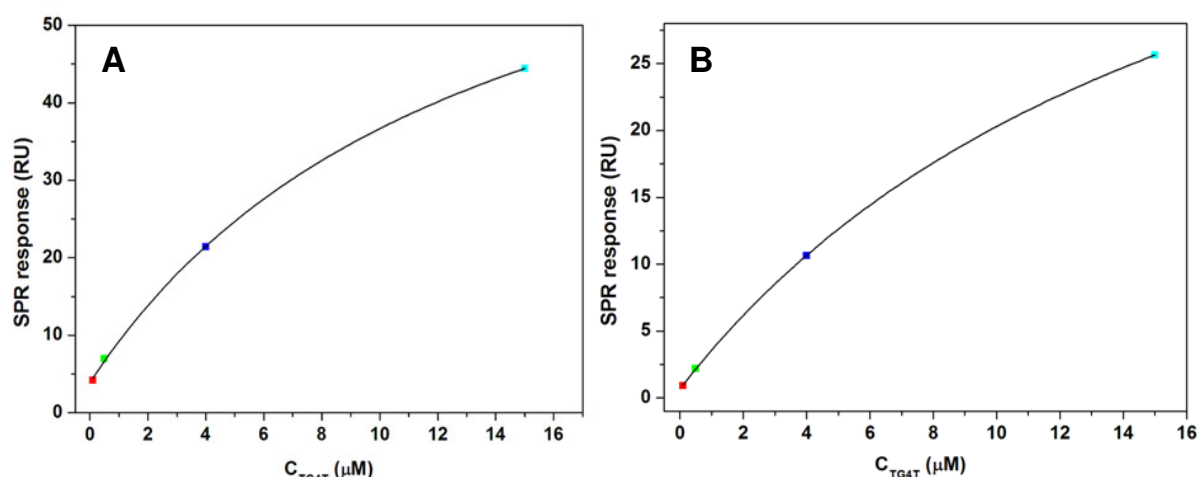


Figure III. 11 SPR binding analysis. A) Dose-response curves for the interaction of the full-length PrP with d[(TGGGGT)₄]. B) Dose-response curves for the interaction of Δ PrP with d[(TGGGGT)₄].

Finally, SPR experiments were performed using the unfolded D12, and the results obtained were in good agreement with ITC data, supporting the conclusion that the binding of DNA and RNA aptamers to PrP requires not only specific sequences, with GG repeats, but also the fold into quadruplex structures.

Structural analysis of the interaction between prion protein and quadruplex structures.

As previously reported, in some cases, the interaction between DNA or RNA aptamers and prion protein led to changes either on the protein and/or on the nucleic acid structure (Cordeiro et al., 2001; Adler et al., 2003). SPR experiments, here performed, have revealed that the interaction of prion protein with D12 and R12 aptamers, could give rise to structural rearrangements of one or both the components of the complexes. Therefore, to evaluate whether PrP or the aptamers undergo structural changes upon interaction, CD titration experiments were carried out, with the only exception for the system full-length PrP-D12, as this interaction leads to precipitation, precluding any structural analysis.

The DNA and RNA aptamers here studied are characterized by the same sequence consisting of four tandem GGA repeats (GGAGGAGGAGGA). These aptamers are able to adopt an intramolecular and parallel G-quadruplex structure in the presence of K^+ ions and at pH near neutrality. Thus, in order to determine whether free

aptamers interfere with the protein CD spectra, far UV CD spectra were registered, in the wavelength range 320-200 nm, for both D12 and R12 aptamers (Fig. III.12).

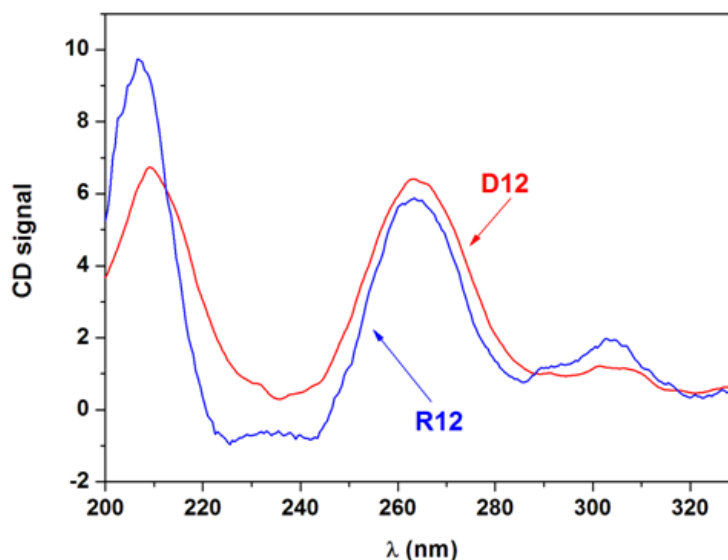


Figure III.12 CD spectra registered for D12 (in red) and R12 (in blue) aptamers in a solution containing K^+ ions at pH 6.0

In both cases, CD spectra showed a positive peak at about 265 nm and another one at about 209 nm. These CD profiles are typical for parallel G-quadruplex folds. Therefore, for the CD titration analysis, it must be taking into account that D12 and R12 aptamers present a significant CD signal in the wavelength range where the secondary structure of the proteins is evaluated. Thus, for each experiment, it was evaluated whether the CD spectrum, corresponding to the complex PrP-aptamer, overlap with that one of the aptamer alone at the same concentration.

In the case of the interaction between Δ PrP and D12, titration experiments revealed no changes of the secondary structure of D12 (Fig. III.13A). Indeed, it was possible to subtract the CD spectra referred to the aptamer alone with that one corresponding to the complex Δ PrP-D12, and the resulting CD spectra showed a progressive decrease of the α -helical content of PrP (Fig. III.13B).

Interestingly, in the molar ratio range $0.3 \leq \Delta$ PrP:D12 ≤ 1 (considering the aptamers as dimers), even if there is a detectable loss of secondary structure of PrP, the CD signal remains almost constant. A molar ratio Δ PrP:D12 of 1:2, leads to a further loss of α -helical structure of prion protein.

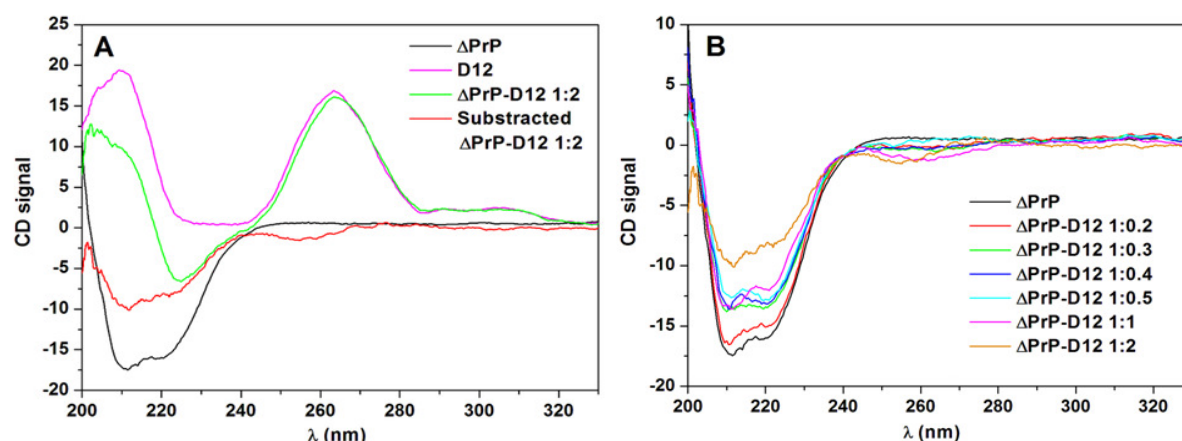


Figure III.13 CD spectra related to the titration of ΔPrP with D12 up to a molar ratio $\Delta\text{PrP}:\text{D12}$ of 1:2. A) CD spectra corresponding to ΔPrP alone, D12 alone, complex $\Delta\text{PrP-D12}$ and the subtracted CD of $\Delta\text{PrP-D12}$. B) CD spectra of $\Delta\text{PrP}:\text{D12}$ complex obtained by subtraction of CD spectra of D12 alone.

Differently, CD spectra related to the interaction of the full-length PrP with R12, showed a loss of secondary structure for both PrP and R12 aptamer (Fig. III.14A,B). In this case, it was not possible to subtract the CD spectra of the RNA alone from the one corresponding to the complex. Anyhow, since the CD signal of R12 at 209 nm is very low at molar ratios within the interval $1:0 \leq \text{PrP}:\text{R12} \leq 1:0.3$ (Fig. III.14C), it is reliable to ascribe the signal decrease observed to an actual loss of protein secondary structure.

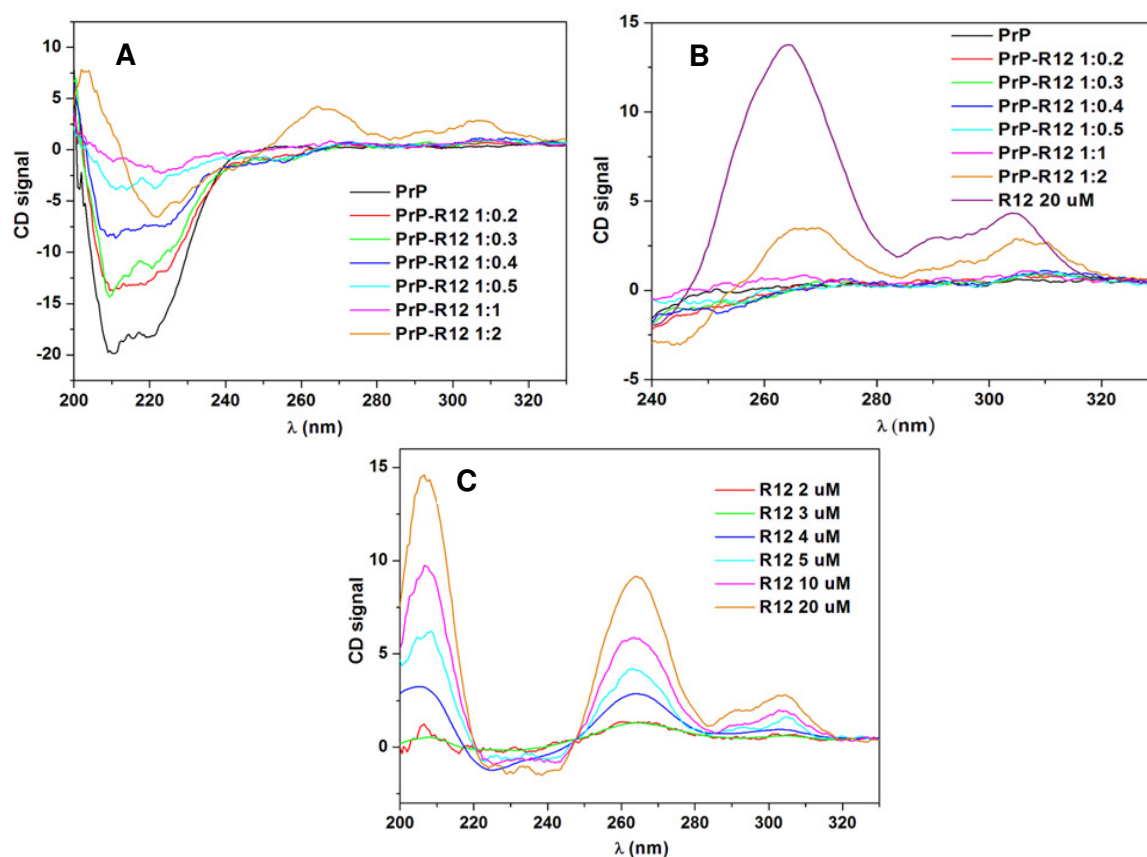


Figure III.14 A) CD spectra, in the wavelength range $330 \div 200$ nm, related to the titration of the full-length PrP with R12 up to a molar ratio of 1:2. B) CD spectra, in the wavelength range $330 \div 240$ nm, related to the complexes PrP-R12. C) CD spectra corresponding to the R12 alone at the same concentrations used for titration with the full-length PrP.

Considering the wavelength range $330 \div 240$ nm, it is possible to evaluate the structural variation of the RNA, without the interference of CD signal from the protein. In fact, there is a complete loss of the secondary structure of R12, up to an equimolar ratio of R12 relative to PrP. For a molar ratio PrP-R12 of 1:2, a CD signal at 265 nm is observed. In Figure III.14B, the CD spectra of R12 alone at the same concentration used for the solution PrP-R12, at molar ratio of 1:2, is shown. Even if a CD signal is observed at this molar ratio, the signal is lower compared to that one corresponding to R12 alone. Thus, this could be due to the unbound R12 present in solution. In fact, ITC experiments showed a binding stoichiometry PrP:R12 of 1:1, which could explain the CD signal at a molar ratio below the stoichiometry value.

A similar behavior was observed for the interaction of Δ PrP with R12. In fact, also in this case, both proteins and R12 lose secondary structure (Fig. III.15), even if the structural loss of R12 is lower with respect to the complete loss of the quadruplex architecture, found in the interaction with the full-length PrP. This difference could be explained considering that in the interaction of R12 with Δ PrP, many contacts are missing, leading to a partially misfold of the quadruplex structure. On the contrary, R12 can fully interact with all the binding sites present on the full-length PrP.

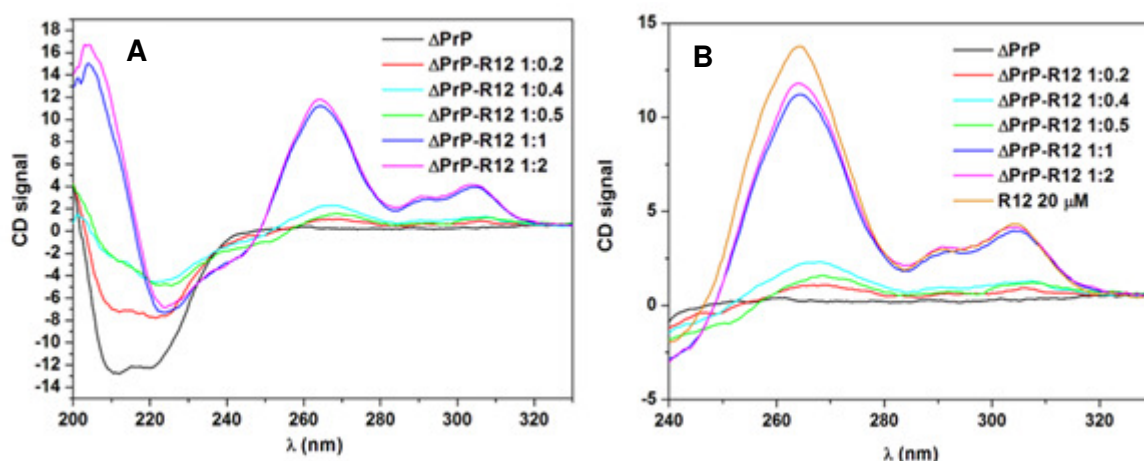


Figure III.15 A) CD spectra, in the wavelength range $330 \div 200$ nm, related to the titration of Δ PrP with R12 up to a molar ratio of 1:2. B) CD spectra, in the wavelength range $330 \div 240$ nm, related to the complexes Δ PrP-R12.

Interestingly, at an equimolar concentration of R12 relative to Δ PrP, CD signal of R12 is observed (Fig. III.15B). From a comparison with the ITC data, the binding stoichiometry resulted for this system was 1:0.5 (protein:aptamer), thus, we can deduce that both proteins and R12 partially lose secondary structure up to a molar ratio Δ PrP:R12 of 1:0.5. Below this molar ratio, the CD signal observed corresponds to free R12 molecules in solution.

Morphological analysis

Since the interaction between the full-length PrP with D12 leads to precipitation upon addition of the aptamer, a question has arisen about the nature of this precipitate: Does the addition of D12 into the solution of PrP lead to the formation of amorphous aggregates, or might D12 induce a conformational variation of the protein, forming fibrils-like structure? To answer to this question, transmission electron microscopy images were collected for the solution containing the complex PrP-D12. Figure III.16

displays the TEM images of PrP in the absence and in the presence of D12. Typical amorphous aggregates are observed for the sample containing PrP and D12. Differently, no aggregates were formed in the D12-free PrP sample.

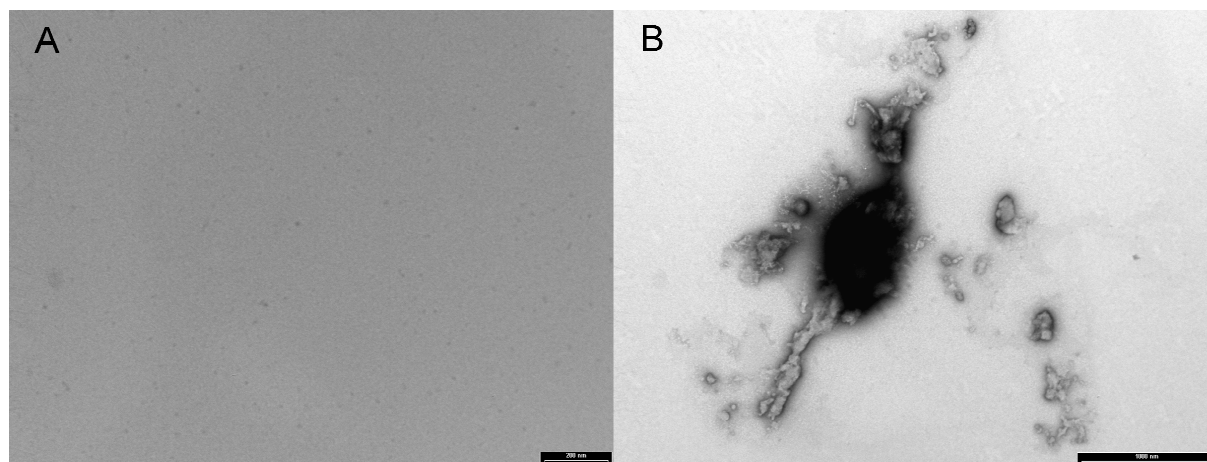


Figure III.16 TEM images corresponding to the full-length PrP without D12 (A), and in the presence of D12 (B). Scale bar: 0.5 μ m.

3.4 Discussion

Despite of all the efforts that have been devoted to understand the influence of nucleic acids on the prion protein and to identify a key sequence shared by the NAs, there is no a single mode of play and neither a specific sequence that binds to PrP.

However, many works have reported that aptamers against prion protein derived from SELEX strategy contain a shared sequence, i.e., a tandem GGA repeat. Among the reported anti-PrP aptamers containing GGA repeats, there are the anti-syrian golden hamster PrP aptamers (Weiss et al., 1997), the aptamer DP7 targeted to amino acids 90–129 of human PrP (Proske et al., 2002), and moreover, the anti-mouse PrP aptamer, called 60–3, containing GGAGG repeat (Sekiya et al., 2006). These studies have highlighted the relevance of this shared sequence for specific binding to PrP. In addition, these aptamers are able to fold into a parallel quadruplex structure, that seems to be another requirement for specific interaction with prion protein.

In a previous work, RNA aptamers against bPrP have been selected, and all the sequences contained a core with four tandem GGA repeats (Murakami et al., 2008). The minimization of these sequences in one contained only the four tandem (GGA)₄, allowed to point out the minimal sequence required to maintain the specificity toward PrP. Therefore, in this thesis work, we studied the interaction of the ovine prion protein with the minimal DNA and RNA sequence containing four tandem GGA repeat, (GGAGGAGGAGGA). In particular, our studies were performed by SPR, as well as by calorimetric (ITC) and spectroscopic approaches (CD), to obtain all the kinetic, thermodynamic and structural features of these interactions. Moreover, various PrP domains were used in order to identify the PrP regions involved in the interaction.

Although several binding studies have been conducted between these aptamers and PrP, no thermodynamic and kinetic characterization so far has been reported. In this regard, ITC and SPR technologies are complementary techniques to obtain a complete understanding of bimolecular interactions. From one side, ITC directly measures the binding enthalpy change and the stoichiometry for the formation of a complex, and thus it allows to distinguish between the enthalpic and entropic contribution to the association process. This reveals the nature of the forces that drive the binding and can provide insight into the nature of the intermolecular contacts formed. From the other side, SPR is capable of determining the rate constants of an interaction, and allows further rationalization of the contribution of individual structural features to the interaction.

The results here obtained clearly demonstrate that: i) the interaction of PrP with both D12 and R12 is different, from the viewpoint of the nature of the forces that drive the formation of PrP-aptamer complexes, ii) the interaction between the full-length PrP and R12 aptamer occurs through the formation of a 1:1 complex in which one molecule of PrP interacts with one R12 dimer molecule, iii) the interaction with the full-length prion protein presumably involves three binding regions in the protein.

Unluckily, only the stoichiometry of the binding between the full-length PrP and R12 was determined, since addition of D12 caused amorphous aggregate formation. This phenomenon precluded the derivation of the thermodynamic parameters. Although we could not extrapolate ITC binding parameters for the interaction of D12 with the full-length PrP, the aggregate formation is a clue to understand how DNA and RNA interact in a different way, and thus, could have different influences on prion biology. Anyhow, the diverse behavior of D12 and R12 with respect to the binding with the full-length PrP can be attributed to the differences in the structure between R12 and D12, described in Section 3.1.3.

From ITC and SPR data, it emerges that the binding features of D12 and R12 differ among the PrP forms here considered. First of all, the binding stoichiometry resulted from ITC experiments was 1:1 (protein-aptamer) for the interaction of R12 with the full-length PrP, while a value of 1:0.5 was obtained for the interaction of both aptamers with Δ PrP (the aptamers are in the dimeric form). Previous work has reported three different binding sites in PrP for nucleic acids; in particular two binding sites located at the ends of the unstructured N-terminal domain, and the third in the C-terminal globular part. Indeed, two lysine clusters, located in the N-terminal domain of PrP, encompass the residues K²⁵KRPKPGGGW³⁴ and W¹⁰¹NKPSKPKT¹¹⁰ in ovine PrP (Lima et al., 2006; Mercey et al., 2006). Regarding the C-terminal domain several studies point to several residues in the structured domain from arginine 136 to alanine 224 (Lima et al., 2006).

It is worth point out that in this work, two PrP forms were used: the full-length PrP (23-234), in which all the three binding sites reported for nucleic acids are present, and a deleted PrP (103-234), lacking only one binding sites, namely, the first lysine cluster. Taking in consideration the ITC and SPR results obtained for both PrP forms, we can conclude that the interaction with D12 and R12 involved the three binding sites of PrP. Moreover, from stoichiometry data, it is conceivable to presume that, since D12 and R12 are dimers, the binding occurs through the interaction of each monomer with the N-terminal and C-terminal domain, respectively. These findings are further confirmed by the different values of the binding enthalpy changes

obtained for the interaction of R12 with both full-length and deleted PrP. Indeed, the more negative $\Delta_b H^\circ$ obtained for the interaction with the full-length protein with respect to that one obtained for Δ PrP indicates that R12 can establish a higher number of contacts since all the dimeric structure is involved in the interaction.

Another important feature, derived from $\Delta_b H^\circ$ values, is related to the interaction of Δ PrP with both aptamers. In fact, these values are markedly different, suggesting a distinct intermolecular contact pattern in the complex formation. Anyhow, the electrostatic interactions between the positive charges of the lysine clusters and the negative charges of the phosphate groups of the aptamers must be the main factor for the high affinity between PrP and both D12/R12 aptamers. Moreover, it was suggested for the ovine PrP-aptamer system that the stacking interaction of the aptamers with a tryptophan residue, located in the second lysine cluster, may also contribute to the binding (Mercey et al., 2006). D12, as well as R12, has two G:G:G:G tetrad planes at the top and bottom of its dimer structure. These planes are suitable for the stacking interaction with the tryptophan residues.

It is worth mentioning that, differently from previous works in which R12 interaction with bPrP resulted to be stronger than the one with D12 (Murakami et al., 2008), our results indicate that the affinity of both aptamers toward ovine PrP is comparable. The different results could be related to the diverse PrP species considered. Anyhow, the K_b values resulted from ITC titration of R12 with both the full-length and the truncated PrP revealed a stronger interaction of this aptamer toward the full-length PrP rather than with Δ PrP, might be due to the lack of the first lysine cluster in the deleted protein.

Another important feature that seems necessary for aptamer binding properties toward prion protein is the folding in a quadruplex architecture. This requirement was confirmed by using the sequence d[(TGGGGT)₄], which can adopt a tetramolecular quadruplex structure in presence of K⁺ ions. The ITC thermodynamic parameters corresponding to the system full-length PrP-(TGGGGT)₄ are roughly comparable to those obtained for the full-length PrP and R12, even if the quadruplex d[(TGGGGT)₄] has a lower affinity toward the full-length compared to R12. Moreover, d[(TGGGGT)₄] interacts with the full-length PrP with a binding stoichiometry of 1:0.5 (protein-NA). Taking into account that the quadruplex d[(TGGGGT)₄] does not form a dimer, it might form a complex in which two PrP molecules interact with one molecule of d[(TGGGGT)₄]. Differently to ITC, SPR measurements were conducted using both the full-length and the deleted protein, and the K_D values obtained are very similar for both the PrP forms, indicating that the interaction with this quadruplex is mediated by the C-terminal domain and could involved one or both binding sites present in the delete protein.

The binding study of the quadruplex d[(TGGGGT)₄] with PrP endorsed the affinity of the GG-containing sequences *versus* PrP and the need of a quadruplex folding. In fact, in a quadruplex structure the arrangement of the negatively charged phosphate groups is unique and different from those of canonical structures such as an A-form duplex. This particular rearrangement, together with the highly density of negative charges, are supposed to be responsible for the high affinity of these aptamers toward PrP (Mashima et al., 2009).

One of the most intriguing aftermaths of nucleic acid binding to PrP is the structural variation underlying the complexes formation. Although ITC titrations directly measure the enthalpy change of the binding reaction, this value contains all the components of the interaction at equilibrium, such as solvation or desolvation effects, buffer ionization effects and conformational changes in the reactants during complex formation, and these contributions cannot be distinguished (Horn et al., 2002). Conversely, SPR experiments allow the measure of the direct binding interaction and a kinetic characterization which takes into account possible structural variations of the components of the binding reaction. Indeed, the SPR experiments related to the interaction of the full-length and the truncated PrP with D12 and R12 revealed a binding reaction consisting of two steps: i) the formation of the initial protein-aptamer complex, and ii) the conformational rearrangement that may take place on the protein and/or on the aptamers upon complex formation.

CD experiments confirmed the structural changes that occur upon interaction of PrP with these aptamers. In particular, CD titration showed that PrP undergoes structural rearrangements upon addition of D12 or R12 aptamers. On the other hand, D12 did not show a structural variation when interacting with Δ PrP, whereas R12 completely or partially loses its quadruplex architecture upon binding with the full-length or the truncated PrP, respectively. These findings reveal an important binding feature that differentiates the type of interaction of D12 and R12 with prion protein and may explain the precipitation phenomena observed upon addition of D12 into the full-length PrP solution. However, these changes in structure of the prion protein when complexed to the nucleic acid would have a biological feedback since this feature is typical of nucleic acid chaperones (Gabus et al., 2001; Cristofari et al., 2002; Silva et al., 2008).

Finally, in this work we want to highlight the possibility to use DNA and RNA aptamers for diagnostic purpose. Indeed, the high specificity of DNA and RNA aptamers toward PrP can be used to enrich PrP from biological samples. RNA aptamers have been successfully used for concentration of PrP^C and PK-resistant PrP taken from serum, urine (Zeiler et al., 2003) and brain homogenate (Davidowitz et al., 2005). Several aptamers, designed for this aim and immobilized on a column cartridge, efficiently bound PrP^C and PrP^{Sc}. This device was able to concentrate PrP from biological fluids, thus showing its potential in improving the current diagnostic tests by lowering the detection threshold (Zeiler et al., 2003). A similar principle was recently tested using magnetic nanoparticles functionalized with a PrP-specific DNA aptamer (Takemura et al., 2006). In spite of their experimentally demonstrated potential, to our knowledge these aptamer-based tools have not yet been commercially developed. We hope that in the future this strategy could be applied as diagnostic tools in double ligand assay systems.

Chapter IV Prion Protein and Aldolase C

4.1 The glycolytic enzyme Aldolase

As mentioned in the Chapter I, the prion protein is able to interact with many partners, including proteins, nucleic acids and glycosaminoglycans. Several studies have been dedicated to the description of the PrP interaction with various macromolecules and the investigation of their role in prion biology. The interactome studies may help to clarify the elusive function not only of the prion protein but also of its biological partners.

Prion protein is mostly a plasma membrane-anchored extracellular glycoprotein, whose localization within the cell is represented by a small fraction. Despite this, the number of identified intracellular partners of PrP is comparable to that of its membranal or extracellular interactors. One of these intracellular proteins that has been identified as a possible biological partner of PrP is aldolase C, one of the three isozymes belonging to the aldolases family. Strom and co-workers have found, through a proteomic approach mainly based on mass spectrometry combined with far-Western immunoblotting and 2D gel electrophoresis, that mouse PrP may interact with heterogeneous nuclear ribonucleoprotein (hnRNP) and Aldolase C (Strom et al., 2006). Indeed, on ligand blots, purified recombinant PrP^{23–231} bound both the proteins from the cytosolic fraction of brain homogenate obtained from *Prnp*-knockout mice.

Very recently, this interaction has acquired a greater significance since it was found that enzymes involved in the glucose metabolism are diversely regulated during the pathology of prion diseases (Watts et al., 2009; Gawinecka et al., 2010).

Fructose-1,6-(bis)phosphate aldolase are ubiquitous enzymes of the glycolytic and gluconeogenic pathways. These enzymes catalyze the reversible cleavage of fructose-1,6-(bis)phosphate (Fru-1,6-P₂) and fructose-1-phosphate (Fru-1-P) to dihydroxy-acetone phosphate (DHAP) and either glyceraldehyde-3-phosphate (G3P) or glyceraldehyde, respectively. There are two distinct classes of aldolases: Class I aldolases, which are present in animals and higher plants and use covalent catalysis through a Schiff-based intermediate; and a class II aldolases, which are present in most bacteria and fungi and require a divalent metal cation as a cofactor for their enzymatic activity (Rutter, 1964).

Among the class I enzymes found in mammals, there are three tissue-specific isozymes of aldolase that have similar molecular masses and catalytic mechanisms: aldolase A, aldolase B and aldolase C. The A isozyme is essentially ubiquitous in all mammalian tissues but is predominantly expressed in muscle and red blood cells. Mutations of the corresponding gene have been associated to haemolytic anaemia and myopathy (Yao et al., 2004). The B isozyme is found in liver, kidney and small intestine and mutations in the gene cause fructose-intolerance, a hereditary disorder (Tolan, 1995). The C isozyme is expressed mainly in the brain, i. e., in hippocampal neurons and in the Purkinje cells of the cerebellum. No gene variants have been found in this tissue.

The aldolase isozymes are similar in sequence, with 66% identity between human A and B, 68% identity between B and C, and 78% identity between A and C (Rottmann et al., 1987). Despite the sequence similarity, they have different catalytic properties, and thus they are involved in different physiological roles. In fact, the three isozymes differ in their affinity for the two physiological substrates, Fru-1,6-P₂ and Fru-1-P. These differences correspond to the demonstrated function of liver aldolase in the aldol cleavage of Fru-1-P during the metabolism of fructose by this tissue. Other catalytic differences suggest aldolase B is tailored for a role in gluconeogenesis while aldolase A is more effective in a degradative glycolytic capacity. In contrast, the physiological role of the glycolytic AldoC is not well-understood.

X-ray crystallographic structures of human muscle aldolase A (Gamblin et al., 1991), human liver aldolase B (Dalby et al., 2001) and human brain aldolase C (Arakaki et al., 2004) demonstrate that these enzymes are structurally similar. The enzyme is homotetrameric, with a subunit molecular mass of 36 kDa (Fig. IV.1A). The subunits are arranged in the tetramer with a local 222 symmetry. The enzyme has a tertiary structure characteristic of the TIM barrel class of proteins, consisting of eight alternating α helices and parallel β -strands, where the Schiff-base lysine is located in the central cavity of the barrel. The C-terminal end is highly mobile and its movement allows the entrance of the substrate and the exit of the reaction product. In Figure IV.1B the 3D structural superposition of the three aldolase isozymes is shown, indicating a highly similar fold.

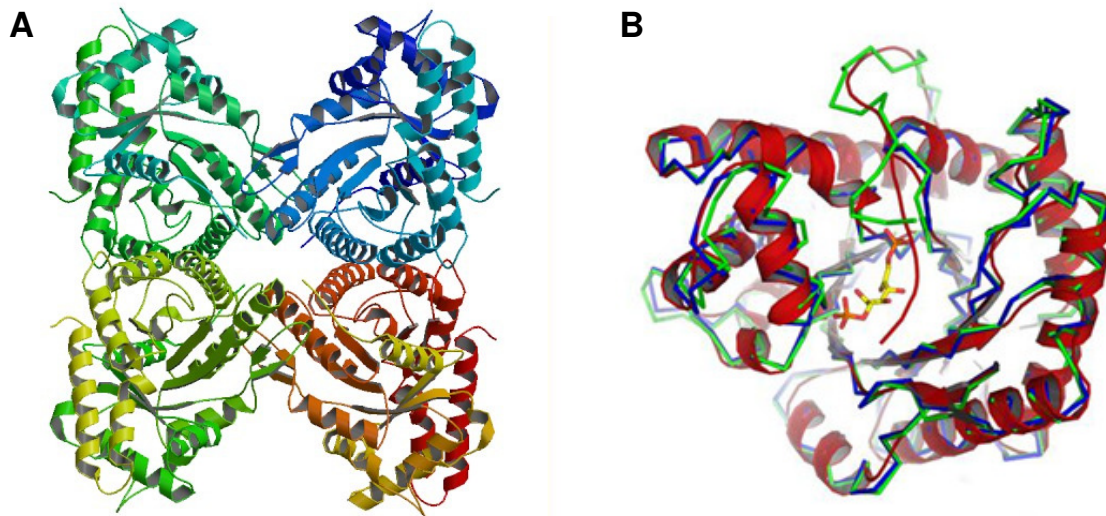


Figure IV.1 A) Ribbon diagram representation of aldolase C tetramer; PDB accession code 1XFB. B) 3D structure superposition of the three aldolase enzymes: AldoC is depicted as a coil overlaid (in blue) with the ribbon structure of AldoA (red) and AldoB (green).

Aldolase enzymes not only play a key role in glycolysis, but also bind to macromolecules unrelated to glycolysis such as F-actin (Wang et al., 1996), vacuolar H⁺-ATPase (Lu et al., 2001), cell surface adhesions (Jewett et al., 2003), and tubulin (Karkhoff-Schweizer et al., 1987). Thus, aldolase may be used for other functions in the cell, a concept that has been described as “moonlighting”. Studies have shown that aldolases associate with target proteins in a tissue-specific manner (Kusakabe et al., 1994).

Regarding aldolase C, the ratio of the specificity constants (k_{cat}/K_m) for the two hexose substrates is in between those of isoenzymes A and B. Although AldoA and AldoB have well-defined roles in glycolysis and gluconeogenesis, the physiological role of AldoC remains elusive. It has been suggested that the occurrence of AldoC in some tissues can substitute for aldolase B in fructose metabolism (Funari et al., 2005). Moreover, aldolase C has been implicated in establishing subsets of neurons during cerebellar development (Ahn et al., 1994) or during differentiation of progenitor cells in the subventricular zones of the developing brain (Staugaitis et al., 2001).

Finally, the identification of aldolase C macromolecular interactors might open new perspectives that could shed light on the mechanisms underlying neuronal function and dysfunction.

4.1.1 The possible physiological role of the PrP-AldoC complex

Strom and co-workers speculated that the interaction of PrP^C with aldolase C could explain the loss of cerebellar Purkinje cells in aged PrP^{0/0} mice (Yamaguchi et al., 2004), a hypothesis supported by the localization of aldolase C in Purkinje cells.

Interestingly, there are many evidences that correlate aldolase C, and in general glycolytic enzymes, with the pathological pattern of prion diseases. In fact, a study of the cerebrospinal fluid (CSF) protein pattern, from patients with sporadic Creutzfeldt-Jakob disease (sCJD), showed that the major alteration in CSF proteome was observed in proteins involved in the glycolysis pathway or involved in glucose metabolism (Gawinecka et al., 2010). Moreover, it has been shown that the expression levels of AldoC in the brains of scrapie-infected mice significantly increase (Jang et al., 2008).

Aldolase C seems to be related also to other neurodegenerative diseases. AldoC is able to specifically interact with the light neurofilament mRNA (Cañete-Soler et al., 2005), which is not transcribed in neurons of patients afflicted with amyotrophic lateral sclerosis (Ge et al., 2003). Thus, the modulation of the expression levels of NF-L by AldoC might have important consequences for understanding causal mechanisms underlying neurodegeneration. Another implication was found in Huntington's diseases (HD); in particular, HD affected mice showed higher activities of some glycolytic enzymes, leading to the suggestion that the neuronal damage in HD tissue may be associated with increased energy metabolism at the tissue level giving rise to modified levels of various intermediary metabolites with pathological consequences (Oláh et al., 2008).

Ultimately, previous results obtained on the correlation of aldolase C with prion protein require further clarifications, especially in view of the possible role that aldolase C might have on prion pathology. Therefore, taking into account that no information about the strength of the binding between prion protein and aldolase C was reported, in this work we have carried out a detailed quantitative analysis of the binding of PrP to aldolase C by SPR; indeed we determined the thermodynamic and kinetic binding constants. Moreover, our interaction study was extended to the other two aldolase isoenzymes, AldoA and AldoB, to investigate whether the binding was sequence specific or not. Interestingly, we identified the PrP C-terminal domain as

the binding region for aldolases. Moreover, the results obtained indicate that the interaction between PrP and aldolases occurs through a 3D-structural recognition, rather than a sequence recognition.

4.2 Experimental procedures

- *Protein production and storage*

The full-length PrP from sheep PrP and the truncated form Δ PrP (103-234) were produced as described in Section II. 2. The lyophilized protein was directly dissolved in buffer sodium acetate 10 mM, pH 5.0. Final protein concentration was measured by optical density at 280 nm as described in Section 2.2. The aldolase enzymes were supplied by the group of Prof. F. Salvatore and Prof. P. Buono, at CEINGE. The enzymes remained stable at 4 °C in Tris-HCl 20 mM, pH 7.4, for at least 2 weeks, and for at least 1 month at -20 °C in 40 %(v/v) glycerol/ Tris-HCl 20 mM, pH 7.4. Glycerol was removed by subjecting the sample dialysis, using Tris-HCl 20 mM pH 7.4, NaCl 150 mM. The concentration of aldolases samples was measured by optical density at 280 nm using an extinction coefficient of 36370, 33390, 36245 M⁻¹ cm² for the isozyme A, B and C, respectively, deduced from amino acid sequence.

- *Circular Dichroism.*

For technical and instrument details see Section 2.2. Far-UV measurements (190-250 nm) were carried out in sodium acetate 10 mM, pH 5.0 at 20 °C using a 0.1 cm optical path length cell and a protein concentration of 0.2 mg·mL⁻¹ for all proteins. CD spectra, recorded with a time constant of 4 s, a 2 nm band width, and a scan rate of 5 nm·min⁻¹, were signal-averaged over at least three scans. The baseline was corrected by subtracting the buffer spectrum.

- *Size-exclusion chromatography with multiangle light scattering*

SEC was performed using AKTA FPLC equipment on a Superdex 200 10/300 GL column. For further details regarding the calibration and equilibration of the columns, see Section 2.2. The elution buffer was Tris-HCl 20 mM pH 7.4, NaCl 100 mM. The eluent flow was 0.5 mL min⁻¹. A total of 0.1÷0.2 mg of proteins were loaded.

Size-exclusion chromatography with multiangle light scattering (MALS) experiments was carried out with the AKTA system coupled to a three-angle (45°, 90° and 135°) Wyatt Minidown EOS light scattering instrument linked to a Wyatt Optilab refractometer (Wyatt Technology Corp., Santa Barbara, CA). These experiments served to determine the molecular mass aldolase C. Molecular masses, polydispersity and root mean square radius calculations were made by ASTRA software, which is supplied with the light scattering device, using a dn/dc value of 0.185 mL g⁻¹.

- *Surface Plasmon Resonance.*

For technical and instrument details see Section 2.2. Both full-length and truncated PrP were immobilized with the same procedure previously described (Section 2.2). Aldolase A, B and C solutions at various concentrations (from 10 nM to 10 μ M) were injected in the running buffer as analytes. Also denaturated aldolases were used as analytes. Aldolases were denaturated trough incubation of the solutions at relatively high temperatures, and the loss of structure was evaluated by CD. PrP covalently

immobilised chip was regenerated using the mobile phase buffer [Glycine 10mM (pH2.5)], injected 180 s after the analyte injection.

Kinetic binding analysis was performed and kinetic constants were calculated from the sensorgrams using the same software as described in Section 2.2. The full binding cycle for each aldolase concentration is well described by a 1:1 interaction model.

4.3 Results

Some bio-physical features of Aldolase C

A comparison among the three aldolases fold shows the high structural similarity (Fig. IV.1B). Indeed, the relatively high sequence identity and the same tridimensional structure, leads to suppose the comparable chemico-physical features for the three aldolases.

To well-characterized the PrP-AldoC binding, a structural analysis has been performed on purified human aldolase C by several biophysical approaches, since in literature, very little is known about aldolase C chemico-physical properties. First, secondary structure analysis was conducted by recording CD spectra of aldolase C samples in the far-UV region (190-250 nm) at pH 7.4 and 20 °C (Fig. IV.2A). Far-UV CD spectra are characterized by the presence of two minima (at 208 and 222 nm) and one maximum (at 195 nm) which are typical fingerprints of α/β proteins (Cantor et al., 1970). Secondary structure analysis by means of the self-consistent method, implemented in the Dichroweb server, resulted in 38% α -helix and 13% β -sheet; such estimates are in line with those determined from the X-ray structure of human aldolase C (Arakaki et al., 2004).

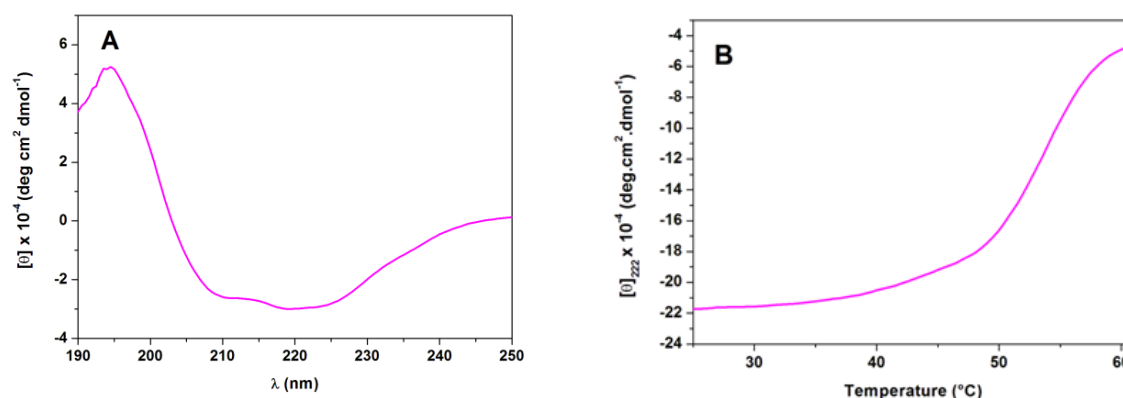


Figure IV.2 Structural analysis of aldolase C by circular dichroism. A) Far-UV CD spectra recorded at 20 °C and pH 7.4. B) CD thermal denaturation curve followed at 222 nm.

Moreover, temperature induced denaturation was performed, by following the molar ellipticity at 222 nm (Fig. IV.2B). Thermal denaturation curve of aldolase C presents a sigmoidal shape with a single inflection point, corresponding to T_m value of 51.5 °C. The CD spectra of denatured species at 80 °C are typical of random coil. The spectrum of cooled samples after denaturation is virtually identical to that of the

denatured protein at 80 °C, thereby indicating the irreversibility of the unfolding process.

For comparison, in Table IV.1 the melting temperature reported in literature and obtained by the same methodology for aldolase A and B are listed, together with the T_m of aldolase C here obtained. Aldolase C has a melting temperature in between those reported for aldolase A and B.

Table IV.1 Comparison of the T_m here obtained for aldolase C with previously reported T_m for aldolase A and B

Human Aldolases	T_m (°C)	References
Aldolase A	54.2	(Esposito et al., 2005)
Aldolase B	50.0	(Malay et al., 2002)
Aldolase C	51.5 ±0.5	

The quaternary structure of aldolase C was analyzed by SEC coupled with a multi-angle light scattering. The SEC profile, shown in Figure IV.3A, revealed that aldolase C elutes at 11.9 mL and the protein is in the tetrameric form. The presence of aldolase C was confirmed loading the fraction collected by SEC on a SDS/PAGE (Fig. IV.3A). The resulting molecular mass, obtained by MALS data, was 164 kDa (within 0.7%). A representative profile obtained by MALS measurements of aldolase C is shown in Figure IV.3B.

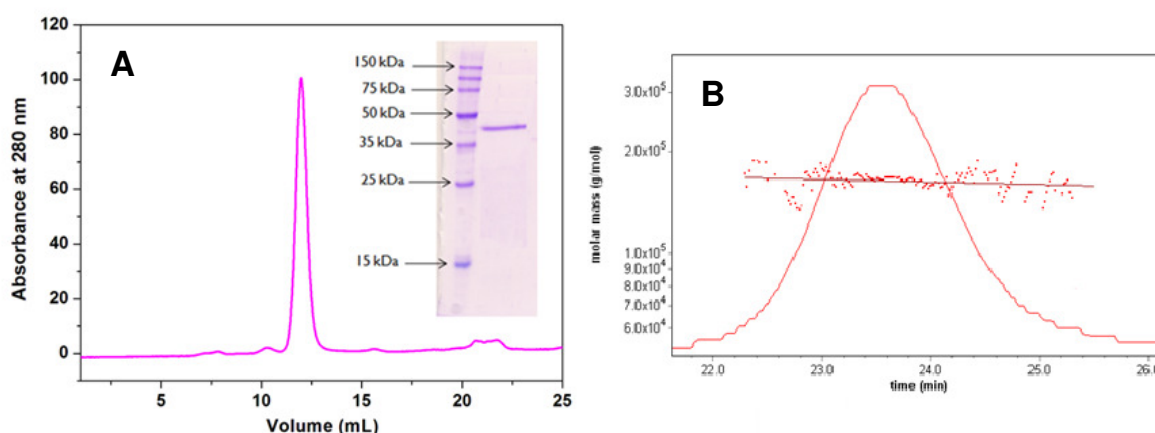


Figure IV.3 Quaternary structure analysis of aldolase C by SEC-MALS. A) SEC chromatogram carried out at pH 7.4 and SDS-PAGE analysis of the fraction collected by SEC. B) Representative SEC-MALS profile in which the molecular mass is shown. The experimental data are represented by dots and the fitting of experimental data is shown by a red line.

PrP-Aldolases interaction resulting from SPR measurements

To evaluate the kinetics and the binding affinity of the interaction between aldolases and PrP (both full length and truncated forms), SPR technology was utilized. During the experiments, we observed a strong non-specific interaction between aldolases and the sensor chip CM5, hampering an accurate measurement of the binding. We spent several efforts in finding the experimental conditions suitable for a reliable measurement. Finally, we found that the addition of the enzyme substrate, fructose-1,6-bisphosphate, eliminated nonspecific interactions between aldolases and CM-

dextran. We speculate that because the natural substrate of aldolase is a sugar, this enzyme is prone to interact with this class of molecules, and thus, may interact with the carboxymethylated dextran surface of the sensor chip. In the presence of fructose-1,6-bisphosphate, the enzyme is saturated by its natural substrate, for which the enzyme has a greater affinity, preventing the interaction with the matrix of the sensor chip.

Kinetic and binding experiments were carried out immobilizing, on the sensor chip, the full-length and the C-terminal PrP and injecting aldolase C at various concentrations in the presence of its substrate Fru-1,6-P₂. Analogously, with the aim to investigate the specificity of the PrP interaction with aldolases, kinetic and binding experiments were carried out also for the interaction of prion protein with the other two isozymes: AldoA and AldoB.

In Figure IV.4, SPR sensorgrams related to the binding of aldolases with the immobilized full-length PrP are shown. The sensorgrams registered for the binding of the three isozymes with Δ PrP are very similar (data not shown). SPR sensorgrams were used to calculate the corresponding kinetic constants k_{on} and k_{off} (Table IV.2) by a global fit of the response data collected during the association and dissociation phases.

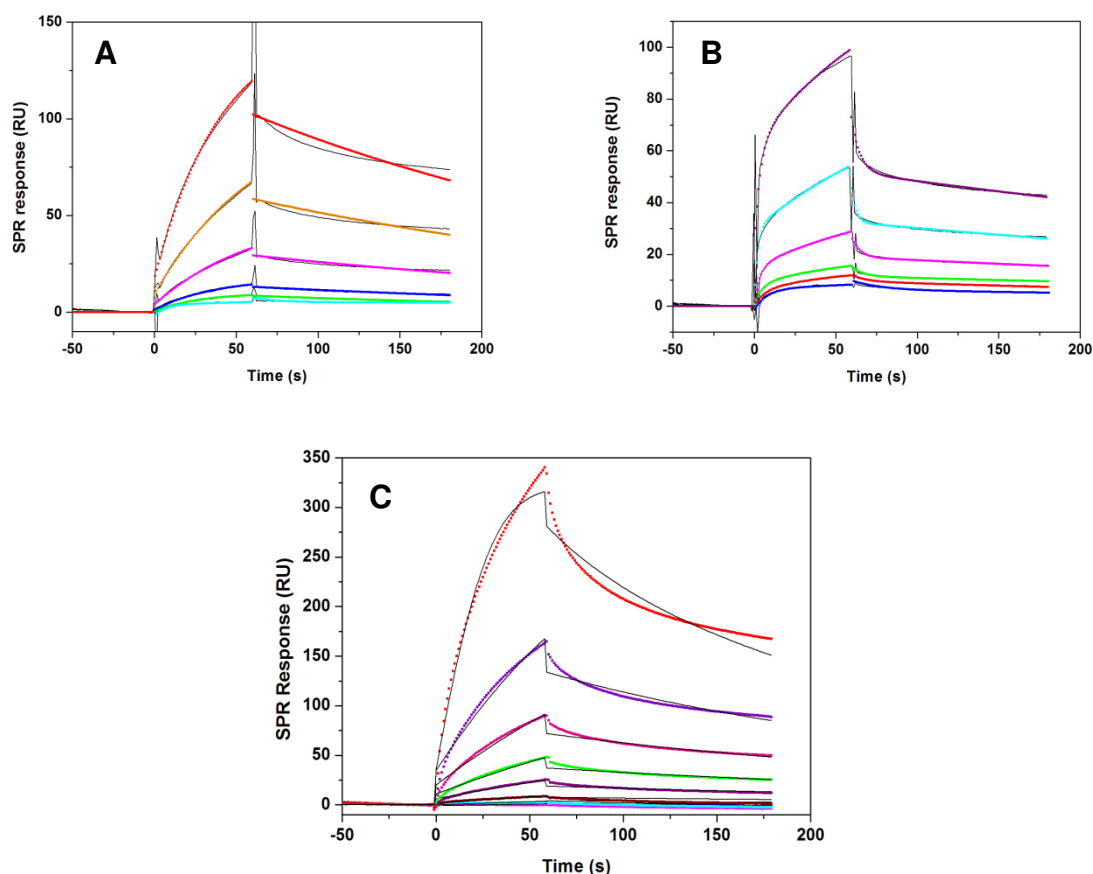


Figure IV.4 SPR sensorgrams corresponding to the interaction of aldolases with the full-length PrP together with the fit obtained applying the 1:1 binding model (dot lines). A) Aldolase A; B) Aldolase B; C) Aldolase C

Kinetic data indicated that the values of k_{on} obtained for the binding of all aldolases with the full-length PrP are within the same order of magnitude (10^3), as well as the values obtained for the system aldolases- Δ PrP (10^4). It is worth noting that the kinetic association constant relative to the interaction of aldolases with Δ PrP, are one order of magnitude higher compared to those obtained with the full-length PrP, indicating a faster association with the C-terminal part of the prion protein. Regarding the kinetic dissociation constant, the values are similar for the binding of the three isozymes to the full-length PrP, whereas these values change significantly for the truncated protein. In fact, k_{off} is smaller for the system Δ PrP-AldoB, suggesting a slower dissociation process for this complex.

Table IV.2 Kinetic and binding analysis of the interaction data between aldolases and PrP. The values of K_D were determined by the dose response curves.

Ligand	k_{on} (1/Ms)	k_{off} (1/s)	K_D (M)
Full-length PrP immobilized			
AldoA	$(5.4 \pm 0.2) \times 10^3$	$(1.0 \pm 0.2) \times 10^{-3}$	$(4.9 \pm 0.4) \times 10^{-6}$
AldoB	$(9.7 \pm 0.2) \times 10^3$	$(3.2 \pm 0.3) \times 10^{-3}$	$(3.4 \pm 0.4) \times 10^{-6}$
AldoC	$(6.4 \pm 0.1) \times 10^3$	$(8.3 \pm 0.1) \times 10^{-3}$	$(9.9 \pm 0.3) \times 10^{-6}$
Δ PrP immobilized			
AldoA	$(1.3 \pm 0.3) \times 10^4$	$(1.5 \pm 0.2) \times 10^{-3}$	$(1.3 \pm 0.4) \times 10^{-6}$
AldoB	$(6.4 \pm 0.2) \times 10^4$	$(6.9 \pm 0.1) \times 10^{-5}$	$(4.2 \pm 0.5) \times 10^{-6}$
AldoC	$(5.3 \pm 0.1) \times 10^4$	$(2.1 \pm 0.1) \times 10^{-4}$	$(3.6 \pm 0.3) \times 10^{-7}$

To determine the binding dissociation constant, SPR sensorgrams at each concentration of aldolase isoenzymes were used to plot the dose-response curve, from which it was possible to estimate the K_D values (Table IV.2). The dose response curves for the interaction of the full-length PrP and AldoA, B and C are depicted in Figure IV.5. The values of K_D are comparable for the binding of all the aldolases with the full-length PrP and Δ PrP, with the only exception of the system Δ PrP-AldoC, which is one order of magnitude lower. These results indicated that aldolases interact with PrP mainly through the C-terminal domain of the protein.

Finally, to study the influence of the folded state of aldolases to the interaction with PrP, SPR measurements were carried out with the unfolded aldolases (see experimental procedures). In fact, since the affinity of aldolases toward the full-length PrP is comparable, we presumed that a 3D-structural recognition drives the interaction between aldolases and prion protein. The results obtained did not show an interaction with prion protein.

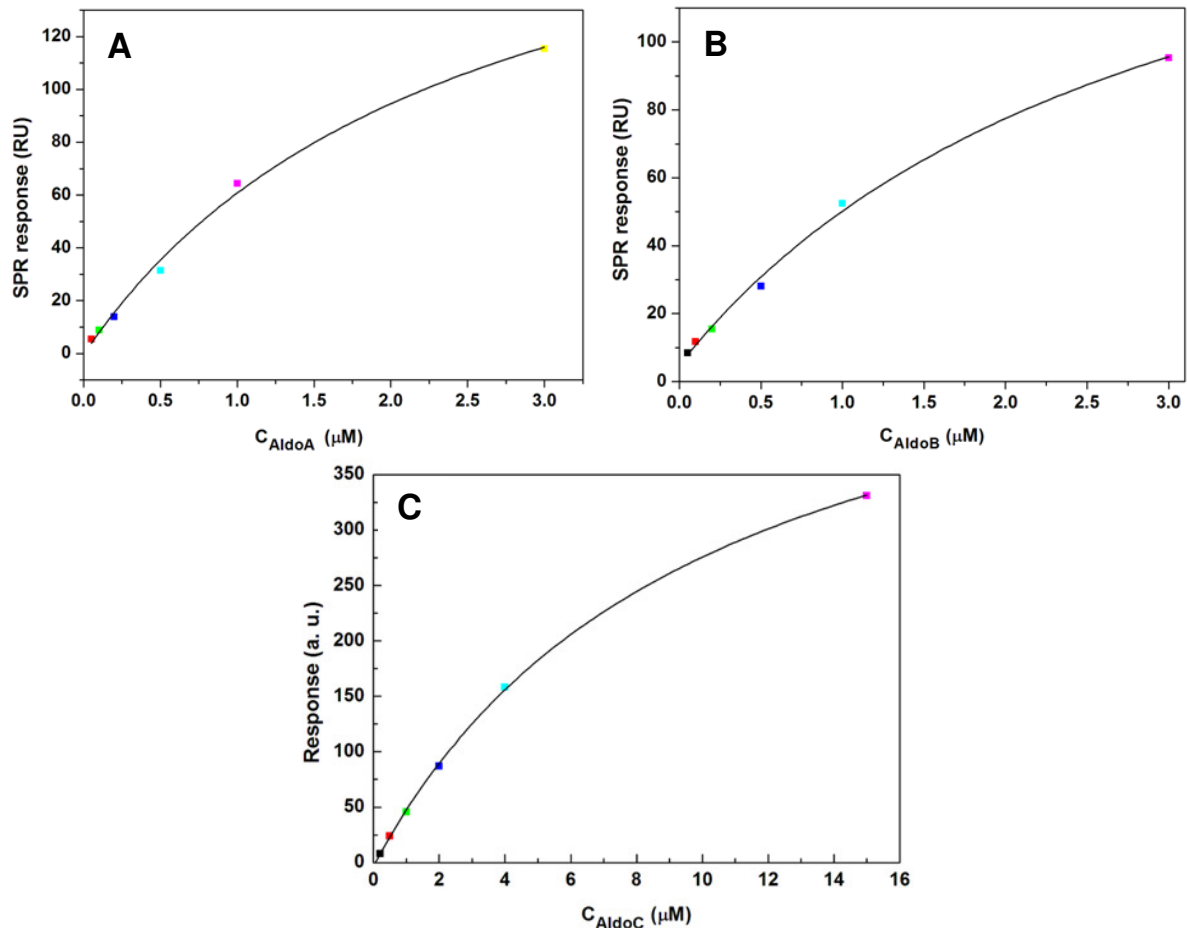


Figure IV.5 SPR binding analysis. Dose-response curves for the interaction of the full-length PrP with AldoA (A) AldoB (B) and AldoC (C).

4.4 Discussion

In recent years, a number of different methods have been used for the identification of PrP-binding molecules. A complex picture is emerging of PrPC as a multifunctional protein, able to interact with a large ensemble of biological macromolecules and, thus, to participate in several cellular processes.

Based on a previous work, where the authors showed the interaction between mouse prion protein with aldolase C (Strom et al., 2006), we confirmed that PrP and AldoC interact *in vitro*. We monitored the formation of the PrP-AldoC complex by SPR, deriving all the kinetic and binding parameters. Moreover, we used both full-length and truncated PrP, which lacks of the N-terminal region to investigate the binding region of prion protein to aldolase C. Both kinetic and binding constants related to the binding of aldolase C with both the full-length and the truncated PrP indicate that the interaction occurs through the structured C-terminal region of PrP, spanning residues 103-234. In fact, the interaction of aldolase C with the Δ PrP is characterized by a faster association and a slower dissociation process, with a higher binding affinity, compared to the kinetic and binding data obtained for the full-length.

The interaction study was extended to the other aldolase isozymes, namely aldolase A and B, that share a relatively high sequence identity and a similar 3D structure with

the aldolase C. In fact, the bio-physical analysis of aldolase C, here performed, has confirmed the similarity among the aldolase isozymes. The SPR experiments have demonstrated that also AldoA and AldoB interact with both full length and truncated forms of PrP, similarly to AldoC. It is worth noting that the interaction of aldolase A and B with Δ PrP has kinetic and binding properties similar to those corresponding to the interaction with the full-length. The results obtained lead to presume that the PrP interacting region for aldolases is the C-terminal folded domain, whereas the N-terminal unstructured domain does not participate in the interaction.

On the basis of the results obtained, it is reasonably to suppose that the binding process between PrP and all aldolase isozymes is based on a 3D-structural recognition and presumably do not involve primary structure recognition. This assumption is supported by the following remarks: i) PrP-aldolase interactions were observed in SPR experiments, in which all the proteins involved were in a folded state accordingly to the far-UV CD spectra recorded for each protein immediately before SPR measurements; ii) Not only do assume human aldolases the same fold but also an essentially identical binding site architecture for PrP, being the SPR experiments performed in the presence of substrate Fru-1,6-P₂; iii) SPR measurements performed with the unfolded aldolases did not reveal any interaction.

Anyhow, the interaction of prion protein with aldolase C seems to be related to the loss of cerebellar Purkinje cells in aged PrP^{0/0} mice (Yamaguchi et al., 2004). As aldolase C and PrP colocalized in Purkinje cells, their interaction in normal cerebellum may be required to maintain the long-term survival of these cells, while the absence of PrP^C in PrP^{0/0} mice may explain the death of cerebellar Purkinje cells in these mice (Strom et al., 2006). It is also worth mentioning that neurotoxicity of doppel (Dpl), the PrP^C homologue, in Purkinje cells of a line of PrP-null mice, Ngsk *Prnp*^{0/0}, varies according to aldolase C expression.

Further evidences for a physiological correlation of PrP^C and aldolase C come from various studies that connect the glycolytic enzymes to prion diseases. In fact, in BSE-infected mouse brain was found an enhanced level of a long aldolase C mRNA transcript (Dandoy-Dron et al., 2000). Moreover, the expression of proteins involved in the glycolytic pathway was found altered in sCJD patients (Gawinecka et al., 2010).

Interaction studies could add, to the current knowledge, more information about the possibility that PrP^C may be part of large multi-molecular complexes, depending on the cellular context and environment, and thereby contribute to diverse cellular functions. Resolving the complexity of PrP^C partners and the functional interactions in neuronal cells should lead to a better understanding of the neurospecificity of PrP^C function. Further research is required to determine the relationship between PrP^C and its biological ligands, how the absence of the interaction is compensated, and whether the loss-of-function of PrP-interactors is related to prion diseases.

Chapter V Conclusion

Prion diseases have occurred in humans and animals for many years. The first cases of human prion disease, CJD, were reported in the 1920s (Creutzfeldt, 1920; Jakob, 1921). The number of human and animal diseases recognized as TSEs has increased steadily and now includes many other variants that may arise either spontaneously, *via* inheritance of a predisposing mutation, or by way of infection, with an incidence of 1:1million. Acquisition of disease by infection has drawn intense interest among both scientists and the general public, especially in light of the outbreak of BSE (“mad cow” disease) in the United Kingdom (Wells et al., 1995) and indications that BSE can likely be transmitted to humans, resulting in a new variant of CJD (Caughey et al., 2001).

Although excellent progresses have been achieved, several important questions in the prion field remain unanswered. Most conspicuously, both the physiological function of PrP^C and the molecular pathways leading to the fatal neurodegeneration in prion diseases remain unknown. The complete knowledge of the biological meaning of PrP and the mechanism of prion replication could build a bridge toward the understanding of fundamental cellular processes that involved this protein and its biological partners, and the development of easily implementable diagnostic tools and effective therapies against prionopathies. These unresolved questions could have a significant impact on other protein misfolding disorders.

In this thesis work, we aimed to add one more piece to the fascinating field of prion protein, by studying the interaction of PrP with three different molecules: a small molecule, methylene blue; DNA and RNA aptamers; and a glycolytic enzyme, Aldolase C. This *in vitro* binding study brought further information on the significance of these interactions to PrP, and on how they may modulate the behavior of both PrP native and oligomer/fibrils states.

Among the wide repertoire of small molecules that have been studied for prion diseases or for other misfolding diseases, the addition of a new potential compound against prionopathies is not suitable, due to the great number of reported compounds that have shown somehow to have an effect on prion conversion but they remained at an *in vitro* level, without further development. This could be ascribed to the fact that some of these compounds do not satisfy the requirements to act in CNS and to be used as a drug for human and animals. For all these reasons, we have sought a molecule which has known toxicological properties, because already used for medical treatments, and is able to target the misfolded proteins in the brain. To this aim, we found that methylene blue is one of the oldest drugs used, and, more interesting, it was already shown to be effective for other amyloidogenic-associated diseases. Thus, it is conceivable to presume that MB, also in a synergistic mechanism with other compounds, could act as a general anti-aggregation compound against many proteinopathies. Our results strongly encourage further studies on animal models for future perspective in clinical trials.

Beside the research of compounds that could act as antagonist of prionopathies, the development of effective diagnostic tools, that allow the early detection of the occurrence of the diseases, is a currently compelling need. DNA and RNA aptamers

have been demonstrated to specifically interact with prion protein, and, in some cases, distinguish between the normal and the pathogenic isoform of prion protein. Although many NA sequences were found to interact with PrP, a common shared sequence containing contiguous guanine was observed for some of these aptamers, in addition to a common fold in a G-quadruplex architecture. Our study of the binding between prion protein and some GG-containing aptamers that fold in G-quadruplexes, have endorsed the importance of these two requirements to maintain the specificity with PrP. Aptamers are gaining more interest not only because they can help to better understand the biological function of PrP, but also because they can be used to enrich PrP from biological samples, and thus, can be a potent tool for diagnostic purposes.

As far as the PrP physiological role is concerned, one of the most used approaches to try to resolve this conundrum, is the study of the interaction partners that could regulate specific actions of PrP, within the cells. Aldolase C, one of the three isoforms of the glycolytic enzyme aldolase, was found to interact with prion protein. Although, it is not yet clear if this interaction occurs *in vivo*, the understanding of the mechanism of recognition between these proteins may help to understand some unresolved mechanisms observed in the cell, also considering the very recent results that correlate the glucose metabolism-associated enzymes to prion pathologies.

We are aware that in most cases, investigations bring more questions than answers, but they add further steps toward a deeper understanding of the mechanisms that drive the living processes.

Appendix I *Other protein-misfolding diseases: the case of phenylalanine hydroxylase*

The protein folding is described as a complex process in which a polypeptide chain reaches its native structure by searching the conformational space through a multidimensional energy surface (Dobson, 2003). Failure to fold correctly, or to remain correctly folded, will give rise to the malfunctioning of living systems and hence to diseases. Some of these diseases result from proteins with a high propensity to misfold, and thus, escaping all the protective mechanism of the cells and forming amyloid fibrils that are deposited in the extracellular space. In this group fall those diseases as Alzheimer's and Parkinson's diseases and prionopathies (Chiti et al., 2006). In other cases, diseases arise from a loss of the biological function due to an incorrect folding of the proteins. Mutations are the most frequent causes of the increased tendency of the proteins to misfold, leading to reduced *in vivo* function. Among mutation-induced misfolding diseases, PKU (caused by mutations in PAH) is considered a paradigm of misfolding metabolic diseases (Gregersen et al., 2006).

The human inborn error of metabolism PKU (OMIM# 261600) is caused by a dysfunction of the liver enzyme PAH (EC 1.14.16.1). PAH catalyzes the rate-limiting step in L-phenylalanine (L-Phe) catabolism in liver, using tetrahydrobiopterin (BH₄) and dioxygen as additional co-substrates. PKU mutations are associated with impairment of PAH activity, leading to accumulation of L-Phe in plasma (that is, hyperphenylalaninemia – HPA) and neurological damage in untreated patients (Scriver et al., 1994). Since the introduction of a dietary treatment fifty years ago, PKU has been the prototype for a treatable genetic disease and, later, for genetic screening in human populations.

About two-thirds of PKU mutations are caused by single amino acid changes in the PAH sequence. A large proportion of all missense mutations, including many of the most common mutations found in patients, display stability and folding defects when they are expressed *in vitro* (Waters, 2003). These variant PAH proteins are found to aggregate when expressed in prokaryote systems, where they appear as both soluble and insoluble aggregates (Leandro et al., 2010). But the presence of amyloid fibrils or insoluble aggregates has never been reported in the liver of PKU-affected individuals, and PKU has, in fact, been classified as a cytosol-associated protein-misfolding disease. The current understanding of PKU is related to a loss-of-function mechanism associated with increased degradation rather than aggregation of the mutants (Waters, 2006).

The full-length *PAH* gene encodes a protein of about 52 kDa (452 amino acids) that in the mature form is assembled as a homotetramer. Each subunit consists of three functional domains: a flexible N-terminal regulatory domain (residues 1-142); a catalytic domain (residues 143-410) which includes binding sites for iron, substrate and cofactor; and a C-terminal oligomerization domain (residues 411-452) which includes a tetramerization motifs (residues 427-452). The crystal structure of PAH has revealed that the tetrameric oligomers are dimers of dimers in which the interaction between the two dimers is mediated by a C-terminal 'arm' (Fusetti et al., 1998).

Recombinant variant proteins containing prevalently missense mutations have been analyzed and characterized *in vitro*. Each exerts a distinct effect on the behavior of the PAH protein, which in many cases predicts the biochemical phenotype (Zschocke, 2003). The effects of a specific mutation on protein function have been studied by various approaches. It is now established that, in most PKU cases, the loss of PAH function is due to decreased stability (Mallolas et al., 1999) increased susceptibility toward aggregation and degradation of PAH mutant proteins (Leandro et al., 2010), thermodynamic instability and/or folding efficiency (Pey et al., 2007).

PAH protein function and its involvement in the PKU diseases is one of the main field studied by the group of Prof. Salvatore and his co-workers (Prof. Daniele) at the research institute CEINGE. In this regard, they previously carried out a molecular analysis of the PAH gene in HPA patients from Southern Italy, and identified and characterized several novel mutations (Daniele et al., 2007; Daniele et al., 2008; Daniele et al., 2009). During my thesis work, in collaboration with the aforementioned group, I carried out a bio-physical study on the wt-PAH protein and some PAH natural mutants, p.I65M, p.N223Y, p.R297L, p.F382L, p.K398N, p.A403V, p.Q419R, to obtain further information about the molecular basis of PKU. To this aim, biophysical characterization of PAH proteins was performed by size-exclusion chromatography, light scattering and circular dichroism, thereby providing novel data on this group of mutant proteins. Our study demonstrate that the oligomerization process and conformational stability are altered by mutations, thus affecting the physiological behavior of the enzyme and endorsing the hypothesis that oligomerization and folding defects of PAH variants are the most common causes of HPA, particularly as regards mild human phenotypes.

For more information see the article enclosed:

Cerreto, M., **Cavaliere, P.**, Carluccio, C., Amato, F., Zagari, A., Daniele, A. and Salvatore, F., 2011. Natural phenylalanine hydroxylase variants that confer a mild phenotype affect the enzyme's conformational stability and oligomerization equilibrium. *Biochim. Biophys. Acta.* **1812**, 1435-1445.

Appendix II *List of publication, communications and research activity in scientific institutions abroad and in Italy*

Publications:

- Cerreto, M., **Cavaliere, P.**, Carluccio, C., Amato, F., Zagari, A., Daniele, A. and Salvatore, F., 2011. Natural phenylalanine hydroxylase variants that confer a mild phenotype affect the enzyme's conformational stability and oligomerization equilibrium. *Biochim. Biophys. Acta.* **1812**, 1435-1445.

Manuscripts in preparation:

- **Cavaliere, P.**, Torrent, J., Prigent, S., Pouwels, K., Granata, V., Pastore, A., Rezaei, H. and Zagari, A. Inhibition insights into PrP oligomerization and fibrillization by methylene blue.
- **Cavaliere, P.**, Pagano, B., Granata, V., Prigent, S., Rezaei, H., Giancola, C. and Zagari, A. High affinity binding of quadruplex DNA and RNA aptamers to ovine prion protein.

Proceedings:

- Cerreto, M., **Cavaliere, P.**, Zagari, A., Daniele, A., Salvatore, F. "Mutation Q301P promotes structural instability and formation of high molecular mass oligomers in the phenylalanine hydroxylase enzyme". *FEBS J.*, vol 278 supplement 1, p.100. 36th FEBS Congress Torino-Italy, 25-30 June 2011
- **Cavaliere, P.**, Prigent, S., Pastore, A., Rezaei, H., Zagari, A. "Effects of Methylene Blue on the Oligomerization Pathway of Prion Protein". *Prion J.*, vol 5 supplement 1-20, pp. 34. PRION 2011 Congress Montreal-Canada, 16-19 May 2011

Communications:

- Pagano, B., **Cavaliere, P.**, Granata, V., Prigent, S., Rezaei, H., Zagari, A., Giancola, C. "Biophysical characterization of interaction between prion and G-quadruplex forming aptamers". Abstract book, pp.54. Third International Meeting on G-quadruplex and G-assembly Sorrento-Italy, 28 June-01 July 2011
- Cerreto, M., **Cavaliere, P.**, Carluccio, C., Zagari, A., Daniele, A., Salvatore, F. "Characterization of the biochemical, biophysical and structural phenotypes of seven PAH natural variants identified in patients affected by Hyperphenylalaninemias". Abstract Book, pag. 524. 42° National Congress SIBioc Roma-Italy, 05-08 October 2010
- **Cavaliere, P.**, Cerreto, M., Carluccio, C., Cappuccio, A., Daniele, A., Zagari, A., Salvatore, F. "Natural phenylalanine hydroxylase mutants provoke

conformational instability and oligomerization defects of the enzyme". Abstract Book, pag. 119. The EMBO meeting 2010 Barcelona-Spain, 04-07 September 2010

- **Cavaliere, P.**, Granata, V., Zagari, A. "Binding of Methylene Blue to Prion Protein Oligomers By Surface Plasmon Resonance". Abstract Book, pag. P33. IX National Congress of Supramolecular chemistry Parma-Italy, 06-09 September 2009

Research activity in Scientific Institutions abroad and in Italy:

- From April 2009 to April 2011, excluding periods spent in France, the research activity on phenylalanine hydroxylase and on the interaction between prion protein and aldolase C were partially carried out at CEINGE- Biotechnologie avanzate Scarl, Naples-Italy. These projects were headed by Prof. F. Salvatore and carried out in collaboration with Prof. P. Buono and Prof. A. Daniele;
- From March to July 2010, September to December 2010, and June to August 2011, the research activity on the effects of methylene blue on the oligomerization and fibrillization of PrP was carried out at INRA "Institute National de la Recherche Agronomique", Jouy en Josas-Paris-France, in collaboration with Dr. H. Rezaei;
- From November 2010 to May 2011, part of the research activity on the interaction between PrP and DNA and RNA aptamers was carried out at the Department of Chemistry, University of Naples "Federico II", Naples-Italy, in collaboration with Prof. C. Giancola.

Acknowledgments

It is somehow trivial to say: “I would like to thank...”

A thesis work is never done by one person, and in my opinion, there is no other job that teaches the true meaning of team work as science research. Once, someone told me: “I have no principle... but my job is based on only one: we work for humanity”. Perhaps, this is the reason why, for this job, sharing what we discover and being in a network, always keeping in touch, is the most important thing.

During these three years, I was witness of ideas generated from a simple and informal conversation between two persons who, although they do not work in the same field, share the same feeling. Therefore, whom do we must thank? Does it really exist a limited group of person that we can list without falling into boredom? I think, it does not. Anyhow, we always try to do our best to thanking all the persons who have taught us how to think in a scientific way, how to manage a science project, how to grow in science. But not only in science. There are also other persons who have taught us what we are now, and what we will be in future.

Most of my research work was carried out at the Department of Biological Sciences, University of Naples “Federico II” (Italy) and partially at the CEINGE, at the INRA and at the Department of Chemistry, University of Naples. Much of this work is the direct result of collaborations with other researchers, and without their help, I could not have come so far. First of all I must say thank to Prof. Adriana Zagari, who allowed me to make the wonderful experience of the doctorate. She was not only my supervisor, but also my guide on this route, showing me how fascinating is the world of science research. I learned from her integrity and professionalism in the work, but also the love for research. She is a real teacher and a guide.

Beside the supervision of our Professor, for us PhD students, there is always someone who teaches us and drives us toward the right direction. For me this person is Vincenzo Granata, with whom I was always worked side by side with confidence to find always the best colleague. Another important component of Zagari’s group is Carla Carluccio. In Carla, I found not only another close collaborator, but also a good friend. Her presence in our team was crucial to make perfect an environment that I wish every PhD student could have in his doctorate experience. Finally, I want to say thank also to Luca Ambrosino, our master student for his sympathy and his kindness.

Prof. Francesco Salvatore has also been instrumental in my doctoral research, having served as the principal investigator for two important works, carried out at CEINGE with his collaborators: Prof. Aurora Daniele and Prof. Pasqualina Buono. My main collaborator in the works performed at CEINGE was Monica Cerreto, who has enjoyed with me for the wonderful work made together. Ultimately, I must say thank to Prof. Salvatore to have introduced me in the world of: listening to biomolecules to silence disease.

A very important experience, during my thesis work, has been the stage at the INRA in Paris, under the supervision of Dr. Human Rezaei. I have been in Rezaei’s lab for almost one year but for me it seems that I have worked there for all my life. It occurs usually in this way when we meet a person or we work somewhere and we feel perfectly comfortable. I have learned too much from this experience. First of all, I must say thanks to Dr. Rezaei. His passion for science, his way to think, project and

manage the work, his enthusiasm and, above all, his goodness have inspired me. He has created a little world where I could learn what science really means and where I have met so many wonderful persons. One of these persons is Joan Torrent. The patience and accuracy with which he conducts his work, has been enlightening for me. He played for me the same role as Vincenzo, teaching me and guiding me.

Another wonderful person (but they are all wonderful) is Stephanie Prigent, who was for me a great support and a guide when I arrived at INRA. Thanks to her, I could enter little by little in the world of prion lab. I have learned from her strength and firmness in work, but more important, I must say thanks to her to have allowed me to be part of her life. Not long after, I have met Katarina Grznarova. Her joy and passion on everything what she does in her life is just fascinating. But the most important thing is that I have gained a best friend. Another fundamental piece in my “parissienne” life, and not only, is Khalid Salamat. He is one of the best persons I have met in my life, professionally and personally. Whatever I can say it would not be enough to say thank to him, for all what he did for me.

I would like also to thank Dr. Annalisa Pastore. She has been instrumental for all what concerned my work in Paris. Her helpfulness and her advices were fundamental for the work made at INRA.

Of course, I cannot forget other incredible persons: Qiaojing, Celine Hernandez, Nesrine, Philipp, Zhou, Lieke, Florian, Olivier, Angelique, Yves, Pierre, Jasmina, Celine Chapuis, Stephanie Steunou, Sylvie, Vincent, Elizabeth. Sorry if I forgot someone.....

All together, they made me feel like home and they will remain indelible in my life.

Last but not least, I would like to thank Prof. Concetta Giancola and her team for the work that actually we are carrying out together, and for hosting me in her lab as part of the family.

Finally, I must thank my family, those to whom I owe what I am. There are no other persons that love me as they do, unconditionally, unreservedly, limitless. They are always, in whatever moment of my life, my landmark. Simply, without them, I could not reach what I have gained till now. They are the reason why I am here.

References

- Adler, V.**, Zeiler, B., Kryukov, V., Kascsak, R., Rubenstein, R. and Grossman, A., 2003. Small, highly structured RNAs participate in the conversion of human recombinant PrP(Sen) to PrP(Res) in vitro. *J. Mol. Biol.* **332**, 47-57.
- Aguzzi, A.**, Baumann, F. and Bremer, J., 2008. The prion's elusive reason for being. *Annu. Rev. Neurosci.* **31**, 439-477.
- Aguzzi, A.** and Calella, A. M., 2009. Prions: Protein Aggregation and Infectious Diseases. *Physiol. Rev.* **89**, 1105-1152.
- Aguzzi, A.** and Polymenidou, M., 2004. Mammalian prion biology: one century of evolving concepts. *Cell* **116**, 313-327.
- Ahn, A. H.**, Dziennis, S., Hawkes, R. and Herrup, K., 1994. The cloning of zebrin II reveals its identity with aldolase C. *Development* **120**, 2081-2090.
- Alper, T.**, Haig, D. A. and Clarke, M. C., 1987. The scrapie agent: evidence against its dependence for replication on intrinsic nucleic acid. *J. Gen. Virol.* **41**, 503-516.
- Arakaki, T. L.**, Pezza, J. A., Cronin, M. A., Hopkins, C. E., Zimmer, D. B., Tolan, D. R. and Allen, K. N., 2004. Structure of human brain fructose 1,6-(bis)phosphate aldolase: linking isozyme structure with function. *Protein Sci.* **13**, 3077-3084.
- Atamna, H.**, Nguyen, A., Schultz, C., Boyle, K., Newberry, J., Kato, H. and Ames, B. N., 2008. Methylene blue delays cellular senescence and enhances key mitochondrial biochemical pathways. *FASEB J.* **22**(703-712).
- Azzalin, A.**, Ferrara, V., Arias, A., Cerri, S., Avella, D., Pisu, M. B., Nano, R., Bernocchi, G., Ferretti, L. and Comincini, S., 2006. Interaction between the cellular prion (PrP^C) and the 2P domain K⁺ channel TREK-1 protein. *Biochem. Biophys. Res. Commun.* **346**, 108-115.
- Barret, A.**, Tagliavini, F., Forloni, G., Bate, C., Salmona, M., Colombo, L., De Luigi, A., Limido, L., Suardi, S., Rossi, G., Auvré, F., Adjou, K. T., Salès, N., Williams, A., Lasmezas, C. and Deslys, J. P., 2003. Evaluation of quinacrine treatment for prion diseases. *J. Virol.* **77**, 8462-8469.
- Baskakov, I. V.**, Legname, G., Baldwin, M. A., Prusiner, S. B. and Cohen, F. E., 2002. Pathway complexity of prion protein assembly into amyloid. *J. Biol. Chem.* **277**, 21140-21148.
- Basler, K.**, Oesch, B., Scott, M., Westaway, D., Wälchli, M., Groth, D. F., McKinley, M. P., Prusiner, S. B. and Weissmann, C., 1986. Scrapie and cellular PrP isoforms are encoded by the same chromosomal gene. *Cell* **46**, 417-428.
- Bera, A.**, Roche, A. C. and Nandi, P. K., 2007. Bending and unwinding of nucleic acid by prion protein. *Biochemistry* **46**, 1320-1328.
- Bjorndahl, T. C.**, Zhou, G. P., Liu, X., Perez-Pineiro, R., Semchenko, V., Saleem, F., Acharya, S., Bujold, A., Sobsey, C. A. and Wishart, D. S., 2011. Detailed biophysical characterization of the acid-induced PrP(c) to PrP(β) conversion process. *Biochemistry* **50**, 1162-1173.
- Blass, N.** and Fung, D., 1976. Dyed but not dead-methylene blue overdose. *Anesthesiology* **45**, 458-459.
- Brandner, S.**, Isenmann, S., Raeber, A., Fischer, M., Sailer, A., Kobayashi, Y., Marino, S., Weissmann, C. and Aguzzi, A., 1996. Normal host prion protein necessary for scrapie-induced neurotoxicity. *Nature* **379**, 339-343.
- Bremer, J.**, Baumann, F., Tiberi, C., Wessig, C., Fischer, H., Schwarz, P., Steele, A. D., Toyka, K. V., Nave, K., Weis, J. and Aguzzi, A., 2010. Axonal prion protein is required for peripheral myelin maintenance. *Nature Neurosci.* **13**, 310-318.
- Büeler, H.**, Aguzzi, A., Sailer, A., Greiner, R. A., Autenried, P., Aguet, M. and Weissmann, C., 1993. Mice devoid of PrP are resistant to scrapie. *Cell* **73**, 1339-1347.
- Calhoun, D. B.**, Vanderkooi, J. M., Holtorn, G. R. and Englander, S. W., 1986. Protein Fluorescence Quenching by Small Molecules: Protein Penetration Versus Solvent Exposure. *Proteins* **1**, 109-115.
- Callaway, N. L.**, Riha, P. D., Wrubel, K. M., McCollum, D. and Gonzalez-Lima, F., 2002. Methylene blue restores spatial memory retention impaired by an inhibitor of cytochrome oxidase in rats. *Neurosci. Lett.* **332**, 83-86.
- Cañete-Soler, R.**, Reddy, K. S., Tolan, D. R. and Zhai, J., 2005. Aldolases A and C are ribonucleolytic components of a neuronal complex that regulates the stability of the light-neurofilament mRNA. *J. Neurosci.* **25**, 4353-4364.
- Cantor, C. R.**, Warshaw, M. M. and Shapiro, H., 1970. Oligonucleotide interactions. III. Circular dichroism studies of the conformation of deoxyoligonucleotides. *Biopolymers* **9**, 1059-1077.

- Caspi, S.**, Halimi, M., Yanai, A., Sasson, S. B., Taraboulos, A. and Gabizon, R., 1998. The anti-prion activity of Congo red. Putative mechanism. *J. Biol. Chem.* **273**, 3484-3489.
- Castilla, J.**, Saa, P., Hetz, C. and Soto, C., 2005. In vitro generation of infectious scrapie prions. *Cell* **121**, 195-206.
- Caughey, B.**, 2001. Interactions between prion protein isoforms: The kiss of death? . *Trends Biochem. Sci.* **26**, 235-242.
- Caughey, B.**, Brown, K., Raymond, G. J., Katzeinstein, G. E. and Thresher, W., 1994. Binding of the protease-sensitive form of PrP (prion protein) to sulfated glycosaminoglycan and congo red. *J. Virol.* **68**, 2135-2141.
- Caughey, B.**, Caughey, W. S., Kocisko, D. A., Lee, K. S., Silveira, J. R. and Morrey, J. D., 2006. Prions and transmissible spongiform encephalopathy (TSE) chemotherapeutics: A common mechanism for anti-TSE compounds? *Accts. Chem. Res.* **39**, 646-653.
- Caughey, B.** and Chesebro, B., 2001. Transmissible spongiform encephalopathies and prion protein interconversions. *Adv. Virus Res.* **56**, 277-311.
- Caughey, B.** and Lansbury, P. T., 2003. Protofibrils, pores, fibrils, and neurodegeneration: Separating the responsible protein aggregates from the innocent bystanders. *Annu. Rev. Neurosci.* **26**, 267-298.
- Caughey, B.** and Race, R. E., 1992. Potent inhibition of scrapie-associated PrP accumulation by congo red. *J. Neurochem.* **59**, 768-777.
- Caughey, B.** and Raymond, G. J., 1993. Sulfated polyanion inhibition of scrapie-associated PrP accumulation in cultured cells. *J. Virol.* **67**, 643-650.
- Caughey, B.**, Raymond, L. D., Raymond, G. J., Maxson, L., Silveira, J. and Baron, G. S., 2003. Inhibition of protease-resistant prion protein accumulation in vitro by curcumin. *J. Virol.* **77**, 5499-5502.
- Caughey, B. W.**, Dong, A., Bhat, K. S., Ernst, D., Hayes, S. F. and Caughey, W. S., 1991. Secondary structure analysis of the scrapie-associated protein PrP 27-30 in water by infrared spectroscopy. *Biochemistry* **30**, 7672-7680.
- Caughey, W. S.**, Raymond, L. D., Horiuchi, M. and Caughey, B., 1998. Inhibition of protease-resistant prion protein formation by porphyrins and phthalocyanines. *Proc. Natl. Acad. Sci. U.S.A.* **95**, 12117-12122.
- Cawein, M.**, Behlen, C. H. n., Lappat, E. J. and Cohn, J. E., 1964. Hereditary diaphorase deficiency and methemoglobinemia. *Arch. Intern. Med.* **113**, 578-585.
- Chakraborty, N.**, Prigent, S., Dreiss, C. A., Noinville, S., Chapuis, C., Fraternali, F. and Rezaei, H., 2010. The oligomerization properties of prion protein are restricted to the H2H3 domain. *FASEB J.* **24**, 3222-3231.
- Chiti, F.** and Dobson, C. M., 2006. Protein misfolding, functional amyloid, and human disease. *Annu. Rev. Biochem.* **75**, 333-366.
- Choi, C. J.**, Kanthasamy, A., Anantharam, V. and Kanthasamy, A. G., 2006. Interaction of metals with prion protein: Possible role of divalent cations in the pathogenesis of prion diseases. *Neurotoxicology* **27**, 777-787.
- Clifton II, J.** and Leikin, J. B., 2003. Methylene blue. *Am. J. Ther.* **10**, 289-291.
- Clodi, E.**, Semrad, K. and Schroeder, R., 1999. Assaying RNA chaperone activity in vivo using a novel RNA folding trap. *EMBO J.* **18**, 3776-3782.
- Cohen, F. E.**, 1999. Protein misfolding and prion diseases. *J. Mol. Biol.* **293**, 313-320.
- Collinge, J.**, 2001. Prion diseases of humans and animals: Their causes and molecular basis. *Annu. Rev. Neurosci.* **24**, 519-550.
- Come, J. H.**, Fraser, P. E. and Lansbury, P. T. J., 1993. A kinetic model for amyloid formation in the prion diseases: importance of seeding. *Proc. Natl. Acad. Sci. U. S. A.* **90**, 5959-5963.
- Cordeiro, Y.**, Machado, F., Juliano, L., Juliano, M. A., Brentani, R. R., Foguel, D. and Silva, J. L., 2001. DNA converts cellular prion protein into the beta-sheet conformation and inhibits prion peptide aggregation. *J. Biol. Chem.* **276**, 49400-49409.
- Cordeiro, Y.** and Silva, J. L., 2005. The hypothesis of the catalytic action of nucleic acid on the conversion of prion protein. *Protein Pept. Lett.* **12**, 251-255.
- Creutzfeldt, H. G.**, 1920. Über eine eigenartige herdformige erkrankung des zentralnervensystems. *Z. Ges. Neurol. Psychiatr.* **57**, 1-19.
- Cristofari, G.** and Darlix, J. L., 2002. The ubiquitous nature of RNA chaperone proteins. *Prog. Nucleic Acid Res. Mol. Biol.* **72**, 223-268.
- Dalby, A. R.**, Tolan, D. R. and Littlechild, J. A., 2001. The structure of human liver fructose-1,6-bisphosphate aldolase. *Acta Crystallogr. D Biol. Crystallogr.* **57**, 1526-1533.

- Dandoy-Dron, F.**, Benboudjema, L., Guillo, F., Jaegly, A., Jasmin, C., Dormont, D., Tovey, M. G. and Dron, M., 2000. Enhanced levels of scrapie responsive gene mRNA in BSE-infected mouse brain. *Brain Res. Mol. Brain Res.* **76**, 173-179.
- Daniele, A.**, Cardillo, G., Pennino, C., Carbone, M. T., Scognamiglio, D., Correra, A., Pignero, A., Castaldo, G. and Salvatore, F., 2007. Molecular epidemiology of phenylalanine hydroxylase deficiency in Southern Italy: a 96% detection rate with ten novel mutations. *Ann. Hum. Genet.* **71**, 185-93.
- Daniele, A.**, Cardillo, G., Pennino, C., Carbone, M. T., Scognamiglio, D., Esposito, L., Correra, A., Castaldo, G., Zagari, A. and Salvatore, F., 2008. Five human phenylalanine hydroxylase proteins identified in mild hyperphenylalaninemia patients are disease-causing variants. *Biochim. Biophys. Acta.* **1782**, 378-384.
- Daniele, A.**, Scala, I., Cardillo, G., Pennino, C., Ungaro, C., Sibilio, M., Parenti, G., Esposito, L., Zagari, A., Andria G. and Salvatore, F., 2009. Functional and structural characterization of novel mutations and genotype-phenotype correlation in 51 phenylalanine hydroxylase deficient families from Southern Italy. *Febs J.* **276**, 2048-2059.
- Davidowitz, E.**, Eljuga, L., Dover, K., Tian, J. and Grossman, A., 2005. Concentration of prion protein from biological samples to increase the limits of detection by immunoassay. *Biotechnol. Appl. Biochem.* **41**, 247-253.
- De Fea, K. A.**, Nakahara, D. H., Calayag, M. C., Yost, C. S., Mirels, L. F., Prusiner, S. B. and Lingappa, V. R., 1994. Determinants of carboxyl-terminal domain translocation during prion protein biogenesis. *J. Biol. Chem.* **269**, 16810-16820.
- De Simone, A.**, Dodson, G. G., Verma, C. S., Zagari, A. and Fraternali, F., 2005. Prion and water: tight and dynamical hydration sites have a key role in structural stability. *Proc. Natl. Acad. Sci. U. S. A.* **102**, 7535-7540.
- De Simone, A.**, Zagari, A. and Derreumaux, P., 2007. Structural and Hydration Properties of the Partially Unfolded States of the Prion Protein. *Biophys. J.* **93**, 1284-1292.
- Deleault, N. R.**, Harris, B. T., Rees, J. R. and Supattapone, S., 2007. Formation of native prions from minimal components in vitro. *Proc. Natl. Acad. Sci. U. S. A.* **104**, 9741-9746.
- Deleault, N. R.**, Lucassen, R. W. and Supattapone, S., 2003. RNA molecules stimulate prion protein conversion. *Nature* **425**, 717-720.
- Di Santo, A. R.** and Wagner, J. G., 1972. Pharmacokinetics of highly ionized drugs. II. Methylene blue: Absorption, metabolism, and excretion in man and dog after oral administration. *J. Pharm. Sci.* **61**, 1086-1090.
- Dobson, C.**, 2003. Protein folding and misfolding. *Nature* **426**, 884-890.
- Donne, D. G.**, Viles, J. H., Groth, D., Mehlhorn, I., James, T. L., Cohen, F. E., Prusiner, S. B., Wright, P. E. and Dyson, H. J., 1997. Structure of the recombinant full-length hamster prion protein PrP(29-231): The N terminus is highly flexible. *Proc. Natl. Acad. Sci. U.S.A.* **94**, 13452-13457.
- Donne, D. G.**, Viles, J. H., Groth, D., Melhorn, I., James, T. L., Cohen, F. E., Prusiner, S. B., Wright, P. E. and Dyson, J. H., 1997. Structure of the recombinant full-length hamster prion protein PrP(29-231): The N terminus is highly flexible. *Proc. Natl. Acad. Sci. U.S.A.* **94**, 13452-13457.
- Eberl, H.**, Tittmann, P. and Glockshuber, R., 2004. Characterization of recombinant, membrane-attached full-length prion protein. *J. Biol. Chem.* **279**, 25058-25065.
- Edenhofer, F.**, Rieger, R., Famulok, M., Wendler, W., Weiss, S. and Winnacker, E. L., 1996. Prion protein PrP^C interacts with molecular chaperones of the Hsp60 family. *J. Virol.* **70**, 4724-4728.
- Eghiaian, F.**, Daubenfeld, T., Quenet, Y., van Audenhege, M., Bouin, A. P., van der Rest, G., Grosclaude, J. and Rezaei, H., 2007. Diversity in prion protein oligomerization pathways results from domain expansion as revealed by hydrogen/deuterium exchange and disulfide linkage. *Proc. Natl. Acad. Sci. U.S.A.* **104**, 7414-7419.
- Eghiaian, F.**, Daubenfeld, T., Quenet, Y., van Audenhege, M., Bouin, A. P., van der Rest, G., Grosclaude, J., and Rezaei, H., 2007. Diversity in prion protein oligomerization pathways results from domain expansion as revealed by hydrogen/deuterium exchange and disulfide linkage. *Proc. Natl. Acad. Sci. U.S.A.* **104**, 7414-7419.
- Ellis, V.**, Daniels, M., Misra, R. and Brown, D. R., 2002. Plasminogen activation is stimulated by prion protein and regulated in a copper-dependent manner. *Biochemistry* **41**, 6891-96.
- Esposito, G.**, Vitagliano, L., Cevenini, A., Amelio, T., Zagari, A. and Salvatore, F., 2005. Unraveling the structural and functional features of an aldolase A mutant involved in the hemolytic anemia and severe rhabdomyolysis reported in a child. *Blood* **105**, 905-906.
- Flechsig, E.**, Shmerling, D., Hegyi, I., Raeber, A. J., Fischer, M., Cozzio, A., von Mering, C., Aguzzi, A. and Weissmann, C., 2000. Prion protein devoid of the octapeptide repeat region restores susceptibility to scrapie in PrP knockout mice. *Neuron* **27**, 399-408.

- Funari, V. A.**, Herrera, V. L., Freeman, D. and Tolan, D. R., 2005. Genes required for fructose metabolism are expressed in Purkinje cells in the cerebellum. *Brain Res. Mol. Brain Res.* **142**, 115-122.
- Fusetti, F.**, Erlandsen, H., Flatmark, T. and Stevens, R. C., 1998. Structure of tetrameric human phenylalanine hydroxylase and its implications for phenylketonuria. *J. Biol. Chem.* **273**, 16962-16967.
- Gabus, C.**, Auxilien, S., Pechoux, C., Dormont, D., Swietnicki, W., Morillas, M., Surewicz, W., Nandi, P. and Darlix, J. L., 2001. The prion protein has DNA strand transfer properties similar to retroviral nucleocapsid protein. *J. Mol. Biol.* **307**, 1011-1021.
- Gabus, C.**, Derrington, E., Leblanc, P., Chnaiderman, J., Dormont, D., Swietnicki, W., Morillas, M., Surewicz, W. K., Marc, D., Nandi, P. and Darlix, J. L., 2001. The prion protein has RNA binding and chaperoning properties characteristic of nucleocapsid protein NCP7 of HIV-1. *J. Biol. Chem.* **276**, 19301-19309.
- Gamblin, S. J.**, Davies, G. J., Grimes, J. M., Jackson, R. M., Littlechild, J. A. and Watson, H. C., 1991. Activity and specificity of human aldolases. *J. Mol. Biol.* **219**, 573-576.
- Gao, C.**, Lei, Y. J., Han, J., Shi, Q., Chen, L., Guo, Y., Gao, Y. J., Chen, J. M., Jiang, H. Y., Zhou, W. and Dong, X. P., 2006. Recombinant neural protein PrP can bind with both recombinant and native apolipoprotein E in vitro. *Acta Biochim. Biophys. Sin.* **38**, 593-601.
- Gatto, B.**, Palumbo, M. and Sissi, C., 2009. Nucleic Acid aptamers based on the g-quadruplex structure: therapeutic and diagnostic potential. *Curr. Med. Chem.* **16**, 1248-1265.
- Gawinecka, J.**, Dieks, J., Asif, A. R., Carimalo, J., Heinemann, U., Streich, J. H., Dihazi, H., Schulz-Schaeffer, W. and Zerr, I., 2010. Codon 129 polymorphism specific cerebrospinal fluid proteome pattern in sporadic Creutzfeldt-Jakob disease and the implication of glycolytic enzymes in prion-induced pathology. *J. Proteome Res.* **9**, 5646-5657.
- Ge, W. W.**, Leystra-Lantz, C., Wen, W. and Strong, M. J., 2003. Selective loss of trans-acting instability determinants of neurofilament mRNA in amyotrophic lateral sclerosis spinal cord. *J. Biol. Chem.* **278**, 26558-26563.
- Gomes, M. P.**, Cordeiro, Y. and Silva, J. L., 2008^a. The peculiar interaction between mammalian prion protein and RNA. *Prion* **2**, 64-66.
- Gomes, M. P.**, Millen, T. A., Ferreira, P. S., e Silva, N. L., Vieira, T. C., Almeida, M. S., Silva, J. L. and Cordeiro, Y., 2008^b. Prion protein complexed to N2a cellular RNAs through its N-terminal domain forms aggregates and is toxic to murine neuroblastoma cells. *J. Biol. Chem.* **283**, 19616-19625.
- Graner, E.**, Mercadante, A. F., Zanata, S. M., Martins, V. R., Jay, D. G. and Brentani, R. R., 2000. Laminin-induced PC-12 cell differentiation is inhibited following laser inactivation of cellular prion protein. *FEBS Lett.* **482**, 257-260.
- Gregersen, N.**, Bross, P., Vang, S. and Christensen, J. H., 2006. Protein misfolding and human disease. *Annu. Rev. Genomics Hum. Genet.* **7**, 103-124.
- Griffith, J. S.**, 1967. Self-replication and scrapie. *Nature* **215**, 1043-1044.
- Gura, T.**, 2008. Hope in Alzheimer's fight emerges from unexpected places. *Nat. Med.* **14**, 894.
- Guttmann, P.** and Ehrlich, P., 1891. Über die Wirkung des Methylenblau bei Malaria. *Berlin. Klin. Woch.* **28**, 953-956.
- Hajieva, P.**, Mocko, J. B., Moosmann, B. and Behl, C., 2009. Novel imine antioxidants at lownanomolar concentrations protect dopaminergic cells from oxidative neurotoxicity. *J. Neurochem.* **110**, 118-132.
- Hajj, G. N.**, Lopes, M. H., Mercadante, A. F., Veiga, S. S., da Silveira, R. B., Santos, T. G., Ribeiro, K. C., Juliano, M. A., Jacchiero, S. G., Zanata, S. M. and Martins, V. R., 2007. Cellular prion protein interaction with vitronectin supports axonal growth and is compensated by integrins. *J. Cell Sci.* **120**, 1915-1926.
- Haraguchi, T.**, Fisher, S., Olofsson, S., Endo, T., Groth, D., Tarentino, A., Borchelt, D. R., Teplow, D., Hood, L., Burlingame, A., Lycke, E., Kobata, A. and Prusiner, S. B., 1989. Asparagine-linked glycosylation of the scrapie and cellular prion proteins. *Arch. Biochem. Biophys.* **274**, 1-13.
- Haslberger, T.**, Bukau, B. and Mogk, A., 2010. Towards a unifying mechanism for ClpB/Hsp104-mediated protein disaggregation and prion propagation. *Biochem. Cell Biol.* **88**(63-75).
- Hegde, R. S.**, Mastrianni, J. A., Scott, M. R., DeFea, K. A., Tremblay, P., Torchia, M., DeArmond, S. J., Prusiner, S. B. and Lingappa, V. R., 1998. A transmembrane form of the prion protein in neurodegenerative disease. *Science* **279**, 827-834.
- Herman, M. I.**, Chyka, P. A., Butler, A. Y. and Rieger, S. E., 1999. Methylene blue by intraosseous infusion for methemoglobinemia. *Ann. Emerg. Med.* **33**, 111-113.

- Horiuchi, M.**, Priola, S. A., Chabry, J. and Caughey, B., 2000. Interactions between heterologous forms of prion protein: binding, inhibition of conversion, and species barriers. *Proc. Natl. Acad. Sci. U.S.A.* **97**, 5836-5841.
- Horiuchi, M.**, Yamazaki, N., Ikeda, T., Ishiguro, N. and Shinagawa, M., 1995. A cellular form of prion protein (PrPC) exists in many non-neuronal tissues of sheep. *J. Gen. Virol.* **76**, 2583-2587.
- Horn, J. R.**, Brandts, J. F. and Murphy, K. P., 2002. van't Hoff and calorimetric enthalpies II: effects of linked equilibria. *Biochemistry* **41**, 7501-7507.
- Hornemann, S.**, Schorn, C. and Wuthrich, K., 2004. NMR structure of the bovine prion protein isolated from healthy calf brains. *EMBO Rep* **5**, 1159-1164.
- Hornsey, V. S.**, Casey, C., McColl, K., Young, H., Drummond, O., McMillan, L., Morrison, A. and Prowse, C. V., 2010. Characteristics of prion-filtered red cells suspended in pathogen-inactivated plasma (MB treated or solvent-detergent treated) for neonatal exchange transfusion. *Vox Sang.* **101**, 28-34.
- Horonchik, L.**, Tzaban, S., Ben-Zaken, O., Yedidia, Y., Rouvinski, A., Papy-Garcia, D., Barritault, D., Vlodavsky, I. and Taraboulos, A., 2005. Heparan sulfate is a cellular receptor for purified infectious prions. *J. Biol. Chem.* **280**, 17062-17067.
- Hosokawa-Muto, J.**, Kamatari, Y. O., Hironori, K., Nakamura, H. K. and Kuwata, K., 2008. Variety of Antiprion Compounds Discovered through an In Silico Screen Based on Cellular-Form Prion Protein Structure: Correlation between Antiprion Activity and Binding Affinity. *Antimicrob. Agents Chemother.* **53**, 765-771.
- Jakob, A.**, 1921. Über eigenartige erkrankungen des zentralnervensystems mit bemerkenswertem anatomischem befunde (spastische pseudosklerose-encephalomyelopathie mit disseminierten degenerationsherden). *Z. Ges. Neurol. Psychiatr.* **64**, 147-228.
- Jang, B.**, Kim, E., Choi, J. K., Jin, J. K., Kim, J. I., Ishigami, A., Maruyama, N., Carp, R. I., Kim, Y. S. and Choi, E. K., 2008. Accumulation of citrullinated proteins by up-regulated peptidylarginine deiminase 2 in brains of scrapie-infected mice: a possible role in pathogenesis. *Am. J. Pathol.*, 1129-1142.
- Jenkins, D. C.**, Sylvester, I. D. and Pinheiro, T. J., 2008. The elusive intermediate on the folding pathway of the prion protein. *FEBS J.* **275**, 1323-1335.
- Jewett, T. J.** and Sibley, L. D., 2003. Aldolase forms a bridge between cell surface adhesins and the actin cytoskeleton in apicomplexan parasites. *Mol. Cell* **11**, 885-894.
- Jinwal, U. K.**, Miyata, Y., Koren, J. r., Jones, J. R., Trotter, J. H., Chang, L., O'Leary, J., Morgan, D., Lee, D. C., Shults, C. L., Rousaki, A., Weeber, E. J., Zuiderweg, E. R., Gestwicki, J. E. and Dickey, C. A., 2009. Chemical manipulation of hsp70ATPase activity regulates tau stability. *J. Neurosci.* **29**, 12079-12088.
- Karkhoff-Schweizer, R.** and Knull, H. R., 1987. Demonstration of tubulin-glycolytic enzyme interactions using a novel electrophoretic approach. *Biochem. Biophys. Res. Commun.* **146**, 827-831.
- Kazlauskaite, J.**, Young, A., Gardner, C. E., Macpherson, J. V., Venien-Bryan, C. and Pinheiro, T. J., 2005. An unusual soluble beta-turn-rich conformation of prion is involved in fibril formation and toxic to neuronal cells. *Biochem. Biophys. Res. Commun.* **328**, 292-305.
- Kellings, K.**, Prusiner, S. B. and Riesner, D., 1994. Nucleic acids in prion preparations: unspecific background or essential component? *Philos. Trans. R. Soc. Lond. B Biol. Sci.* **343**, 425-430.
- Keniry, M. A.**, 2000. Quadruplex structures in nucleic acids. *Biopolymers* **56**, 123-46.
- Keshet, G. I.**, Bar-Peled, O., Yaffe, D., Nudel, U. and Gabizon, R., 2000. The cellular prion protein colocalizes with the dystroglycan complex in the brain. *J. Neurochem.* **75**, 1889-1897.
- Kettani, A.**, Gorin, A., Majumdar, A., Hermann, T., Skripkin, E., Zhao, H., Jones, R. and Patel, D. J., 2000. A dimeric DNA interface stabilized by stacked A:(G:G:G:G):A hexads and coordinated monovalent cations. *J. Mol. Biol.* **297**, 627-644.
- Kim, H.**, Chatani, E., Goto, Y. and Paik, S., 2007. Seed-dependent accelerated fibrillation of alpha-synuclein induced by periodic ultrasonication treatment. *J Microbiol Biotechnol* **17**, 2027-2032.
- Kocisko, D. A.**, Vaillant, A., Lee, K. S., Arnold, K. M., Bertholet, N., Race, R. E., Olsen, E. A., Juteau, J. M. and Caughey, B., 2006. Potent anti-scrapie activities of degenerate phosphorothioate oligonucleotides. *Antimicrob. Agents Chemother.* **50**, 1034-1044.
- Kocisko, D. A.**, Vaillant, A., Lee, K. S., Arnold, K. M., Bertholet, N., Race, R. E., Olsen, E. A., Juteau, J. M. and Caughey, B., 2006. Potent antiscrapie activities of degenerate phosphorothioate oligonucleotides. *Antimicrob. Agents Chemother.* **50**, 1034-1044.
- Korth, C.**, May, B. C., Cohen, F. E. and Prusiner, S. B., 2001. Acridine and phenothiazine derivatives as pharmacotherapeutics for prion disease. *Proc. Natl. Acad. Sci. U.S.A.* **98**, 9836-9841.

- Kupfer, A.**, Aeschlimann, C., Wermuth, B. and Cerny, T., 1994. Prophylaxis and reversal of ifosfamid encephalopathy with methylene-blue. *Lancet* **343**, 763-764.
- Kurschner, C.** and Morgan, J. I., 1995. The cellular prion protein (PrP) selectively binds to Bcl-2 in the yeast two-hybrid system. *Brain Res. Mol. Brain Res.* **30**, 165-168.
- Kusakabe, T.**, Motoki, K. and Hori, K., 1994. Human aldolase C: Characterization of the recombinant enzyme expressed in *Escherichia coli*. *J. Biochem.* **115**, 1172-1177.
- Kuwata, K.**, Li, H., Yamada, H., Legname, G., Prusiner, S. B., Akasaka, K. and James, T. L., 2002. Locally Disordered Conformer of the Hamster Prion Protein: A Crucial Intermediate to PrP^{Sc}. *Biochem.* **41**, 12277-12283.
- Kuwata, K.**, Nishida, N., Matsumoto, T., Kamatari, Y. O., Hosokawa-Muto, J., Kodama, K., Nakamura, H. K., Kimura, K., Kawasaki, M., Takakura, Y., Shirabe, S., Takata, J., Kataoka Y. and Katamine, S., 2007. Hot spots in prion protein for pathogenic conversion. *Proc. Natl. Acad. Sci. U. S. A.* **104**, 11921-11926.
- Lakowicz, J. R.**, 1999. Principles of Fluorescence Spectroscopy. Plenum Press, New York.
- Lashuel, H. A.**, Hartley, D., Petre, B. M., Walz, T., Lansbury, P. T. J. and 418:291., 2002. New class of inhibitors of amyloid-beta fibril formation. Implications for the mechanism of pathogenesis in Alzheimer's disease. *Nature* **418**, 291.
- Lasmezas, C. I.**, Deslys, J. P., Robain, O., Jaegly, A., Beringue, V., Peyrin, J. M., Fournier, J. G., Hauw, J. J., Rossier, J. and Dormont, D., 1997. Transmission of the BSE agent to mice in the absence of detectable abnormal prion protein. *Science* **275**, 402-405.
- Laughlan, G.**, Murchie, A. I. H., Norman, D. G., Moore, M. H., Moody, P. C., Lilley, D. M. and Luisi, B., 1994. The high-resolution crystal structure of a parallel-stranded guanine tetraplex. *Science* **265**, 520-524.
- Leandro, J.**, Simonsen, N., Saraste, J., Leandro, P. and Flatmark, T., 2010. Phenylketonuria as a protein misfolding disease: The mutation pG46S in phenylalanine hydroxylase promotes self-association and fibril formation. *Biochim. Biophys. Acta.* **1812**, 106-120.
- Lee, Y. J.**, Savtchenko, R., Ostapchenko, V. G., Makarava, N. and Baskakov, I., 2011. Molecular structure of amyloid fibrils controls the relationship between fibrillar size and toxicity. *PLoS One* **6**, e20244.
- Legname, G.**, Baskakov, I. V., Nguyen, H. O., Riesner, D., Cohen, F. E., DeArmond, S. J. and Prusiner, S. B., 2004. Synthetic mammalian prions. *Science* **305**, 673-676.
- Lima, L. M.**, Cordeiro, Y., Tinoco, L. W., Marques, A. F., Oliveira, C. L., Sampath, S., Kodali, R., Choi, G., Foguel, D., Torriani, I., Caughey, B. and Silva, J. L., 2006. Structural insights into the interaction between prion protein and nucleic acid. *Biochemistry* **45**, 9180-9187.
- Lu, B. Y.** and Chang, J. Y., 2002. Isolation and characterization of a polymerized prion protein. *Biochem. J.* **364**, 81-87.
- Lu, M.**, Holliday, L. S., Zhang, L., Dunn Jr., W. A. and Gluck, S. L., 2001. Interaction between aldolase and vacuolar H⁺-ATPase: Evidence for direct coupling of glycolysis to the ATP-hydrolyzing proton pump. *J. Biol. Chem.* **276**, 30407-30413.
- Málaga-Trillo, E.**, Solis, G. P., Schrock, Y., Geiss, C., Luncz, L., Thomanetz, V. and Stuermer, C. A., 2009. Regulation of embryonic cell adhesion by the prion protein. *PLoS Biol.* **7**, e55.
- Malay, A. D.**, Prociou, S. L. and Tolan, D. R., 2002. The temperature dependence of activity and structure for the most prevalent mutant aldolase B associated with hereditary fructose intolerance. *Arch. Biochem. Biophys.* **408**, 295-304.
- Mallolas, J.**, Vilaseca, M. A., Campistol, J., Lambruschini, N., Cambra, F. J., Estivill, X. and Mila, M., 1999. Mutational spectrum of phenylalanine hydroxylase deficiency in the population resident in Catalonia: genotype-phenotype correlation. *Hum. Genet.* **105**, 468-73.
- Mallucci, G.**, Dickinson, A., Linehan, J., Kohn, P. C., Brandner, S. and Collinge, J., 2003. Depleting neuronal PrP in prion infection prevents disease and reverses spongiosis. *Science* **302**, 871-874.
- Mallucci, G. R.**, White, M. D., Farmer, M., Dickinson, A., Khatun, H., Powell, A. D., Brandner, S., Jefferys, J. G. and Collinge, J., 2007. Targeting cellular prion protein reverses early cognitive deficits and neurophysiological dysfunction in prion-infected mice. *Neuron* **53**, 325-335.
- Maness, P. F.** and Schachner, M., 2007. Neural recognition molecules of the immunoglobulin superfamily: signaling transducers of axon guidance and neuronal migration. *Nat. Neurosci.* **10**, 19-26.
- Manson, J. C.**, Jamieson, E., Baybutt, H., Tuzi, N. L., Barron, R., McConnell, I., Somerville, R., Ironside, J., Will, R., Sy, M. S., Melton, D. W., Hope, J. and Bostock, C., 1999. A single amino acid alteration (101L) introduced into murine PrP dramatically alters incubation time of transmissible spongiform encephalopathy. *EMBO J.* **18**, 6855-6864.

- Marc, D.**, 2010. Aptamers to explore prion protein interactions with nucleic acids. *Front. Biosci.* **15**, 550-563.
- Marsh, R. F.**, Semancik, J. S., Medappa, K. C., Hanson, R. P. and Rueckert, R. R., 1974. Scrapie and transmissible mink encephalopathy: search for infectious nucleic acid. *J. Virol.* **13**, 993-996.
- Masel, J.**, Jansen, V. A. and Nowak, M. A., 1999. Quantifying the kinetic parameters of prion replication. *Biophys. Chem.* **77**(139-152).
- Mashima, T.**, Matsugami, A., Nishikawa, F., Nishikawa, S. and Katahira, M., 2009. Unique quadruplex structure and interaction of an RNA aptamer against bovine prion protein. *Nucleic Acids Res.* **37**, 6249-6258.
- Matsugami, A.**, Ouhashi, K., Kanagawa, M., Liu, H., Kanagawa, S., Uesugi, S. and Katahira, M., 2001. An intramolecular quadruplex of (GGA)(4) triplet repeat DNA with a G:G:G:G tetrad and a G(:A):G(:A):G(:A):G heptad, and its dimeric interaction. *J. Mol. Biol.* **313**, 255-269.
- McKinley, M. P.**, Bolton, D. C. and Prusiner, S. B., 1983. A protease-resistant protein is a structural component of the scrapie prion. *Cell* **35**, 57-62.
- Meier, P.**, Genoud, N., Prinz, M., Maissen, M., Rulicke, T., Zurbriggen, A., Raeber, A. J. and Aguzzi, A., 2003. Soluble dimeric prion protein binds PrP(Sc) in vivo and antagonizes prion disease. *Cell* **113**, 49-60.
- Mercey, R.**, Lantier, I., Maurel, M.-C., Grosclaude, J., Lantier, F. and Marc, D., 2006. Fast, reversible interaction of prion protein with RNA aptamers containing specific sequence patterns. *Arch. Virol.* **151**, 2197-2214.
- Mercey, R.**, Lantier, I., Maurel, M. C., Grosclaude, J., Lantier, F. and Marc, D., 2006. Fast, reversible interaction of prion protein with RNA aptamers containing specific sequence patterns. *Arch. Virol.* **151**, 2197-2214.
- Millhauser, G. L.**, 2004. Copper binding in the prion protein. *Acc. Chem. Res.* **37**, 79-85.
- Mironov, A. J.**, Latawiec, D., Wille, H., Bouzamondo-Bernstein, E., Legname, G., Williamson, R. A., Burton, D., DeArmond, S. J., Prusiner, S. B. and Peters, P. J., 2003. Cytosolic prion protein in neurons. *J. Neurosci.* **23**, 7183-7193.
- Mouillet-Richard, S.**, Ermonval, M., Chebassier, C., Laplanche, J. L., Lehmann, S., Launay, J. M. and Kellermann, O., 2000. Signal transduction through prion protein. *Science* **289**(1925-1928).
- Murakami, K.**, Nishikawa, F., Noda, K., Yokoyama, T. and Nishikawa, S., 2008. Anti-bovine prion protein RNA aptamer containing tandem GGA repeat interacts both with recombinant prion protein and its b isoform with high affinity. *Prion* **2**, 73-78.
- Nandi, P. K.** and Leclerc, E., 1999. Polymerization of murine recombinant prion protein in nucleic acid solution. *Arch. Virol.* **144**, 1751-1763.
- Necula, M.**, Breydo, L., Milton, S., Kaye, R., van der Veer, W. E., Tone, P. and Glabe, C. G., 2007. Methylene Blue Inhibits Amyloid A β Oligomerization by Promoting Fibrillization. *Biochem.* **46**, 8850-8860.
- Nicolla, A. J.**, Trevitt, C. R., Tattumb, M. H., Rissea, E., Quartermann, E., Ibarra, A. A., Wright, C., Jackson, G. S., Sessions, R. B., Farrow, M., Walthod, J. P., Clarke, A. R. and Collinge, J., 2010. Pharmacological chaperone for the structured domain of human prion protein. *Proc. Natl. Acad. Sci. U. S. A.* **107**, 17610-17615.
- O'Leary, J. L.**, Petty, J., Harris, A. B. and Inukai, J., 1968. Supravital staining of mammalian brain with intra-arterial methylene blue followed by pressurized oxygen. *Stain Technol.* **43**, 197-201.
- Oesch, B.**, Westaway, D., Wälchli, M., McKinley, M. P., Kent, S. B., Aebersold, R., Barry, R. A., Tempst, P., Teplow, D. B., Hood, L., Prusiner, S. B. and Weissmann, C., 1985. A cellular gene encodes scrapie PrP 27-30 protein. *Cell* **40**, 735-746.
- Oláh, J.**, Klivényi, P., Gardián, G., Vécsei, L., Orosz, F., Kovacs, G. G., Westerhoff, H. V. and Ovádi, J., 2008. Increased glucose metabolism and ATP level in brain tissue of Huntington's disease transgenic mice. *FEBS J.* **275**, 4740-4755.
- Oz, M.**, Lorke, D. E. and Petroianu, G. A., 2009. Methylene blue and Alzheimer's disease. *Biochem Pharmacol* **78**(8), 927-32.
- Palmer, M. S.**, Dryden, A. J., Hughes, J. T. and Collinge, J., 1991. Homozygous prion protein genotype predisposes to sporadic Creutzfeldt-Jakob disease. *Nature* **352**, 340-342.
- Pan, K. M.**, Baldwin, M., Nguyen, J., Gasset, M., Serban, A., Groth, D., Mehlhorn, I., Huang, Z., Fletterick, R. J., Cohen, F. E. and Prusiner, S. B., 1993. Conversion of α -helices into β -sheets features in the formation of the scrapie prion proteins. *Proc. Natl. Acad. Sci. U.S.A.* **90**, 10962-10966.
- Pan, T.**, Wong, B. S., Liu, T., Li, R., Petersen, R. B. and Sy, M. S., 2002. Cell-surface prion protein interacts with glycosaminoglycans. *Biochem. J.* **368**, 81-90.

- Paolella, G.**, Buono, P., Mancini, F. P., Izzo, P. and Salvatore, F., 1990. Structure and expression of mouse aldolase genes. Brain-specific aldolase C aminoacid sequence is closely related to aldolase A. *European Journal of Biochemistry* **156**, 229-235.
- Parkin, E. T.**, Watt, N. T., Hussain, I., Eckman, E. A., Eckman, C. B., Manson, J. C., Baybutt, H., Turner, A. J. and Hooper, N. M., 2007. Cellular prion protein regulates beta-secretase cleavage of the Alzheimer's amyloid precursor protein. *Proc. Natl. Acad. Sci. U.S.A.* **104**, 11062-11067.
- Pastore, A.** and Zagari, A., 2007. A structural overview of the vertebrate prion proteins. *Prion* **1**, 185-197.
- Peter, C.**, Hongwan, D., Kupfer, A. and Lauterburg, B. H., 2000. Pharmacokinetics and organ distribution of intravenous and oral methylene blue. *Eur. J. Clin. Pharmacol.* **56**, 247-250.
- Petrakis, S.** and Sklaviadis, T., 2006. Identification of proteins with high affinity for refolded and native PrP^C. *Proteomics* **6**, 6476-6484.
- Pey, A. L.**, Stricher, F., Serrano, L. and Martinez, A., 2007. Predicted effects of missense mutations on native-state stability account for phenotypic outcome in phenylketonuria, a paradigm of misfolding diseases. *Am. J. Hum. Genet.* **81**, 1006-1024.
- Pfeifer, A.**, Eigenbrod, S., Al-Khadra, S., Hofmann, A., Mitteregger, G., Moser, M., Bertsch, U. and Kretzschmar, H., 2006. Lentivector-mediated RNAi efficiently suppresses prion protein and prolongs survival of scrapie-infected mice. *J. Clin. Invest.* **116**, 3204-3210.
- Proske, D.**, Gilch, S., Wopfner, F., Schatzl, H. M., Winnacker, E. L. and Famulok, M., 2002. Prion-protein-specific aptamer reduces PrP^{Sc} formation. *Chembiochem.* **3**, 717-725.
- Prusiner, S. B.**, 1982. Novel proteinaceous infectious particles cause scrapie. *Science* **216**, 136-144.
- Prusiner, S. B.**, 1998. Prions. *Proc. Natl. Acad. Sci. U.S.A.* **95**, 13363-13383.
- Prusiner, S. B.**, Scott, M., Foster, D., Pan, K. M., Groth, D., Mirenda, C., Torchia, M., Yang, S. L., Serban, D., Carlson, G. A., Hoppe, P. C., Westaway, D. and DeArmond, S. J., 1990. Transgenic studies implicate interactions between homologous PrP isoforms in scrapie prion replication. *Cell* **63**, 673-686.
- Rezaei, H.**, 2008. Prion protein oligomerization. *Curr. Alzheimer Res.* **5**, 572-578.
- Rezaei, H.**, Choiset, Y., Eghiaian, F., Treguer, E., Mentre, P., Debey, P., Grosclaude, J. and Haertle, T., 2002. Amyloidogenic unfolding intermediates differentiate sheep prion protein variants. *J. Mol. Biol.* **322**, 799-814.
- Rezaei, H.**, Eghiaian, F., Perez, J., Doublet, B., Choiset, Y., Haertle, T. and Grosclaude, J., 2005. Sequential generation of two structurally distinct ovine prion protein soluble oligomers displaying different biochemical reactivities. *J. Mol. Biol.* **347**, 665-679.
- Rezaei, H.**, Marc, D., Choiset, Y., Takahashi, M., Hui Bon Hoa, G., Haertlé, T., Grosclaude, J. and Debey, P., 2000. High yield purification and physico-chemical properties of full-length recombinant allelic variants of sheep prion protein linked to scrapie susceptibility. *Eur. J. Biochem.* **267**, 2833-2839.
- Rhie, A.**, Kirby, L., Sayer, N., Wellesley, R., Disterer, P., Sylvester, I., Gill, A., Hope, J., James, W. and Tahiri-Alaoui, A., 2003. Characterization of 2'-fluoro-RNA aptamers that bind preferentially to disease-associated conformations of prion protein and inhibit conversion. *J. Biol. Chem.* **278**, 39697-39705.
- Riek, R.**, Hornemann, S., Wider, G., Billeter, M., Glockshuber, R. and Wuthrich, K., 1996. NMR structure of the mouse prion protein domain PrP(121-321). *Nature* **382**, 180-182.
- Riek, R.**, Hornemann, S., Wider, G., Glockshuber, R. and Wüthrich, K., 1997. NMR characterization of the full-length recombinant murine prion protein, mPrP (23-231). *FEBS Lett.* **413**, 282-288.
- Riek, R.**, Hornemann, S., Wider, G., Glockshuber, R. and Wüthrich, K., 1997. NMR characterization of the full-length recombinant murine prion protein, mPrP(23-231). *FEBS Lett.* **413**, 282-288.
- Riha, P. D.**, Bruchey, A. K., Echevarria, D. J. and Gonzalez-Lima, F., 2005. Memory facilitation by methylene blue: Dosedependent effect on behavior and brain oxygen consumption. *Eur. J. Pharmacol.* **511**, 151-158.
- Rottmann, W. H.**, Deselms, K. R., Niclas, J., Camerato, T., Holman, P. S., Green, C. J. and Tolan, D. R., 1987. The complete amino acid sequence of the human aldolase C isozyme derived from genomic clones. *Biochimie* **69**, 137-145.
- Rutter, W. J.**, 1964. Evolution of aldolase. *Fed. Proc.* **23**, 1248-1257.
- Rybner, C.**, Finel-Szermanski, S., Felin, M., Sahraoui, T., Rousseau, C., Fournier, J. G., Sève, A. P. and Botti, J., 2002. The cellular prion protein: a new partner of the lectin CBP70 in the nucleus of NB4 human promyelocytic leukemia cells. *J. Cell. Biochem.* **84**, 408-419.

- Safar, J.**, Wille, H., Itri, V., Groth, D., Serban, H., Torchia, M., Cohen, F. E., Prusiner, S. B. E. p. s. h. P. and molecules with different conformations. *Nat. Med.* **4**, 1998. Eight prion strains have PrP^{Sc} molecules with different conformations. *Nat. Med.* **4**, 1157-1165.
- Safar, J. G.**, Kellings, K., Serban, A., Groth, D., Cleaver, J. E., Prusiner, S. B. and Riesner, D., 2005. Search for a prion-specific nucleic acid. *J. Virol.* **79**, 10796-10806.
- Sakai, T.** and Hohjoh, H., 2006. Gene silencing analyses against amyloid precursor protein (APP) gene family by RNA interference. *Cell Biol. Int.* **30**, 952-956.
- Sanchez-Ruiz, J. M.**, 1992. Theoretical analysis of Lumry-Eyring models in differential scanning calorimetry. *Biophys. J.* **61**, 921-935.
- Schirmer, R. H.**, Adler, H., Pickhardt, M. and Mandelkow, E., 2011. "Lest we forget you - methylene blue ...". *Neurobiol Aging*. **32**, 2325.e7-2325.e16.
- Scott, M.**, Foster, D., Mirenda, C., Serban, D., Coufal, F., Wälchli, M., Torchia, M., Groth, D., Carlson, G., DeArmond, S. J., Westaway, D. and Prusiner, S. B., 1989. Transgenic mice expressing hamster prion protein produce species-specific scrapie infectivity and amyloid plaques. *Cell* **59**, 847-857.
- Scriver, C. R.**, Eisensmith, R. C., Woo, S. L. C. and Kaufman, S., 1994. The hyperphenylalaninemias in man and mouse. *Annu. Rev. Genet.* **28**, 141-165.
- Sekiya, S.**, Noda, K., Nishikawa, F., Yokoyama, T., Kumar, P. K. and Nishikawa, S., 2006. Characterization and application of a novel RNA aptamer against the mouse prion protein. *J. Biochem.* **139**, 383-390.
- Shulman-Peleg, A.**, Shatsky, M., Nussinov, R. and Wolfson, H. J., 2008. Prediction of interacting single-stranded RNA bases by protein-binding patterns. *J Mol Biol* **379**, 299-316.
- Silva, J. L.**, Gomes, M. P., Vieira, T. C. and Cordeiro, Y., 2010. PrP interactions with nucleic acids and glycosaminoglycans in function and disease. *Front. Biosci.* **15**, 132-150.
- Silva, J. L.**, Lima, L. M., Foguel, D. and Cordeiro, Y., 2008. Intriguing nucleic-acid-binding features of mammalian prion protein. *Trends Biochem. Sci.* **33**, 132-40.
- Silveira, J. R.**, Raymond, G. J., Hughson, A. G., Race, R. E., Sim, V. L., Hayes, S. F. and Caughey, B., 2005. The most infectious prion protein particles. *Nature* **437**, 257-261.
- Sim, V. L.** and Caughey, B., 2009. Recent advances in prion chemotherapeutics. *Infect Disord. Drug Targets*. **9**, 81-91.
- Simoneau, S.**, Rezaei, H., Salès, N., Kaiser-Schulz, G., Lefebvre-Roque, M., Vidal, C., Fournier, J.-G., Comte, J., Wopfner, F., Grosclaude, J., Schätzl, H. and Lasmèzas, C. I., 2007. In Vitro and In Vivo Neurotoxicity of Prion Protein Oligomers. *PLoS Pathog.* **3**, e125.
- Spielhauser, C.** and Schatzl, H. M., 2001. PrP^C directly interacts with proteins involved in signaling pathways. *J. Biol. Chem.* **276**, 44604-44612.
- Stahl, N.**, Baldwin, M. A., Teplow, D. B., Hood, L., Gibson, G. W., Burlingame, A. L. and Prusiner, S. B., 1993. Structural studies of the scrapie prion protein using mass spectrometry and amino acid sequencing. *Biochemistry* **32**, 1991-2002.
- Stahl, N.**, Borchelt, D. R., Hsiao, K. and Prusiner, S. B., 1987. Scrapie prion protein contains a phosphatidylinositol glycolipid. *Cell* **51**, 229-240.
- Staugaitis, S. M.**, Zerlin, M., Hawkes, R., Levine, J. M. and Goldman, J. E., 2001. Aldolase C/zebrin II expression in the neonatal rat forebrain reveals cellular heterogeneity within the subventricular zone and early astrocyte differentiation. *J. Neurosci.* **21**, 6195-6205.
- Steele, A. D.**, Lindquist, S. and Aguzzi, A., 2007. The prion protein knockout mouse: a phenotype under challenge. *Prion* **1**, 83-93.
- Stefani, M.** and Dobson, C. M., 2003. Protein aggregation and aggregate toxicity: new insights into protein folding, misfolding diseases and biological evolution. *J Mol Med (Berl)* **81**(11), 678-99.
- Stefani, M.** and Dobson, C. M., 2003. Protein aggregation and aggregate toxicity: new insights into protein folding, misfolding diseases and biological evolution. *J. Mol. Med.* **81**, 678-699.
- Strom, A.**, Diecke, S., Hunsmann, G. and W., S. A., 2006. Identification of prion protein binding proteins by combined use of far-Western immunoblotting, two dimensional gel electrophoresis and mass spectrometry. *Proteomics* **6**, 26-34.
- Sun, G.**, Guo, M., Shen, A., Mei, F., Peng, X., Gong, R., Guo, D., Wu, J., Tien, P. and Xiao, G., 2005. Bovine PrP^C directly interacts with α B-crystalline. *FEBS Lett.* **579**, 5419-5424.
- Sunyach, C.**, Jen, A., Deng, J., Fitzgerald, K. T., Frobert, Y., Grassi, J., McCaffrey, M. W. and Morris, R., 2003. The mechanism of internalization of glycosylphosphatidylinositol-anchored prion protein. *EMBO J.* **22**, 3591-3601.
- Swietnicki, W.**, Morillas, M., Chen, S. G., Gambetti, P. and Surewicz, W. K., 2000. Aggregation and fibrillization of the recombinant human prion protein huPrP90-231. *Biochemistry* **39**, 424-431.

- Tagliavini, F.**, McArthur, R. A., Canciani, B., Giaccone, G., Porro, M., Bugiani, M., Lievens, P. M., Bugiani, O., Peri, E., Dall'Ara, P., Rocchi, M., Poli, G., Forloni, G., Bandiera, T., Varasi, M., Suarato, A., Cassutti, P., Cervini, M. A., Lansen, J., Salmona, M. and Post, C., 1997. Effectiveness of anthracycline against experimental prion disease in Syrian hamsters. *Science* **276**, 1119-1122.
- Takemura, K.**, Wang, P., Vorberg, I., Surewicz, W., Priola, S. A., Kanthasamy, A., Pottathil, R., Chen, S. G. and Sreevatsan, S., 2006. DNA aptamers that bind to PrP(C) and not PrP(Sc) show sequence and structure specificity. *Exp. Biol. Med. (Maywood)* **231**, 204-214.
- Taniguchi, S.**, Suzuki, N., Masuda, M., Hisanaga, S., Iwatsubo, T., Goedert, M. and Hasegawa, M., 2005. Inhibition of heparin-induced tau filament formation by phenothiazines, polyphenols, and porphyrins. *J Biol Chem* **280**, 7614-7623.
- Taniguchi, S.**, Suzuki, N., Masuda, M., Hisanaga, S., Iwatsubo, T., Goedert, M. and Hasegawa, M., 2005. Inhibition of heparin-induced tau filament formation by phenothiazines, polyphenols, and porphyrins. *J. Biol. Chem.* **280**, 7614-7623.
- Telling, G. C.**, Parchi, P., DeArmond, S. J., Cortelli, P., Montagna, P., Gabizon, R., Mastriani, J., Lugaresi, E., Gambetti, P. and Prusiner, S. B., 1996. Evidence for the formation of the pathologic isoform of the prion protein enciphering and propagating prion diversity. *Science* **274**, 2079-2082.
- Telling, G. C.**, Scott, M., Mastrianni, J., Gabizon, R., Torchia, M., Cohen, F. E., Dearmond, S. J. and Prusiner, S. B., 1995. Prion propagation in mice expressing human and chimeric PrP transgenes implicates the interaction of cellular PrP with another protein. *Cell* **83**, 79-90.
- Tilly, G.**, Chapuis, J., Vilette, D., Laude, H. and Vilotte, J. L., 2003. Efficient and specific down-regulation of prion protein expression by RNAi *Biochem. Biophys. Res. Commun.* **305**, 548-551.
- Tjong, H.** and Zhou, H. X., 2007. DISPLAR: an accurate method for predicting DNA-binding sites on protein surfaces. *Nucleic Acids Res.* **35**, 1465-1477.
- Tolan, D. R.**, 1995. Molecular basis of hereditary fructose intolerance: mutations and polymorphisms in the human aldolase B gene. *Human Mutation* **6**, 210-218.
- Tuerk, C.** and Gold, L., 1990. Systematic evolution of ligands by exponential enrichment: RNA ligands to bacteriophage T4 DNA polymerase. *Science* **249**, 505-510.
- Tuite, M. F.** and Serio, T. R., 2010. The prion hypothesis: from biological anomaly to basic regulatory mechanism. *Nat. Rev. Mol. Cell Biol.* **11**, 823-833.
- Turk, E.**, Teplow, D. B., Hood, L. E. and Prusiner, S. B., 1988. Purification and properties of the cellular and scrapie hamster prion proteins. *Eur. J. Biochem.* **176**, 21-30.
- van Bebber, F.**, Paquet, D., Hruscha, A., Schmid, B. and Haass, C., 2010. Methylene blue fails to inhibit Tau and polyglutamine protein dependent toxicity in zebrafish. *Neurobiol. Dis.* **39**, 265-271.
- Vogtherr, M.**, Grimme, S., Elshorst, B., Jacobs, D. M., Fiebig, K., Griesinger, C. and Zahn, R., 2003. Antimalarial Drug Quinacrine Binds to C-Terminal Helix of Cellular Prion Protein. *J. Med. Chem.* **46**, 3563-3564.
- Wainwright, M.** and Amaral, L., 2005. The phenothiazinium chromophore and the evolution of antimalarial drugs. *Trop. Med. Int. Health* **10**, 501-511.
- Walker, L. C.**, Callahan, M. J., Bian, F., Durham, R. A., Roher, A. E. and Lipinski, W. J., 2002. Exogenous induction of cerebral β -amyloidosis in β APP-transgenic mice. *Peptides* **23**, 1241-1247.
- Walter-Sack, I.**, Rengelshausen, J., Oberwittler, H., Burhenne, J., Mueller, O., Meissner, P. and Mikus, G., 2009. High absolute bioavailability of methylene blue given as an aqueous oral formulation. *Eur. J. Clin. Pharmacol.* **65**, 179-189.
- Wang, F.**, Wang, X., Yuan, C. G. and Ma, J., 2010. Generating a prion with bacterially expressed recombinant prion protein. *Science* **327**, 1132-1135.
- Wang, J.**, Morris, A. J., Tolan, D. R. and Pagliaro, L., 1996. The molecular nature of the F-actin binding activity of aldolase revealed with site-directed mutants. *J. Biol. Chem.* **271**, 6861-6865.
- Ward, R. L.**, Porter, D. D. and Stevens, J. G., 1974. Nature of the scrapie agent: evidence against a viroid. *J. Virol.* **14**, 1099-1103.
- Waters, P. J.**, 2003. How PAH gene mutations cause hyperphenylalaninemia and why mechanism matters: insights from in vitro expression. *Hum. Mutat.* **21**, 357-369.
- Waters, P. J.**, 2006. Molecular bases of phenylketonuria: insights from functional studies in vitro. In: Blau N (ed) PKU and BH4: advances in phenylketonuria and tetrahydrobiopterin SPS Verlagsgesellschaft, Heilbronn, pp 277-310.

- Watts, J. C.**, Huo, H., Bai, Y., Ehsani, S., Jeon, A. H., Shi, T., Daude, N., Lau, A., Young, R., Xu, L., Carlson, G. A., Williams, D., Westaway, D. and Schmitt-Ulms, G., 2009. Interactome analyses identify ties of PrP and its mammalian paralogs to oligomannosidic N-glycans and endoplasmic reticulum-derived chaperones. *PLoS Pathog.* **5**, e1000608.
- Weiss, S.**, Proske, D., Neumann, M., Groschup, M. H., Kretzschmar, H. A., Famulok, M. and Winnacker, E. L., 1997. RNA aptamers specifically interact with the prion protein PrP. *J. Virol.* **71**, 8790-8797.
- Weissmann, C.**, 2004. The state of the prion. *Nat. Rev. Microbiol.* **2**, 861-871.
- Wells, G. A.** and Wilesmith, J. W., 1995. The neuropathology and epidemiology of bovine spongiform encephalopathy. *Brain Pathol.* **5**, 91-103.
- Westaway, D.**, Goodman, P. A., Mirenda, C. A., McKinley, M. P., Carlson, G. A. and Prusiner, S. B., 1987. Distinct prion proteins in short and long scrapie incubation period mice. *Cell* **51**, 651-662.
- Wischik, C. M.**, Edwards, P. C., Lai, R. Y., Roth, M. and Harrington, C. R., 1996. Selective inhibition of Alzheimer disease-like tau aggregation by phenothiazines. *Proc. Natl. Acad. Sci. U.S.A.* **93**, 11213-11218.
- Wüthrich, K.** and Riek, R., 2001. Three-dimensional structures of prion proteins. *Adv. Protein. Chem.* **57**, 55-82.
- Yamaguchi, N.**, Sakaguchi, S., Shigematsu, K., Okimura, N. and Katamine, S., 2004. Doppel-induced Purkinje cell death is stoichiometrically abrogated by prion protein. *Biochem. Biophys. Res. Commun.* **319**, 1247-1252.
- Yamashita, M.**, Nonaka, T., Arai, T., Kametani, F., Buchman, V. L., Ninkina, N., Bachurin, S. O., Akiyama, H., Goedert, M. and Hasegawa, M., 2009. Methylene blue and dimebon inhibit aggregation of TDP-43 in cellular models. *FEBS Lett.* **583**, 2419-2424.
- Yamashita, M.**, Nonaka, T., Arai, T., Kametani, F., Buchman, V. L., Ninkina, N., Bachurin, S. O., Akiyama, H., Goedert, M. and Hasegawa, M., 2009. Methylene blue and dimebon inhibit aggregation of TDP-43 in cellular models. *FEBS Lett.* **14**, 2419-2424.
- Yao, D. C.**, Tolan, D. R., Murray, M. F., Harris, D. J., Darras, B. T., Geva, A. and Neufeld, E. J., 2004. Hemolytic anemia and severe rhabdomyolysis caused by compound heterozygous mutations of the gene for erythrocyte/muscle isozyme of aldolase, ALDOA(Arg303X/Cys338Tyr). *Blood* **103**, 2401-2403.
- Zahn, R.**, 2003. The octapeptide repeats in mammalian prion protein constitute a pH-dependent folding and aggregation site. *J. Mol. Biol.* **334**, 477-488.
- Zeiler, B.**, Adler, V., Kryukov, V. and Grossman, A., 2003. Concentration and removal of prion proteins from biological solutions. *Biotechnol. Appl. Biochem.* **37**, 173-82.
- Zschocke, J.**, 2003. Phenylketonuria mutations in Europe. *Hum. Mutat.* **21**, 345-356.



Natural phenylalanine hydroxylase variants that confer a mild phenotype affect the enzyme's conformational stability and oligomerization equilibrium

Monica Cerreto ^{a,1}, Paola Cavaliere ^{a,b,1}, Carla Carluccio ^{a,c}, Felice Amato ^a, Adriana Zagari ^{a,b}, Aurora Daniele ^{a,d,e,*}, Francesco Salvatore ^{a,c,e,**}

^a CEINGE–Biotecnologie Avanzate Scarl, Naples, Italy

^b Dipartimento di Scienze Biologiche, Università di Napoli “Federico II”, Naples, Italy

^c Dipartimento di Biochimica e Biotecnologie Mediche, Università di Napoli “Federico II”, Naples, Italy

^d Dipartimento di Scienze Ambientali, Seconda Università di Napoli, Caserta, Italy

^e IRCCS – Fondazione SDN, Naples, Italy

ARTICLE INFO

Article history:

Received 8 March 2011

Received in revised form 19 July 2011

Accepted 20 July 2011

Available online 27 July 2011

Keywords:

BH4 responsiveness

Number and brightness

PAH conformational stability

PAH oligomerization equilibrium

Hyperphenylalaninemia

Phenylalanine hydroxylase

ABSTRACT

Hyperphenylalaninemias are genetic diseases prevalently caused by mutations in the phenylalanine hydroxylase (PAH) gene. The wild-type PAH enzyme is a homotetramer regulated by its substrate, cofactor and phosphorylation. We reproduced a full-length wild-type protein and seven natural full-length PAH variants, p.I65M, p.N223Y, p.R297L, p.F382L, p.K398N, p.A403V, and p.Q419R, and analyzed their biochemical and biophysical behavior. All mutants exhibited reduced enzymatic activity, namely from 38% to 69% of wild-type activity. Biophysical characterization was performed by size-exclusion chromatography, light scattering and circular dichroism. In the purified wild-type PAH, we identified the monomer in equilibrium with the dimer and tetramer. In most mutants, the equilibrium shifted toward the dimer and most tended to form aggregates. All PAH variants displayed different biophysical behaviors due to loss of secondary structure and thermal destabilization. Specifically, p.F382L was highly unstable at physiological temperature. Moreover, using confocal microscopy with the number and brightness technique, we studied the effect of BH4 addition directly in living human cells expressing wild-type PAH or p.A403V, a mild mutant associated with BH4 responsiveness in vivo. Our results demonstrate that BH4 addition promotes re-establishment of the oligomerization equilibrium, thus indicating that the dimer-to-tetramer shift in p.A403V plays a key role in BH4 responsiveness. In conclusion, we show that the oligomerization process and conformational stability are altered by mutations that could affect the physiological behavior of the enzyme. This endorses the hypothesis that oligomerization and folding defects of PAH variants are the most common causes of HPAs, particularly as regards mild human phenotypes.

© 2011 Elsevier B.V. All rights reserved.

1. Introduction

Phenylketonuria (PKU, Online Mendelian Inheritance in Man database: 261600) and its hyperphenylalaninemia (HPA) variants

Abbreviations: BH4, (6R)-L-erythro-5,6,7,8-tetrahydrobiopterin; CD, circular dichroism; Δ 13-PAH, PAH missing residues 1–13; DSC, differential scanning calorimetry; Ek, enterokinase; HPA, hyperphenylalaninemia; IPTG, isopropylthio- β -D-galactoside; L-Phe, phenylalanine; LS, light scattering; MALS, multiangle light scattering; MBP, maltose-binding protein; N&B, number and brightness; PKU, phenylketonuria; SEC, size-exclusion chromatography

* Correspondence to: A. Daniele, CEINGE–Biotecnologie Avanzate Scarl, Via Gaetano Salvatore 486, 80145 Naples, Italy.

** Correspondence to: F. Salvatore, CEINGE–Biotecnologie Avanzate Scarl and Dipartimento di Biochimica e Biotecnologie Mediche, Università di Napoli “Federico II”, Via Sergio Pansini 5, Ed.19, 80131 Naples, Italy. Tel.: +39 0817463133; fax: +39 0817463650.

E-mail address: salvator@unina.it (F. Salvatore).

¹ These authors contributed equally to this paper.

represent the most common inherited disorder of amino acid metabolism transmitted by an autosomal recessive mode [1]. The primary cause of HPA is a dysfunction of phenylalanine hydroxylase (PAH; EC 1.14.16.1). In the liver, this enzyme metabolizes L-Phenylalanine (L-Phe) to L-Tyrosine (L-Tyr) using (6R)-L-erythro-5,6,7,8-tetrahydrobiopterin (BH4) as cofactor. More rarely, forms of HPAs can also be caused by a lack of the BH4 cofactor due to defective cofactor biosynthesis and regeneration [2]. Untreated PKU patients present an abnormal phenotype, with growth failure, microcephaly, seizures and permanent neurologic damage because their body fluids contain elevated levels of L-Phe and its neurotoxic metabolites (phenylpyruvate, phenylacetate and phenyllactate) [1,3].

The major manifestations of the disease, which start at birth, are prevented by severe dietary restriction of L-Phe [4] and, in selected cases, by BH4 supplementation, which reduces L-Phe levels and increases L-Phe tolerance in HPA patients [5]. Several new therapeutic strategies based on the biochemistry and pathogenetic features of PKU are currently being investigated [6,7].

The human PAH gene, mapped on 12q23.2, consists of 13 exons encompassing 171 kb. The full-length PAH cDNA encodes a protein of about 52 kDa (452 amino acids) that in the mature form is assembled as a homotetramer. Each subunit consists of three functional domains: a flexible N-terminal regulatory domain (residues 1–142); a catalytic domain (residues 143–410) that includes binding sites for iron, substrate and cofactor; and a C-terminal oligomerization domain (residues 411–452) with dimerization (residues 411–426) and tetramerization motifs (residues 427–452) [8] (Fig. 1). The crystal structure of PAH has revealed that the tetrameric oligomers are dimers of dimers in which the interaction between the two dimers is mediated by the C-terminal ‘arm’ [8].

The tetrameric and dimeric forms of PAH are in equilibrium [9,10] and have different catalytic properties because the tetramer, but not the dimer, demonstrates a positive kinetic cooperativity with respect to L-Phe [11]. In particular, substrate activation results in conformational changes involving the tertiary as well as the quaternary structure [12] and drives the tetramer–dimer equilibrium toward the tetrameric form [13]. Further regulation mechanisms require binding of BH4 [12] and phosphorylation [14].

The clinical and metabolic features associated to HPA are complex [15] and various genotype–phenotype correlation studies have been performed [16–18]. In addition, at molecular level, about 600 mutations have been identified, most of which are point mutations scattered throughout the whole PAH gene (<http://www.pahdb.mcgill.ca>), although frequencies differ among populations and geographic areas [16–18].

Recombinant variant proteins containing prevalently missense mutations have been analyzed and characterized in vitro; each mutation exerts a distinct effect on the behavior of the PAH protein, which in many cases allows the prediction of the biochemical phenotype [19–21]. The effects of a specific mutation on protein functions have been studied with different approaches, i.e., enzyme assay, in vivo isotopic studies and in vitro expression. Moreover, the crystal structures of human and rat PAH [8,22] provided the structural basis of HPA [23]. It is now established that, in most HPA cases, the loss of PAH function is due to decreased stability [21,24], increased susceptibility toward aggregation and degradation of PAH mutant proteins [19,24,25], thermodynamic instability [26] and/or folding efficiency [27]. About 75% of PAH mutations, characterized by high residual activity, have been found to be associated with BH4

responsiveness, both in vitro [28–30] and in vivo [4,5]. It has recently been speculated that pharmacological doses of BH4 may augment the conformational stability and the amount of functional PAH [31].

We previously carried out a molecular analysis of the PAH gene in HPA patients from Southern Italy, and identified and characterized several novel mutations [32–34]. In the present study, we analyzed the wild-type PAH protein and some PAH natural mutants to obtain further information about the molecular basis of HPAs and the mechanism of BH4 responsiveness. To this purpose, we reproduced, by in vitro mutagenesis, the wild-type and seven natural variants of PAH: p.I65M, p.N223Y, p.R297L, p.F382L, p.K398N, p.A403V, and p.Q419R, and characterized the biophysical–biochemical properties of the above-mentioned purified full-length proteins in order to understand the impact of each mutation on the activity, oligomeric structure and stability of PAH. In addition, we investigated the mechanism underlying BH4 responsiveness using p.A403V, which is one of the most frequent mutations in our geographic area [32], and is associated with a BH4-responsive mild phenotype [35].

2. Material and methods

2.1. Construction of PAH expression plasmid and site-directed mutagenesis

PAH wild-type and mutant constructs were obtained by modifying the pMAL Xa PAH plasmid, kindly provided by Drs CR. Scriver and P. Waters (McGill University-Montreal Children's Hospital Research Institute, Montreal, Canada), to digest the fusion protein MBP-PAH with enterokinase (Ek) [9]. The Ek site was inserted downstream the sequence encoding the factor Xa site, by site-directed mutagenesis using the primers 5'gatgacgatgacaagtctactgcggctctgg3' and 5'gccctaactcccttcctactgtactgttc3' and the Quick Site-directed mutagenesis kit (Stratagene, CA, USA). GFP was amplified by PCR from pEGFP-N1 (Clontech, CA, USA) using the primers: 5'acattaggtacagccatggtgagcaaggcgag3' and 3'gtatgatgaattctccacccttgtacagctg 5' and cloned into pcDNA3 (Invitrogen, Carlsbad, CA) using Kpn1 and EcoR1 sites. PAH cDNA was amplified from pMAL Xa Ek PAH by using the primers: 5'catcattgaattctccactcggctctgg3' and 3'cgtaatcgccgcttactttttctggag 5' and cloned downstream GFP, using EcoR1 and Not1 sites. Sequence analysis confirmed the correct frame.

Mutations were introduced into pMAL Xa Ek PAH and pcDNA3-GFP-PAH using mutagenic primers and the Quick Site-directed mutagenesis kit (Table 1). The modified plasmid and the mutant clones were sequenced to verify the introduction of each single mutation. Commercial MBP was obtained from New England Biolabs (Ipswich, MA, USA).

2.2. Expression, purification and N-terminal sequencing of the PAH protein

pMAL Xa Ek PAH expression plasmids were transformed into *Escherichia coli* BL21 cells and the colonies were selected using Luria-Broth plates with ampicillin (0.1 mg mL⁻¹). Bacteria were grown to 2 × 10⁸ cells/mL (A_{600nm} ~ 0.5) and overexpression of wild-type and variant MBP-PAH fusion proteins was induced with 1 mM isopropylthio-β-D-galactoside (IPTG) for 16 h at 37 °C. Cells were harvested by centrifugation and treated according to the instruction manual of the pMAL protein fusion and purification system (New England Biolabs). The fusion protein was digested overnight at room temperature with Ek (New England Biolabs) to obtain wild-type and mutant forms of PAH without the MBP tag, using 0.5 ng of enzyme for each 50 µg fusion protein. The mixture was then applied to a hydroxyapatite column (1 cm × 10 cm, Bio-Rad Laboratories, CA, USA) and subjected to several washes with 20 mM sodium phosphate, 200 mM NaCl (pH 7.2). Proteins were then eluted with 0.5 M Na phosphate, pH 7.2 and subsequently MBP was isolated from the

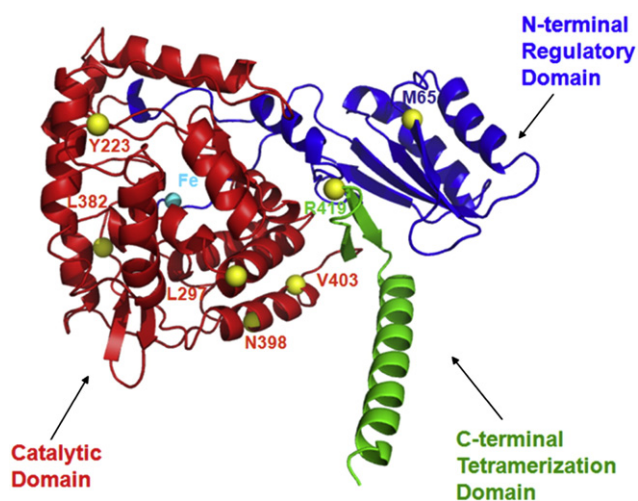


Fig. 1. Full-length composite model of the PAH monomer structure and distribution of the HPA-related missense mutations studied in this paper. The N-terminal regulatory domain is shown in blue, the catalytic domain in red and the tetramerization domain in green. The Fe ion is shown as a cyan sphere at the center of the catalytic domain; the mutation sites are marked as yellow balls.

Table 1

The seven mutant forms of PAH reproduced in vitro as recombinant products and analyzed. The primer pairs used to produce the pMAL Xa Ek PAH plasmid.

Mutant forms of PAH	Mutagenic primers (forward)	Mutagenic primers (reverse)
Ek site	5'GATGACGATGACAAGTCTACTGCGGTCTCTGG3'	5'GCCCTAACTCCCTTCCCTACTGCTACTGTTC3'
p.I65M	5'ACCTGACCCACATGGAATCTAGACCTTCTC3'	5'GAGAAGGTCTAGATTCCATGTGGGTCAAGT3'
p.N223Y	5'CATGAAGATTACATCCCCAGCTGGAAGAC3'	5'GTCTTCCAGCTGGGGAATGTAATCTTCATG3'
p.R297L	5'TGTTTTCAGATCTCAGCTTGCCAGTTT3'	5'AAACTGGGCAAGCTGAGATCTGAAACA3'
p.F382L	5'ACTGTACAGGAGTTGCAGCCCTGTATTAC3'	5'GTAATACAGGGCTGCAACTCCGTGACAGT3'
p.K398N	5'GCCAAGGAGAACGTAAGAACTTTGCTGCC3'	5'GGCAGCAAAAGTTCCTACGTTCTCTTGGC3'
p.A403V	5'GAAAGTAAGAACTTTGTTGCCACA3'	5'CCGAGGTATTGTGCAACAAAGTTC3'
p.Q419R	5'ATACACCCGAAGGATTGAGG3'	5'CCTCAATCCTTCGGGTGTAT3'

cleavage mixture by re-binding to amylose resin. PAH was finally purified by size-exclusion chromatography with a HiLoad 16/60 Superdex 200 column (GE Healthcare, UK). Protein concentrations were determined spectrophotometrically with the use of the absorption coefficient A280 or the dye-binding Bradford assay (Bio-Rad Laboratories). The N-terminal amino acid sequence of PAH was determined by Edman degradation on an automated Procise H49 sequencer (Applied Biosystems, MA, USA).

It has been reported [36] that, during the various steps of recombinant protein production, some labile Asn residues are deamidated; however, any possible deamidation of these residues, which would in the activity assay produce substrate inhibition, would most likely be the same in the presence of wild-type and of the variant forms of PAH we have employed.

2.3. Concentration and storage of proteins

The concentration of proteins was determined both by the micro BCA protein assay and spectrophotometrically. The final protein concentration was measured based on optical density at 280 nm using, for the extinction coefficient, a value of 49,780, 66,350 and 115,630 M⁻¹ cm⁻¹ for PAH, MBP and the fused wild-type MBP-PAH respectively, deduced from the amino acid composition of the protein. We used a SpeedVac concentrator (Thermo Scientific, Rockford, IL, USA) to concentrate the protein solutions because ultra-filtration led to considerable sample loss. All protein samples, if not utilized within few days, were stored at -20 °C in their elution buffer (see below).

2.4. PAH activity and thermal inactivation assay

Enzymatic activity analysis was carried out on a whole equilibrium mixture of oligomeric species of purified full-length wild-type and mutant PAH (see Supplementary Table S1). The activity was assayed in the presence of 0.25 µCi L-[¹⁴C] Phe (Amersham, Buckinghamshire, UK; 460 µCi/mmol); 0.25 mM cold L-Phe, 1.3 units of beef liver catalase; 0.8 mM BH4; 250 mM Tris HCl pH 7.8, 1 µg of protein; final volume: 100 µL. The reaction was conducted at 25 °C with an incubation time of 1 h [32–34]. After centrifugation at room temperature and maximum speed, an aliquot of each supernatant was applied on a thin-layer chromatography system and the amount of [¹⁴C] radio-labeled L-Phe converted to [¹⁴C] radio-labeled L-Tyr was measured. The mean PAH activities were calculated from three sets of experiments. The residual activities of mutant PAH enzymes were expressed as a percentage of wild-type enzyme activity. The same assay was used for the thermal inactivation analysis of the wild-type protein and of the p.F382L mutant. Thermal inactivation of both proteins was determined by measuring the decay of tyrosine production as a function of temperature in the 32–58 °C range.

2.5. Electrophoresis and immunoblotting

SDS/PAGE was performed at 100 V (2 h) in a 10% (w/v) polyacrylamide gel. The purification of all proteins was verified after staining with Colloidal Coomassie. The absence of MBP contamination in all preparations was determined by western blot analyses.

Immunoblotting was performed using affinity-purified rabbit anti-hPAH [32–34] and mouse anti-MBP (New England Biolabs) as primary antibodies. The enhanced chemiluminescence system from Amersham (GE Healthcare) was used for immunodetection.

2.6. Size-exclusion chromatography with multiangle light scattering

Size-exclusion chromatography (SEC) was performed using Akta FPLC chromatography equipment (GE Healthcare) on a Superdex 200 10/300 GL column. The column was previously calibrated for molecular mass using a Gel Filtration High Molecular Weight calibration kit (GE Healthcare) constituted by ovalbumin (44 kDa), conalbumin (75 kDa) and aldolase (158 kDa). Before each run, the column was equilibrated with at least two column volumes of elution buffer and each run was performed at both 4 °C and room temperature (20–23 °C). The elution buffer was Tris-HCl 20 mM pH 7.4, NaCl 100 mM (buffer A) and, in a few cases, Na-phosphate 20 mM pH 7.0, KF 150 mM (buffer B).

The eluent flow was 0.5 mL min⁻¹. Only freshly prepared or recently defrosted proteins were loaded on the column because storage at 4 °C for more than one week led to sample aging. A total of 0.1–0.2 mg of proteins were loaded. At room temperature, the elution profile was monitored at three UV absorption wavelengths (280 nm, 215 nm and 258 nm). At 4 °C, UV absorption was measured only at 280 nm. The chromatograms were deconvoluted by Unicorn software, supplied with the FPLC device, to calculate the percentage of single species. All chromatograms were normalized in the (0.0–1.2) range.

At room temperature, size-exclusion chromatography with multiangle light scattering (MALS) experiments was carried out with the AKTA system coupled to a three-angle (45°, 90° and 135°) Wyatt Minidown EOS light scattering instrument linked to a Wyatt Optilab refractometer (Wyatt Technology Corp., Santa Barbara, CA). These experiments served to determine the sizes of oligomers of wild-type and mutant PAH. Molecular masses, polydispersity and root mean square radius calculations were made by ASTRA software, which is supplied with the light scattering device, using a dn/dc value of 0.185 mL g⁻¹.

2.7. Circular dichroism

Circular dichroism (CD) analysis was performed on commercial MBP, on the fused wild-type MBP-PAH tetrameric sample and on the most abundant species of cleaved PAH proteins after SEC purification. In the case of the cleaved wild-type PAH, CD experiments were performed with both the tetrameric form and the whole equilibrium mixture. A 2-day dialysis at 4 °C against Tris-HCl 20 mM pH 7.4 (buffer C) was conducted to eliminate NaCl before CD experiments. All CD spectra were recorded with a Jasco J-810 spectropolarimeter equipped with a Peltier temperature control system (model PTC-423-S). The spectropolarimeter was calibrated with an aqueous solution of D-10-(+)-camphorsulfonic acid at 290 nm. The molar ellipticity per mean residue, $[\theta]$ in deg cm² dmol⁻¹, was calculated from the equation $[\theta] = [\theta]_{\text{obs}} \text{mrw} / (10 \text{ l C})^{-1}$, where $[\theta]_{\text{obs}}$ is the ellipticity measured in degrees, mrw is the mean residue molecular weight (111.5 Da), C is the protein concentration in

g mL^{-1} , and l is the optical path length of the cell in cm. Far-UV (ultraviolet) measurements (190–260 nm) were carried out at 20 °C using a 0.2 cm optical path length cell and a protein concentration in the range 0.10–0.15 mg mL^{-1} . CD spectra, recorded with a time constant of 4 s, a 1-nm bandwidth, and a scan rate of 20 nm min^{-1} , were signal averaged over at least three scans. The baseline was corrected by subtracting the buffer spectrum. Thermal denaturation curves were recorded over the 20–80 °C temperature range and by monitoring the CD signal at 222 nm. After preliminary trials within the scan rate interval of $0.5 \div 2.0$ °C min^{-1} , all curves were recorded using a 0.2-cm path length cell and a scan rate of 1.0 °C min^{-1} . Irreversibility of the denaturation was verified by recording, after cooling to 20 °C, the spectra of samples subjected to a first temperature scan. All denaturation curves were normalized in an interval of 0.0–1.0. The T_m values were determined from the first derivatives of the denaturation curves after noise reduction by using the standard analysis program provided with the instrument.

2.8. Cell culture

HeLa cells were grown in D-MEM high glucose medium (Invitrogen) containing 10% heat inactivated fetal bovine serum (Invitrogen), 1% penicillin/streptomycin, at 37 °C in 5% CO_2 . Transfections of both wild-type PAH and the p.A403V mutant were carried out using the ProFection Mammalian Transfection System (Promega, WI, USA) in accordance with the manufacturer's protocol. Cells were plated on 35-mm glass bottom dishes (MatTek, MA) for imaging.

2.9. Confocal microscopy and number and brightness analysis

Constructs containing GFP-PAH fusion proteins were transfected in HeLa cells and experiments were started 18 h after transfection. To evaluate BH4 responsiveness, transfected cells were treated with 60 μM BH4 in aqueous solution. Analyses were performed 6 h later. Number and brightness (N&B) analysis was performed according to Gratton and colleagues [37,38] using a Zeiss LSM 510 META confocal microscope. Cells grown for 4 days on bottom glass dishes were imaged *in vivo* in CO_2 -independent medium (150 mM NaCl, 5 mM KCl, 1 mM CaCl_2 , 1 mM MgCl_2 , and 20 mM Hepes, pH 7.4). Fifty frame time series were acquired with a LSM 510 META equipped with a plan apo 63 \times oil-immersion (NA 1.4) objective lens using the following settings: 488 nm Argon laser, 25% of output power, 1.5% transmission, 505–550 nm emission, gain equal to 850, offset 0.1, and digital gain 1. Scanning parameters were: 512 \times 512 frame window, 25.61 μs /pixel dwell time, no average, zoom 6 \times , ROI (x,y) 256 \times 64, and pinhole corresponding to 1 μm optical slice. Data from each cell were analyzed with the simFCS software (Globals Software, East Villa Grove, IL 61956, USA). Briefly, data analysis was performed pixel-by-pixel over time to calculate variance and average intensity. Correction was applied to take into account the analog detection of fluorescence by the photomultiplier tubes of the confocal microscope. Briefly, the correction parameters S , offset and σ_0 were determined, for each experiment, by plotting the measured average intensity ($\langle I \rangle$) vs average variance ($\langle \text{Var} \rangle$) of 50 frame time series acquired using same settings as above, but setting 4 different values of laser transmission percentages. Moreover, filters and beam splitters were configured to obtain reflection images to detect the defined amount of light originating directly from the laser. The obtained plots were linearly interpolated and the equation of straight line ($R \geq 0.99$) was used to extract the parameters S and offset based on the following equation: $\langle \text{Var} \rangle = S \cdot \langle I \rangle + \text{offset}$. The parameter σ_0 was estimated from time-series acquired with laser off, as the half maximum width of the histogram peak of the “dark”-counts. Its value was constantly lower than 0.1, and consequently was approximated to zero in all the calculations. Brightness (B) was calculated pixel by pixel from the

following equation $B = V(x,y)/(S \cdot I_{x,y})$, where $I = I_{\text{m}} - \text{offset}$ (I_{m} : measured average fluorescence).

The number of molecule subunits constituting each oligomer was calculated with the following calibration procedure: the brightness of monomeric GFP and of GFP-based molecules made by two or three GFP moieties fused in tandem in expression vector pcDNA3.1 and expressed in HeLa cells were measured with the same experimental settings described above. The measured B values for monomeric, dimeric and trimeric GFP and the corresponding number of subunits were linearly interpolated to obtain the experimental equation describing the dependence of brightness on the number of GFP subunits: $B = k \cdot n_{\text{sub}} + c$. This equation was used to calculate the unknown number of GFP subunits corresponding to the measured brightness. The following formula $B = \sum (B_i^2 n_i) / \sum (B_i n_i)$ provides the brightness of multiple species (B_i) whose number is n_i in a single pixel, is combined in the measured brightness (B). This formula is used to interpret non integer subunit values obtained by the above procedure.

2.10. Structural analysis

The effect of the mutations on the 3D structure was investigated by analyzing the structural environment of each substituted residue in the PAH crystal structures deposited in the Protein Data Bank (PDB). Since no crystal structure of any full-length enzyme is available, various models were used: tetrameric human PAH lacking residues 1–117 (pdbcode 2pah); dimeric truncated human PAH lacking residues 1–117 and 425–452 (PDB code 1kw0); and the dimeric rat PAH, from residue 19 to 427 (pdbcode 1phz), which encompasses the regulatory domain. A composite monomeric model that included the three domains was built by superimposing the secondary structure elements of the respective catalytic domains of the rat (1phz) and human structures (2pah and 1kw0). The structural superposition was performed using the program O [39].

3. Results

3.1. Enzymatic activity analysis of wild-type and mutant forms of PAH

We measured the enzymatic activity of the equilibrium mixture of the wild-type and mutant forms of PAH to investigate the effect of the mutations on catalytic activity. As shown in Fig. 2, the residual activities of the mutant PAH enzymes, expressed as a percentage of wild-type enzyme activity, were: $38 \pm 3\%$ (p.I65M), $48 \pm 14\%$ (p.N223Y), $60 \pm 12\%$ (p.R297L), $69 \pm 11\%$ (p.F382L), $58 \pm 9\%$ (p.K398N), $43 \pm 4\%$ (p.A403V) and $63 \pm 5\%$ (p.Q419R). In our conditions, we found in multiple experiments that isolated oligomeric species are not stable and evolve toward the equilibrium mixture (see

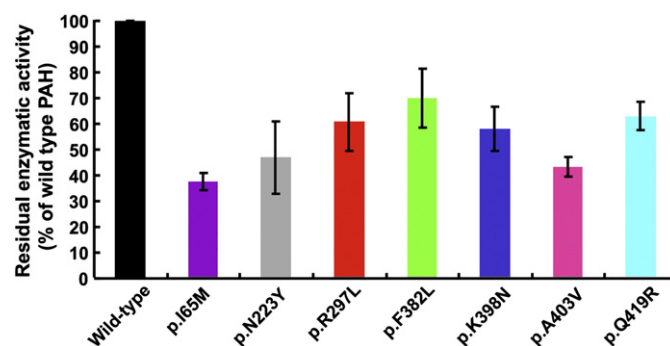


Fig. 2. Enzymatic activity of the PAH mutants expressed as percentage of wild-type PAH activity. The activity was measured by the amount of [^{14}C] Tyr produced by [^{14}C] Phe as analyzed by thin layer chromatography. Mean values and the standard deviation derived from three sets of independent experiments for each construct are shown expressed as percentage of wild-type PAH activity. The experimental assay conditions are reported in Section 2.4.

also below under Section 3.2); hence the activity of the isolated tetramers and dimers was not possible to be measured with accuracy.

3.2. Oligomerization equilibrium of wild-type and mutant forms of PAH

The oligomerization equilibrium for the fused MBP-PAH protein, the purified cleaved wild-type protein, and the missense mutants was analyzed by SEC (Fig. 3a,b). SEC runs were carried out at both 4 °C and room temperature. The elution profile was essentially the same at both temperatures, therefore only the data at room temperature are reported. Unless specified otherwise, SEC measurements were carried at a constant pH of 7.4 (buffer A). The SEC profiles revealed that wild-type and most of the mutant forms of PAH elute as tetramers and dimers although monomers and aggregates are also present, depending on the mutation of the protein. Fig. 3a shows the SEC profiles of proteins in which the tetramer is the most abundant species, i.e., the fused protein, the cleaved wild-type PAH and mutant p.R297L. Fig. 3b shows the profiles of the wild-type PAH (as reference) and of mutants p.I65M, p.N223Y, p.F382L, p.K398N, p.A403V and p.Q419R in which dimer is the dominant species. The peaks corresponding to tetramer, dimer and monomer species elute at 11.5 mL, 13.1 mL and 14.7 mL respectively (Fig. 3a,b).

The presence of the PAH protein was confirmed in each of the fractions obtained by SEC (Fig. 3a) after separation by SDS/PAGE and Western blot analysis using anti-PAH serum (Fig. 3c). This result demonstrates the existence of a monomeric form of the PAH enzyme. This form was probably underestimated in previous studies because it was masked by MBP. Western blot analysis also showed that samples did not contain MBP after cleavage (Fig. 3c).

The percentage of PAH oligomeric species is reported in Fig. 4 (see also Supplementary Table S1). The tetramer and dimer species of the wild-type PAH were separately collected and stored for less than one week at 4 °C. Subsequently, SEC analysis of tetramers and dimers showed that the tetramer shifts back toward the dimer and the monomer, while the dimer is fairly stable, since about 90% of the protein applied was recovered in the dimeric form (data not shown), according to literature data [21].

All chromatographic runs were done in conjunction with MALS. The masses resulting from MALS measurements in wild-type PAH mutants were 203 kDa (within 1%) and 102 kDa (within 3%) for tetramer species and dimer species, respectively. Because of the small quantities of monomer, we were not able to calculate its molecular mass. A representative profile of wild-type PAH obtained from MALS is shown in Fig. 5.

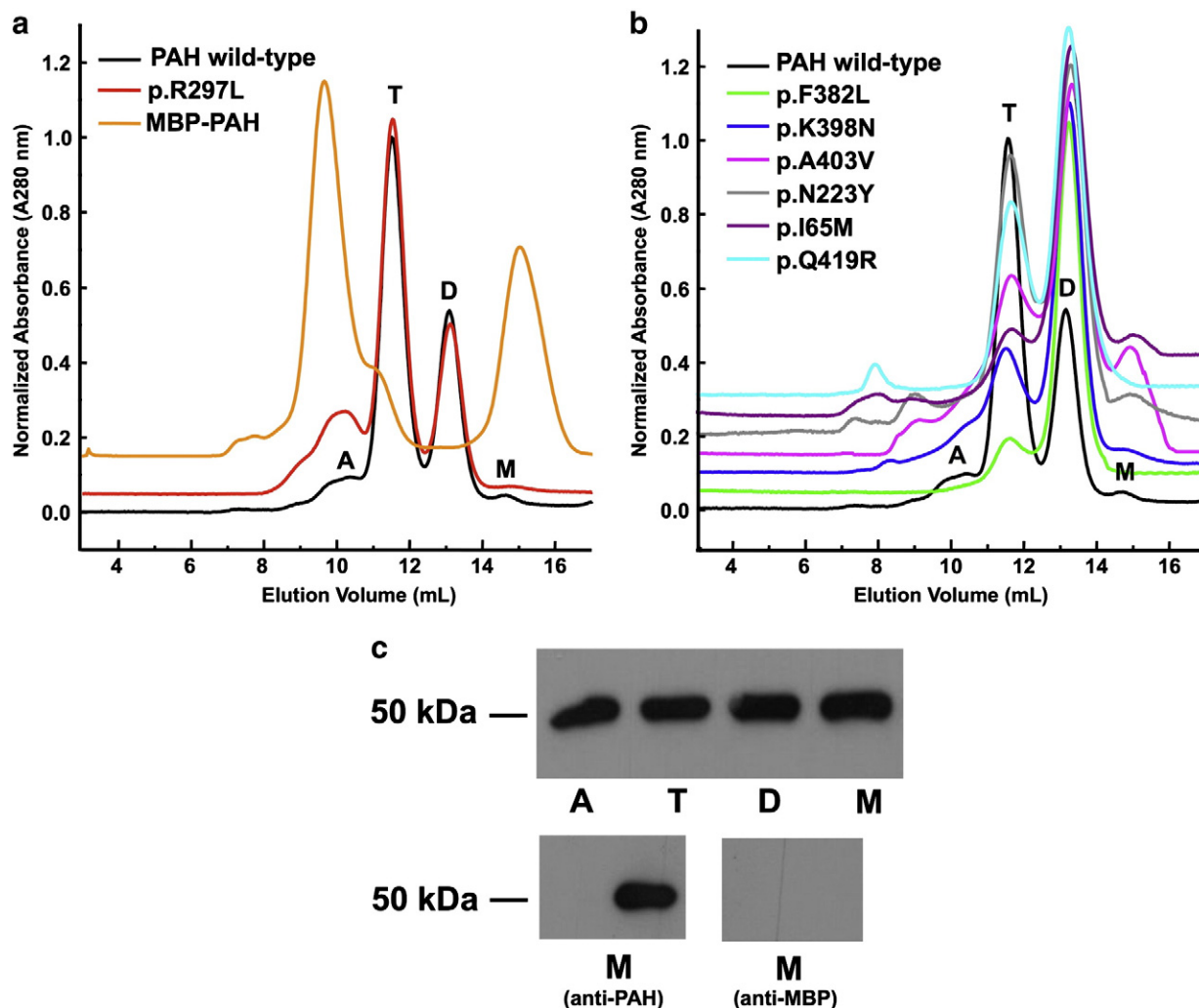


Fig. 3. Chromatographic profiles of the PAH natural variants and immunoblotting of wild-type PAH. a) Size exclusion chromatographic (SEC) runs carried out in buffer A (see text) and normalized in the 0.0–1.2 interval. All curves are shifted along the ordinate axis by 0.05n, n integer ($1 \leq n \leq 5$), with respect to the wild-type PAH curve. b) SEC runs of wild-type and other mutant recombinant PAH proteins. All curves are shifted along the ordinate axis by 0.05n, n integer ($1 \leq n \leq 5$), with respect to the wild-type PAH curve, to better visualize the single curves. c) Western blot analysis using the anti-PAH antibody of each of the fractions in panel a) obtained from wild-type (depicted as a black curve in a); peak A) aggregated forms, possibly multimeric; peak T) tetramer; peak D) dimer; peak M) monomer. Western blot analysis of the wild-type PAH monomer (peak M of panel a) with anti-PAH or anti-MBP antibodies.

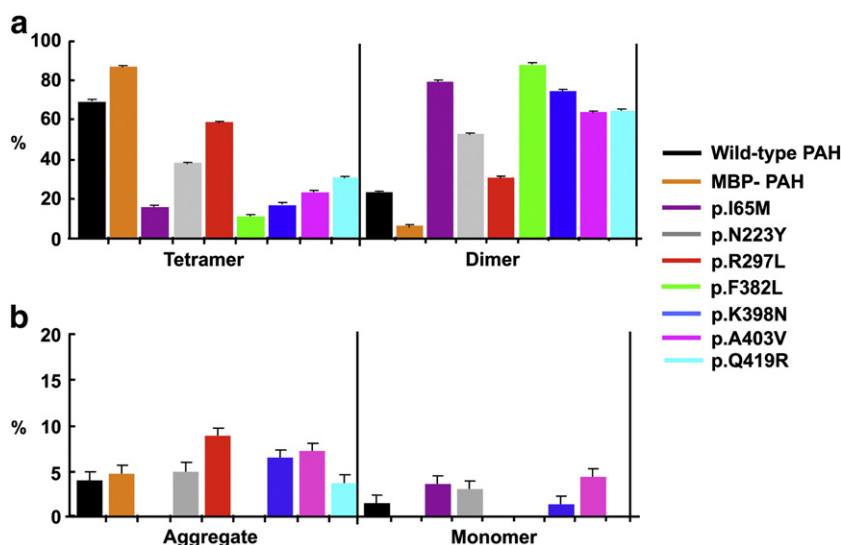


Fig. 4. Percentage of the molecular species of the recombinant wild-type PAH protein and its mutants. The histograms indicate a) the percentage of tetramers and dimers, and b) the percentage of aggregate and monomers of recombinant wild-type PAH, MBP-PAH, p.I65M, p.N223Y, p.R297L, p.F382L, p.K398N, p.A403V and p.Q419R. All data with standard deviations were calculated on at least triplicate runs carried out at 20 °C.

3.3. Thermal stability and inactivation

The dominant oligomeric species of wild-type PAH and mutants, collected after gel filtration and dialyzed against buffer C, were analyzed by CD. The CD spectra of all samples were recorded in the far-UV region (190–250 nm), in buffer C, pH 7.4, at 20 °C. Fig. 6a shows the normalized spectra for wild-type PAH and selected mutants, together with the spectrum for the fused wild-type MBP-PAH. In the spectra of Fig. 6a, the maximum centered at 195 nm and the two broad minima centered at 208 and 222 nm are indicative of the presence of both α and β secondary structure elements. The spectra profiles do not differ significantly from each other, but the molar ellipticity of all the mutants is much lower than that of wild-type enzyme. Therefore, these spectra provide evidence for local unfolding of the mutants.

We also recorded the thermal denaturation curves in the 20–80 °C temperature range by monitoring the molar ellipticity at 222 nm (Fig. 6b) of the most abundant oligomeric species of cleaved PAH proteins (Figs. 3a,b; 4, Supplementary Table S1). The far-UV CD spectra of denatured species of all samples at 80 °C are typical of random coil (data not shown). The spectrum of cooled samples after denaturation is virtually identical to that of the denatured protein at

80 °C (data not shown), thereby confirming the irreversibility of the unfolding process, as previously reported [24,40]. In the case of the wild-type PAH, the denaturation curve of the equilibrium mixture was also recorded; for comparison purposes, this curve and that of the tetramer are shown in Fig. 6c. It is clear that the denaturation process depends on the oligomeric species.

The sigmoidal denaturation curve obtained with the fused wild-type MBP-PAH protein shows two inflection points, with a plateau, corresponding to the two melting temperatures of the two proteins. Visual inspection of the denaturation curves (Fig. 6b) of the cleaved PAH proteins shows a sigmoidal shape with a single inflection point. Differently, a detailed analysis of the curves through the first derivatives, revealed two midpoints corresponding to two transitions (data not shown), according to literature data [40]. As shown in Table 2, the melting temperatures of the PAH proteins range from 33 to 57 °C. The thermal denaturation curve of mutant p.F382L is significantly shifted to lower temperatures with respect to the wild-type PAH (Fig. 6b). Therefore, we carried out the thermal inactivation assay of the wild-type PAH and the p.F382L mutant at temperatures between 32 and 58 °C (Fig. 6d). Consistently, the p.F382L mutant was much more temperature sensitive than the wild-type enzyme. In fact, under these conditions a lower amount of Tyr was produced (Fig. 6d), and the half-inactivation temperature was close to 44 °C, which well agrees with the value of $T_{m2} = 43.6$ °C obtained by CD. These findings show that the stability of specific mutants, such as p.F382L, can markedly diverge from that of the wild-type protein.

3.4. N&B analysis

Confocal microscopy observation of cells expressing GFP-wild-type PAH and GFP-A403V fusion proteins revealed a cytoplasmic localization of PAH and its mutant p.A403V, as expected (Fig. 7a,b). No fluorescence was detected in the cell nuclei. To estimate the number of subunits constituting wild-type PAH and the p.A403V mutant at steady state in live cells, the recently developed N&B technique was performed on cells expressing the fusion proteins treated and not with BH4 for 6 h. The “brightness” of the GFP-wild-type PAH fusion protein was 1.091 and 1.099 upon BH4 treatment, which, at the t-test, was not significantly different from values obtained without BH4 treatment. On the contrary, in cells expressing the GFP-A403V fusion protein there was a statistically significant ($p < 0.001$) shift of brightness from 1.047 without BH4 to 1.094 upon its addition.

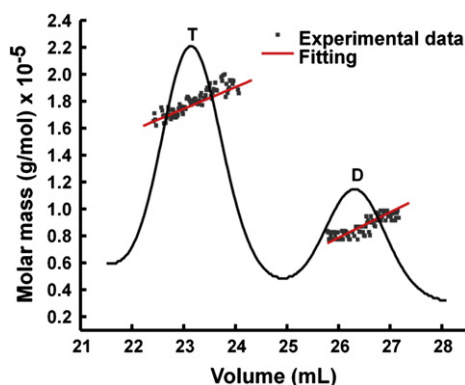


Fig. 5. SEC-MALS analysis of wild-type PAH. Representative profile of wild-type PAH obtained from light scattering and refractive index detectors. The molecular mass is shown. The experimental data are represented by squares and the fitting of experimental data is shown by a red line.

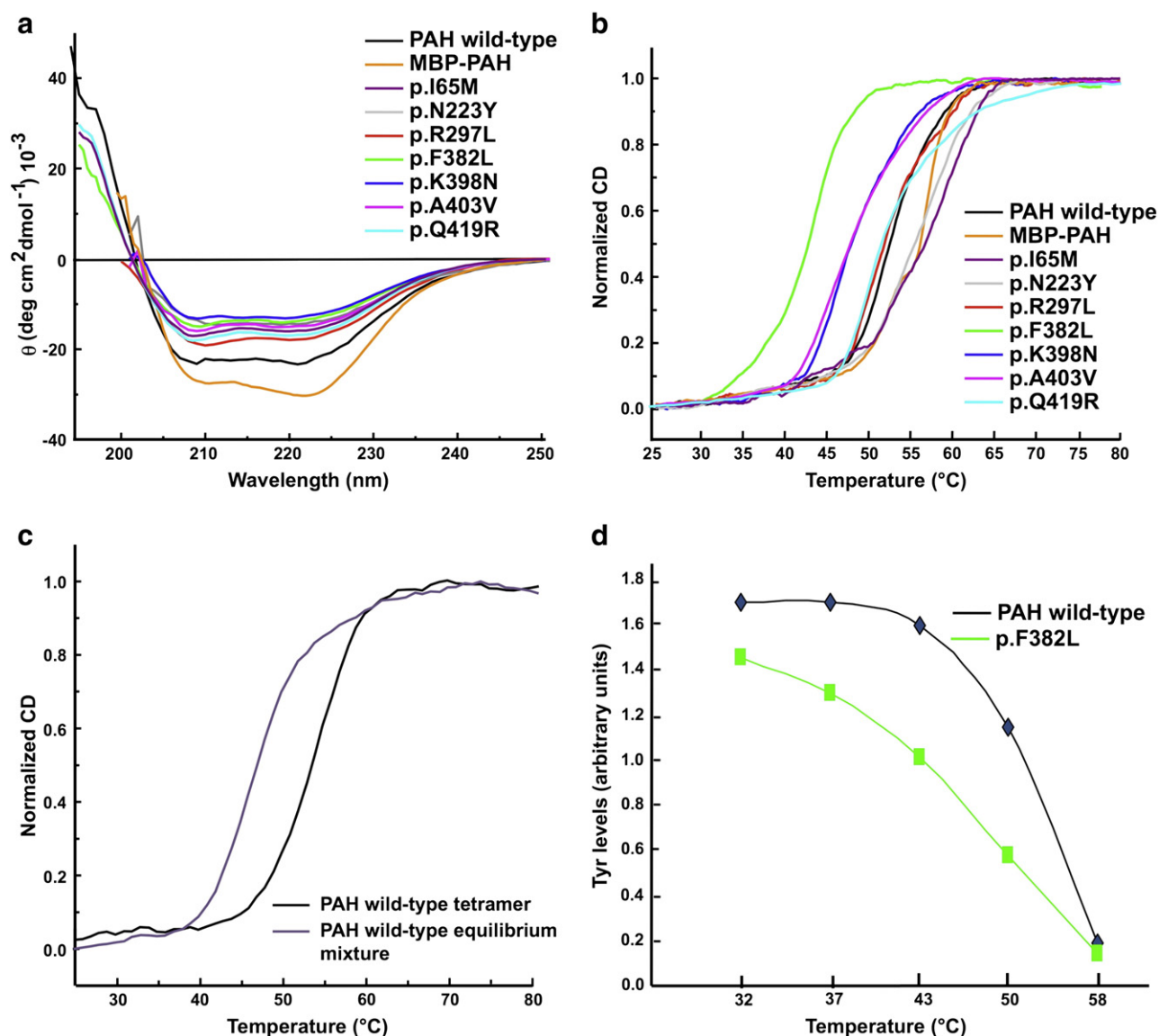


Fig. 6. CD measurements. a) Far-UV spectra recorded in buffer C (see text) at 20 °C. b) CD-monitored thermal unfolding curves in the 25–80 °C temperature range. The change of the molar ellipticity at 222 nm was monitored versus the temperature. The most abundant oligomeric form was considered for each PAH protein. c) Thermal denaturation of the tetrameric form and of the equilibrium mixture of cleaved wild-type PAH. d) Thermal inactivation assay of wild-type and F382L PAH. Proteins were incubated at increasing temperatures and the amount of produced tyrosine was determined.

These brightness values were used to calculate the number of subunits that constitute each PAH oligomer at steady state, namely wild-type and p.A403V before and after BH4 administration (see [Material and methods](#) for details). Briefly, a calibration curve (number of subunits vs brightness) was constructed using reference GFP-based

molecules constituted by 1, 2 or 3 GFP monomers and measuring their brightness in the same experimental conditions used above. The reference curve obtained (which was perfectly linear) was used to extrapolate the unknown number of subunits from the brightness of GFP-PAHs. The wild-type PAH conserved an average number of subunits (see [Material and methods](#) for definition of “average number of subunits”) equal to approximately 3.1, which reflects the presence of tetramers and dimers in equilibrium. The addition of BH4 did not affect this number. Differently, exposure of the A403V-PAH mutant form to BH4 caused the subunit number to increase from 2.4 to 3.1, this latter being the same as that of the wild-type enzyme (Fig. 7c).

4. Discussion

4.1. The oligomerization equilibrium is shifted toward the dimeric form in PAH mutants

To characterize the oligomeric state of PAH in solution, we performed SEC with on-line detection of LS and refractive index signals. This approach allowed us to measure the molecular mass of

Table 2
Melting temperatures inferred by first derivative of unfolding curves.^a

Forms of PAH	T _{m1} ± 1.0 (°C)	T _{m2} ± 1.0 (°C)
Wild-type PAH	52.2	57.6
MBP-PAH	52.0	57.5
p. I65M	53.0	59.2
p.N223Y	54.2	57.6
p.R297L	50.8	59.0
p.F382L	32.6	43.6
p.K398N	46.4	53.6
p.A403V	46.0	55.6
p.Q419R	50.1	57.3

All experiments were conducted in buffer C (see [Material and methods](#)).

^a See also Fig. 6b.

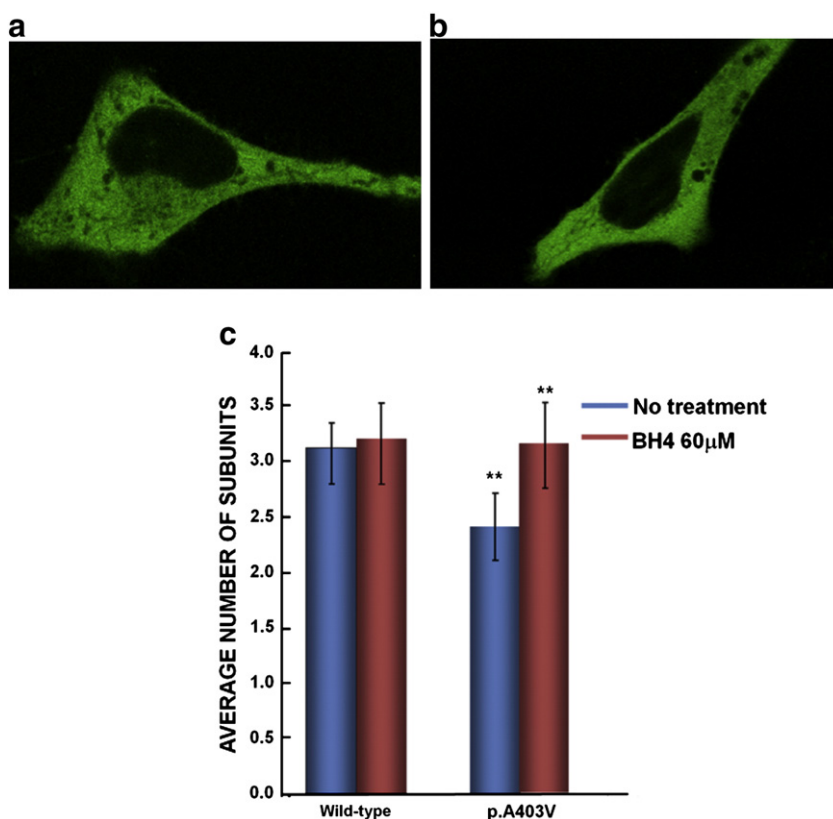


Fig. 7. N&B analysis. a) Confocal microscopy images of cells expressing GFP-wild-type PAH protein and b) GFP-p.A403V mutant protein. c) Histograms showing the oligomeric state of both GFP-wild-type PAH and GFP-p.A403V mutant in untreated (blue bars) and BH4-treated (red bars) cells. Asterisks above the bars indicate statistical significance for the p.A403V mutant protein.

the eluted peaks independently of their shape and/or amino acid composition and elution volume. The operative conditions used in the SEC experiments were the same for all samples. No substrate, cofactor or any other compound was added and only a buffer at physiological pH (buffer A; pH 7.4) was used because a lower pH and the addition of L-Phe can affect the oligomeric equilibrium [10].

In line with previous data [10,21,24], the SEC profile of the fused wild-type MBP-PAH protein revealed that tetramer was the dominant species (88.4%), whereas the dimeric form was less abundant and the monomeric form was absent. Differently, all three species were obtained in the cleaved full-length wild-type enzyme (see Fig. 4 and Supplementary Table S1 for the relative percentages). The observation of three distinct peaks demonstrates that self-association of monomers or dimers is slow on the time scale of separation. Previous studies showed that both fused and truncated/cleaved forms of wild-type and mutant enzymes consist of an equilibrium mixture of dimeric and tetrameric species in a ratio that depends on the protein nature and on the experimental conditions used [10,24].

Only in a few cases in which proteins were expressed in a coupled *in vitro* transcription–translation eukaryotic system [41,42] was the monomeric form also detected. Here, we report evidence that a monomer species occurs in the equilibrium mixture of PAH albeit in a low amount. The presence of a monomer species may have been underestimated in previous studies for several reasons: i) because of its low abundance, ii) because the fused protein was analyzed [24] or iii) because the cleaved wild-type PAH was analyzed in the presence of MBP which co-elutes with the PAH monomer [10]. Western blot analysis (Fig. 3c) and re-chromatography of the isolated tetramer of wild-type PAH, which regenerate the dimer and the monomer peak (data not shown), indicate that the monomer contributes to the equilibrium mixture. The equilibrium mixture of the PAH enzyme can be described as follows: $4M \rightleftharpoons 2D \rightleftharpoons T$.

The oligomerization process of the mutants is clearly disturbed by the mutation, except in the case of mutant p.R297L that has a SEC profile similar to that of the wild-type enzyme although it lacks a monomer (Fig. 3a). For all the other mutants (p.I65M, p.N223Y, p.F382L, p.K398N, p.A403V and p.Q419R), the equilibrium was shifted toward the dimeric enzyme (Fig. 3b). In any event, all mutants present a reduced activity of the enzyme because of the diverse composition of the equilibrium mixture. This confirms that oligomerization defects of PAH variants are one of the most common causes of HPAs.

4.2. Thermal stability and defect at the secondary structure level of PAH mutants

The CD spectrum of wild-type PAH is characterized by typical fingerprints of α/β proteins (Fig. 6a), in line with the known 3D structure [43]. Despite the similarity of CD spectra profiles in the wild-type and mutant forms of PAH, the latter present a partial loss of secondary structure with respect the wild-type folded structure, their molar ellipticity being significantly decreased (Fig. 6a). This loss occurs for all the mutants except for mutant p.R297L in which the loss is less pronounced. Therefore, the CD spectra have provided evidence for a folding defect at secondary structure level. To characterize further all the PAH mutants, we estimated the α -helical content using the equation of Richardson and Makhatazde [44]. The calculations showed a progressive decrease of the α -helical content of the PAH mutants (see Supplementary Table S2).

Thermal denaturation of all the PAH proteins proved to be an irreversible process as previously reported [40]. Therefore, the thermodynamic features of the enzyme cannot be further characterized. As expected for the wild-type MBP-PAH fused protein, the two steps in the sigmoidal curve correspond to two independent unfolding processes for the two proteins. Indeed, the two melting

temperatures (Table 2) correspond to the independent structural collapse of PAH (52.0 °C) and MBP (57.5 °C), respectively (see also Supplementary data for details).

Earlier differential scanning calorimetry, fluorescence and CD experiments indicated that, upon heating, two partially overlapping transitions occur with an apparent melting temperature T_{m1} of about 46 °C and a T_{m2} of about 54 °C, respectively [14,40]. Apart from rare exceptions, two transitions were identified also in the mutants. Their melting temperatures diverged from that of wild-type PAH within a range from −6 to +2 °C [24,45]. On the other hand, unfolding experiments conducted on the truncated PAH (aa 112–452) revealed only one cooperative transition centered at about 54 °C [40]. Therefore, the first transition was interpreted as a denaturation of the N-terminal regulatory domain and the second, partially overlapping transition as a denaturation of the catalytic-tetramerization domain [40].

Unfolding experiments were carried out for wild-type PAH and mutants in buffer C and the ellipticity at 222 nm was monitored as a function of temperature. Two overlapping transitions occurred for the wild-type PAH and all the mutants. For the wild-type PAH, the T_{m1} and T_{m2} were 52.2 °C and 57.6 °C, slightly different from previous reports [24,40,45]. This discrepancy is due to the species studied. If the denaturation process is followed using only the PAH tetramer, as in our case, the melting temperatures are T_{m1} = 52.2 °C and T_{m2} = 57.6 °C. On the other hand, if all the species present in the oligomerization equilibrium are considered, the T_{m1} well agrees with that reported previously (T_{m1} = 46.1 °C) (Fig. 6c) [24,40,45]. To verify that the unfolding process depends only on the oligomerization equilibrium, we carried out unfolding experiments in the same buffer and scan-rate conditions used in previous studies (buffer B, scan-rate 0.7 °C/min) [40,45], and obtained a T_{m1} and T_{m2} of 52.0 °C and 54.8 °C, respectively. Indeed, a small destabilization has been reported for most of the previously described mutants, as shown by a decrease in ΔT_m of about a couple of degrees. There are only a few instances where ΔT_m decreases down to ~6 °C [45]. For example, T_{m1} and T_{m2} decreased by as much as 42.6 °C and 52.0 °C and 40.7 °C and 50.2 °C, respectively in the non-natural mutants p.N223D and p.T427P with respect to wild-type enzyme T_{m1} and T_{m2} [45].

The melting temperatures of mutants p.I65M and p.N223Y indicate a very marginal stability gain, being only a couple of degrees higher with respect to the wild-type enzyme (Table 2). Furthermore, the denaturation curves of p.R297L and p.Q419R are similar, and the denaturation slopes differ only slightly from that of the wild-type enzyme, which indicates that the thermal stability is hardly affected. For mutants p.K398N and p.A403V, however, the T_{m1} is about 6° lower and the T_{m2} about 2–3° lower with respect to the wild-type, thereby indicating a loss of stability. Interestingly, the T_{m1} (33.0 °C) and T_{m2} (43.6 °C) of mutant p.F382L are about 20 °C and 14 °C lower with respect to those of the wild-type enzyme, which indicates that this enzyme variant has a high thermal structural instability.

The results of thermal denaturation experiments of the p.F382L mutant suggest that the replacement of L-Phe by L-Leu at position 382 leads to temperature-dependent functional alterations. These results were confirmed by the thermal inactivation assay performed on the p.F382L mutant and, for comparison, on the wild-type PAH. Indeed, the half-inactivation temperature obtained for this mutant (~44 °C) well agrees with the T_{m2} of 43.6 °C obtained by CD (Fig. 6b and d, Table 2).

4.3. Mapping the mutations to search for structural alterations

For the present study, we built a composite model of the full-length human enzyme and used it as a template for structural analysis of the wild-type and mutant proteins. Mutations p.I65M and p.Q419R fall in the regulatory and tetramerization domain, respectively; mutations p.N223Y, p.R297L, p.F382L, p.K398N and p.A403V fall in

the large catalytic domain. All mutations are far from the active and cofactor binding sites. All, except mutations at positions 65 and 403, are located on the surface of the molecule in hydrated regions. In Fig. 1, the position of the seven mutations is drawn on the monomer structure. There are four previously identified variants at codon 65 (p.I65T, p.I65V, p.I65N, and p.I65S). The PAH database contains in vitro expression data only for p.I65T, namely, increased proteolytic degradation in pulse-chase experiments, increased aggregation and decreased solubility. The residual activity of the I65T/V mutants, tested in different in vitro systems, was about 21–29% (<http://www.pahdb.mcgill.ca>).

Ile65 is located in a hydrophobic environment of the regulatory domain. In the mutant enzyme p.I65M, the Ile change to a somewhat larger but differently shaped Met may distort the hydrophobic packing of the region [30]. In addition, Ile 65 makes a favorable interaction with the catalytic domain of another subunit within the dimer (the Ile65 oxygen atom is hydrogen-bonded to the hydroxyl group of Tyr 216). As a result, both the tertiary structure and the quaternary structure are perturbed. These data are in line with the dimer abundance (Fig. 4 and Supplementary Table S1).

Asn223 is located in a solvent exposed loop [46]. In mutant p.N223Y the structural perturbation is mainly due to tyrosine solvent exposure that may affect the function. It has been proposed that this residue is embodied in an intra-domain hinge bending region [45] that is involved in the conformational transition induced by substrate binding. Overall, its properties are similar to those of the wild-type enzyme, except that the dimeric form is favored over the tetramer. Mutant p.R297L exhibits properties very similar to those of the wild-type enzyme. Interestingly, two other mutants reported in the database, i.e., p.R297C and p.R297H, which are also associated with a mild phenotype, indicate that mutations at this site are not critical [32].

Mutant p.F382L is the one that differs most from the wild-type enzyme. It occurs prevalently as a dimer (88.3%). Moreover, the mutation falls in a region rich in aromatic residues. L-Phe forms various stacking aromatic interactions with the aromatic residues Tyr356 and Tyr277 in the wild-type enzyme [33]. The replacement by Leu, despite the hydrophobic nature of this residue, breaks the aromatic network and results in marked destabilization. This is in line with larger ΔT_{m1} (19.6 °C) and ΔT_{m2} (14.0 °C) and with a lower inactivation temperature compared to the wild-type protein (Fig. 6d). This is the largest difference observed so far for a PAH mutant. This highlights that L-Phe in position 382 is crucial for the stability of this aromatic amino acid-rich region.

Lys398 is located at the tetramer interface, although it is not directly engaged in intersubunit interactions. The positively charged Lys is embedded in a negatively charged environment because of the presence of Asp394 and Glu390 [43]. The high dimer/tetramer ratio observed for mutant p.K398N (75.0/17.2, Fig. 4 and Supplementary Table S1) is in line with tetramer destabilization. Also the structural stability was decreased. In fact, T_{m1} and T_{m2} were lower than that of the wild-type enzyme being 5.6 and 4.0 °C, respectively (Table 2). Q419 lies in a hydrated region at the dimer/tetramer interface. The substitution of Gln by an Arg generates unfavorable ionic interactions with a nearby Arg241 that destabilize the tetramer. The thermal stability of p.Q419R is not significantly affected by the mutation.

4.4. BH4 effect and the dimer–tetramer p.A403V equilibrium

In this study, we investigated the effect of BH4 on p.A403V that, in our geographic area, is the most frequent mutant in mild, BH4-responsive patients [32,33]. To this aim, we used the N&B technique that has been successfully employed to discern minor changes in molecular composition [37,38]. We monitored the fluorescent molecular forms of GFP-wild-type PAH and the GFP-A403V mutant after transient transfection of HeLa cells. The addition of BH4 to the

wild-type enzyme did not cause any change. Differently, BH4 addition to cells expressing the p.A403V mutant promoted a shift from dimeric to tetrameric molecular forms.

The BH4 responsiveness in HPA has been the subject of numerous studies. Various mechanisms have been proposed to explain BH4-responsiveness, namely: increased enzyme activity [1,30,47,48], correction or compensation of the BH4 decreased affinity, protection toward catalytic inactivation and chaperone-like activity that, by stabilizing the protein, protects it from proteolytic degradation [1,15,30]. In addition, BH4 supplementation may restore the optimal concentration of BH4 cofactor in hepatocytes [28,46]. In our study, the N&B technique revealed that the addition of BH4 to HeLa living cells influences the oligomerization equilibrium of the p.A403V mutant by shifting it toward a tetrameric quaternary structure.

4.5. Concluding remarks

About 600 mutations associated with the PKU/HPA phenotype have been identified in the PAH gene. The resulting phenotypes range from mild to severe HPA. This study demonstrates that our seven gene variants reduce the enzymatic activity to 38–69% of that of wild-type activity and affect the oligomerization state, thermal stability and folding of PAH protein. Perturbation of these biophysical and biochemical features may, therefore, be considered major disease-causing alterations, also in mild phenotypic forms of HPAs. In addition to the well recognized effect of BH4 on the stability of PAH mutants [30], we provide the first evidence, obtained with the N&B technique, that in cellulose exposure to BH4 influences the oligomerization equilibrium of the p.A403V mutant. Therefore, we surmise that, in this case, a shift from dimer to tetramer plays a major role in BH4 responsiveness.

Acknowledgements

This study was supported by grants from Regione Campania (Convenzione CEINGE-Regione Campania, G.R. 27/12/2007), from Ministero dell'Istruzione, dell'Università e della Ricerca-Rome PS35-126/IND, from IRCCS – Fondazione SDN, and from Ministero Salute, Rome, Italy.

We thank Simona Monti and Nina Dathan for their suggestions and advices regarding SEC. Pompea del Vecchio and Vincenzo Granata are acknowledged for their comments regarding CD measurements. We are grateful to Jean Ann Gilder (Scientific Communication srl) for revising and editing the text, and to Vittorio Lucignano for graphic editorial help in figure composition.

Appendix A. Supplementary data

Supplementary data to this article can be found online at doi:10.1016/j.bbdis.2011.07.012.

References

- [1] C.R. Scriver, The PAH gene, phenylketonuria, and a paradigm shift, *Hum. Mutat.* 28 (2007) 831–845.
- [2] N. Blau, B. Thony, R.G.H. Cotton, K. Hyland, Disorders of tetrahydrobiopterin and related biogenic amines, in: C.R. Scriver, A.L. Beaudet, W.S. Sly, D. Valle, B. Vogelstein (Eds.), *The Metabolic and Molecular Bases of Inherited Disease*, McGraw-Hill, New York, 2001, pp. 1725–1776.
- [3] R.A. Williams, C.D. Mamotte, J.R. Burnett, Phenylketonuria: an inborn error of phenylalanine metabolism, *Clin. Biochem. Rev.* 29 (2008) 31–41.
- [4] M. Giovannini, E. Verduci, E. Salvatici, L. Fiori, E. Riva, Phenylketonuria: dietary and therapeutic challenges, *J. Inher. Metab. Dis.* 30 (2007) 145–152.
- [5] H.L. Levy, A. Milanowski, A. Chakrapani, M. Cleary, P. Lee, F.K. Trefz, C.B. Whitley, F. Feillet, A.S. Feigenbaum, J.D. Bechuk, H. Christ-Schmidt, A. Dorenbaum, Efficacy of sapropterin dihydrochloride (tetrahydrobiopterin, 6R-BH4) for reduction of phenylalanine concentration in patients with phenylketonuria: a phase III randomised placebo-controlled study, *Lancet* 370 (2007) 504–510.
- [6] M. Cerreto, R. Nistico, D. Ombrone, M. Ruoppolo, A. Usiello, A. Daniele, L. Pastore, F. Salvatore, Complete reversal of metabolic and neurological symptoms in PKU mice after PAH-HD-Ad vector treatment, *Hum. Gene Ther.* 11 (2009) 1391.
- [7] F.J. Van Spronsen, G.M. Enns, Future treatment strategies in phenylketonuria, *Mol. Genet. Metab.* 99 (2010) 90–95.
- [8] F. Fusetti, H. Erlandsen, T. Flatmark, R.C. Stevens, Structure of tetrameric human phenylalanine hydroxylase and its implications for phenylketonuria, *J. Biol. Chem.* 273 (1998) 16962–16967.
- [9] A.P. Doskeland, A. Martinez, P.M. Knappskog, T. Flatmark, Phosphorylation of recombinant human phenylalanine hydroxylase: effect on catalytic activity, substrate activation and protection against non-specific cleavage of the fusion protein by restriction protease, *Biochem. J.* 313 (1996) 409–414.
- [10] A. Martinez, P.M. Knappskog, S. Olafsdottir, A.P. Doskeland, H.G. Eiken, R.M. Svebak, M. Bozzini, J. Apold, T. Flatmark, Expression of recombinant human phenylalanine hydroxylase as fusion protein in *Escherichia coli* circumvents proteolytic degradation by host cell proteases. Isolation and characterization of the wild-type enzyme, *Biochem. J.* 306 (Pt 2) (1995) 589–597.
- [11] S. Kaufman, The phenylalanine hydroxylating system, *Adv. Enzymol. Relat. Areas Mol. Biol.* 67 (1993) 77–264.
- [12] O.A. Andersen, A.J. Stokka, T. Flatmark, E. Hough, 2.0 Å resolution crystal structures of the ternary complexes of human phenylalanine hydroxylase catalytic domain with tetrahydrobiopterin and 3-(2-thienyl)-L-alanine or L-norleucine: substrate specificity and molecular motions related to substrate binding, *J. Mol. Biol.* 333 (2003) 747–757.
- [13] A. Doskeland, T. Ljones, T. Skotland, T. Flatmark, Phenylalanine 4-monooxygenase from bovine and rat liver: some physical and chemical properties, *Neurochem. Res.* 7 (1982) 407–421.
- [14] F.F. Miranda, M. Thörölfsson, K. Teigen, J.M. Sanchez-Ruiz, A. Martinez, Structural and stability effects of phosphorylation: localized structural changes in phenylalanine hydroxylase, *Protein Sci.* 13 (2004) 1219–1226.
- [15] C.R. Scriver, P.J. Waters, Monogenic traits are not simple: lessons from phenylketonuria, *Trends Genet.* 15 (1999) 267–272.
- [16] S. Giannattasio, I. Dianzani, P. Lattanzio, M. Spada, V. Romano, F. Cali, G. Andria, A. Ponzone, E. Marra, A. Piazza, Genetic heterogeneity in five Italian regions: analysis of PAH mutations and minihaplotypes, *Hum. Hered.* 52 (2001) 154–159.
- [17] P. Guldborg, F. Rey, J. Zschocke, V. Romano, B. Francois, L. Michiels, K. Ullrich, G.F. Hoffmann, P. Burgard, H. Schmidt, C. Meli, E. Riva, I. Dianzani, A. Ponzone, J. Rey, F. Guttler, A European multicenter study of phenylalanine hydroxylase deficiency: classification of 105 mutations and a general system for genotype-based prediction of metabolic phenotype, *Am. J. Hum. Genet.* 63 (1998) 71–79.
- [18] J. Zschocke, Phenylketonuria mutations in Europe, *Hum. Mutat.* 21 (2003) 345–356.
- [19] H.G. Eiken, P.M. Knappskog, J. Apold, T. Flatmark, PKU mutation G46S is associated with increased aggregation and degradation of the phenylalanine hydroxylase enzyme, *Hum. Mutat.* 7 (1996) 228–238.
- [20] M. Thörölfsson, K. Teigen, A. Martinez, Activation of phenylalanine hydroxylase: effect of substitutions at Arg68 and Cys 237, *Biochem. J.* 42 (2003) 3419–3428.
- [21] P.M. Knappskog, T. Flatmark, J.M. Aarden, J. Haavik, A. Martinez, Structure/function relationships in human phenylalanine hydroxylase. Effect of terminal deletions on the oligomerization, activation and cooperativity of substrate binding to the enzyme, *Eur. J. Biochem.* 242 (1996) 813–821.
- [22] B. Kobe, I.G. Jennings, C.M. House, B.J. Michell, K.E. Goodwill, B.D. Santasiero, R.C. Stevens, R.G. Cotton, B.E. Kemp, Structural basis of autoregulation of phenylalanine hydroxylase, *Nat. Struct. Biol.* 6 (1999) 442–448.
- [23] P.J. Waters, M.A. Parniak, B.R. Akerman, A.O. Jones, C.R. Scriver, Missense mutations in the phenylalanine hydroxylase gene (PAH) can cause accelerated proteolytic turnover of PAH enzyme: a mechanism underlying phenylketonuria, *J. Inher. Metab. Dis.* 22 (1999) 208–212.
- [24] S.W. Gersting, K.F. Kemter, M. Staudigl, D.D. Messing, M.K. Danecka, F.B. Lagler, C.P. Sommerhoff, A.A. Roscher, A.C. Muntau, Loss of function in phenylketonuria is caused by impaired molecular motions and conformational instability, *Am. J. Hum. Genet.* 83 (2008) 5–17.
- [25] T. Gjetting, M. Petersen, P. Guldborg, F. Guttler, In vitro expression of 34 naturally occurring mutant variants of phenylalanine hydroxylase: correlation with metabolic phenotypes and susceptibility toward protein aggregation, *Mol. Genet. Metab.* 72 (2001) 132–143.
- [26] P.J. Waters, M.A. Parniak, B.R. Akerman, C.R. Scriver, Characterization of phenylketonuria missense substitutions, distant from the phenylalanine hydroxylase active site, illustrates a paradigm for mechanism and potential modulation of phenotype, *Mol. Genet. Metab.* 69 (2000) 101–110.
- [27] A.L. Pey, F. Stricher, L. Serrano, A. Martinez, Predicted effects of missense mutations on native-state stability account for phenotypic outcome in phenylketonuria, a paradigm of misfolding diseases, *Am. J. Hum. Genet.* 81 (2007) 1006–1024.
- [28] C. Aguado, B. Perez, M. Ugarte, L.R. Desviat, Analysis of the effect of tetrahydrobiopterin on PAH gene expression in hepatoma cells, *FEBS Lett.* 580 (2006) 1697–1701.
- [29] M. Staudigl, S.W. Gersting, M.K. Danecka, D.D. Messing, M. Woidly, D. Pinkas, K.F. Kemter, N. Blau, A.C. Muntau, The interplay between genotype, metabolic state and cofactor treatment governs phenylalanine hydroxylase function and drug response, *Hum. Mol. Genet.* 20 (2011) 2628–2641.
- [30] H. Erlandsen, A.L. Pey, A. Gamez, B. Perez, L.R. Desviat, C. Aguado, R. Koch, S. Surendran, S. Tyrling, R. Matalon, C.R. Scriver, M. Ugarte, A. Martinez, R.C. Stevens, Correction of kinetic and stability defects by tetrahydrobiopterin in phenylketonuria patients with certain phenylalanine hydroxylase mutations, *Proc. Natl. Acad. Sci. U. S. A.* 101 (2004) 16903–16908.
- [31] A.C. Muntau, S.W. Gersting, Phenylketonuria as a model for protein misfolding diseases and for the development of next generation orphan drugs for patients with inborn errors of metabolism, *J. Inher. Metab. Dis.* 33 (2010) 649–658.

- [32] A. Daniele, G. Cardillo, C. Pennino, M.T. Carbone, D. Scognamiglio, A. Correr, A. Pignero, G. Castaldo, F. Salvatore, Molecular epidemiology of phenylalanine hydroxylase deficiency in Southern Italy: a 96% detection rate with ten novel mutations, *Ann. Hum. Genet.* 71 (2007) 185–193.
- [33] A. Daniele, G. Cardillo, C. Pennino, M.T. Carbone, D. Scognamiglio, L. Esposito, A. Correr, G. Castaldo, A. Zagari, F. Salvatore, Five human phenylalanine hydroxylase proteins identified in mild hyperphenylalaninemia patients are disease-causing variants, *Biochim. Biophys. Acta* 1782 (2008) 378–384.
- [34] A. Daniele, I. Scala, G. Cardillo, C. Pennino, C. Ungaro, M. Sibilio, G. Parenti, L. Esposito, A. Zagari, G. Andria, F. Salvatore, Functional and structural characterization of novel mutations and genotype–phenotype correlation in 51 phenylalanine hydroxylase deficient families from Southern Italy, *FEBS J.* 276 (2009) 2048–2059.
- [35] T. Bardelli, M.A. Donati, S. Gasperini, F. Ciani, F. Belli, N. Blau, A. Morrone, E. Zammarchi, Two novel genetic lesions and a common BH4-responsive mutation of the PAH gene in Italian patients with hyperphenylalaninemia, *Mol. Genet. Metab.* 77 (2002) 260–266.
- [36] R.N. Carvalho, T. Solstad, E. Bjørge, J.F. Barroso, T. Flatmark, Deamidations in recombinant human phenylalanine hydroxylase. Identification of labile asparagine residues and functional characterization of Asn→Asp mutant forms, *J. Biol. Chem.* 278 (2003) 15142–15152.
- [37] M.A. Digman, C.M. Brown, P. Sengupta, P.W. Wiseman, A.F. Horwitz, E. Gratton, Measuring fast dynamics in solutions and cells with a laser scanning microscope, *Biophys. J.* 89 (2010) 1317–1327.
- [38] R.B. Dalal, M.A. Digman, A.F. Horwitz, V. Vetri, E. Gratton, Determination of particle number and brightness using a laser scanning confocal microscope operating in the analog mode, *Microsc. Res. Technol.* 71 (2008) 69–81.
- [39] T.A. Jones, J.Y. Zou, S.W. Cowan, M. Kjeldgaard, Improved methods for building protein models in electron density maps and the location of errors in these models, *Acta Crystallogr. A* 47 (1991) 110–119.
- [40] M. Thörölfsson, B. Ibarra-Molero, P. Fojan, S.B. Peterson, J.M. Sanchez-Ruiz, A. Martinez, I. Phenylalanine binding and domain organization in human phenylalanine hydroxylase: a differential scanning calorimetry study, *Biochem.* 41 (2002) 7573–7585.
- [41] E. Bjørge, P.M. Knappskog, A. Martinez, R.C. Stevens, T. Flatmark, Partial characterization and three-dimensional-structural localization of eight mutations in exon 7 of the human phenylalanine hydroxylase gene associated with phenylketonuria, *Eur. J. Biochem.* 257 (1998) 1–10.
- [42] A.L. Pey, B. Perez, L.R. Desviat, M.A. Martinez, C. Aguado, H. Erlandsen, A. Gamez, R.C. Stevens, M. Thörölfsson, M. Ugarde, A. Martinez, Mechanisms underlying responsiveness to tetrahydrobiopterin in mild phenylketonuria mutations, *Hum. Mutat.* 24 (2004) 388–399.
- [43] H. Erlandsen, F. Fusetti, A. Martinez, E. Hough, T. Flatmark, R.C. Stevens, Crystal structure of the catalytic domain of human phenylalanine hydroxylase reveals the structural basis for phenylketonuria, *Nat. Struct. Biol.* 4 (1997) 995–1000.
- [44] J.M. Richardson, G.I. Makhataadze, Temperature dependence of thermodynamics of helix-coil transition, *J. Mol. Biol.* 335 (2004) 1029–1037.
- [45] A.J. Stokka, R.N. Carvalho, J.F. Barroso, T. Flatmark, Probing the role of crystallographically defined/predicted hinge-bending regions in the substrate-induced global conformational transition and catalytic activation of human phenylalanine hydroxylase by single-site mutagenesis, *J. Biol. Chem.* 279 (2004) 26571–26580.
- [46] S. Kure, K. Sato, K. Fujii, Y. Aoki, Y. Suzuki, S. Kato, Y. Matsubara, Wild-type phenylalanine hydroxylase activity is enhanced by tetrahydrobiopterin supplementation in vivo: an implication for therapeutic basis of tetrahydrobiopterin-responsive phenylalanine hydroxylase deficiency, *Mol. Genet. Metab.* 83 (2004) 150–156.
- [47] N. Blau, H. Erlandsen, The metabolic and molecular bases of tetrahydrobiopterin-responsive phenylalanine hydroxylase deficiency, *Mol. Genet. Metab.* 82 (2004) 101–111.
- [48] A.C. Muntau, W. Roschinger, M. Habich, H.H. Demmelmair, B. Hoffmann, C.P. Sommhoff, A.A. Roscher, Tetrahydrobiopterin as an alternative treatment for mild phenylketonuria, *N. Engl. J. Med.* 347 (2002) 2122–2132.

Further reading

- [49] V. Novokhahny, K. Ingham, Thermodynamics of maltose binding protein unfolding, *Protein Sci.* 6 (1997) 141–146.

Appendix A. Supplementary data

Selection of the operative conditions for CD measurements

Any compound that absorbs in the region of interest (250-190 nm) should be avoided. Salt absorption, particularly of alogen anions hampers the protein CD spectra below 200 nm. In addition, their presence increases the high tension voltage leading to a detector saturation. Consequently, we extensively dialyzed all protein samples before CD measurements to eliminate salts.

Analysis of the α -helical content of PAH proteins

To estimate approximately the fractional helical content from the ellipticity at 222 nm, the following equation was used [44]:

$$f_h = ([\theta] - [\theta]_c) / ([\theta]_h - [\theta]_c) \quad \text{Eq.1}$$

where f_h is the fractional helical content, $[\theta]_h$ and $[\theta]_c$ are the molar ellipticities of the full helical and full coiled states, respectively, which are given by $[\theta]_h = (-40000 + 250T) [1 - (2.5/N_{\text{res}})]$ and $[\theta]_c = (640 - 45T)$, where T is the temperature (Celsius degrees). The results, reported in Supplementary Table S2, show a decrease of the α -helical content from 65% (wt-hPAH) to 35%, for the mutant p.K398N. The percentages are over-estimated in comparison with high resolution experimental X-ray structure [8, 22].

Thermal unfolding of MBP at pH 7.4

Previous studies show that thermal unfolding of MBP is characterized by a single two-state transition, of which T_m is largely affected by experimental conditions [49]. In particular, pH and the presence of maltose can influence the melting of MBP. T_m values were reported only for pH ≤ 3.4 or pH ≥ 8.3 ; T_m are 52.6°C and 62.6°C at pH 3.4 and 8.3 respectively [49]. Furthermore, because MBP is widely used as a carrier protein for the production of recombinant fusion proteins,

several studies evaluated unfolding of the fused protein [24]. Since no data are available at neutral pH values, and taking into account that all our measurements were performed at pH7.4, we recorded the thermal unfolding curve of commercial MBP by monitoring the molar ellipticity θ at 222 nm, in buffer C, at pH 7.4. In the case of MBP, the T_m was 57.5°C. This value coincides with the T_{m2} of the fused protein MBP-PAH (Table 2, Fig. 6b).

Supplementary Table S1. Percentages of molecular species

	Aggregates (%)		Tetramer (%)		Dimer (%)		Monomer(%)	
Wild-type PAH	4.0 ± 1.0	30 ^{Ref 21}	70.7 ± 0.4	53 ^{Ref 21}	23.9 ± 0.6	12 ^{Ref 21}	1.4 ± 0.9	nd ^{Ref 21}
MBP-PAH	4.8 ± 0.9	38 ^{Ref 10,41}	88.4 ± 0.3	86.2 ^{Ref 10}	6.8 ± 0.8	13.8 ^{Ref 10}	Nd	nd ^{Ref 21}
p.I65M	Nd		16.5±0.5		80.1±0.3		3.4±0.8	
p.N223Y	5.0±1.0		38.9±0.5		53.2±0.5		2.9±0.8	
p.R297L	8.9±0.8		60.0±0.3		31.1±0.4		Nd	
p.F382L	Nd		11.7±0.4		88.3±0.3		Nd	
p.K398N	6.5 ± 0.9		17.2 ± 0.5		75.0±0.4		1.3±0.9	
p.A403V	7.3 ± 0.8		23.8 ± 0.4		64.8 ± 0.3		4.1±0.8	
p.Q419R	3.7 ± 1.0		31.4 ± 0.4		64.9 ± 0.3		Nd	

Supplementary Table S2. α -helical content of PAH proteins obtained through the Eq. 1

PAH protein	α -helical content
PAH WT	65%
I65M	45%
N223Y	40%
R297L	51%
F382L	38%
K398N	35%
A403V	42%
Q419R	48%